

**THE EFFECT OF SOLID CARRIERS IN FLUIDIZED BED FOR  
FENTON PROCESS IN TREATING RECALCITRANT  
WASTEWATERS**

**MUSTAPHA MOHAMMED BELLO**

**FACULTY OF ENGINEERING  
UNIVERSITY OF MALAYA  
KUALA LUMPUR**

**2018**

**THE EFFECT OF SOLID CARRIERS IN FLUIDIZED BED FOR  
FENTON PROCESS IN TREATING RECALCITRANT  
WASTEWATERS**

**MUSTAPHA MOHAMMED BELLO**

**THESIS SUBMITTED IN FULFILMENT OF THE  
REQUIREMENTS FOR THE DEGREE OF DOCTOR OF  
PHILOSOPHY**

**FACULTY OF ENGINEERING  
UNIVERSITY OF MALAYA  
KUALA LUMPUR**

**2018**

**UNIVERSITY OF MALAYA**  
**ORIGINAL LITERARY WORK DECLARATION**

Name of Candidate: Mustapha Mohammed Bello

Registration/Matric No: KHA150037

Name of Degree: Doctor of Philosophy

Title of Thesis (“this work”): The Effect of Solid Carriers in Fluidized Bed for Fenton process in Treating Recalcitrant Wastewaters

Field of study: Environmental Engineering

I do solemnly and sincerely declare that:

- (1) I am the sole author/writer of this Work;
- (2) This Work is original;
- (3) Any use of any work in which copy right exists was done by way of fair dealing and for permitted purposes and any excerpt or extract from, or reference to or reproduction of any copyright work has been disclosed expressly and sufficiently and the title of the work and its authorship have been acknowledged in this Work;
- (4) I do not have any actual knowledge nor do I ought reasonably to know that the making of this Work constitutes an infringement of any copyright work;
- (5) I hereby assign all and every rights in the copyright of this Work to the University of Malaya (“UM”), who henceforth shall be owner of copyright in this Work and that any reproduction or use in any form by any means whatsoever is prohibited without the consent of UM having been first had and obtained;
- (6) I am fully aware that if in the course of making this Work I have infringed any copyright whether intentionally or otherwise, I may be subject to legal action or any other action as may be determined by UM.

Candidate’s Signature

Date:

Subscribed and solemnly declared before,

Witness’s Signature

Date:

Name:

Designation:

# THE EFFECT OF SOLID CARRIERS IN FLUIDIZED BED FOR FENTON PROCESS IN TREATING RECALCITRANT WASTEWATERS

## ABSTRACT

Fluidized bed Fenton (FBF) process is a modification of Fenton oxidation that can reduce sludge generation and enhance process performance. The fluidized solid carriers can enhance mass transfer and provide surface for the precipitation of iron oxide, thus reducing sludge generation. Furthermore, the iron oxide-coated carrier can act as a heterogeneous Fenton catalyst, further enhancing process performance. Despite the potentials of FBF process, many aspects of the process, such as the effect of carrier and its possible interaction with Fenton's reagent are yet to be fully established. Considering the importance of carrier on the process performance, understanding its effect and interaction with Fenton's reagent/pollutants is necessary for effective optimization of the process. Thus, this study is aimed at filling these gaps through theoretical and experimental approaches.

A fluidized bed Fenton process was developed and its performance was evaluated through the degradation of a model pollutant, Reactive Black 5 (RB5). The FBF process was first optimized using  $\text{SiO}_2$  as the carrier. Quantum chemical calculations was then used to predict the possible interactions among the  $\text{SiO}_2$ , Fenton's reagent and RB5. The results of the quantum chemical calculations were subsequently validated through experimental investigations of the effect of  $\text{SiO}_2$  and interaction with the Fenton's reagent. To further enhance the cost-effectiveness of the FBF process, the feasibility of using a palm kernel shell granular activated carbon (PKSGAC) as an alternative low-cost carrier was investigated. The performance of the PKSGAC was compared with that of  $\text{SiO}_2$ .

Using  $\text{SiO}_2$ , the FBF process can remove 80% of the initial COD and more than 99% of the initial color under optimum conditions. This COD removal was about 15 to 20% higher than conventional Fenton oxidation. Under constant  $\text{SiO}_2$  loading, the most

significant parameters affecting the FBF process are the initial concentration of  $\text{Fe}^{2+}$  and the concentration of the pollutant. The analysis of quantum chemical parameters shows that there are possible interactions between  $\text{SiO}_2$ , Fenton's reagent and the pollutant. For example, with a comparatively higher  $E_{\text{HOMO}}$  of -8.72 eV,  $\text{SiO}_2$  shows a tendency to donate electrons to  $\text{Fe}^{3+}$  ( $E_{\text{HOMO}} = -18.74$  eV), which explains the crystallization of iron oxide on the carriers. Analysis of frontier orbitals also shows that  $\text{SiO}_2$  can take up electrons from  $\text{H}_2\text{O}$ ,  $\text{H}_2\text{O}_2$ , and  $\text{H}_3\text{O}^+$  molecules due to its lower energy. Analysis of enthalpy and Gibb's free energies further revealed that beside crystallization of iron oxide, other interactions such as complexation between  $\text{SiO}_2$  and  $\text{H}_2\text{O}_2$ , can occur in the process. These results are supported by the experimental results and surface analysis of the carrier. The overall results show that solid carriers contribute to the removal of pollutants through adsorption and may also form complexes with  $\text{H}_2\text{O}_2$ . However, due to the synergy of oxidation and adsorption, the overall process performance is enhanced in the presence of solid carriers. Comparing the PKSGAC with  $\text{SiO}_2$ , PKSGAC offers a higher performance in terms of treatment efficiency and hydrodynamic characteristics, making it a potential alternative to the commonly used carrier.

**Keywords:** Fenton oxidation, Fluidized bed Reactor, Recalcitrant wastewater, Fluidized carriers, Quantum chemical calculations.

# KESAN PENGANGKUT PEPEJAL DALAM TURUS TERBENDALIR BAGI PROSES FENTON UNTUK MERAWAT AIRSISA DEGIL

## ABSTRAK

Proses Turus Terbendalir Fenton (FBF) merupakan modifikasi pengoksidaan Fenton yang boleh mengurangkan penghasilan enapcemar dan meningkatkan prestasi proses. Lapisan pengangkut pepejal terbendalir boleh meningkatkan pemindahan jisim dan menyediakan permukaan bagi pemendakan oksida besi, seterusnya mengurangkan penghasilan enapcemar. Selain itu, pengangkut bersadur oksida besi boleh bertindak sebagai mangkin Fenton heterogen, seterusnya meningkatkan prestasi proses. Namun, walaupun FBF berpotensi, banyak aspek bagi proses ini, seperti kesan pengangkut dan interaksi yang mungkin dengan reagen Fenton masih belum dibangunkan sepenuhnya. Mempertimbangkan kepentingan pengangkut ke atas prestasi proses, memahami kesannya dan interaksi dengan reagen Fenton / bahan pencemar adalah perlu bagi optimasi proses yang berkesan. Maka, kajian ini bertujuan untuk mengisi kekurangan ini melalui pendekatan teori dan ujikaji.

Proses Turus Terbendalir Fenton telah dibangunkan dan prestasinya telah dinilai melalui degradasi model bahan pencemar, Reactive Black 5 (RB5). Proses FBF terlebih dahulu dioptimumkan menggunakan  $\text{SiO}_2$  sebagai pengangkut. Pengiraan kimia kuantum kemudiannya digunakan untuk meramalkan kemungkinan interaksi di antara  $\text{SiO}_2$ , reagen Fenton dan RB5. Keputusan yang diperolehi daripada pengiraan kimia kuantum kemudiannya disahkan melalui ujikaji eksperimen tentang pengaruh  $\text{SiO}_2$  dan interaksi dengan reagen Fenton. Bagi meningkatkan lagi keberkesanan kos proses FBF, kemungkinan untuk menggunakan karbon teraktif berbutir dari tempurung kelapa sawit (PKSGAC) sebagai alternatif bagi pengangkut berkos rendah telah dikaji. Prestasi PKSGAC telah dibandingkan dengan  $\text{SiO}_2$ .

Pada keadaan optima, proses FBF mampu menyingkirkan COD awal dan warna awal masing-masing sehingga 80% dan 99% dengan menggunakan SiO<sub>2</sub>. Penyingkiran COD ini adalah kira-kira 15 - 20% lebih tinggi daripada proses pengoksidaan Fenton lazim. Pada bebanan SiO<sub>2</sub> malar, parameter yang paling ketara mempengaruhi proses FBF adalah kepekatan awal Fe<sup>2+</sup> dan kepekatan bahan pencemar. Analisis parameter kimia kuantum menunjukkan bahawa terdapat kemungkinan interaksi di antara SiO<sub>2</sub>, reagen Fenton dan bahan pencemar. Sebagai contoh, dengan E<sub>HOMO</sub> yang agak tinggi iaitu -8.72 eV, SiO<sub>2</sub> menunjukkan kecenderungan untuk menyumbang elektron kepada Fe<sup>3+</sup> (E<sub>HOMO</sub> = -18.74 eV), yang menerangkan penghabluran oksida besi ke atas pengangkut. Analisis orbital sempadan juga menunjukkan bahawa SiO<sub>2</sub> boleh mengambil elektron daripada molekul H<sub>2</sub>O, H<sub>2</sub>O<sub>2</sub>, dan H<sub>3</sub>O<sup>+</sup> oleh kerana tenaganya yang lebih rendah. Entalpi dan tenaga Gibb bebas juga menunjukkan bahawa selain penghabluran oksida besi, interaksi lain seperti kompleks di antara SiO<sub>2</sub> dan H<sub>2</sub>O<sub>2</sub> boleh berlaku dalam proses tersebut. Keputusan ini disokong oleh keputusan ujikaji dan analisis permukaan pengangkut. Keputusan keseluruhan menunjukkan bahawa pengangkut pepejal menyumbang kepada penyingkiran bahan pencemar melalui penjerapan dan mungkin juga membentuk kompleks dengan H<sub>2</sub>O<sub>2</sub>. Namun, disebabkan oleh sinergi pengoksidaan dan penjerapan, prestasi keseluruhan proses dipertingkatkan dengan kehadiran pengangkut pepejal. Melalui perbandingan di antara PKSGAC dengan SiO<sub>2</sub>, PKSGAC menawarkan prestasi yang lebih tinggi dari segi kecekapan rawatan dan ciri-ciri hidrodinamik, menjadikannya alternatif yang berpotensi kepada pengangkut yang lazim digunakan.

**Kata kunci:** Pengoksidaan Fenton, Reaktor Turus Terbendalir, Airsisa Degil, Pengangkut Terbendalir, Pengiraan Kimia Kuantum

## ACKNOWLEDGMENTS

All glory be to Almighty Allah, in whose favor this thesis has been produced. My sincere gratitude goes to my supervisor, Prof. Ir. Dr. Abdul Aziz Abdul Raman, for his guidance and support throughout the period of my studies. This thesis is a product of his excellent supervision.

During this work, I shared long hours with my laboratory colleagues, many of whom have contributed to this thesis in one way or another. Notable among them is Dr. Anam Asghar who has always been there for me throughout this journey. Ali Sherlala, Dr. Archina Buthiyyapan and Huda Hassan have all been part of the journey. My gratitude to the entire staff of the Department of Chemical Engineering and the Faculty of Engineering.

I feel sad that my parents are not there to rejoice with me over this feat. They would have been very happy and proud. May Allah have mercy on them. Whilst they departed long time ago, they have left me in the safe hands of grandparents, brothers and sisters, uncles and aunts, and cousins who are too numerous to mention. This family brought me up to be what I am today. I owe this feat, and those before it, to them.

Whilst I was spending hours in the laboratory in the course of producing this thesis, my wife was patiently supporting me. Fatima provided me with the necessary spiritual support that sustain my pursuit of this study. It was in the middle of this study that our first child, Muhammad, was born. Despite her own study and the hurdles of childbirth, she was always there for me. This thesis is dedicated to you, my love, and to Muhammad, the fruit of our love.

## TABLE OF CONTENTS

ABSTRACT .....	iii
ABSTRAK .....	v
ACKNOWLEDGMENTS .....	vii
TABLE OF CONTENTS .....	viii
LIST OF FIGURES .....	xiii
LIST OF TABLES .....	xvi
LIST OF SYMBOLS AND ABBREVIATIONS .....	xvii
LIST OF APPENDICES .....	xxi
<b>CHAPTER 1: INTRODUCTION.....</b>	<b>1</b>
1.1 Background .....	1
1.2 Problem Statement .....	4
1.3 Aim and Objectives of the Study .....	5
1.4 Scope of the Study .....	5
1.5 Thesis Outline .....	6
<b>CHAPTER 2: LITERATURE REVIEW.....</b>	<b>9</b>
2.1 Introduction .....	9
2.2 Advanced Oxidation Processes .....	9
2.3 Types of Advanced Oxidation Processes .....	11
2.3.1 Photocatalysis .....	12
2.3.2 Ozonation.....	14
2.3.3 Ultrasound irradiation .....	17
2.4 Fenton Oxidation.....	19
2.4.1 Fundamentals of Fenton Oxidation .....	20

2.5. Limitations of Fenton Oxidation .....	22
2.6 Fluidized Bed Technology .....	26
2.6.1 Classifications of Fluidized Bed Reactor .....	28
2.7 Applications of Fluidized Bed Reactor in Wastewater Treatment.....	30
2.8 Fluidized Bed Fenton Process .....	34
2.8.1 Mechanism of Fluidized Bed Fenton Process .....	34
2.9 Operational Parameters of Fluidized Bed Fenton .....	36
2.9.1 Fenton-based Parameters .....	37
2.9.1.1 pH.....	37
2.9.1.2 Hydrogen peroxide.....	39
2.9.1.3 Iron.....	40
2.9.2 Fluidized Bed-based Parameters.....	41
2.9.2.1 Shape and cross-sectional area of reactor .....	42
2.9.2.2 Aspect ratio of reactor .....	44
2.9.2.3 Reactor internals.....	45
2.9.2.4 Particle size and surface characteristics .....	47
2.9.2.5 Particle loading.....	49
2.9.2.6 Particle density .....	51
2.9.2.7 Superficial fluid velocity.....	52
2.10 Applications of Fluidized Bed Fenton in Wastewater Treatment.....	54
2.11 Summary of Literature Review .....	59
<b>CHAPTER 3: METHODOLOGY .....</b>	<b>62</b>
3.1 Introduction .....	62
3.2 Chemicals and Materials .....	62
3.3 Characterization of Carriers .....	63
3.3.1 Particle Size Distribution.....	63

3.3.2 Zeta Potential .....	63
3.3.3 Brunner-Emmet-Taylor Surface Analysis .....	63
3.3.4 Field Emission Scanning Electron Microscopy/Energy Dispersive X-ray...	65
3.3.5 Fourier Transform Infrared Spectroscopy .....	65
3.4 Experimental Setup .....	65
3.4.1 Fluidized-Bed Fenton Experiments .....	65
3.4.2 Conventional Fenton Experiments .....	66
3.5 Reactor Hydrodynamics.....	67
3.6 Experimental Design and Process Optimization.....	67
3.6.1 Selection of Design Domains.....	68
3.7 Analytical Methods .....	72
3.7.1 Inductively Couple Plasma .....	72
3.7.2 Chemical Oxygen Demand (COD).....	72
3.7.3 Color Removal.....	72
3.7.4 pH Measurement.....	73
3.8 Quantum Computational Method.....	73
3.8.1 Quantum Chemical Parameters .....	75
3.8.2 Thermodynamic Parameters .....	76
3.9 Safety Measures .....	77
<b>CHAPTER 4: PERFORMANCE OF FLUIDIZED BED FENTON PROCESS ....</b>	<b>79</b>
4.1. Degradation of Reactive Black 5 .....	79
4.2 Kinetic of COD Removal by Fluidized Bed Fenton .....	82
4.3 Comparison of Fluidized Bed Fenton and Conventional Fenton.....	85
4.4 Development of Response Surface Models .....	89
4.4.1 Fitness of the response surface models.....	91
4.4.2 Contribution of model terms to COD and color removals .....	92

4.4.3 Sensitivity of COD and color removal to changes in variables.....	95
4.5 Effects of Operational Parameters on COD Removal.....	97
4.5.1 Effect of Fenton’s reagent .....	97
4.5.2 Effect of pH .....	102
4.5.3 Effect of process time .....	103
4.6 Optimization of Fluidized Bed Fenton Process .....	105
4.7 Summary.....	107
<b>CHAPTER 5: EFFECT OF CARRIERS ON FLUIDIZED BED FENTON .....</b>	<b>108</b>
5.1 Quantum Chemical Calculations.....	108
5.1.1 Quantum Chemical Parameters .....	109
5.1.1.1 HOMO-LUMO Energies.....	111
5.1.1.2 HOMO-LUMO Energy gap .....	113
5.1.1.3 Global Hardness and Global Softness.....	114
5.1.1.4 Electrophilicity Index.....	115
5.1.2 Thermodynamic feasibility of interactions.....	116
5.2 Experimental Results of the Effect of Carrier.....	119
5.2.1 Adsorption of pollutant on the surface of carrier.....	119
5.2.2 Effect of carrier loading.....	122
5.2.3 Interaction of carrier with Fenton’s reagent .....	124
5.2.3.1 Fourier Transform Infrared Analysis .....	124
5.2.3.2 Morphology and Elemental Composition of SiO <sub>2</sub> .....	126
5.2.4 Iron removal in fluidized bed Fenton .....	128
5.3 Summary.....	129
<b>CHAPTER 6: PALM KERNEL SHELL ACTIVATED CARBON AS CARRIER.....</b>	<b>131</b>

6.1 Characteristics of Palm Kernel Shell Granular Activated Carbon.....	131
6.1.1 Particle size distribution .....	131
6.1.2 Textural analysis .....	132
6.1.3 Zeta potential .....	133
6.1.4 Morphology and elemental composition of palm kernel shell .....	134
6.1.5 Analysis of surface functional groups .....	137
6.2 Performance of Palm Kernel Shell Activated Carbon .....	138
6.2.1 Effect of pH on the performance of palm kernel Shell.....	139
6.2.2 Adsorption of pollutant by palm kernel shell .....	142
6.2.3 Effect of palm kernel shell loading.....	144
6.2.4 Comparison of palm kernel shell and SiO <sub>2</sub> .....	147
6.2.4.1 Comparison of performance for pollutant removal.....	147
6.2.4.2 Hydrodynamic Characteristics .....	149
6.3 Summary. ....	150
<b>CHAPTER 7: CONCLUSION AND RECOMMENDATIONS .....</b>	<b>151</b>
7.1 Conclusion .....	151
7.2 Recommendation for Future Work .....	153
7.3 Knowledge Contribution.....	154
7.4 Potential Real Applications of the Study .....	155
REFERENCES.....	156
LIST OF PUBLICATIONS AND PAPERS PRESENTED .....	175
APPENDICES .....	177

## LIST OF FIGURES

Figure 1.1: Details of fluidized bed Fenton process .....	3
Figure 2.1: Flowchart of Literature review .....	10
Figure 2.2: Common types of advanced oxidation processes .....	11
Figure 2.3: Basic mechanism of photocatalysis .....	14
Figure 2.4: Principles of acoustic cavitation .....	18
Figure 2.5: Advantages of homogeneous Fenton oxidation .....	19
Figure 2.6: Major limitations of Fenton oxidation.....	23
Figure 2.7: Fluidized bed reactor in wastewater treatment.....	27
Figure 2.8: Classification of fluidized bed reactor.....	29
Figure 2.9: Applications of fluidized bed reactor in wastewater treatment.....	31
Figure 2.10: Mechanism of fluidized bed Fenton process .....	35
Figure 2.11: Operational parameters of fluidized bed Fenton process .....	37
Figure 3.1: Flowchart of methodology .....	64
Figure 3.2: Schematic of the fluidized bed Fenton process .....	66
Figure 3.3 Central composite design flowchart .....	70
Figure 4.1: Steps in evaluating fluidized bed Fenton process.....	79
Figure 4.2: COD and color removals .....	80
Figure 4.3: Degradation of Reactive Black 5 .....	81
Figure 4.4: Kinetic orders for COD removal .....	84
Figure 4.6: COD removal by fluidized bed Fenton and conventional Fenton.....	86
Figure 4.7: Color removal by fluidized bed Fenton and conventional Fenton .....	87
Figure 4.8: Contributions of model terms to COD removal .....	93
Figure 4.9: Contributions of model terms to color removal.....	94
Figure 4.10: Perturbation plots for COD removal .....	95

Figure 4.11: Perturbation plot for color removal .....	96
Figure 4.12: Effect of Dye/Fe <sup>2+</sup> and H <sub>2</sub> O <sub>2</sub> /Fe <sup>2+</sup> on COD removal.....	99
Figure 4.13: Effect of Dye/Fe <sup>2+</sup> on color removal .....	100
Figure 4.14: Effects of pH and Dye/Fe <sup>2+</sup> on COD removal.....	102
Figure 4.15: Effects of Dye/Fe <sup>2+</sup> and Time on COD removal .....	104
Figure 5.1: Flow of discussion on the effect of SiO <sub>2</sub> .....	108
Figure 5.2: Optimized geometry of Reactive Black 5 dye.....	109
Figure 5.3: Optimized geometries of molecules .....	110
Figure 5.4: Energy level diagram of the studied molecules.....	111
Figure 5.5: Global hardness versus softness of the molecules.....	114
Figure 5.6: Electronegativity versus electrophilicity index .....	115
Figure 5.7: Contribution of different components to color removal.....	120
Figure 5.8: Effect of SiO <sub>2</sub> loading on COD removal .....	123
Figure 5.9: FTIR of SiO <sub>2</sub> (a) before and (b) after fluidized bed Fenton .....	125
Figure 5.10: FESEM of SiO <sub>2</sub> (a) before treatment (b) after treatment.....	126
Figure 5.11: Elemental mapping of SiO <sub>2</sub> (a) before and (b) after treatment.....	127
Figure 5.12: Iron removal by fluidized bed Fenton and conventional Fenton.....	128
Figure 6.1: Particle size distribution of palm kernel shell.....	132
Figure 6.2: N <sub>2</sub> adsorption/desorption isotherm of palm kernel shell .....	132
Figure 6.3: Point of zero charge of palm kernel shell .....	134
Figure 6.4: SEM of palm kernel before fluidized bed Fenton .....	135
Figure 6.5: SEM of palm kernel shell after fluidized bed Fenton.....	135
Figure 6.6: FTIR of palm kernel shell (a) before and (b) after fluidized bed Fenton ...	137
Figure 6.7: Effect of pH on COD removal.....	139
Figure 6.8: Effect of pH on color removal .....	141
Figure 6.9: Contribution of adsorption to COD removal.....	142

Figure 6.10: Contribution of adsorption to color removal .....	143
Figure 6.11: Effect of palm kernel shell loading on COD removal .....	145
Figure 6.12: Effect of palm kernel shell loading on color removal .....	146
Figure 6.13: COD removal by palm kernel shell and SiO <sub>2</sub> .....	148

University of Malaya

## LIST OF TABLES

Table 2.1: Limitations of Fenton oxidation and possible solutions .....	24
Table 2.2: Effects of pH on Fenton oxidation.....	38
Table 2.3: Applications of fluidized bed Fenton in wastewater treatment .....	55
Table 3.1 Chemicals and materials used.....	62
Table 3.2: Experimental ranges of the process variables.....	71
Table 3.3: Details of the chemical species for quantum analysis .....	74
Table 3.4: Safety measures .....	78
Table 4.1: Percentage COD and color removal.....	80
Table 4.2: Reaction order for COD removal.....	83
Table 4.3: Response surface models for COD and color removals .....	89
Table 4.4: Fitness of the response surface models.....	91
Table 4.5: Constrains for the optimization of color and COD removals .....	106
Table 4.6: Results of numerical optimization for COD and color removal.....	106
Table 5.1: Total and Gibb's free energies of the reactants and products.....	117
Table 5.2: Interaction energies of possible complexes .....	118
Table 5.3: COD removal by different processes.....	121
Table 5.4: Elemental composition of the carrier.....	127
Table 6.1: Textural properties of palm kernel shell.....	133
Table 6.2: Elemental composition of palm kernel shell.....	136

## LIST OF SYMBOLS AND ABBREVIATIONS

<b>List of Abbreviations</b>	<b>Unit</b>
ANOVA : Analysis of variance	[-]
AOPs : Advanced oxidation processes	[-]
AY36 : Acid yellow 36	[-]
B3LYP : Beck's 3-parameter Lee-Yang-Parr	[-]
BBD : Box-Behnken design	[-]
BET : Brunauer-Emmett-Teller	[-]
BPA : Bisphenol A	[-]
CCD : Central composite design	[-]
COD : Chemical oxygen demand	[mg/L]
DFT : Density functional theory	[-]
DMSO : Dimethyl sulfoxide	[-]
DOE : Design of experiment	[-]
DTFBR : Draft tube fluidized bed reactor	[-]
EA : Electron affinity	[eV]
EDC : Endocrine disrupting chemicals	[-]
EDX : Energy dispersive x-ray	[-]
EDTA : Ethylenediaminetetraacetic acid	[-]
FBBR : Fluidized bed bioreactor	[-]
FBF : Fluidized bed Fenton	[-]
FBR : Fluidized bed reactor	[-]
FC-CCD : Face-centered central composite design	[-]
FESEM : Field emission scanning electron microscope	[-]
FTIR : Fourier transform infrared	[-]
HF : Hartree Fock	[-]
HOMO : Highest occupied molecular orbital	[eV]
HPLC : High performance liquid chromatography	[-]
HRT : Hydraulic retention time	[s]
ICP : Inductively couple plasma	[-]
IFBBR : Inverse fluidized bed bioreactor	[-]

IFBR	: Inverse fluidized bed reactor	[-]
IP	: Ionic potential	[eV]
LPM	: Liter per minute	[-]
LUMO	: Lowest unoccupied molecular orbital	[eV]
MEA	: Monoethanolamine	[-]
MFC	: Microbial fuel cell	[-]
PKSGA	: Palm kernel shell granular activated carbon	[-]
PPCPs	: Pharmaceutical and personal care products	[-]
RB2	: Reactive blue 2	[-]
RB5	: Reactive black 5	[-]
RO16	: Reactive orange 16	[-]
RSM	: Response surface methodology	[-]
TFT-LCD	: Thin film transistor liquid crystal display	[-]
UV	: Ultraviolet	[-]
WWTP	: Wastewater treatment plant	[-]
XPS	: X-ray photoelectron spectroscopy	[-]
<b>Formulas</b>		
$Al_2O_3$	: Aluminium oxide	[-]
$CO_2$	: Carbon dioxide	[-]
$Fe^{2+}$	: Iron (II) ions	[-]
$Fe^{3+}$	: Iron (III) ions	[-]
$Fe_3O_4$	: Magnetite	[-]
$\alpha-Fe_2O_3$	: Hematite	[-]
$\gamma-Fe_2O_3$	: Maghemite	[-]
$FeOOH$	: Iron hydroxide	[-]
$\alpha-FeOOH$	: Goethite	[-]
$FeSO_4 \cdot 7H_2O$	: Iron sulphate heptahydrate	[-]
$H_2O$	: Water	
$H_2O_2$	: Hydrogen peroxide	[-]
HCl	: Hydrochloric acid	[-]
$H_2SO_4$	: Sulphuric acid	[-]
NaOH	: Sodium hydroxide	[-]

$\text{OH}^\bullet$	: Hydroxyl radical	[-]
$\text{O}_2^{\cdot-}$	: Superoxide radical	[-]
$\text{SiO}_2$	: Silica	[-]
$\text{ZnO}$	: Zinc oxide	[-]

#### Notations/symbols

D	: Reactor diameter	[m]
H	: Height of reactor	[m]
$P_L$	: Solid particle loading	[g/L]
Q	: Liquid flow rate	[m <sup>3</sup> /s]
$Q_a$	: Air flow rate	[m <sup>3</sup> /s]
T	: Temperature	[°C]
$U_{mf}$	: Minimum superficial velocity	[m/s]
$U_L$	: Superficial Liquid velocity	[m/s]
$U_g$	: Superficial gas velocity	[m/s]
V	: Volume	[m <sup>3</sup> ]
S	: Entropy	[-]
P	: Pressure	[N/m <sup>2</sup> ]
T	: Temperature	[°C]
$\eta$	: Global hardness	[eV]
$\sigma$	: Global softness	[eV]
$\chi$	: Electronegativity	[eV]
$\mu$	: Chemical potential	[eV]
$\omega$	: Electrophilicity index	[eV]
$G^\circ$	: Gibb's free energy	[kcal/mol]
$H^\circ$	: Enthalpy	[kcal/mol]
$h$	: Planck's constant	[J.s]
$\nu$	: Frequency of light	[s <sup>-1</sup> ]
$a_s$	: Specific surface area	[m <sup>-1</sup> ]
$\varepsilon$	: Expanded bed porosity	[-]
d	: Support particle diameter	[m]

$\psi$	: Form factor	[-]
$dp$	: Pressure drop	[N/m <sup>2</sup> ]
$dz$	: Bed height	[m]
$\varepsilon_s$	: Solid phase holdup	[-]
$\varepsilon_L$	: Liquid phase holdup	[-]
$\varepsilon_g$	: Gas phase holdup	[-]
$\rho_s$	: Solid density	[kg/m <sup>3</sup> ]
$\rho_l$	: Liquid density	[kg/m <sup>3</sup> ]
$\rho_g$	: Gas density	[kg/m <sup>3</sup> ]
$\mu$	: Dynamic viscosity of water	[g/m/h]
$g$	: Acceleration of gravity	[m/h <sup>2</sup> ]
$Y$	: Response/dependent variable	[-]
$\beta$	: Model term	[-]
$k$	: Number of variables	[-]
$\varepsilon$	: Model's error term	[-]
$b_i$	: Regression coefficient	[-]
$C_0$	: Initial COD	[mg/L]
$C_t$	: Final COD	[mg/L]
$k_1$	: First-order rate constant	[s <sup>-1</sup> ]
$k_2$	: Second-order rate constant	[L.mg <sup>-1</sup> s <sup>-1</sup> ]
$k'_2$	: Pseudo-second-order rate constant	[L mg <sup>-1</sup> ]

## LIST OF APPENDICES

APPENDIX A: Literature on application of fluidized bed Fenton process .....	177
APPENDIX B: Response surface model data.....	180

University of Malaya

## CHAPTER 1: INTRODUCTION

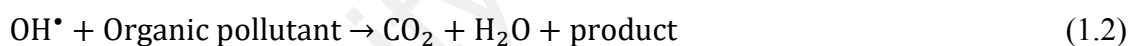
### 1.1 Background

The rapid industrialization in different parts of the world is exerting intense pressure on the environment. Industrial processes generate large quantities of wastewater containing various pollutants, which may end up in the environment. These pollutants include recalcitrant organic compounds such as synthetic dyes, pesticides, pharmaceuticals and personal care products (PPCP). Although wastewater treatment plants (WWTP) have been well established, various studies have confirmed the presence of recalcitrant pollutants in the effluents of conventional WWTP (Casas & Bester, 2015; Luo et al., 2014; Mailler et al., 2016). Thus, conventional wastewater treatment processes do not effectively remove recalcitrant pollutants.

Recalcitrant pollutants can pose serious threat to public health and the environment, besides limiting potential reuse of the wastewater. For example, chronic toxicity and endocrine disruption have been linked with the presence of PPCP in the environment (Perdigo et al., 2010). Due to the limitation of conventional wastewater treatment technologies in removing recalcitrant pollutants, efforts have been intensified to find alternative technologies that could effectively remove these pollutants from the environment (Ahmadi, Ramavandi, & Sahebi, 2015; Alalm, Tawfik, & Ookawara, 2015a). Although some physico-chemical treatments can remove recalcitrant pollutants from wastewater, they usually transfer the pollutants to another medium where further treatment may still be required (Ahmadi et al., 2015). Biodegradation is a slow process and mostly convert the organic pollutants to some intermediates, which can still accumulate in the environment (Bilinska, Gmurek, & Ledakowicz, 2016). Therefore, technologies that can effectively eliminate recalcitrant pollutants are needed.

Advanced oxidation processes (AOPs) have received a significant interest as effective technologies for the removal of recalcitrant pollutants. AOPs are characterized by the generation of a reactive hydroxyl radical through different processes as discussed by Glaze, Kang, & Chapin, (1987). The hydroxyl radical (OH•) is a powerful and non-selective oxidant (oxidation potential = 2.8 eV) that can degrade organic pollutants. The most common AOPs are Fenton oxidation, photocatalysis, ultrasound cavitation, ozonation and electrochemical oxidation.

Fenton oxidation is among the most effective AOPs due to the rapid production of OH• in acidic medium (Asghar, Raman, & Daud, 2015). It involves a homogeneous reaction between ferrous iron (Fe<sup>2+</sup>) and hydrogen peroxide (H<sub>2</sub>O<sub>2</sub>) to produce OH• as shown in Equation 1.1. The generated OH• further oxidizes organic pollutant as shown in Equation 1.2 (Alalm et al., 2015a).



Despite its effectiveness, some drawbacks have hindered the practical applications of Fenton oxidation. One of these is the production of excessive iron sludge, which poses difficulty in disposal and can result in a secondary pollution (Neyens & Baeyens, 2003). Other limitations include narrow range of operational pH and high chemical consumption (Guo, Yuan, Zhang, & Yu, 2017). Thus, addressing these limitations represents an on-going research effort in the field of Fenton oxidation for wastewater treatment.

One of the approaches that can be used in addressing these limitations is the application of fluidized bed reactor (FBR) in Fenton oxidation, termed fluidized bed Fenton (FBF). FBR possess excellent features that can be exploited to enhance mass transfer rate and reduce sludge generation in Fenton oxidation (Andalib et al., 2014). The fluidized carriers

promote iron nucleation and crystal growth on the surface of the solids, inducing the crystallization of iron oxide (Garcia-Segura, Bellotindos, Huang, Brillas, & Lu, 2016). The crystallization of iron oxides reduces sludge generation and further introduces a heterogeneous Fenton reaction into the system. Besides these, the excellent mixing provided by fluidization can enhance process performance.

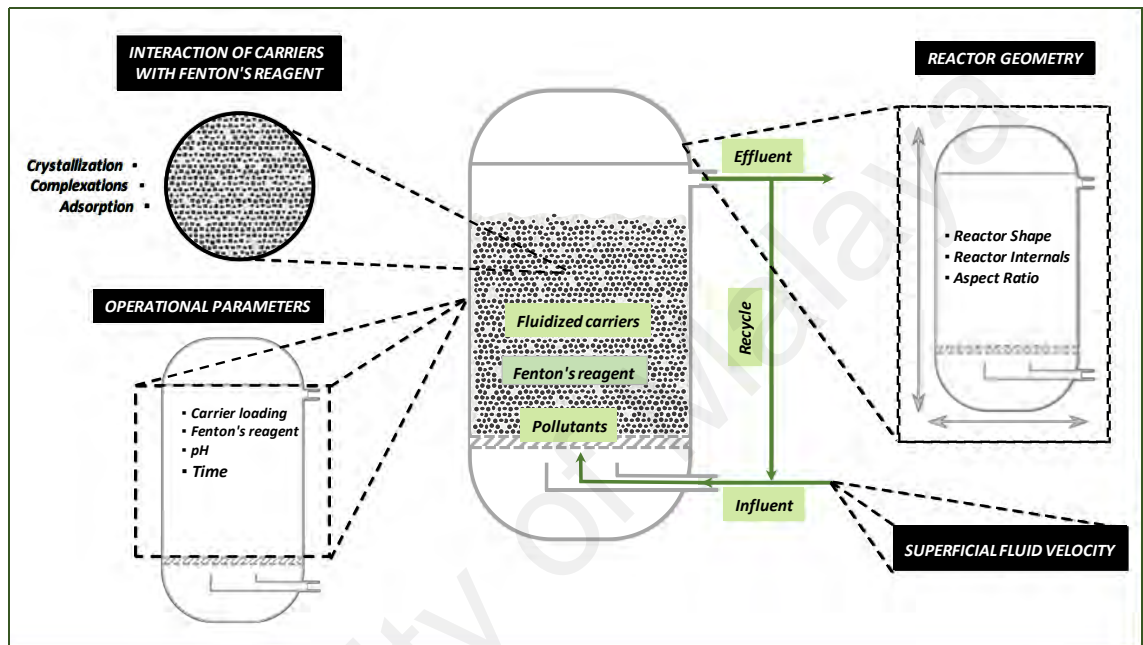


**Figure 1.1: Details of fluidized bed Fenton process**

Figure 1.1 shows the different parameters involved in FBF process, which comprise those related to the Fenton oxidation, fluidized carriers and reactor hydrodynamics. The presence of solid carriers increases the complexity of the process, posing challenges to process optimization and control. The carrier may also interact with Fenton's reagent and the organic pollutants. Thus, understanding the nature of these interactions is an important consideration for successful application of FBF process. However, previous studies have not given much attention to these important aspects. It is noteworthy that proper process description and optimization can only be effectively done when the effect of the carrier and its interactions with Fenton's reagent are understood. However, due to the heterogeneity of the FBF process, experimental investigation alone cannot easily describe the complex interactions in the process. In this regard, computational modeling

techniques, such as quantum chemical simulation, can assist in studying the interactions in the FBF process. The combination of theoretical and experimental approaches can therefore provide an effective method for studying these complex interactions, with the aim of enhancing the performance of the FBF process.

## **1.2 Problem Statement**

The introduction of fluidized solid carriers into Fenton oxidation brings complexity into an otherwise simple process. This brings additional parameters that must be optimized for effective process performance. In addition, the solid carriers can interact with the Fenton's reagent, which may lead to either synergistic or antagonistic effects on the pollutant removal. Consequently, the effect of solid carrier and its interaction with Fenton's reagent are important considerations for process optimization. However, previous studies have largely focused on evaluating the performance of the process, leaving these important aspects largely unreported.

Considering the importance of the solid carrier, it is necessary to understand its effect and interaction with Fenton's reagent and organic pollutants. However, due to the inherent complexity of the FBF process, process description through experimental approach alone can be daunting. Thus, appropriate computational modeling techniques can assist in this regard. Approaches such as quantum chemical calculations and response surface methodology can provide platforms that can be used to study and optimize the complex interactions involved in FBF process. Therefore, this study adopts both theoretical and experimental approaches to investigate the effect of fluidized carriers on the performance of FBF process, with the aim of enhancing the performance of the process. In addition, the study also investigates the feasibility of using an alternative low-cost carrier with the view of enhancing the performance of the FBF process.

Specifically, the study attempts to answer these questions:

1. Can response surface methodology technique be used to investigate the effect of operational parameters towards enhancing the performance of FBF process?
2. Can quantum chemical calculations and experimental investigation be used to investigate the complex interaction among the fluidized solid carriers, Fenton's reagent and organic pollutant?
3. Can the performance of the FBF process be enhanced through the use of an alternative low-cost carrier?

### **1.3 Aim and Objectives of the Study**

The aim of this study is to enhance the performance of FBF process through clarifying the effect of fluidized carrier and its interactions with Fenton's reagent and organic pollutant. The specific objectives are:

1. To evaluate the performance of FBF process in degrading recalcitrant organic pollutant and investigate the effect of operational parameters on the performance.
2. To investigate the effect of fluidized carrier in FBF process and its interaction with Fenton's reagent and organic pollutant through theoretical and experimental approaches.
3. To investigate the potential of palm kernel shell granular activated carbon (PKSGAC) as an alternative carrier in FBF process.

### **1.4 Scope of the Study**

This study is limited to the application of a laboratory scale FBF process for the degradation of recalcitrant pollutants. The major focus of the study is the effect of fluidized carrier on the process performance and its interaction with Fenton' reagent and organic pollutants. Consequently, the study does not cover the effect of hydrodynamics

on the process performance. However, preliminary studies were conducted to establish the minimum fluidization velocity and understand the fluidization patterns in the system. Since the focus of study is the effect of solid carriers and its interaction with Fenton's reaction, a model organic pollutant was used instead of a real wastewater. The use of synthetic wastewater will allow a more proper evaluation since the reaction matrix is known. In order to study the effect of the fluidized carrier, the most commonly used carrier, SiO<sub>2</sub>, was used in this study. Thus, the detailed study on the effect of carrier and interaction with other parameters was conducted considering only SiO<sub>2</sub> as a representative carrier. A second carrier, PKSGAC, was evaluated as a possible alternative to the SiO<sub>2</sub>. Thus, these two carriers were considered in the study. For the quantum chemical calculations, all optimizations were restricted to Beck's 3-parameter Lee-Yang-Parr (B3LYP) level of study using 6-311++G (d,p) as a basis set.

## **1.5 Thesis Outline**

This section explains the arrangement of the thesis, which comprises seven chapters as follows:

### **Chapter 1: Introduction**

This chapter introduces the whole study by giving a brief background information, highlighting the problem statement and outlining the objectives of the study. The chapter also provides the justification and scope of the study.

### **Chapter 2: Literature Review**

This chapter presents the literature review, which critically analyzed relevant previous studies, identifying the existing gaps and placing the current study in context. The chapter discusses the development of AOPs, with emphasis on Fenton oxidation. It then discussed the fundamentals and limitations of Fenton oxidation. The development of FBF process

as alternative solution to the limitations of Fenton oxidation is then highlighted. The last part of the chapter summarized the major findings of the literature review, highlighting the research gaps that are to be addressed by the current study.

### **Chapter 3: Methodology**

This chapter presents the overall materials and methods that are necessary to achieve the objectives of the study. The chemicals/materials utilized are first presented, followed by the experimental set-ups for both FBF process and conventional Fenton oxidation. The procedure for response surface methodology and steps for performing quantum chemical simulations and calculations are then presented.

### **Chapter 4: Performance of Fluidized Bed Fenton Process**

This chapter deals with the performance of FBF process. It discussed the degradation of a model pollutant, RB5, by the FBF process and the effects of operational parameters on the process performance. It also discussed the development of response surface methodology model for predicting the dye degradation, comparison of FBF process and conventional Fenton oxidation as well as the process optimization.

### **Chapter 5: Effect of carriers in fluidized bed Fenton process**

This chapter deals with the effect of fluidized carrier and its interaction with Fenton's reagent and organic pollutant. It presents the results of quantum chemical simulation and experimental investigations of the interactions of SiO<sub>2</sub>, Fenton's reagent and RB5. In the first part, the results of quantum chemical parameters and thermodynamic analysis were presented. In the second part details, the experimental results and spectroscopic analysis were presented.

## **Chapter 6: Palm Kernel Shell as a Carrier in Fluidized Bed Fenton Process**

This chapter presents feasibility study on the use of palm kernel shell granular activated carbon as alternative carrier in FBF process. It discussed the characteristics of the proposed carrier and its performance in the FBF process. The chapter also discusses the comparison of palm kernel shell activated carbon and SiO<sub>2</sub> as carriers.

## **Chapter 7: Conclusion and Recommendations**

This chapter concludes the thesis by highlighting the major conclusions, their implications and recommendations for future work.

University of Malaya

## CHAPTER 2: LITERATURE REVIEW

### 2.1 Introduction

This chapter presents a critical review of relevant literatures that are necessary to achieve the objectives of this work. Figure 2.1 depicts the outline of the literature review presented in this chapter. It includes discussions on the fundamentals and types of AOPs, Fenton oxidation and its limitations in the treatment of recalcitrant wastewater, development of fluidized bed Fenton process as a solution to the limitations of conventional Fenton oxidation, as well as examples of the applications of fluidized bed Fenton process to remove recalcitrant pollutants. Since the basis of fluidized bed Fenton process stems from fluidization technology, the basics of fluidized bed technology are also covered. At the end of the chapter, a summary of the literature review is presented, highlighting the identified research gaps that formed the basis of this study.

### 2.2 Advanced Oxidation Processes

AOPs is a term used generally to refer to processes that are characterized by the generation of hydroxyl radicals ( $\text{OH}^\bullet$ ) capable of degrading organic pollutants. The  $\text{OH}^\bullet$  is a very reactive radical with a redox potential of 2.8 eV that can react with organic pollutant in the order of  $10^9 \text{ M}^{-1} \text{ S}^{-1}$ , converting them to some intermediates, carbon dioxide and water (Neyens & Baeyens, 2003). Traditionally, the discussion on AOPs was limited to processes involving ozone, hydrogen peroxide and ultraviolet radiation as put forward by Glaze and co-workers (Glaze et al., 1987). Although their discussion was mainly on ozone, hydrogen peroxide and ultraviolet radiation, the field of AOPs has grown widely since then. Nowadays, the term is used broadly, involving many processes such as Fenton oxidation, photocatalysis, ozonation, ultraviolet radiation (UV), sonolysis, electrochemical oxidation and supercritical water oxidation. Figure 2.2 shows the

common AOPs used for wastewater treatment. AOPs have proven effective in the treatment of recalcitrant organic pollutants. Unlike conventional treatments, which either separate the pollutants from the wastewater or convert them to some intermediate compounds, AOPs are capable of mineralizing organic pollutants (Ahmadi et al., 2015).

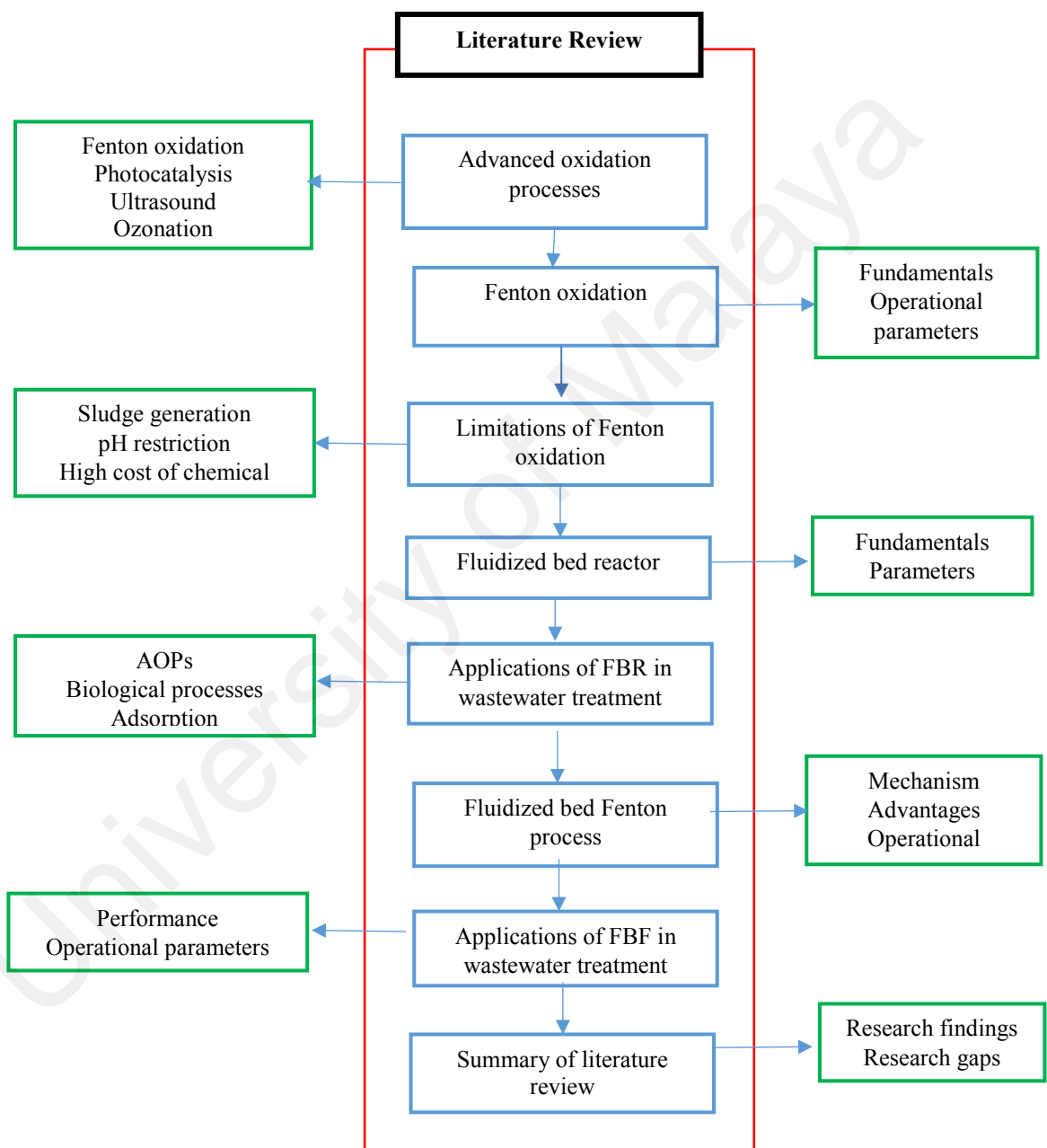


**Figure 2.1: Flowchart of Literature review**

A significant progress has been recorded in the field of AOPs, which are largely fueled by the advances in material engineering and the concerted efforts of researchers working

in the field. Dewil et al. (2017) have recently offered some new perspectives on AOPs, discussing, among others, integrating AOPs with other treatment technologies, solar-driven AOPs and the emerging electrochemical oxidation.

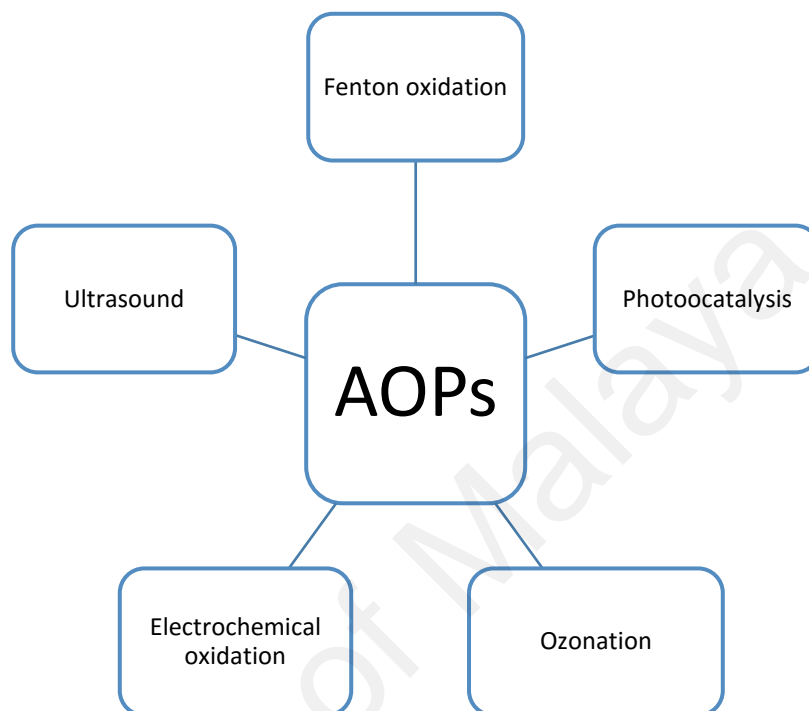


**Figure 2.2: Common types of advanced oxidation processes**

The effectiveness of AOPs has led to their wide investigations by researchers working on developing treatment technologies for recalcitrant wastewaters. Due to the high oxidation power of  $\text{OH}^\bullet$ , organic pollutants are rapidly and effectively degraded. However, complete mineralization is not always economically feasible because of the high energy and chemical requirements of some of the AOPs. Although some of the AOPs such as Fenton and ozonation have been applied at industrial scales, many of the emerging AOPs are still under laboratory investigations.

### **2.3 Types of Advanced Oxidation Processes**

Several approaches can be used in classifying AOPs. While the common approach is to classify AOPs based on the process used to generate  $\text{OH}^\bullet$  (Figure 2.2), other

classifications can be based on whether the process is homogeneous or heterogeneous, and whether a source of energy is required or not. However, classifying AOPs based on the process used in generating the oxidant seems more practical. Discussion on other classification methods has been presented earlier by Poyatos et al. (2010).

In the context of OH<sup>•</sup> generating methods, the most common types of AOPs are Fenton oxidation, photocatalysis, ozonation and sonolysis. Recently, however, electrochemical oxidation is receiving a significant attention as another effective AOP. Fenton oxidation consists of a reaction between Fe<sup>2+</sup> and H<sub>2</sub>O<sub>2</sub> to produce OH<sup>•</sup> (Alalm et al., 2015a). Photocatalysis uses semiconductor metal oxides, such as TiO<sub>2</sub>, in the presence of irradiation (UV or Visible) to produce OH<sup>•</sup> (Dong, Zhang, He, Dong, & Wang, 2014). Ozonation involves the use of ozone, a powerful oxidant with a high thermodynamic oxidation potential (Aparicio, Eiroa, Kennes, & Veiga, 2007). Although photolysis using UV can generate OH<sup>•</sup>, it is not very effective and is usually combine with other AOPs (Lin, Zhang, & Yuan, 2014). Previous studies have shown that combining two or more AOPs is more effective than individual process due to the synergistic higher generation of OH<sup>•</sup>, lower catalyst consumption and a possible reduction in process time (Miralles-Cuevas et al., 2014).

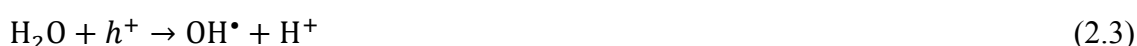
The commonly used AOPs are briefly discussed in the following subsections. However, due to the central position of Fenton oxidation in this work, it is discussed separately in section 2.4.

### **2.3.1 Photocatalysis**

Photocatalysis is a form of AOPs where semiconductor catalysts (such as TiO<sub>2</sub>, ZnO, etc.) and a source of light (Ultraviolet or Visible) are utilized to generate the oxidizing agent. Generally, photocatalysis is based on the ability of the photocatalyst to simultaneously

adsorb reactants and absorb photons efficiently (Herrmann, 2010). As a wastewater treatment process, photocatalysis offers many advantages such as complete mineralization of pollutants, operating under ambient condition and low operational cost. The fundamentals and mechanism of photocatalysis have been well documented (Bora & Mewada, 2017; Herrmann, 2010; Meng, Jin, Chow, & Saint, 2010; Mohamed & Bahnemann, 2012).

The basic principle of photocatalysis involves illuminating the surface of a semiconductor with photon energy ( $h\nu$ ) equal to or greater than the bandgap energy of the material. This excites an electron from the valence band to the conducting band, leaving behind an empty band that will lead to the creation of an electron-hole pair ( $e^- - h^+$ ). Considering  $\text{TiO}_2$  as the photocatalyst, Equation 2.1 to Equation 2.6 show the typical reactions while Figure 2.3 shows the basic mechanism of photocatalysis. The degradation of pollutants occurs by the  $\text{OH}^\bullet$  (Equation 2.5) and superoxide radical anions ( $\text{O}_2^{\bullet-}$ ) (Equation 2.6). One of the major challenges in photocatalysis is the prevention of the reaction (recombination) that occurs in Equation 2.2. Recombination of the generated charge carriers reduces the overall quantum efficiency and prevent the oxidation of target pollutants (Choi, Termin, & Hoffmann, 1994).



( $\rightarrow \rightarrow \rightarrow$ : indicates intermediates that depend on the type of pollutant)

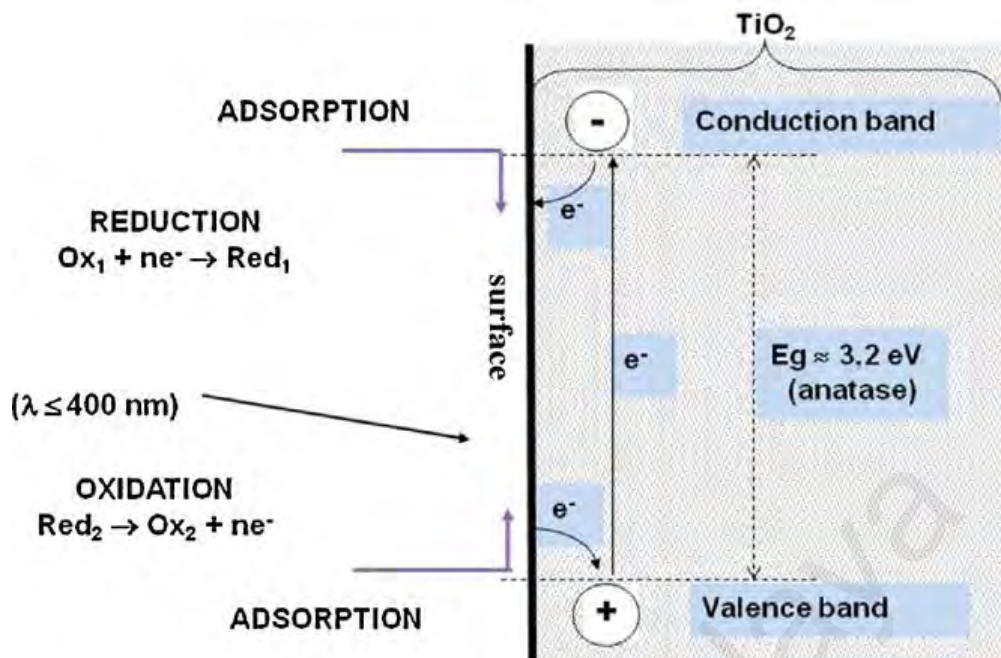


**Figure 2.3: Basic mechanism of photocatalysis (Herrmann, 2010)**

The reviewed literature showed that photocatalysis is an effective method to remove recalcitrant pollutants from the environment. While TiO<sub>2</sub> has been the mostly commonly used photocatalyst, there is growing interest in the development of other materials with photocatalytic abilities. In particular, development of photocatalysts that can be used to remove pollutants under visible irradiation is vigorously pursued. The availability of such materials will extend the application of photocatalyst under natural solar irradiation, enhancing the cost-effectiveness of the technology.

### 2.3.2 Ozonation

Ozone (O<sub>3</sub>) is one of the strongest chemical oxidants, having a very high thermodynamic oxidation potential (2.07eV). Ozonation is a well-established oxidation process for wastewater treatment that can effectively oxidize recalcitrant organic pollutants. Although ozone is a powerful oxidant, its oxidation reactions are rather selective and may be considered slow for wastewater treatment applications (Glaze et al., 1987). However, the use of catalysts (catalytic ozonation) and integrating ozonation with other AOPs have been pursued as possible ways to improve its effectiveness. Some of the strategies being

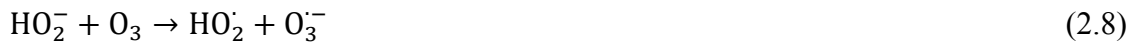
adopted to enhance the performance of ozonation have been presented recently (Gomes, Costa, Quinta-ferreira, & Martins, 2017).

The mechanism of ozonation has been discussed by previous researchers (Glaze et al., 1987; Gomes et al., 2017; Umar, Roddick, Fan, & Abdul, 2013). In a classical ozonation, organic pollutants are oxidized through direct reaction with molecular ozone and/or indirect reaction with  $\text{OH}^\bullet$  that is generated from the decomposition of ozone (Broséus et al., 2009). While oxidation by direct molecular ozone may be limited to the degradation of multiple bonds and aromatic compounds, degradation by the  $\text{OH}^\bullet$  is very fast and nonselective (Broséus et al., 2009; Glaze et al., 1987).

The pH condition and wastewater matrix determine whether direct or indirect oxidation will dominate. Direct oxidation dominates under acidic conditions or in the presence of radical scavengers that can hinder the chain reaction necessary to decompose ozone (Umar et al., 2013). On the other hand, indirect oxidation dominates under basic conditions or in the presence of compounds that promote radical-type chain reactions and  $\text{OH}^\bullet$  formation (Irmak, Erbatur, & Akgerman, 2005; Staehelin & Hoigne, 1985). However, in real wastewaters, radical scavengers (e.g. carbonate) are always present and therefore, oxidation by molecular ozone may be the dominant mechanism (Nakada et al., 2007; Umar et al., 2013).

Equation 2.7 to Equation 2.14 show the chain reactions that occur in the decomposition of ozone in an aqueous medium. The reactions occur in three stages of initiation, propagation and termination as outlined below (Irmak et al., 2005; Umar et al., 2013).

Initiation stage involves the decomposition of ozone by  $\text{OH}^-$ , resulting in the formation of hydroperoxide ion ( $\text{HO}_2^-$ ) as shown in Equation 2.7. The  $\text{HO}_2^-$  further reacts with ozone to form  $\text{H}_2$  and  $\text{O}_3^-$  as described in Equation 2.8.



In the propagation stage, ozone further decomposes into ozonide ion ( $\text{O}_3^-$ ) by reacting with  $\text{O}_2^-$  as shown in Equation 2.9. The ozonide ion then reacts with  $\text{H}^+$  to form  $\text{HO}_3\cdot$  as shown in Equation 2.10, which is further converted to  $\text{OH}\cdot$  through the reaction shown in Equation 2.11 and Equation 2.12. Further reactions may occur, producing  $\text{HO}_4\cdot$  and  $\text{HO}_2\cdot$  as shown in Equation 2.13 and Equation 2.14 respectively.



Termination stage may involve the recombination of  $\text{OH}\cdot$ ,  $\text{HO}_2\cdot$  and  $\text{O}_2$ .

The reviewed literature showed that despite the high cost of ozonation, it is one of the most widely established AOPs for water treatment. In ozonation, degradation of pollutant can occur either through direct oxidation by ozone or indirectly by generating hydroxyl radicals. The pH of the solution determines which of the two routes dominates. However, since degradation through hydroxyl radicals is more effective, most of the studies have reported the use of catalytic ozonation to favor the indirect oxidation. This represents the research trend in the application of ozonation for recalcitrant wastewater treatment.

### 2.3.3 Ultrasound irradiation

Ultrasound is a form of AOPs where ultrasound irradiation is used to induce an acoustic cavitation capable of generating OH<sup>•</sup>. Although the generation of OH<sup>•</sup> is emphasized, the cavitation also results in the generation of local hot spots that can induce pyrolytic degradation of the pollutants. Thus, pollutants removal in ultrasound consists of the degradation by OH<sup>•</sup> and the pyrolytic destruction by the generated heat (Chowdhury & Viraraghavan, 2009). In the literature, different names are used to denote the use of ultrasound irradiation for wastewater treatment, such as sonolysis, sonication, and sonochemistry. However, the basic process remains the same.

Cavitation is induced in a liquid whenever the intensity of the applied ultrasound exceeds the cavitation thresholds of the liquid. This results in the formation, growth and collapse of bubbles in the liquid as depicted in Figure 2.4. By these growth and collapse cycles, negative and positive pressures are exerted on the liquid respectively by the sound waves (Chowdhury & Viraraghavan, 2009). When the negative pressure reaches a certain threshold level, the average distance between the liquid molecules would exceed the critical molecular distance required to keep the liquid together (Chowdhury & Viraraghavan, 2009; Mason & Lorimer, 1988; Suslick, 1989). At this point, the liquid would break down, forming cavitation bubbles under high temperatures (up to 5000 K) and pressures (up to 1000 atm) (Suslick, 1990). These bubbles consist of compressed gas and vapor, which generate localized hot spots capable of pyrolyzing water molecules into hydroxyl and hydrogen radicals as shown in Equation 2.15 (Wang & Xu, 2012). Details on the principles and theories of sonochemistry have been discussed in the literature (Adewuyi, 2005; Adewuyi, 2001; Gogate, 2008; Mason & Lorimer, 1988; Suslick, 1990; Wang & Xu, 2012).



The  $\text{OH}^\bullet$  then react with the target organic pollutant, oxidizing them as shown in Equation 2.16. A side reaction may also occur, where  $\text{OH}^\bullet$  recombines to form  $\text{H}_2\text{O}_2$  according to Equation 2.17.

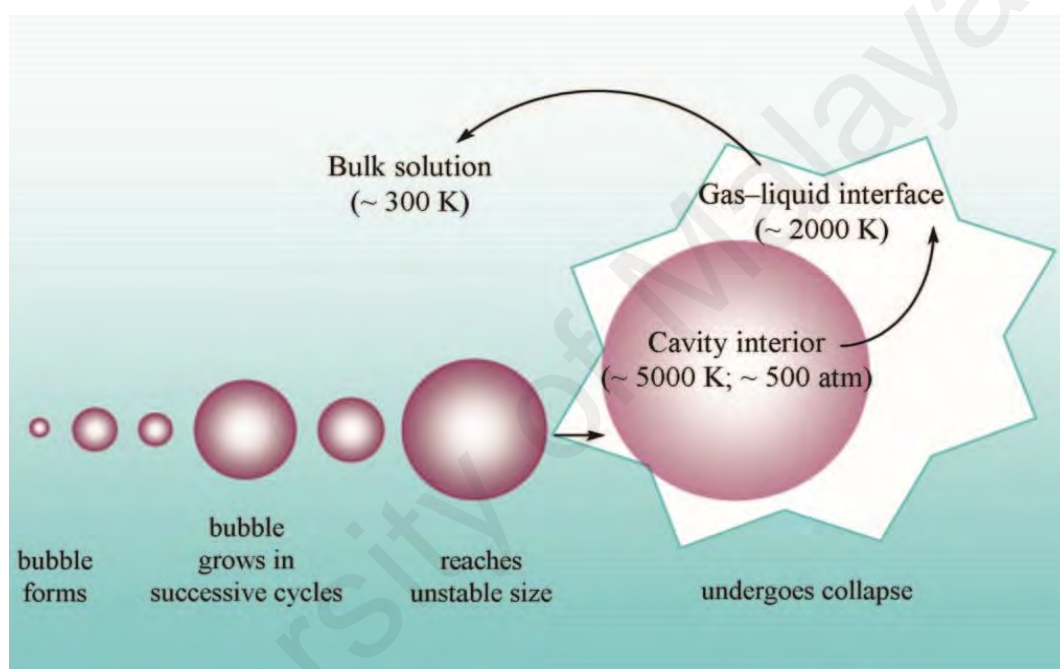
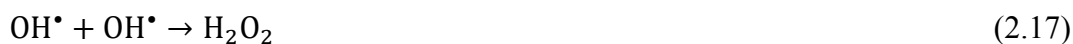


**Figure 2.4: Principles of acoustic cavitation (Wang and Xu, 2012)**

The reviewed literature shows that the application of ultrasound cavitation as an advanced oxidation process is relatively new, and studies on its applications are limited compared to other AOPs. Nevertheless, there is a growing interest in its application since it can achieve pollutant degradation through both hydroxyl radical oxidation and pyrolytic effect. In addition, the process can be easily integrated with other wastewater treatment technology, making it versatile.

## 2.4 Fenton Oxidation

Fenton oxidation is one of the most effective AOPs for the treatment of recalcitrant organic pollutants. The process is based on the use of Fenton's reagent ( $\text{Fe}^{2+}$  and  $\text{H}_2\text{O}_2$ ) to generate  $\text{OH}^\bullet$ . Although Fenton's reagent was proposed as an analytical reagent since 1894, its application as an oxidant for the destruction of organic contaminants was only explored some 60 years later (Huang, Dong, & Tang, 1993). Since then, a lot of development has been recorded in the application of Fenton oxidation for wastewater treatment. The major advantages of Fenton oxidation for wastewater treatment were highlighted by Huang et al. (1993) and depicted in Figure 2.5. These include: (1) no toxic organic byproducts are formed during the oxidation processes (2) Fenton's reagent are nontoxic and readily available; (3) there is no mass transfer limitation due to its homogeneous catalytic nature; (4) the process is simple and does not require any special equipment. Despite these advantages, Fenton oxidation has some drawbacks such as requirement of acidic working environment (pH around 3) and excessive sludge generation, which limit its application.

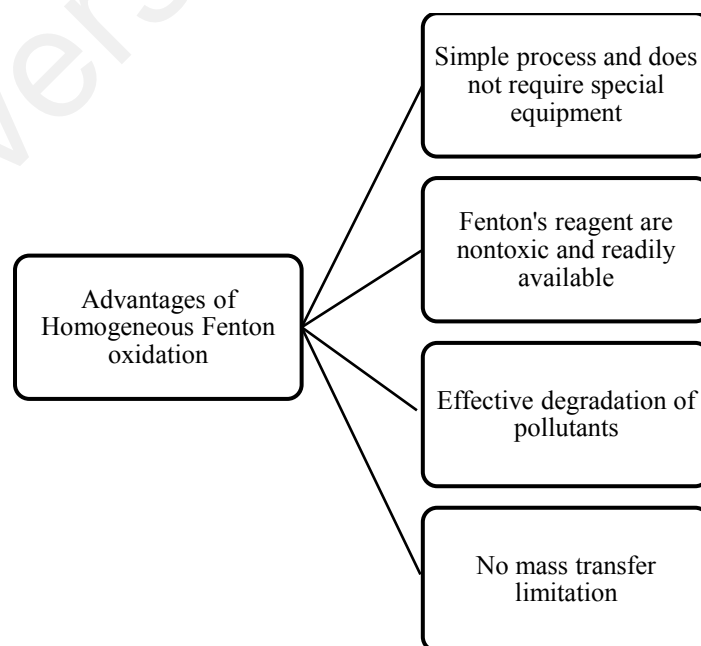


**Figure 2.5: Advantages of homogeneous Fenton oxidation**

The earliest studies on Fenton oxidation focused largely on the treatment efficiency and the influence of operating parameters. Subsequent studies were mainly on the process intensification by combining homogeneous Fenton oxidation with other treatment processes such as ultraviolet irradiation, ultrasonic, adsorption and biological treatment. Recently, studies have been focusing on addressing some of the limitations of classical Fenton via the development of heterogeneous Fenton and other alternatives such as FBF process.

#### 2.4.1 Fundamentals of Fenton Oxidation

In a classical Fenton oxidation,  $\text{Fe}^{2+}$  reacts with  $\text{H}_2\text{O}_2$  to generate  $\text{OH}^\bullet$  according to Equation 2.18 to Equation 2.20 (Alalm et al., 2015a). The generated  $\text{OH}^\bullet$  then react with organic pollutants, converting them to  $\text{CO}_2$  and  $\text{H}_2\text{O}$  (Neyens & Baeyens, 2003). The first stage of the process is a fast decomposition of  $\text{H}_2\text{O}_2$  by the  $\text{Fe}^{2+}$ , which generates substantial amount of  $\text{OH}^\bullet$ . In the second stage,  $\text{Fe}^{3+}$  reacts slowly with  $\text{H}_2\text{O}_2$ , producing less  $\text{OH}^\bullet$ . Although Fenton oxidation is described in these simple steps, the process is much more complex, involving many other reactions. Generally, these processes can be broadly grouped into initiation, propagation and termination reactions (Munoz, de Pedro, Casas, & Rodriguez, 2015).



Conventional Fenton oxidation utilizes  $\text{Fe}^{2+}/\text{Fe}^{3+}$  as homogeneous catalysts to enhance the decomposition of  $\text{H}_2\text{O}_2$ . Since there is negligible mass transfer in homogeneous Fenton oxidation, the readily available  $\text{Fe}^{2+}$  reacts very fast with the  $\text{H}_2\text{O}_2$  to produce  $\text{OH}^\bullet$  (Buthiyappan et al., 2016). Once produced,  $\text{OH}^\bullet$  reacts with organic compounds through

either of the three mechanisms of hydroxyl addition, hydrogen abstraction or electron transfer (Huang et al., 1993). Hydroxyl addition occurs with organic compounds having aromatic system or carbon-carbon multiple bonds as shown in Equation 2.21. Hydrogen abstraction occurs with unsaturated organic compounds as described in Equation 2.22 whereas electron transfer occurs when  $\text{OH}^\bullet$  interacts with inorganic ions such as the reaction described by Equation 2.23.



Fenton oxidation has been widely used for the removal of various recalcitrant pollutants such as dyes (Dias, Oliveira, Arcanjo, Moura, & Pacheco, 2016; Ribeiro, Starling, Leão, & de Amorim, 2017), pharmaceutical contaminants (Alalm, Tawfik, & Ookawara, 2015b; Mackul'ak et al., 2015), agrochemical pollutants (Navarro, Fenoll, Vela, Ruiz, & Navarro, 2011; Saini, Raghunath, Pandey, & Kumar, 2016) and other recalcitrant pollutants. In most of these applications, effective degradation of pollutants has been reported. However, most of these studies have been on the application of Fenton oxidation for the removal of pollutants under synthetic condition.

The process begins with pH adjustment since Fenton oxidation is significantly affected by pH of the solution. The wastewater is then transferred into the reactor followed by the addition of  $\text{Fe}^{2+}$ . The addition of  $\text{H}_2\text{O}_2$ , either in steps or at once, initiates the Fenton process which proceeds according to the rate of reaction. One of the major challenges in Fenton oxidation is to ensure the use of optimum process parameters, particularly the dosages of  $\text{Fe}^{2+}$  and  $\text{H}_2\text{O}_2$ . Excess amount of Fenton's reagent may lead to scavenging effects, which will negatively affect the process performance. Thus, these process parameters are usually established through preliminary experiments. Once the designed

process time is reached, the pH of the solution is raised above 10 to quench the H<sub>2</sub>O<sub>2</sub> (Chou, Huang, & Huang, 1999). After settling, the solution is filtered to remove iron sludge prior to analyses. The performance of Fenton oxidation is routinely reported in terms of the percentage degradation of the target pollutants, COD and/or TOC removal. Fenton process is affected by many parameters such as concentrations of H<sub>2</sub>O<sub>2</sub> and Fe<sup>2+</sup>, solution pH, reaction time, and presence of scavenging ions.

The reviewed literature has shown that Fenton oxidation is widely applied in the removal of recalcitrant organic pollutants from wastewater. The basic principle of Fenton reaction shows that it is controlled by the Fenton's reagent, solution pH and the concentration of the pollutant. Despite its effectiveness, some limitations are associated with Fenton oxidation. Most of the limitations of Fenton oxidation stem from the operational parameters and the need to precisely control them. For example, the need to control the pH strictly at the narrow acidic pH range and the sludge generation pose practical disadvantage to Fenton oxidation.

## **2.5. Limitations of Fenton Oxidation**

Although Fenton oxidation is effective in the degradation of recalcitrant pollutants, it possesses few drawbacks which have hindered its industrial applications. These limitations are depicted in Figure 2.6. Fenton oxidation is strongly affected by the solution pH and requires the working pH to be kept in the acidic range of 2.8 – 3.5. The need for a precise control of pH and the difficulty of working in acidic condition hinder the applications of Fenton oxidation (Usman, Hanna, & Haderlein, 2016). Higher pH leads to complexation reactions and precipitation of iron oxides, leading to the production of excessive sludge. Thus, sludge generation represents another drawback of conventional Fenton oxidation (Barros, Steter, Lanza, & Tavares, 2016; Martínez-Huitle & Brillas, 2009). Sludge generation introduces the risk of secondary pollution and the need for

further sludge treatment and disposal. The requirement for additional treatment of sludge is a source of concern as the cost of treating the generated sludge can be up to 35 – 50% of the total operating cost of the wastewater treatment (Neyens & Baeyens, 2003). Additional drawbacks of Fenton oxidation include high consumption of  $H_2O_2$  (Asghar et al., 2015), difficulty in optimizing the reagent concentrations (Amorim, Leão, Moreira, Fabris, & Henriques, 2013) and the necessity to neutralize the treated wastewater before disposal.

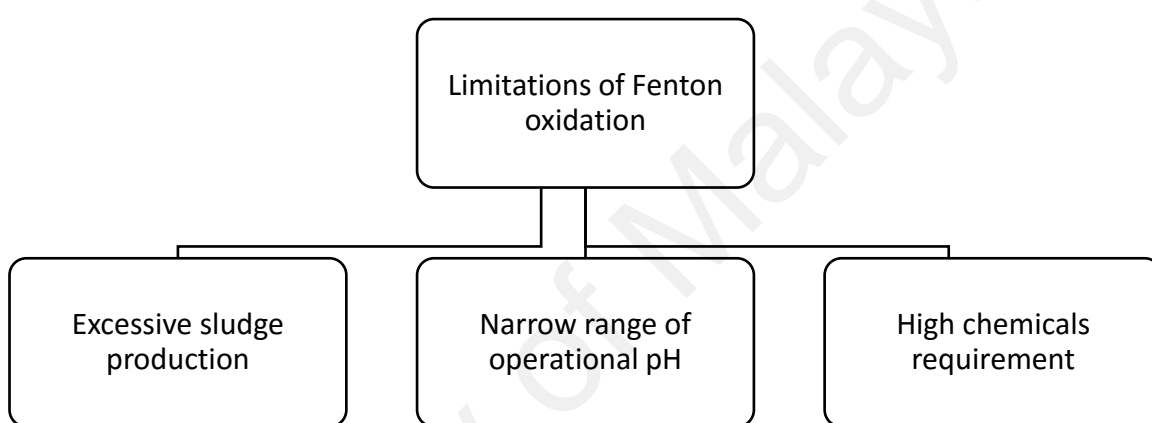


**Figure 2.6: Major limitations of Fenton oxidation**

Despite these limitations, the efficacy of Fenton oxidation in the degradation of recalcitrant pollutants makes it attractive and hence the topic of interest to many researches. Thus, addressing these limitations represents ongoing research efforts. Many strategies have been taken to address the drawbacks of conventional Fenton oxidation, particularly the pH limitation and sludge generation (Table 2.1). One of these is the development of heterogeneous Fenton oxidation, where heterogeneous catalysts are used as alternative to the homogeneous process ( $Fe^{2+}$ ) (Munoz et al., 2015). Another one involves the application of fluidized bed reactor to conduct Fenton oxidation with the aim of reducing the sludge generation. Of recent, various strategies are being developed for conducting Fenton oxidation at near neutral pH such as the addition of chelating agent and natural organic acids (Villegas-Guzman, Giannakis, Torres-Palma, & Pulgarin,

2017). Clarizia et al. (2017) have presented a review on the recent studies on strategies to conduct homogeneous Fenton at near neutral pH.

In heterogeneous Fenton oxidation, iron oxides or other supported catalysts are utilized as the active sites to generate ferric iron. Since the catalyst is not readily soluble, the production of ferric sludge is potentially eliminated and thus, the operation pH range can be wider. For example, Hou et al. (2017) developed a surface heterogeneous Fenton catalyst consisting of hydroxylamine, goethite and hydrogen peroxide and applied it in degrading various recalcitrant organic pollutants. The heterogeneous catalyst performed optimally at pH of 5 with no detectable iron ions in the solution.

**Table 2.1: Limitations of Fenton oxidation and possible solutions**

S/N	Limitation	Causes	Possible solutions	Reference
1	Requirement of acidic pH (small range of operational pH)	Production of OH <sup>•</sup> requires acidic pH (2.8 – 3.5) Acidic pH is required to keep Fe <sup>2+</sup> in soluble form pH above 4 promotes complex formation and sludge generation	Use of heterogeneous catalyst (iron oxide and other transition metal oxides) Use of chelating agents such as EDTA, oxalate, etc	(Clarizia et al., 2017; Ma, Yang, Wen, & Liu, 2017; Pouran, Abdul Raman, & Wan Daud, 2014; Usman et al., 2016)
2	Excessive sludge generation	Precipitation of iron oxide Neutralization of the Fenton reaction	Fluidized bed Fenton process Heterogeneous Fenton Modification and using sludge as heterogeneous catalyst	(Garcia-Segura, Bellotindos, Huang, Brillas, & Lu, 2016; Lima et al., 2017)
3	Chemical consumption/cost of chemicals (H <sub>2</sub> O <sub>2</sub> )	Large amount of H <sub>2</sub> O <sub>2</sub> may be necessary to completely mineralize pollutants Due to non-selectivity of Fenton, H <sub>2</sub> O <sub>2</sub> is scavenged by other anions/cations present	Use of MFCs and other technologies capable of in situ production of H <sub>2</sub> O <sub>2</sub> Other alternative oxidants	(Asghar et al., 2015; Li et al., 2016; Yinhan Wang, Feng, Li, Gao, & Yu, 2016)

Iron oxides in various forms such as goethite ( $\alpha$ -FeOOH), magnetite ( $\text{Fe}_3\text{O}_4$ ), hematite ( $\alpha\text{Fe}_2\text{O}_3$ ) and maghemite ( $\gamma\text{Fe}_2\text{O}_3$ ) are utilized as catalysts in Fenton and Fenton-like processes. However,  $\text{Fe}_3\text{O}_4$  and  $\alpha\text{FeOOH}$  are the most widely used heterogeneous catalysts (Pouran et al., 2014). Nowadays, with increased interest in nanotechnology, magnetite-based nanoparticles (MNPs) are being investigated as heterogeneous catalysts in Fenton oxidation (Davarnajad & Azizi, 2016; Munoz et al., 2015; Rusevova, Kopinke, & Georgi, 2012). The availability of magnetite and the ease of separation of the NPs from the wastewater matrix are obvious advantages of MNPs (Chun et al., 2012).

Although iron is abundant and relatively inexpensive, the cost of  $\text{H}_2\text{O}_2$  is relatively high, especially where the concentration of the target pollutant is high. Additionally, the presence of scavenging compounds in real wastewater can increase the  $\text{H}_2\text{O}_2$  requirement. Consequently, the amount of  $\text{H}_2\text{O}_2$  required to degrade a certain pollutant in industrial wastewater can be as high as 4 to 20 times the pollutant concentration (Asghar et al., 2015). To reduce the cost associated with  $\text{H}_2\text{O}_2$  purchase and transportation, research is being intensified on the in-situ production of  $\text{H}_2\text{O}_2$ . Among the possible methods for in-situ  $\text{H}_2\text{O}_2$  production, the use of electrochemical technology and microbial fuel cells (MFCs) have attracted recent interest (Wang et al., 2016). For example, Li et al. (2016) investigated the production of  $\text{H}_2\text{O}_2$  from MFC, achieving up to  $11.9 \text{ mg L}^{-1} \text{ h}^{-1} \text{ cm}^{-1}$ . Thus, when properly explored, MFCs has the potential towards reducing the cost of Fenton oxidation through the in-situ generation of  $\text{H}_2\text{O}_2$ .

As highlighted earlier, excessive sludge generation is perhaps the major drawback of homogeneous Fenton oxidation. Thus, another alternative which has recently been explored towards addressing this drawback is the application of FBR in homogeneous Fenton oxidation, termed fluidized bed Fenton (FBF) process. In FBF process, fluidized solid particles are used to provide surfaces that induce the removal of iron via

crystallization (Chen, Matira, Lu, & Dalida, 2016; Garcia-Segura et al., 2016). Additionally, the fluidization can enhance the treatment performance of FBF process due to excellent mixing and enhanced mass transfer.

The reviewed literature showed that there is growing research effort to develop solutions to the limitations conventional Fenton oxidation. Three main approaches have been commonly reported as possible solutions. These include heterogeneous Fenton oxidation, FBF process and strategies to applied Fenton oxidation under circumneutral pH. Among these, FBF process has received wide interest due to its practical advantage. Details on FBF process are covered in subsequent sections.

Since the principles of fluidization are adopted to reduce sludge generation and improve process performance of Fenton oxidation, it is imperative that the fundamentals of fluidized bed technology are understood for proper description of the FBF process. Thus, the subsequent section discusses the principles of fluidized bed technology, factors affecting it and its applications in wastewater treatment. Thereafter, the principles of FBF and its applications are reviewed.

## **2.6 Fluidized Bed Technology**

The basic concept of fluidized bed involves passing a fluid through a static bed of solid particles with a superficial velocity sufficient to overcome the drag force of the particles and suspend them in the medium (Figure 2.7). The suspended particles acquired the properties of the fluid and behave as though they were also fluid. As the fluid is first introduced into the static bed at a low velocity, it simply passes through the voids of the solid particles and the bed remains fixed. As the velocity increases, the bed expands until the particles become suspended when the buoyancy force balances the drag and gravitational forces. At a particular velocity, the minimum fluidization velocity ( $U_{mf}$ ), the

pressure drop across the bed equals the weight of the particles and the bed becomes completely suspended (Khan et al., 2014).

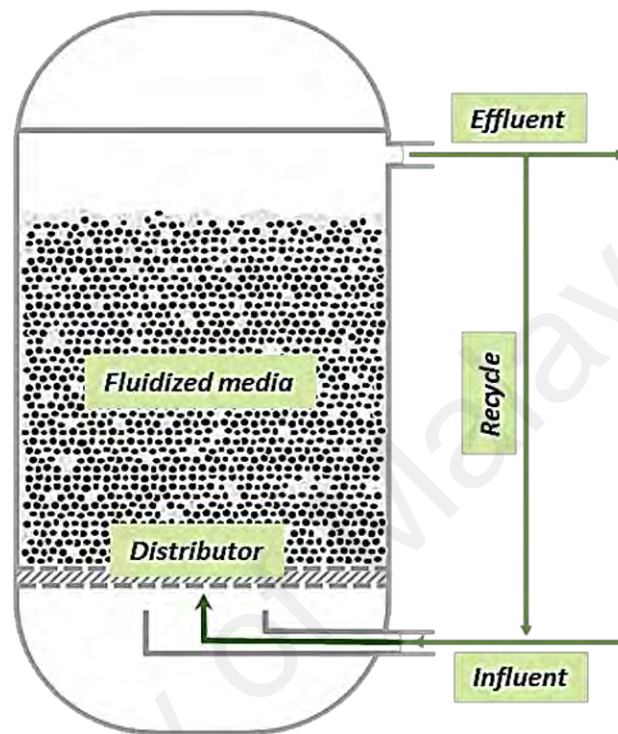


**Figure 2.7: Fluidized bed reactor in wastewater treatment**

The magnitude of the fluidization velocity will determine the nature of the flow regime, which can be a smooth fluidization, bubbling fluidization, slugging fluidization, turbulent fluidization or pneumatic conveying regimes (Yang, 2003). In addition, the characteristics of the fluidized particle, the up-flow velocity of the fluid and its viscosity will also affect the degree of bed expansion. FBR is an intrinsically multiphase flow system (solid-gas, solid-liquid, or solid-liquid-gas), which may involve heat and mass transfer.

The principle of fluidization has been employed in various industrial processes such as catalytic cracking, coal metal refining, gasification, wastewater treatment and other numerous applications. The major advantage of fluidized bed technology is the excellent

particles mixing, which enhances heat and mass transfer in the process (Andalib et al., 2014). Owing to these excellent features, FBR is among the most widely used reactors in chemical and environmental applications (Si, Zhou, & Guo, 2011).

FBR has been commonly used in biological wastewater treatments, with industrial treatment plants in existence as far back as 1970s. However, the earliest application of FBR in AOPs can be traced back to the work of Chou et al. (1999). Almost a decade later, Anotai et al. (2009) reported on the kinetics of Fenton oxidation of nitrobenzene and iron crystallization using FBR. The obvious advantage of using FBR in Fenton oxidation is that the fluidized solids facilitate the crystallization of iron oxides generated from the homogeneous Fenton reaction (Garcia-Segura et al., 2016).

Although several classifications of FBR are discussed in the literature, most of these classifications are not applicable to wastewater treatment. It is therefore pertinent that these classifications are reviewed for better understanding. The next section presents the classifications of FBR that are applicable to wastewater treatment.

### **2.6.1 Classifications of Fluidized Bed Reactor**

Many types of FBR such as bubbling fluidized bed, circulating fluidized bed, turbulent fluidized bed, floating fluidized bed, twin fluidized bed and many other classifications according to the flow regime and reactor design are utilized (Jordening & Buchholz, 1999). However, these classifications are used in specific chemical applications, mostly involving very high fluid velocities typically not applicable to wastewater treatment. Thus, the classification presented here is based on the application of FBR in wastewater treatment as shown in Figure 2.8.

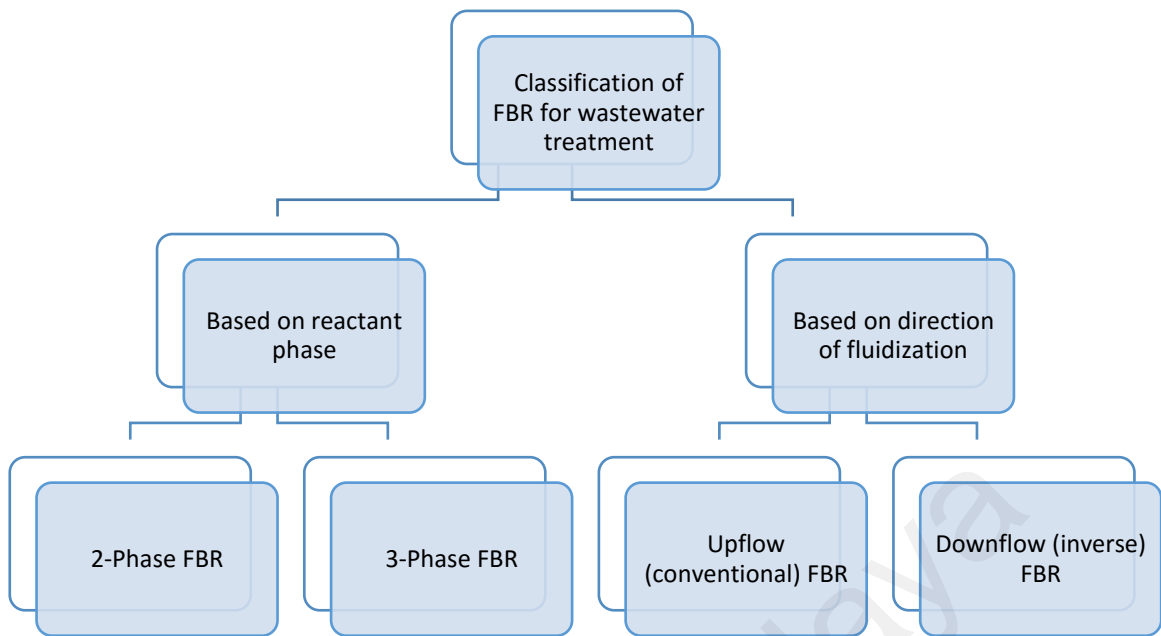


**Figure 2.8: Classification of fluidized bed reactor**

The two-phase FBR is a liquid-solid process in which the fluidization is brought about by the liquid. The solid phase can be a variety of support materials or catalysts, while fluidization is provided by the flow of wastewater through the reactor bed. The three-phase FBR is a gas-liquid-solid system, where aeration is added to the typical liquid-solid FBR. In this case, the fluidization is provided by the concurrent/countercurrent flow of the liquid and gas through the reactor bed. The three-phase system was developed to enhance the performance of the two-phase system through the supply of oxygen (Choi, Min, Lee, & Lee, 2000). However, the three-phase system is more complex and problems such as particle elutriation and increased agitation are commonly encountered.

FBR can also be classified according to direction of the fluid flow. Conventional FBR utilizes solids that have higher densities than the fluid phase and the fluidization is achieved by the upward fluid flow from the bottom of the reactor. However, FBR with downward fluid flow can also be utilized and is referred to as inverse fluidized bed reactor (IFBR) (Lakshmi, Balamurugan, Sivakumar, Samuel, & Velan, 2000). In IFBR, the solid particles are lighter than the fluid phase and fluidization is achieved by the downward

fluid flow counter to the net buoyancy of the particles (Nikolov, Farag, & Nikov, 2000). The IFBR is argued to offer superior hydrodynamic characteristics compared to the upward flow FBR. However, the major drawback of IFBR is that it usually requires higher superficial fluid velocity (Buffiere, Moletta, & Elmaleh, 1998).

The principles of fluidized bed technology have been reviewed and the literature has shown that FBR offers excellent properties that can be advantageous in wastewater treatment. The superior performance of FBR is largely due to the solid fluidization, which enhances mass transfer and prevent dead-zones in the reactor. The applications of FBR in wastewater treatment has been widely reported, especially in biological treatment, AOPs and adsorption. These applications are discussed in the next section.

## **2.7 Applications of Fluidized Bed Reactor in Wastewater Treatment**

The applications of FBR in wastewater treatments dates back to early 1970s where FBR was applied in biological wastewater treatment. There was increased progress in the subsequent years and full-scale fluidized bed bioreactors (FBBR) were already in operation by 1984 (Heijnen, Mulder, Enger, & Hoeks, 1989). On the other hand, the applications of FBR in AOPs is comparatively recent, with the earliest studies appearing in 1990s. The works of Diz and Novak (1998) and Chou and Huang (1999) are the earliest reported studies on the use of FBR in AOPs.

The application of FBR in wastewater treatment has received wide interest due to its effectiveness compared to fixed-bed contacting devices (Burghate & Ingole, 2013). The excellent mixing and high mass transfer rates are some of the attractive features of FBR (Andalib et al., 2014). With the solid particles vigorously agitated by the fluidization, excellent mixing is achieved and the temperature gradient can be minimized or eliminated in FBR (Dora, Mohanty, Roy, & Sarangi, 2013). The common applications of FBR are in

AOPs, biological treatment and adsorption. Therefore, these applications are discussed in this section based on Figure 2.9.

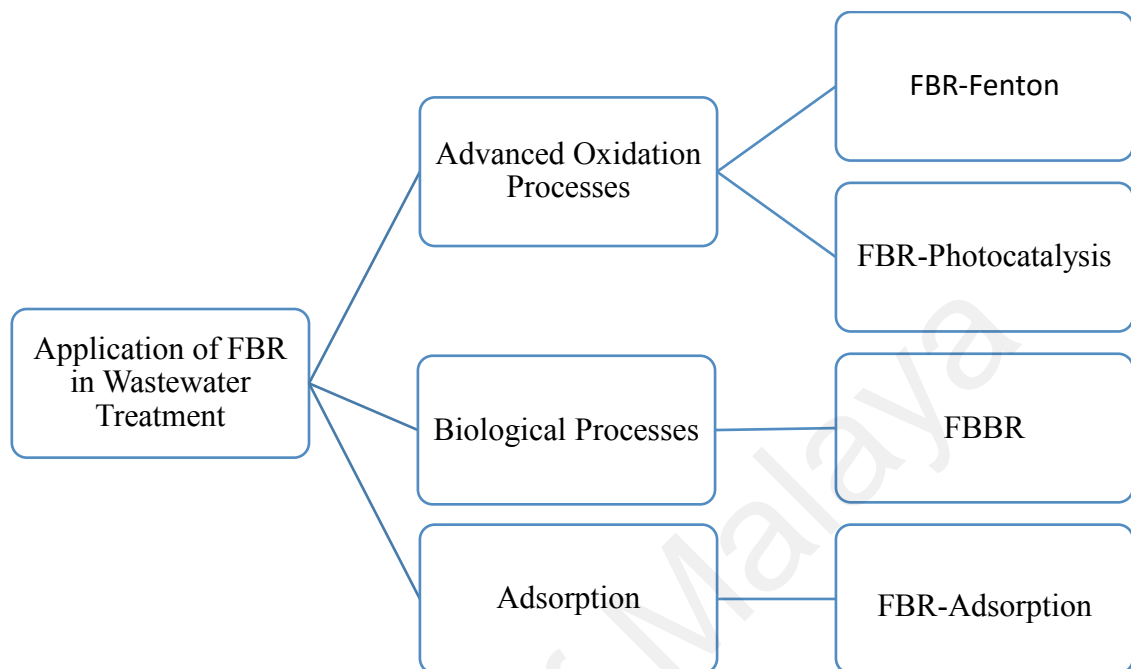


**Figure 2.9: Applications of fluidized bed reactor in wastewater treatment**

Since several chemical reactions occurs in AOPs for the generation of hydroxyl radicals, the choice of a suitable reactor is an important consideration. Due to the excellent features of FBR, many researchers have investigated its application in AOPs. Combining FBR technology with AOPs can improve performance and enhance catalyst reusability (Tisa, Aziz, & Mohd, 2014). In AOPs, FBR has been commonly used in Fenton oxidation and Photocatalysis.

FBR has been used in Fenton oxidation as a possible solution to some of the limitations of Fenton oxidation. Besides excellent mixing, the fluidized particles provide surfaces for iron nucleation and crystallization, thereby reducing the sludge generation and enhancing the process performance (Anotai et al., 2009). FBR can combine the effectiveness of homogeneous Fenton oxidation and the low sludge production of heterogeneous Fenton oxidation. Consequently, the performance of FBR-Fenton is superior to that of

conventional Fenton oxidation (Liu, Li, Mei, Wang, & Sellamuthu, 2014). The use of FBR-Fenton to degrade various recalcitrant pollutants such as textile dyes (Su et al., 2011), dimethyl sulfoxide (Bellotindos, Lu, Methatham, & Lu, 2014), acetaminophen (Luna, Briones, Su, & Lu, 2013), monoethanolamine (Su, Chen, Anotai, & Lu, 2013) and phenol (Muangthai, Ratanatamsakul, & Lu, 2010) have been reported.

The application of FBR in photocatalysis has also been reported. Although powder photocatalyst has a large specific surface area, which enhances mass transfer during wastewater treatment, it is necessary to have a downstream separation stage which increases the cost of treatment (Pozzo, Giombi, Baltanás, & Cassano, 2000). To overcome this, photocatalysts supported on larger materials such as  $\text{Al}_2\text{O}_3$ ,  $\text{SiO}_2$  or perlite are used in photocatalysis. This solves some of the challenges of using nanoparticles including the need for downstream separation and possible particles elutriation. Due to the excellent features of FBR, many publications have appeared on its application in photocatalysis. It is believed that besides excellent mixing and enhanced mass transfer, FBR may enhance light penetration and exposure of the interior of the reaction matrix (Nam, Kim, & Han, 2002).

FBR has been traditionally applied in biological wastewater treatment processes. The process comprises microorganisms-coated particles in wastewater, which are sufficiently fluidized to keep the phases thoroughly mixed (Vinod & Reddy, 2005). The fluidized support materials normally have large specific surface areas, which maximize surface contact between microorganisms and the pollutants. Consequently, the performance of FBR is higher than the conventional biological treatment systems (Alfredo, López, & Rodríguez, 2013). Burghate & Ingole, (2013) argued that FBBR offers the stability and ease of operation of a trickling filter and the high efficiency of activated sludge. For example, it was reported that FBBR operated at lower HRT and gave better performance

than a stirred tank reactor (Gonzalez, Herrera, Garcia, & Pena, 2001). Fluidization enhances gas-liquid mass transfer, which promotes good pollutant-biomass contact and suitable oxygen transfer rate (Pen & Jose, 2008). The fluidization can also reduce preferential flow paths, bed clogging and other challenges encountered in fixed-bed reactors (Jaafari, Mesdaghinia, Nabizadeh, & Hoseini, 2014).

The application of FBR in adsorption process for wastewater treatment has also been reported. The use of FBR in adsorption can eliminate many operational problems encountered in fixed-bed column adsorption such as clogging, temperature gradient, channeling and dead zones. For example, Dora et al. (2013) studied the adsorption of Arsenic (III) using cashew nut shell in a three-phase FBR and achieved a removal efficiency of 92.55%. The adsorption was affected by the gas and liquid velocities, particle size and initial static bed height. Kulkarni et al., (2013) investigated the adsorption of phenol from wastewater in an FBR using coconut shell activated carbon. The adsorption was affected by the initial phenol concentration, flowrate and bed particle size. Jovanovic et al. (2014) conducted studies on the hydrodynamics and adsorption of Cu (II) from aqueous solution using FBR packed with Zeolite beads. The process was achieved a maximum adsorption capacity of 23.3 mg/g.

The reviewed literature shows that FBR has been successfully utilized in different wastewater treatment technologies, particular biological, adsorption and AOPs. While in most cases the application of FBR was to enhance process performance, the technology is also being used to address some drawbacks such as the sludge generation in Fenton oxidation.

## 2.8 Fluidized Bed Fenton Process

The major limitations of Fenton oxidation have been discussed and some of the possible solutions were highlighted. Some of these limitations can be addressed by the application of FBR in Fenton oxidation. FBF is therefore a combination of conventional Fenton oxidation and fluidized carriers. The fluidized carrier in the reactor can provide surfaces for iron crystallization, which reduces the sludge generated and increases catalyst reusability (Anotai et al., 2009). Furthermore, the fluidization can enhance process performance due to excellent mixing (Liu et al., 2014). To fully understand the process, the basics of FBF process are presented in the next section.

### 2.8.1 Mechanism of Fluidized Bed Fenton Process

FBF process is a combination of fluidized bed technology and conventional Fenton oxidation. Thus, besides the processes involved in conventional Fenton oxidation, additional processes occur due to the presence of the fluidized solid carriers (Figure 2.10). The reaction mechanisms that occur in FBF process have been discussed previously (Chen, Ren, Ding, & Gao, 2015; Chou & Huang, 1999) and include (i) homogeneous reaction between the Fenton's reagent ( $\text{Fe}^{2+}/\text{H}_2\text{O}_2$ ); (ii) heterogeneous chemical oxidation (iron oxide/ $\text{H}_2\text{O}_2$ ); (iii) crystallization of the  $\text{Fe}^{3+}$  on the fluidized carriers; (iv) reductive dissolution of iron oxide; and (v) oxidation of the organic pollutant. The processes are clearly depicted in Figure 2.10. It can be seen that some of these reactions are similar to those in conventional Fenton such as (a) homogeneous  $\text{OH}^\bullet$  production from  $\text{Fe}^{2+}$  and  $\text{H}_2\text{O}_2$ , (b) oxidation of organic matter by the  $\text{OH}^\bullet$ , (c) conversion of  $\text{Fe}^{2+}$  to  $\text{Fe}^{3+}$ , and (d) part of the  $\text{Fe}^{3+}$  is converted back to  $\text{Fe}^{2+}$ . The remaining reactions are brought about by the presence of the carriers and include (e) crystallization of the ferric hydrolysis product on the surface of the carrier, forming the ferric oxide (f) heterogeneous production of  $\text{OH}^\bullet$

through the reaction of the ferric oxide and  $\text{H}_2\text{O}_2$ , (g) reductive dissolution of iron oxide to  $\text{Fe}^{2+}$  (Ratanatamskul, Chintitanun, Masomboon, & Lu, 2010).

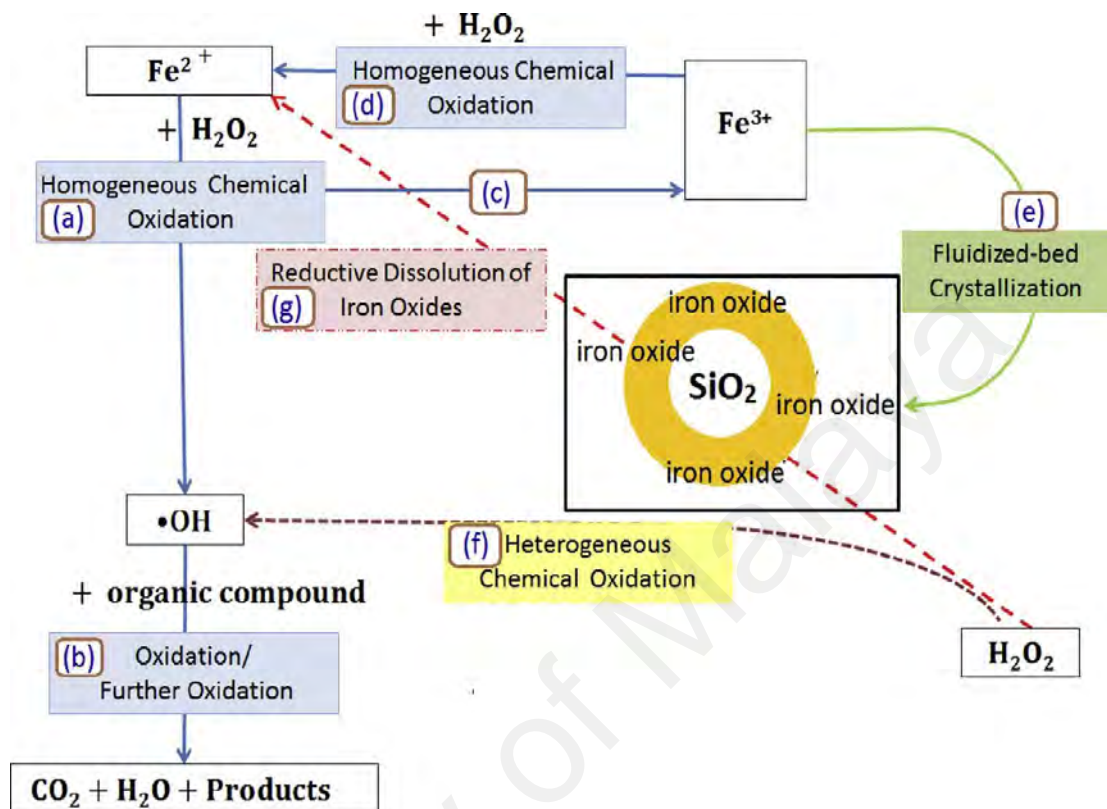


**Figure 2.10: Mechanism of fluidized bed Fenton process** (Adapted from Matira et al., 2015).

At the start of the process, the homogeneous reaction between  $\text{Fe}^{2+}$  and  $\text{H}_2\text{O}_2$  dominates. With the precipitation of the iron (III) ions onto the surface of the carriers, heterogeneous reaction is further introduced into the process. The formed iron oxide usually exist in form of  $\text{FeOOH}$  and acts as a heterogeneous catalyst for decomposing  $\text{H}_2\text{O}_2$  (Ratanatamskul, Narkwittaya, Masomboon, & Lu, 2011). This reduces the ferric requirement and the subsequent sludge generation.

The kinetic oxidation of organic pollutants in FBF process occurs in two stages. The first stage is characterized by the rapid formation of  $\text{OH}^\bullet$  due to the fast reaction between  $\text{Fe}^{2+}$  and  $\text{H}_2\text{O}_2$ . Most of the pollutant degradation is achieved in this stage, which occurs in the first few minutes of the process. The second stage is characterized by a slow reaction

between  $\text{Fe}^{3+}$  and  $\text{H}_2\text{O}_2$  which produces  $\cdot\text{OH}_2$  with a lower redox potential (1.65 eV) compared to  $\text{OH}\cdot$  (2.8 eV) (Luna et al., 2013). This stage dominates the remaining part of the process. For example, Chen et al. (2016) reported that the first stage in the degradation of dimethyl sulfoxide occurs in the first 3 minutes while the second stage dominates the remaining 3-120 minutes. However, the duration each stage would depend on the type of pollutants and other process parameters.

The reviewed literature has shown that the basic mechanism of FBF process consists of the reactions of homogeneous Fenton oxidation and the heterogeneous reactions occasioned by the presence of the fluidized carrier. Consequently, the parameters affecting the process are related to the Fenton's reactions and the fluidization process. Thus, successful application of FBF process in wastewater treatment depends on careful design and understanding of these operational parameters. Thus, the major operational parameters that can affect the performance of FBF process are reviewed in the next section.

## **2.9 Operational Parameters of Fluidized Bed Fenton**

Combining conventional Fenton oxidation with a fluidized bed technology introduces additional parameters into the relatively simple process. Besides the process parameters encountered in conventional Fenton process (pH,  $\text{H}_2\text{O}_2$ ,  $\text{Fe}^{2+}$ ), other parameters such as carriers (type, size, loading), superficial fluid velocity and reactor geometry are significant in FBF process. Thus, these parameters are discussed under two categories; (1) Fenton oxidation-related parameters, and (2) Fluidized bed-related parameters as shown in Figure 2.11.

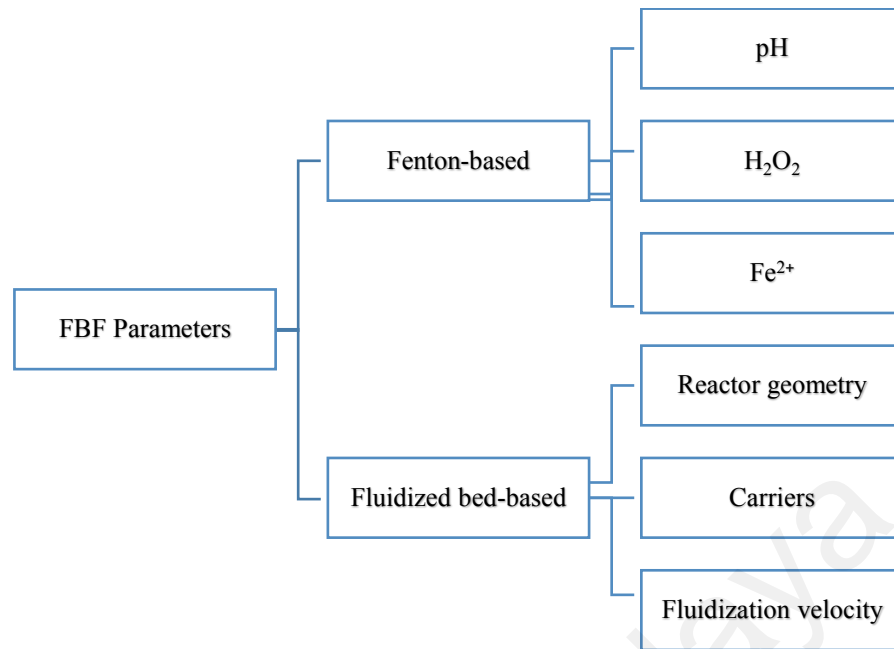


**Figure 2.11: Operational parameters of fluidized bed Fenton process**

### 2.9.1 Fenton-based Parameters

The Fenton-based parameters include the Fenton reagent ( $\text{H}_2\text{O}_2$  and  $\text{Fe}^{2+}$ ) pH, temperature, pollutant concentration and the nature of reaction matrix. However, the Fenton's reagent and pH are the most critical factors due to their effect on the generation of  $\text{OH}^\bullet$ . The production of  $\text{OH}^\bullet$ , the major driver of Fenton oxidation, depends on the decomposition of the oxidant ( $\text{H}_2\text{O}_2$ ) and the catalyst ( $\text{Fe}^{2+}$ ) that speeds up the decomposition. On the other hand, the catalytic role of the catalyst depends largely on the solution pH. The effects of these parameters are discussed in this section.

#### 2.9.1.1 pH

pH is one of the most significant parameters affecting Fenton oxidation. The production of  $\text{OH}^\bullet$  is controlled by the pH of the reaction medium. Rapid formation of  $\text{OH}^\bullet$  and subsequent efficient degradation of pollutants by Fenton oxidation occur at acidic pH, in the range of 2.8 – 3.5 (Pouran, Abdul Aziz, & Wan Daud, 2015; Villegas-Guzman et al., 2017). The pH of the solution has to be controlled within this range to ensure ferrous and

ferric irons maintain their catalytic ability (Clarizia et al., 2017). This is one of the major limitations of Fenton oxidation for industrial wastewater treatment. The need to control the pH in the narrow acidic range would increase the cost of the wastewater treatment. Consequently, research is being intensified on the application of Fenton oxidation at near-neutral pH in order to overcome this limitation (Clarizia et al., 2017). Table 2.2 shows some of the possible ways in which pH outside the optimum range can affect the Fenton oxidation.

**Table 2.2: Effects of pH on Fenton oxidation**

pH below optimum	Reference	pH above optimum	Reference
Scavenging of OH <sup>•</sup> by excess H <sup>+</sup>	(Tang & Huang, 1996)	Deficiency of H <sup>+</sup> which hampers OH <sup>•</sup> formation	(Pouran et al., 2015)
Formation of [Fe(H <sub>2</sub> O)] <sup>2+</sup> which has low oxidative power	(Shemer, Kunukcu, & Linden, 2006)	Decomposition of H <sub>2</sub> O <sub>2</sub> to O <sub>2</sub> and H <sub>2</sub> O	(Acisli, Khataee, Darvishi Cheshmeh Soltani, & Karaca, 2017)
Prevent the interaction between Fe <sup>3+</sup> and H <sub>2</sub> O <sub>2</sub>	(Pignatello, 1992)	Decline in the oxidative power of OH <sup>•</sup>	(Kim & Vogelphohl, 1998)
H <sub>2</sub> O <sub>2</sub> may be unstable to formed H <sub>3</sub> O <sub>2</sub> <sup>+</sup> which impedes production of OH <sup>•</sup>	(Chen, Wu, & Chung, 2009)	Formation of FeOOH which has lower oxidative power	(Villegas-Guzman et al., 2017)

pH values above or below the optimum level inhibit the formation of OH<sup>•</sup>. At higher pH, the catalytic role of iron is impaired because Fe<sup>3+</sup> precipitates as iron oxy-hydroxide, which have lower catalytic role than Fe<sup>2+</sup> (Vitale, Bernatene, & Pomilio, 2016). On the other hand, pH below the optimum range promotes the production of Fe<sup>2+</sup>-H<sub>2</sub>O<sub>2</sub> complex, which has a lower reactivity compared to OH<sup>•</sup> (Ratanatamskul, Narkwittaya, Masomboon, & Lu, 2010). It was also reported that the oxidation power of OH<sup>•</sup> decreases

with increasing pH (Kwon, Lee, Kang, & Yoon, 1999). Therefore, optimum pH is necessary to ensure effective performance of the FBF process.

The reviewed literature shows that the major implications of pH are that the reactivity of OH<sup>•</sup> and the catalytic role of Fe<sup>2+</sup> are significantly affected by the solution pH. The optimum pH according to most of the studies on homogeneous Fenton oxidation is in the range of 2.8 to 3.5. Thus, the need to maintain such acidic condition for effective process performance is one of the major limitations of Fenton oxidation.

### 2.9.1.2 Hydrogen peroxide

In Fenton oxidation, H<sub>2</sub>O<sub>2</sub> acts as the oxidant, producing OH<sup>•</sup> through a catalytic reaction with iron. Thus, the concentration of H<sub>2</sub>O<sub>2</sub> determines the potential OH<sup>•</sup> that can be generated in the reaction. The efficiency of Fenton oxidation increases with increase in H<sub>2</sub>O<sub>2</sub> concentration since more OH<sup>•</sup> can be potentially available. However, this trend is only applicable below the optimum concentration, which depends on the concentration of the pollutant. When the concentration of H<sub>2</sub>O<sub>2</sub> exceeds the optimum level, the process performance will decrease because of scavenging effect of the excess H<sub>2</sub>O<sub>2</sub> (Ahmadi et al., 2015). Scavenging occurs when excess H<sub>2</sub>O<sub>2</sub> acts as radical scavenger and react with the OH<sup>•</sup>, converting it to a less reactive hydroperoxyl radical (HO<sub>2</sub><sup>•</sup>) as shown in Equation 2.24 and Equation 2.25 (Li, Priambodo, Wang, Zhang, & Huang, 2015). This will decrease the concentration of OH<sup>•</sup> available for the degradation of the pollutant.



However, the effect of H<sub>2</sub>O<sub>2</sub> on the process is closely linked to the amount of Fe<sup>2+</sup>. Therefore, the ratio of H<sub>2</sub>O<sub>2</sub> to Fe<sup>2+</sup> is equally important. Indeed, some researchers have reported the effect of H<sub>2</sub>O<sub>2</sub> vis-à-vis the concentration of Fe<sup>2+</sup> (Su et al., 2011). In a study

to establish the optimum condition for degrading 2,4-Dichlorophenol using a fluidized bed Fenton process,  $\text{H}_2\text{O}_2$  was found to be the major parameter affecting the process (Muangthai et al., 2010a). When the concentration of  $\text{H}_2\text{O}_2$  was increased, a corresponding increase in the pollutant degradation was obtained at constant  $\text{Fe}^{2+}$  dosage. Wang et al. (2015) applied FBF process to degrade Orange G and observed that the degradation was enhanced with increasing  $\text{H}_2\text{O}_2$  concentration. When the concentration was increased beyond 25mg/L, the process performance decreased, pointing to the effect of excess  $\text{H}_2\text{O}_2$ .

The optimum concentration  $\text{H}_2\text{O}_2$  varied among the reported studies due to differences in the nature and concentration of the target pollutants, as well as other process parameters. However, all the studies have shown that the reaction rate increases with an increase in  $\text{H}_2\text{O}_2$  concentration until the optimum amount is reached. High concentration may inhibit the degradation due to the scavenging effect of the  $\text{H}_2\text{O}_2$ . Therefore, the optimum concentration of  $\text{H}_2\text{O}_2$  depends largely on the concentration of the target pollutant and the extent of degradation required.

The reviewed literature on the effect of  $\text{H}_2\text{O}_2$  shows that the concentration of  $\text{H}_2\text{O}_2$  has a positive effect on the process performance. This is attributed to the higher generation of  $\text{OH}^\bullet$  with increasing  $\text{H}_2\text{O}_2$ . However, the production of  $\text{OH}^\bullet$  also depends on the concentration of  $\text{Fe}^{2+}$  and the solution pH. Thus, it is more practical to consider the concentration of  $\text{H}_2\text{O}_2$  vis-à-vis the concentration of  $\text{Fe}^{2+}$  under the optimum pH. The next section discussed how  $\text{Fe}^{2+}$  can affect the process performance.

### **2.9.1.3 Iron**

In Fenton oxidation,  $\text{Fe}^{2+}$  acts as a catalyst for the decomposition of  $\text{H}_2\text{O}_2$  to generate  $\text{OH}^\bullet$ . Thus, an increase in the concentration of  $\text{Fe}^{2+}$  will enhance pollutant degradation

due to more generation of  $\text{OH}^\bullet$ . However, excess amount of  $\text{Fe}^{2+}$  can lead to a decrease in the process performance (Muangthai et al., 2010). Excess  $\text{Fe}^{2+}$  can act as a radical scavenger and compete with the organic pollutant for the available  $\text{OH}^\bullet$ . Furthermore, excess  $\text{Fe}^{2+}$  can lead to other undesirable effects such as excessive sludge generation and turbidity in the reactor, decreasing the process performance (Wang et al., 2015). This underscores the importance of establishing the optimum dosage of  $\text{Fe}^{2+}$  vis-à-vis the amount of  $\text{H}_2\text{O}_2$ .

The positive correlation between the concentration of  $\text{Fe}^{2+}$  and the performance of FBF has been consistently observed in the literature. For example, Ratanatamskul & Narkwittaya (2010) reported that the degradation of 2,6-dimethylaniline by FBF process increased from 83 to 100% when  $\text{Fe}^{2+}$  was increased from 1 to 5 mM, with the optimum amount around 2.5 mM. In another study, Briones et al. (2012) investigated the removal of acetaminophen using FBF process and reported that acetaminophen degradation increased with increasing  $\text{Fe}^{2+}$  concentration, especially at acidic pH.

Although  $\text{Fe}^{2+}$  has a positive effect on the process performance, its concentration must be optimized since excess amount will lead to scavenging effect. However, the concentration required would depend on the target pollutant as well as the amount of the  $\text{H}_2\text{O}_2$  used. It has also been established that the catalytic role of  $\text{Fe}^{2+}$  decreased with increasing pH. This is one of the reasons why the performance of Fenton oxidation is more effective at lower pH values.

### **2.9.2 Fluidized Bed-based Parameters**

Successful application of FBR requires knowledge of the major operation parameters that affect fluidization and hydrodynamics of the system. However, despite the extensive applications of FBR, fluidization is still an empirical science (Yang, 2003) and a single

systematic design approach is yet to emerge. Instead, the design is largely application-specific and relies on empirical correlations (Onysko, Robinson, & Budman, 2002) and experience of the designer (Zhang, Wei, Feng, & Zhu, 2012). The absence of a robust methodology and the reliance on heuristic may lead to various problems such as insufficient or over-fluidization, poor treatment performance and reactor failure. Although attempts have been made to understand the operational parameters, large-scale applications of FBR still pose significant challenge (Reinhold, Merrath, Lennemann, & Markl, 1996). Some of the parameters that may affect the performance of FBR include reactor geometry, aspect ratio, reactor internals, particle size and density, particle loading and fluid superficial velocity. These parameters are discussed in this section.

#### **2.9.2.1 Shape and cross-sectional area of reactor**

Reactor configuration is an important parameter that affects mixing and particle distribution in FBR (Choi & Shin, 1999). Particle mixing plays an important role in the performance of FBR since it affects both heat and mass transfer (Yan et al., 2009). For wastewater treatment, it is necessary to obtain high mass transfer rate and uniform temperature in the reactor through fluid-particle interactions.

Although FBR is conventionally cylindrical, other shapes such as square columns have been used. Dead-zones are encountered more frequently in square columns where the sharp corners of the reactor promote their occurrences. The presence of dead-zones inhibits proper particle mixing in the reactor. In their comparative study on the effect of bed geometry on mixing rate, Gorji-kandi et al. (2015) concluded that mixing rate is greater in a cylindrical bed than a square bed FBR. This was attributed to the presence of dead-zones at the corners of the square reactor. The presence of slow fluidization on the wall of the reactor had been confirmed earlier (Efstathios & Michaelides, 2013).

Therefore, it is necessary to choose appropriate shape of the reactor for effective wastewater treatment.

The cross-sectional area of the reactor is another parameter that can affect the hydrodynamics and treatment performance of FBR. Generally, FBR can be a flatbed or a tapered-bed system. Conventional FBRs are flatbed reactors with uniform cross-sectional areas. However, wash-out of particles has been commonly encountered when there is a high superficial velocity. To overcome this challenge, Scott and Hancher introduced the concept of tapered-bed FBR in 1976 (Parthiban, Iyer, & Sekaran, 2007). In tapered FBR, the cross-sectional area of the reactor is made narrower at the bottom (tapered-in) or both bottom and top (tapered-in tapered-out) (Askaripour & Dehkordi, 2015). This results in a stable feed introduction as well as minimizes eddies and back mixing that could arise in flatbed FBR. However, it is necessary to ensure appropriate taper angle so that turbulent flow due to sudden expansion is avoided.

A comparative study on the performance of a flatbed FBR and a tapered FBR showed that the latter has superior treatment performance and better hydrodynamic characteristics (Huang, Yan, & Wu, 2000). Three FBRs having  $0^\circ$ ,  $2.5^\circ$  and  $5^\circ$  taper angles were compared in the study. The hydrodynamics characteristics and performance of the three FBRs were in the following increasing order  $5^\circ \rightarrow 2.5^\circ \rightarrow 0^\circ$ . A previous study by Wu and Huang (1996) had reported that COD removal efficiency of a tapered FBR was higher than a flatbed FBR when the taper angle does not exceed  $5^\circ$ .

The reviewed literature shows that the selection of appropriate cross-sectional area can prevent the formation of dead-zones in the system. Since dead-zones occur at the wall of the reactor, rectangular reactor is more prone to dead-zones than cylindrical shape due to the sharp corners in the former. On the other hand, the shape of the reactor can be used to control the superficial fluid velocity, minimizing eddies and back mixing. The reviewed

literature has shown that although conventional FBR has a flatbed, using tapered bed reactors can ensure stable dynamic and prevent possible particle wash-out.

### **2.9.2.2 Aspect ratio of reactor**

Aspect ratio, defined as the ratio of the static bed height to the reactor diameter, is an important design parameter of FBR. The aspect ratio has an influence on fluid circulation velocity and consequently on the phase mixing in the reactor (Weipeng, Yumei, Guangji, & Chao, 2014). Large aspect ratio promotes bubble coalescence and higher solid holdup. This reduces both gas/liquid holdup and the interphase mixing. Conversely, a low aspect ratio promotes higher liquid/gas holdup and encourages interphase mixing (Sabarunisha & Radha, 2014).. Therefore, low aspect ratio can reduce the fluid flow rate requirement and hence lower the process cost (Ochieng, Odiyo, & Mutsago, 2003). It is therefore necessary to select the appropriate aspect ratio for proper design and successful application. Typical ranges of aspect ratio for laboratory scale FBR ranges from 5 to 25 while that of technical plants ranges from 2 to 5 (Jordening & Buchholz, 1999). Laboratory scale FBR usually have small diameters in relation to the reactor column height and the corresponding static bed height. Since the reactor volume is small, a small diameter and a relatively high static bed height can give the necessary solid loading. In the case of full scale FBR, a long and narrow column may result in slugging effect (Kunii & Levenspiel, 1991) and hence the diameter is usually made relatively bigger to achieve the necessary degree of fluidization. However, a very large diameter may pose challenges to uniform fluidization. Therefore, a compromise is usually necessary (Jordening & Buchholz, 1999). For example, Ochieng et al. (2002) found an aspect ratio of 10 to be the optimum in their treatment of brewery wastewater using laboratory-scale FBR.

Aspect ratio relates the amount of solids to the reactor diameter and can affect fluid pumping requirement through variation in solid/fluid holdups. Appropriate aspect ratio

must be designed to ensure proper phase mixing and optimum fluid pumping requirement. In some cases, an internal structure can be incorporated into the reactor to enhance phase mixing. These are called reactor internals and are discussed in the next section.

### **2.9.2.3 Reactor internals**

Another parameter that affects FBR performance is the presence of an internal structure in the reactor. Internals, such as tubes and baffles, are sometimes introduced into the reactor to modify the flow structures and improve particles fluidization. Reactor internals promotes uniform mixing which result in effective fluidization (Qin, Shen, Zhou, & Liu, 2014). Although the main purpose of internals is to ensure uniform fluidization, additional benefits such as enhanced phase contact, controlled solid holdup and improved radial mixing are obtained (Jin, Wei, & Wang, 2003). The downside of the internals is that they can increase the complexity of system design and operation (Dutta & Suciu, 1992).

Baffles (wire mesh, ring, perforated plate etc.) and tubes (draft tubes, horizontal and vertical banks, etc.) are the most commonly used internals in wastewater treatments. Many studies have been reported on reactor internals such as vertical internals (Ramamoorthy & Subramanian, 1981), horizontal tubes (Olowson, 1994), perforated baffles (Zhao, Zhong, & Xu, 1992), ring-type internals (Zhu, Salah, & Zhou, 1997) and other variations. In general, internals have effects on the bubble behavior, flow distribution and phase mixing.

Studies have shown that introducing a draft tube into FBR can enhance the process performance. Wang et al. (2015) reported that an FBR with internal draft tube gave a higher decolorisation and TOC removal compared with conventional FBR in their study for orange G degradation. Similarly, Nam et al. (2009) reported similar findings when they compared the performance of conventional FBR and FBR with an internal draft tube

(DTFBR). The DTFBR showed superior performance under all the conditions investigated which was attributed to the more uniform distribution of the catalyst.

In another study, Vinod & Reddy (2005) used a draft tube FBR for the treatment of phenolic wastewater, achieving up to 96 % removal efficiency. Interestingly, Wei et al. (2000) compared the hydrodynamics of FBR with conventional internal draft tube and with convergence-divergence draft tube. Results showed that gas holdup is higher in the FBR with convergence-divergence draft tube than the conventional draft tube FBR. Conversely, liquid circulation velocity was found to be lower in the convergence-divergence draft tube reactor, perhaps due to the decrease in the velocity caused by the divergence/convergence tube.

However, Nam et al. (2002) reported that internal draft tube has a negligible effect on the performance of FBR in the oxidation of methyl orange. The degradation was found to depend on other parameters rather than the reactor internals. However, the range of gas flow rates tested in the study may have been too low to make a significant difference in the hydrodynamics of the two different reactors. To buttress that, the authors reported the superiority of the DTFBR over the conventional FBR in a more recent study (Nam et al., 2009).

The reviewed literature has shown that reactor geometry can affect the reactor hydrodynamics and therefore influences the treatment performance of FBR. This occurs due to the excellent mixing and particle fluidization. Although internal structures such as draft-tubes are commonly introduced into the reactor to enhance fluidization, they could increase system complexity. Therefore, reactor geometry is an important parameter that must be carefully designed. Since reactor geometry can affect particle mixing and fluidization, information about the properties of the fluidized particle must be obtained for proper design. The next section discussed the effects of solid particles.

#### 2.9.2.4 Particle size and surface characteristics

The properties of support materials such as particle size, density and surface characteristics can affect the process performance of FBR (Wirsum, Fett, Iwanowa, & Lukjanow, 2001). The choice of support material would therefore determine, to a great extent, the process engineering (Jordening & Buchholz, 1999). The effects of particle loading, density, size and surface properties on the reactor performance are discussed in this section.

Particle size is an important parameter that affects fluidization as well as mass transfer in the reactor. In fact, it has been argued that particle size could be the most important factor that govern mass transfer in a three-phase FBR (Kim & Kang, 1997). Although developed for gas-solid fluidization, Geldart classification of particles can be useful in classifying solids for wastewater applications. Geldart (1973) classified solid particles into four groups (A, B, C and D) based on their mean size and density difference between the particles and the fluidizing medium. Group A are particles with small mean size between 30 to 100  $\mu\text{m}$ , group B ranges between 100 to 800  $\mu\text{m}$ , group C has mean size less than 20  $\mu\text{m}$  while group D has a mean size above 1 mm. For each classification, different flow regimes and bed behavior are observed.

Both heat and mass transfer in FBR increase with increase in particle size. This is because large particles have the capability to break up and disintegrate large bubbles (Nguyentien, Patwari, Schume, & Deckwer, 1984). For a given liquid velocity, larger particles would result in a better mass transfer and subsequent reactor performance than smaller ones (Begum & Radha, 2015). In a study to investigate the effect of zeolite diameter used as a carrier, it was reported that larger diameter (0.5 – 0.8 mm) gave higher COD removals than smaller ones (0.2 – 0.5 mm) (Fernández et al., 2008). Therefore, it is generally

believed that mass transfer coefficient in FBR increases with increase in bed particle diameter.

However, large particles can increase bed pressure drop (Dora, Mohanty, & Roy, 2012) which will consequently increase the fluidization requirement (Midha, Jha, & Dey, 2012). Lakshmi et al. (2000) investigated the effect of particle diameter on the minimum fluidization velocity in a two-phase IFBR using LDPE and propylene particles. They reported that the minimum fluidization velocity increased with increase in particle diameter for the two types of particles investigated. This was attributed to the increase in the Archimedes number which increases with increase in particle diameter.

Surface characteristic of the carrier is another important parameter that can affect the performance of FBR. Solid particles can be hydrophobic or hydrophilic. Unlike hydrophobic particles, hydrophilic particles mix readily with water, which improve mass transfer coefficient for up-flow fluidization (Kim & Kang, 1997). However, for inverse fluidization, the reverse is the case. Han et al., (2003) compared hydrophobic and hydrophilic particles having the same density and concluded that hydrophobic are better than hydrophilic particles for inverse fluidization. This was attributed to the retardation of rising bubbles near the hydrophobic particles which subsequently increased the gas holdup. A similar concept of hydrophobic/hydrophilic was discussed by Choi & Shin (1999) and observed by Buffiere et al. (1998) during their study of an IFBR. Kim & Kangt (1997) had equally discussed this in terms of the wettability of the particles. This shows the importance of surface properties of FBR support materials in wastewater treatment.

Particles with high specific surface areas, good physicochemical and fluido-dynamic properties should therefore be used as support materials (Pen & Jose, 2008). Silica, quartz sand, granular activated carbon, vitreous coke, glass beads, PVC, are some of the common support materials used in FBR (Buffiere et al., 1998). The particle diameter of the support

materials is usually less than 1 mm, though larger particles have also been used (Vinod & Reddy, 2005). The specific area of bed materials after fluidization can be calculated using the following formula:

$$a_s = \frac{6(1-\varepsilon)}{d \psi} \quad (2.26)$$

It can be seen that from the reviewed literature that heat and mass transfer have a positive correlation with particle size. However, large particles can increase bed pressure drop in the reactor. Although different particle size can be used in FBR, the particle sizes commonly utilized in FBR for wastewater treatment fall under Geldart's group B and D. The surface properties of the particles are also important since, for example, hydrophilic particles mix well with water and can promote mass transfer compared to hydrophobic particles. It is pertinent to note that the effect of particle size and surface properties on the process performance is also related to the particle loading in the reactor. Thus, the effect of particle loading is discussed in the next section.

#### **2.9.2.5 Particle loading**

For successful application, it is necessary to understand the effect of particle loading on the hydrodynamics of FBR (Delebarre, Morales, & Ramos, 2004). The initial static bed height is the height of the solid particles in the reactor prior to fluidization. Theoretically, the initial static bed height does not affect the minimum fluidization velocity ( $U_{mf}$ ) in a conventional FBR (Jena, Roy, & Meikap, 2009). This is because fluidization is achieved when the upward inertial and drag forces exerted on the particles equal the buoyant weight of the bed. Lakshmi et al. (2000) studied the effect of bed height on  $U_{mf}$  in a two-phase FBR and reported that constant velocity is obtained for all bed heights investigated.

However, Delebarre et al. (2004) studied the influence of particle loading on fluidization characteristics of FBR and concluded that the initial static bed height has effect on  $U_{mf}$ . An increase in particle loading led to an increase in  $U_{mf}$ . However, there were some inaccuracies in the bed height measurements which might have affected the authors' conclusion. Previous study by Garcia et al. (1999) had reported a small influence of particle loading on the liquid velocity of the system. In the case of IFBR, however, the fluidization velocity decreases with increase in particle loading (Han et al., 2003).

For a given reactor diameter, particle loading can affect the oxygen mass transfer rate in a three-phase FBR. However, the influence of particle loading on oxygen transfer rate is rather complex. High particle loading promotes bubble coalescence, which in turns reduces the interfacial area of gas-liquid and hence the oxygen mass transfer (Abdel-Aziz, El-Abd, & Bassyouni, 2016). Large bubbles will move faster, resulting in a shorter residence time and consequent low gas hold up. It was reported that an increased particle loading of 15% caused a 30% drop in oxygen mass transfer in a three-phase FBR (Yu, Ji, & Yue, 1999).

The initial static bed also affects the pressure drop across the reactor bed. At  $U_{mf}$ , the pressure drop is equal to the weight of the particles divided by the cross-sectional area of the bed. The pressure drop in FBR is the sum of the frictional pressure drop and the static pressure drop. However, the static pressure drop is usually negligible and the total pressure drop is then due to the frictional pressure drop only (Askaripour & Dehkordi, 2016). Therefore, the frictional pressure drop required to counterbalance the weight of the bed increases with increase in initial static bed height (Dora et al., 2012). Thus, it is necessary to use appropriate aspect ratio to ensure optimum performance of the system.

The major effect of particle loading is on the pressure drop in the reactor. Increasing the particle loading will lead to an increase in the frictional pressure necessary to counter the

increased weight. However, the effect of particle loading on the pressure drop is also dependent on the particle density. Thus, the effect of particle density is discussed in the next section.

#### **2.9.2.6 Particle density**

The density and the surface properties of the particles would determine the required superficial fluid velocity under a given bed height (Han et al., 2003). The density of the carrier has a positive correlation with the up-flow fluid velocity (Escudero, 2010). Similarly, the porosity of the materials will positively affect the superficial velocity requirement (Jordening & Buchholz, 1999). The use of light particles will result in low fluid pumping requirement and thereby low operational cost (Midha et al., 2012). In such case, however, the aspect ratio should be as low as possible in order to achieve bed homogeneity at low gas/liquid flow rates (Ochieng et al., 2002).

In the case of an IFBR, the minimum fluidization velocity decreases with increase in particle density. A study on the minimum fluidization velocity requirement between a low density polyethylene (LDPE) ( $940 \text{ kg/m}^3$ ) and polypropylene (PP) ( $840 \text{ kg/m}^3$ ) revealed that the LDPE particles required lesser fluidization velocity than the PP particles (Lakshmi et al., 2000). This is because the upward buoyance force increases as the particle density decreases, and thus higher liquid velocity is required to achieve fluidization.

Under a constant initial static bed height, the density of the carrier will affect the bed pressure drop. Dense particles increase the weight of the initial static bed height and this increases the pressure drop necessary to counterbalance the weight (Dora et al., 2012). A correlation of gas velocity, phase holdups and pressure drop can give further insights on the influence of the hydrodynamic characteristics on the process performance as shown in Equation 2.27 and Equation 2.28.

$$-\frac{dp}{dz} = (\varepsilon_s \rho_s + \varepsilon_L \rho_L + \varepsilon_g \rho_g)g \quad (2.27)$$

$$\varepsilon_s + \varepsilon_L + \varepsilon_g = 1 \quad (2.28)$$

Clearly from Equation 2.27, the use of dense particles could lead to an increase in pressure drop, which consequently increases power consumption. On the other hand, very low densities could lead to particle wash-out. However, a careful design and reactor internal can minimize this problem (Ochieng et al., 2002).

In this section, the effect of particle density on the pressure drop and minimum fluidization velocity is discussed. Although the reactor geometry and properties of fluidized solid can affect fluidization, it is important to understand the influence of superficial fluidization velocity on the process performance. The next section discussed the influence of superficial fluid velocity.

### 2.9.2.7 Superficial fluid velocity

Superficial fluid velocity ( $U_f$ ) refers to the volumetric flow rate of the fluid divided by the cross-sectional area of the reactor.  $U_f$  is responsible for the particles fluidization and therefore influences the particles mixing, heat and mass transfer rate in the reactor (Mostoufi & Chaouki, 2001). Therefore, it is necessary to understand how  $U_f$  affect FBR performance.  $U_f$  is required to be within two extremes, the minimum fluidization velocity ( $U_{mf}$ ) and the terminal fluidization velocity ( $U_t$ ).  $U_{mf}$  is the lowest fluid velocity necessary to initiate particles fluidization while  $U_t$  is the fluid velocity at which particles are carried out with the fluid flow (Jovanovic et al., 2014).

$U_{mf}$  is an important parameter which is closely related to the power requirement of the system (Ochieng et al., 2003). A high  $U_{mf}$  will result in a high fluidization power requirement. Therefore, it is necessary to control  $U_f$  slightly above  $U_{mf}$  with as much

accuracy and precision as possible (Delebarre et al., 2004).  $U_{mf}$  can be calculated using Equation 2.29.

$$U_{mf} = 16.50 \frac{d^2(\rho_s - \rho)g}{\mu} \quad (2.29)$$

Increasing  $U_f$  leads to an increase in liquid circulation and mixing rate, thus a shorter reaction time. However, this is only true up to the optimum  $U_f$ . On the other hand, a high  $U_f$  can result in particle wash-out from the reactor (Jaafari et al., 2014). Therefore, selection of optimum  $U_f$  is necessary to ensure successful operation of the FBR.

Although liquid velocity dominates in a three-phase FBR, the flow regime depends on the ratio of the superficial liquid velocity to the superficial gas velocity. Both velocities have to be properly designed and controlled. For a counter-current system, a small liquid velocity to gas velocity ratio is necessary to have high mass transfer coefficients (Forster, 1980). However, for a concurrent flow system, a high ratio will give a well dispersed bubbles and hence high oxygen transfer rate while a low ratio would result in bubble coalescence and low oxygen transfer rate (Yu et al., 1999). Both superficial liquid and gas velocities will affect solid and liquid holdups. Increasing superficial liquid velocity will cause solid particles to expand faster and hence reduces the solid holdup (Akilamudhan, Sivakumar, Mohanraj, & Senthilkumar, 2014). This will in turn increase the liquid holdup. On the other hand, gas holdup increases with increase in superficial gas velocity (Wei et al., 2000).

Nikolov et al. (2000) reported that liquid velocity has a weak effect on the oxygen transfer and gas velocity has a strong effect in a three phase IFBR. In general, the smaller the amount of air supplied, the more economical the process would be which is desirable for industrial applications (Vimonses, Jin, Chow, & Saint, 2010).

Sabarunisha & Radha (2014) studied the hydrodynamic behavior of an inverse FBR for phenol degradation and reported that COD removal increased with an increase in the superficial gas velocity. This was attributed to the higher gas holdup, volumetric mass transfer coefficient and oxygen transfer rate due to the increased gas velocity. The highest COD and phenol degradation rates were obtained at a gas velocity of 0.220 m/s. Above this optimum value, however, the degradation efficiencies became lower. At gas velocities above the optimum value, larger bubbles are formed which dominate over the interfacial area, resulting in lower mass transfer.  $U_f$  is affected by the properties of bed materials as well as the aspect ratio of the reactor (Zhong, Jin, Zhang, Wang, & Xiao, 2008).

After reviewing the basic principles of FBF process and the major operational parameters that can affect its performance, it is important to discuss the specific applications of the process to remove different recalcitrant pollutants. Thus, the next section reviewed the specific applications of FBF process in the removal of various recalcitrant pollutants.

## **2.10 Applications of Fluidized Bed Fenton in Wastewater Treatment**

FBF process has been used for the degradation of various recalcitrant pollutants such as dyes, pharmaceuticals, phenolic compounds and other organic pollutants. Most of these studies have been on synthetic wastewater. Table 2.3 summarizes some recent applications of FBF process to remove recalcitrant pollutants while a more detailed list can be found in Table A1 in the appendices. It can be seen from Table 2.3 and Table A1 that FBF process has been applied in the treatment of wastewater containing various recalcitrant pollutants under different conditions. The carriers commonly used include  $\text{SiO}_2$  and  $\text{Al}_2\text{O}_3$ . These studies have shown that the FBF can reduce iron sludge generation and improve process performance of conventional Fenton. These previous studies are discussed in this section.

**Table 2.3: Applications of fluidized bed Fenton in wastewater treatment**

Target pollutants	Reactor and Support Material Properties	Operational Conditions	Performance	Reference
DMSO	H: 140 cm D: 5.2 cm Solid: silica D <sub>p</sub> : 0.42-0.5 mm P <sub>L</sub> : 68.97 g/L	pH: 3 Fe <sup>2+</sup> : 5 mM H <sub>2</sub> O <sub>2</sub> : 32.5 mM HRT: 240 min	DMSO: 95.22% COD: 34.38%	(Chen et al., 2016)
AY36	Solid: NP; D <sub>p</sub> : 0.6 – 1 mm	pH: 3.7; H <sub>2</sub> O <sub>2</sub> : 1.7 mM	Degradation: 99.2%	(Aghdasinia, Bagheri, Vahid, & Khataee, 2016)
Hospital wastewater: COD	V: 1.5 L D: 0.053 mm H: 1330 mm Solid: Silica D <sub>p</sub> : 0.42-0.59 mm P <sub>L</sub> : 40g/L	pH: 3 Fe <sup>2+</sup> : 5 mM H <sub>2</sub> O <sub>2</sub> : 50 mM HRT: 90 min Q: :12 L/min	COD: 98%	(Anand, Adish Kumar, Rajesh Banu, & Ginni, 2015)
Orange G	Coaxial cylinder V: 1.5 L D: 35 mm, H: 300 mm Solid: iron oxide (BT4) D <sub>p</sub> : 0.42-0.59 mm P <sub>L</sub> : 6 g/L	pH: 3 T: 25 °C H <sub>2</sub> O <sub>2</sub> : 25 mg/L UV: 15 W, 365 nm	TOC: 78.9% Color: 92%	(Wang et al., 2015)
BPA	Cylindrical V: 1.5 L Solid: Iron oxide (BT4)	pH: 3 H <sub>2</sub> O <sub>2</sub> : 0.7 mmol/L HRT: 180 min UV: 15 W, 365 nm	TOC: 90%	(Li et al., 2015)
DMSO	Solid: D <sub>p</sub> : 0.42-0.5	pH: 3; Fe <sup>2+</sup> : 5 mM; H <sub>2</sub> O <sub>2</sub> : 32.5 mM HRT: 2 h	Degradation: 98% TOC removal: 34.38%	(Matira, Chen, Lu, & Dalida, 2015)
DMSO	Cylindrical glass V: 1.3 L D: 5.23 cm, H: 133 cm, Solid: SiO <sub>2</sub>	pH: 3 Fe <sup>2+</sup> : 5 mM H <sub>2</sub> O <sub>2</sub> : 60 mM HRT: 2 h	DMSO: 98%	(Bellotindos et al., 2014)
Phthalocyanine (PC)	Cylindrical Fiber glass H: 400 mm D: 25 mm Solid: Fe (II)/γ-Al <sub>2</sub> O <sub>3</sub> , P <sub>L</sub> : 60 g/L	pH: 2 – 4 UV light: 254 nm	PC: 95%	(Cheng et al., 2014)
Organic silicone wastewater	Cylindrical Plexiglass V: 3.92 L D: 8 cm H: 78 cm Solid: quartz D <sub>p</sub> : 0.5 – 0.8 mm	pH: 3.5 HRT: 60 min H <sub>2</sub> O <sub>2</sub> /Fe <sup>2+</sup> 13.6:1 Q: 3 mL/h	COD: 95% TOC: 85%	(Liu et al., 2014)
O-toluidine	Solid: SiO <sub>2</sub> ; D <sub>p</sub> : 0.46 – 0.55 mm	pH: 3 Fe <sup>2+</sup> : 1 mM; H <sub>2</sub> O <sub>2</sub> : 17 mM HRT: 120 min	Degradation: 100% COD removal: 62%	(Su, Fan, Anotai, & Lu, 2014)

Wang et al. (2015) studied the removal of an azo dye by a 3-phase FBF with waste iron oxide as a heterogeneous catalyst. The process achieved more than 92% decolorisation and 78.9% TOC removal under the conditions investigated (50 mg/L dye, 25 mg/L H<sub>2</sub>O<sub>2</sub>, 600 mg/L iron oxide and pH 3). The decolorisation was attributed to the homogeneous Fenton reaction while the heterogeneous Fenton was responsible for the TOC removal.

Aghdasinia et al. (2016) reported the degradation of Acid Yellow 36 (AY36) by FBF process. The effect of H<sub>2</sub>O<sub>2</sub>, initial concentration of AY36, pH and catalyst concentration on the process performance were investigated. The results showed that the most significant factor was the initial dye concentration, followed by pH and H<sub>2</sub>O<sub>2</sub> concentration. It is pertinent to point out that the authors used low dye concentrations (5 – 25 mg/L), which is quite lower than the concentrations typically encountered in real textile wastewater.

FBF process has been investigated for the degradation of acetaminophen. Luna et al. (2013) investigated the kinetic of degradation of Acetaminophen by a FBF. The process achieved up to 99.6% degradation of 5 mM acetaminophen under the following condition: pH 3, 25 mM H<sub>2</sub>O<sub>2</sub>, 0.5 mM Fe<sup>2+</sup> and 40 min of reaction time. The degradation followed a pseudo second-order reaction kinetics and increased as both Fe<sup>2+</sup> and H<sub>2</sub>O<sub>2</sub> were increased. However, scavenging effect was observed with excess H<sub>2</sub>O<sub>2</sub> concentration.

Briones et al. (2012) conducted an optimization study for the degradation of acetaminophen using FBF process. The authors investigated the optimum pH, Fe<sup>2+</sup> and H<sub>2</sub>O<sub>2</sub> concentration for acetaminophen degradation. The optimum operating parameters were initial pH: 3.22, Fe<sup>2+</sup>: 0.06 mM and H<sub>2</sub>O<sub>2</sub>: 19.87 mM. The ACT degradation reached 97.8% while iron removal from the solution reached 62.92%. The ACT degradation increased with increase in the concentrations of H<sub>2</sub>O<sub>2</sub> and Fe<sup>2+</sup> while the effect of pH was found to be more pronounced at low Fe<sup>2+</sup> concentration.

FBF process has been used for the degradation of BPA. Li et al. (2015) investigated the removal of BPA by FBF process with waste iron oxide as heterogeneous catalyst. The process was able to remove 90% of the initial TOC using 2 g/L iron oxide, 0.74 mmol/L  $\text{H}_2\text{O}_2$ , and pH 3 and 180 min reaction time. The interesting part of the study is that the waste iron oxide performed better than pure iron oxide, making the process economically attractive. In a similar study, Huang and Huang (2009) studied the mineralization of phenol using FBF process with iron oxide as heterogeneous catalyst. After 180 min reaction time, the process achieved 98% mineralization of phenol.

Muangthai et al. (2010) studied the degradation of 2,4-dichlorophenol (2,4-DCP) using FBF process and achieved degradation, COD and iron removal efficiencies of 99%, 61% and 14% respectively under optimum condition (pH 3, 100 g of  $\text{SiO}_2$ , 0.25 mM of  $\text{Fe}^{2+}$  and 10 mM of  $\text{H}_2\text{O}_2$ ). Although the performance the FBF was not much higher than the conventional Fenton in term of COD removal, FBF achieved higher iron removal, indicating its ability to reduce sludge generation through crystallization of iron oxide.

Anotai et al. (2010) studied the oxidation of aniline by FBF and electro-Fenton. The aniline oxidation was 70-97% in the FBF process and 80-95% in the electro-Fenton. Also, the TOC removal per  $\text{H}_2\text{O}_2$  was higher in the FBF process. In a similar study, Ratanatamskul et al. (2010b) studied the oxidation of 2,6-dimethylaniline using FBF and compared its performance with conventional Fenton process. Both  $\text{Fe}^{2+}$  and  $\text{H}_2\text{O}_2$  concentrations have a significant effect and can promote the degradation up to 100%.

Su et al. (2014) investigated the degradation of o-toluidine by FBF using  $\text{SiO}_2$  carriers and synthetic  $\text{Fe}/\text{SiO}_2$  as catalyst. Under optimum condition, 80% and 100% of the o-toluidine was degraded in 60 min by the  $\text{SiO}_2$  and  $\text{Fe}/\text{SiO}_2$  systems respectively in the pH range of 2-4. The removal efficiencies of COD in the  $\text{SiO}_2$  carriers and  $\text{Fe}/\text{SiO}_2$  catalyst systems were about 62% and 73%, respectively after 120 min. Also, Anotai et al. (2012b)

investigated the influence of process parameters on the removal of o-toluidine by FBF. The solution pH,  $\text{Fe}^{2+}$  and  $\text{H}_2\text{O}_2$  were found to be significant factor whereas the carrier loading was found to be insignificant. The optimal conditions were pH  $3\pm 0.5$ , 1 mM of  $\text{Fe}^{2+}$ , and 17 mM of  $\text{H}_2\text{O}_2$ , corresponding to o-toluidine and COD removals of 99.8% and 61.8%, respectively.

Matira et al. (2015) investigated the removal of DMSO by FBF process and obtained a removal efficiency of 95.22% and 34.38% COD removal under optimum conditions (pH 3, 5 mM  $\text{Fe}^{2+}$ , 32.5 mM  $\text{H}_2\text{O}_2$ , 68.97 g/L  $\text{SiO}_2$  and 2h reaction time). The authors did not observe any  $\text{Fe}^{2+}$  scavenging effect on the degradation of DMSO within the range of  $\text{Fe}^{2+}$  concentrations investigated. Although it is generally known that the rate of  $\text{OH}^\bullet$  production increases with increased in  $\text{Fe}^{2+}$  concentration, excessive  $\text{Fe}^{2+}$  can lead to scavenging of the  $\text{OH}^\bullet$  thereby decreasing their availability (Muangthai et al., 2010). On the other hand, increasing the  $\text{H}_2\text{O}_2$  beyond some amount led to scavenging effects.

In another study for DMSO degradation, Bellotindos et al. (2014) investigated the effects of operational parameters on the FBF performance. The authors studied the effect of  $\text{Fe}^{2+}$ ,  $\text{H}_2\text{O}_2$ , and pH on the degradation of the DMSO as well as COD and TOC removals. The highest DMSO removal, 98%, was obtained at pH 3, 60 mM of  $\text{H}_2\text{O}_2$  and 5 mM of  $\text{Fe}^{2+}$ . All the operating parameters have positive effects on the DMSO degradation in the following order  $\text{Fe}^{2+} > \text{H}_2\text{O}_2 > \text{pH}$ . Compared with convention Fenton oxidation, the process achieved more DMSO removal (about 43%). Although the authors achieved a relatively higher DMSO degradation compared to Chen et al. (2016), the amount of  $\text{H}_2\text{O}_2$  used is nearly twice. Similarly, Matira et al. (2015) achieved up to 95.22% DMSO degradation using only 32.5 mM  $\text{H}_2\text{O}_2$  and 5 mM of  $\text{Fe}^{2+}$ .

Su et al. (2013) studied the removal of MEA from aqueous solution by FBF process. Under optimum condition (3 mM  $\text{Fe}^{2+}$  and 50 mM  $\text{H}_2\text{O}_2$ , pH 3, 1 h reaction time), MEA

removal efficiency reached 76%. The performance of the FBF was 15 – 20% higher than conventional Fenton. In another study, Anotai et al. (2012a) achieved a higher removal efficiency (98.9%) but at a higher catalyst concentration (5 mM Fe<sup>2+</sup> and 60 mM H<sub>2</sub>O<sub>2</sub>) and longer reaction time (2 h).

Liu et al. (2014) treated recalcitrant organic silicone wastewater using an FBF process with different carriers. Under the optimum condition, the process could remove 95% and 85% of the initial COD and TOC respectively. The removal rates of the COD and TOC were found to increase by 20% and 15% respectively, compared to the conventional Fenton. XRD analysis indicated the presence of iron oxide on the surface of the carriers, indicating the crystallization ability of the process. Thus, the total iron removal was higher in the FBF process.

In this section, the applications of FBF process to remove recalcitrant pollutants have been reviewed. It is evident from the reviewed literature that FBF process exhibited superior performance compared to conventional Fenton and that sludge generation is reduced through the crystallization of iron oxide on the fluidized carriers. Most of the reported studies have been on the process performance and the effect of operational parameters on the performance. However, the effect of the fluidized solids have not been fully studied.

## **2.11 Summary of Literature Review**

Drawbacks such as the requirement of acidic condition and sludge generation have hindered the practical applications of homogeneous Fenton oxidation in wastewater treatment. Addressing these limitations is therefore one of the important research topics in the field of advanced oxidation processes. This is evident in the increasing number of publications on approaches such heterogeneous Fenton oxidation, FBF process and homogeneous Fenton at circumneutral pH. Among these approaches, FBF process has

been widely investigated as an alternative to reduce sludge generation and enhance the performance of Fenton oxidation. The reviewed literature has shown that FBF can reduce the sludge generation and improve the performance of conventional Fenton oxidation.

Although the use of FBF process can address some of the limitations of Fenton oxidation, there are some challenges that must be addressed for successful application of the process. The fluidized carriers bring complexity into the relatively simple Fenton process. Thus, process optimization is one of the major challenges in FBF process. The working of FBR is largely empirical, making process optimization and control challenging. Currently, only a few publications have appeared on process optimization in FBF process where only the Fenton-based parameters are considered. The effect of the fluidized carrier is largely neglected, perhaps due to the inherent complexity of the process. Although the experimental study of the effect of carriers could be laborious, appropriate modeling and simulation techniques can be useful in this perspective.

The major objective of FBF process is to reduce the sludge generation of homogeneous Fenton oxidation through the use of the fluidized carriers. Thus, the effect of the fluidized carrier is an important consideration in process design and development. Currently,  $\text{SiO}_2$  is the most commonly used carrier and its effect on the process performance has not been investigated. In addition, the possible interactions between the fluidized carriers, Fenton's reagent and organic pollutants have not been studied. Consequently, it not clear how the fluidized carriers may interact with the classical Fenton reactions. These information are necessary for successful application of the FBF process since the effectiveness of the process can be enhanced through the manipulation of the fluidized carriers.

This study is therefore aimed at filling some of the research gaps highlighted above. Specifically, the effect of operational parameters on the performance of FBF process and the interaction of the fluidized carrier with Fenton's reagent and organic pollutants are

investigated with the aim of enhancing the effectiveness of FBF process for recalcitrant wastewater treatment. To further enhance the process, the feasibility of using a low-cost material as an alternative carrier will be investigated.

University of Malaya

## CHAPTER 3: METHODOLOGY

### 3.1 Introduction

This chapter describes the chemicals, equipment and procedures adopted to achieve the aim and objectives of this study. Figure 3.1 depicts the activities that were conducted to achieve the research objectives. It describes the detailed chemicals, equipment, analyses and procedure for the experimental approach adopted in the study. It also gives the detailed information about theoretical approach used for the quantum chemical calculations.

### 3.2 Chemicals and Materials

Table 3.1 provides details of chemicals and materials used in the study. All chemicals used were of analytical grade and were used without further purification.

**Table 3.1 Chemicals and materials used**

Material	Properties	Use(s)	Supplier
NaOH	Molecular weight:	pH adjustment	Sigma-Adrich
H <sub>2</sub> O <sub>2</sub>	Molecular weight: Content: 33 %	Oxidant in Fenton reaction	Sigma-Adrich
FeSO <sub>4</sub> .7H <sub>2</sub> O	Molecular weight:	Catalyst in Fenton reaction	Sigma-Adrich
H <sub>2</sub> SO <sub>4</sub>	Molecular weight:	pH adjustment	Sigma-Adrich
SiO <sub>2</sub>	Particle size: 0.2 – 1 mm	Carrier in FBF process	Sigma-Adrich
Reactive black 5	Molecular weight:	Model pollutant	Sigma-Adrich
PKSGAC	Activation: physical Particle size: 0.5 – 1.7 mm	Carrier in FBF process	Pacific Activated Carbon
Glass beads	Particle size: 2 mm	Support material in FBF process	Sigma-Adrich
Deionized water		Sample preparation	-
COD kits		Analysis of pollutant degradation	Sigma-Adrich

All chemicals were obtained from Sigma-Adrich Company, except PKSGAC, which was supplied by Pacific Activated Carbon, Malaysia. The activated carbon was produced

through a physical activation process. The activated carbon was subsequently washed with distilled water to remove impurities and then dried at 110 °C for 24 h.

### **3.3 Characterization of Carriers**

#### **3.3.1 Particle Size Distribution**

The particle size distributions of the carriers were measured using a Malvern Mastersizer 2000 (Malvern Instrument, Ltd) with a normal sensitivity and using water as the dispersant.

#### **3.3.2 Zeta Potential**

Zeta potential is an indirect measure of the net charge on the surface of particles and is an important parameter for understanding the surface interactions between molecules. The zeta potential of the carriers was measured using Malvern Zetasizer Version 6.20 (Malvern Instruments Ltd) with water as dispersant. The zeta potential was recorded as an average of 100 runs at 2.00 mm measurement position using attenuation factor of 6. The results were recorded for different pH in order to determine the point of zero charge.

#### **3.3.3 Brunner-Emmet-Taylor Surface Analysis**

The surface area and porosity of the carrier carbon was determined through N<sub>2</sub> adsorption-desorption isotherm at 77 K on a Micrometrics ASAP 2020 (TRISTAR II 3020 Kr) surface area analyzer using Brunauer-Emmett-Teller and Barrett-Joyner-Halenda (BJH) methods.

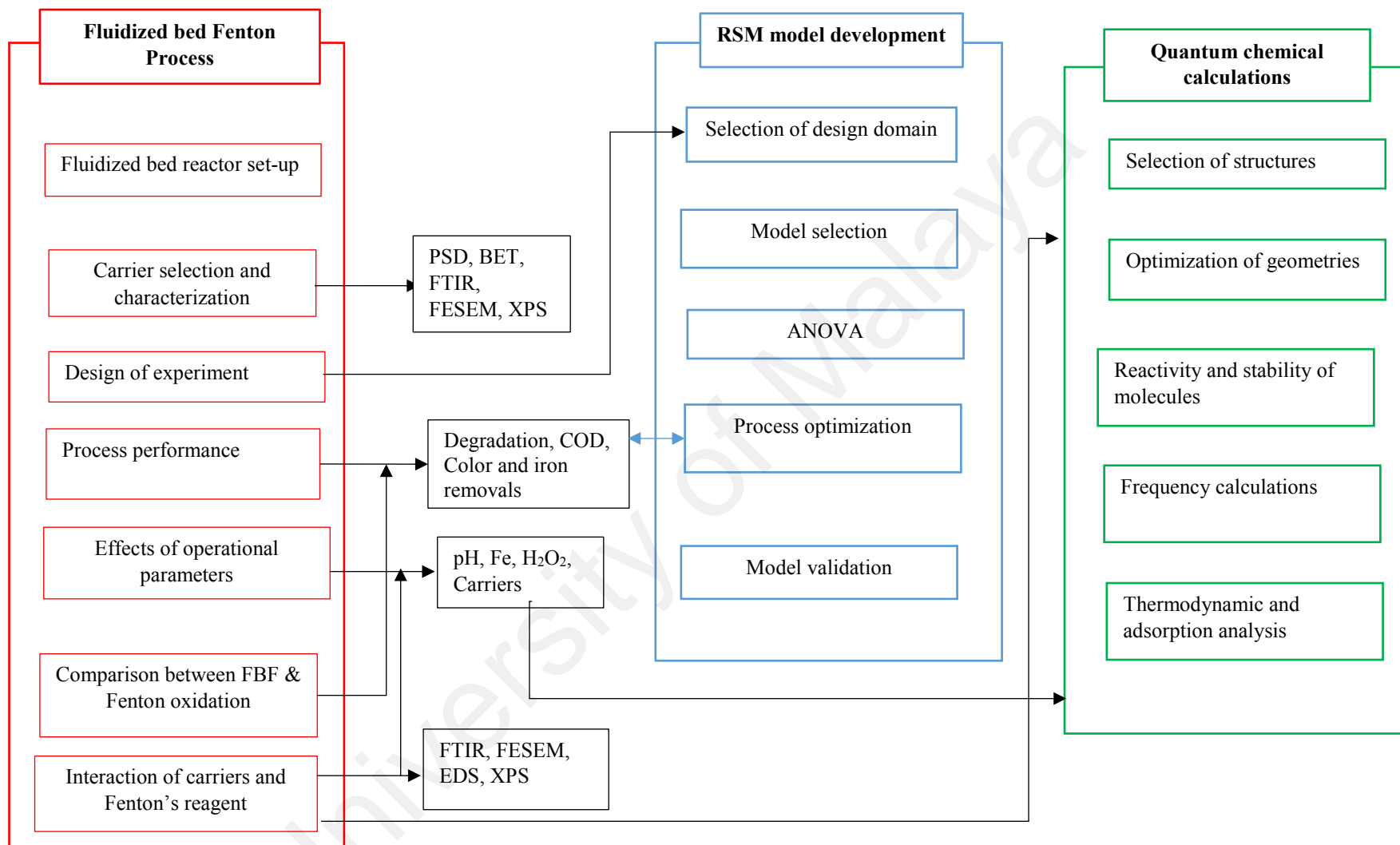


Figure 3.1: Flowchart of methodology

### **3.3.4 Field Emission Scanning Electron Microscopy/Energy Dispersive X-ray**

The surface morphology of the carriers before and after the treatment was investigated by Field Emission Scanning Electron Microscope (FESEM) using a Cross-Beam FIB workstation equipped with GEMINI FESEM Colum (ZEISS Gemini). The elemental compositions of the carriers before and after the fluidized bed Fenton experiments were examined by the Energy Dispersive X-ray (EDX) Spectroscopy using GEMINI EDAX-ZEISS.

### **3.3.5 Fourier Transform Infrared Spectroscopy**

To investigate the change in the surface functional groups of the carriers after the fluidized bed Fenton process, the surface characteristics of the carriers before and after the treatment was examined through Fourier Transform Infrared Spectroscopy (FT-IR) using a Perkin Elmer Spectrometer (Frontier) with light in the range of 500 – 4000  $\text{cm}^{-1}$ . The spectra of the carriers before and after the fluidized bed Fenton process were then compared.

## **3.4 Experimental Setup**

### **3.4.1 Fluidized-Bed Fenton Experiments**

The FBR consisted of a storage tank, recirculation section, magnetic pump and a flow meter (Figure 3.2). The reactor is a glass column of 1.35 L capacity. The magnetic pump was used to pump the wastewater solution from the storage tank to the reactor at a predetermined flow rate. Glass beads (2 mm) was packed at the bottom of the reactor to act as a distributor. The carriers, either  $\text{SiO}_2$  granules or PKSGAC were placed above the glass beads to a known height. Internal recirculation was used to control the fluidization of the carriers to the desired level. The wastewater was placed in the storage tank and the pH was adjusted using NaOH or  $\text{H}_2\text{SO}_4$ . The wastewater was then pumped from the

bottom of the glass column where the carriers were fluidized. After the equalization of the fluidized media, the desired amount of  $\text{Fe}^{2+}$  was added into the system in form of  $\text{FeSO}_4 \cdot 7\text{H}_2\text{O}$ . The addition of the required  $\text{H}_2\text{O}_2$  initiated the Fenton reaction. Samples were collected at pre-determined intervals and the pH of the sample was raised above 10 with NaOH to quench the  $\text{H}_2\text{O}_2$  (Chou et al., 1999). The samples were allowed to settle and then filtered through a  $0.45 \mu\text{m}$  filter before analysis.

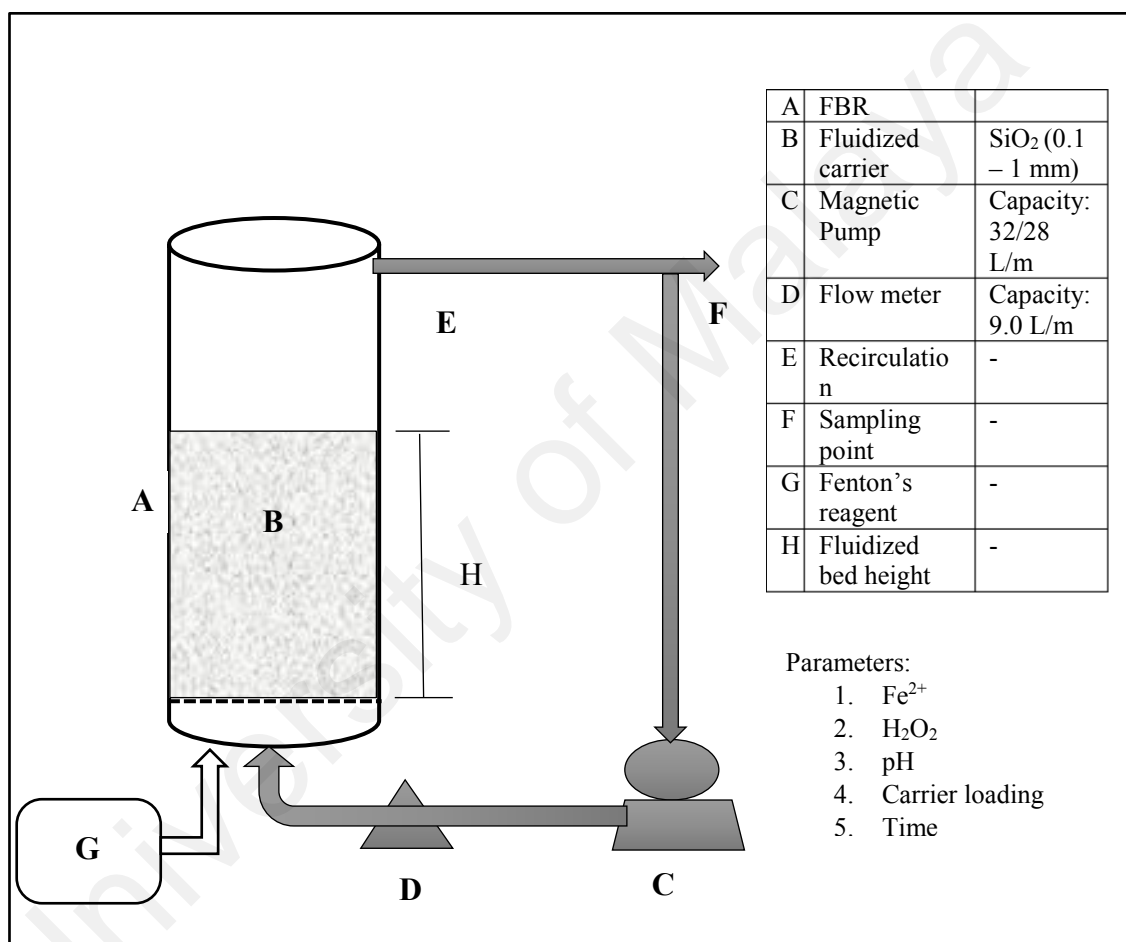


**Figure 3.2: Schematic of the fluidized bed Fenton process**

### 3.4.2 Conventional Fenton Experiments

For the conventional Fenton, Erlenmeyer flask (500 mL) was used for the degradation of the model RB5. Synthetic wastewater with a known concentration of RB5 was placed in the flask, followed by pH adjustment using NaOH or  $\text{H}_2\text{SO}_4$ . A known quantity of  $\text{FeSO}_4 \cdot 7\text{H}_2\text{O}$  was added into the mixture followed by the addition of  $\text{H}_2\text{O}_2$  which initiated

the Fenton oxidation. Magnetic stirrer was used to provide the necessary mixing at 250 rpm. Samples were collected at pre-determined intervals and NaOH was added to quench the reaction. After settling, the samples were filtered through a 0.45  $\mu\text{m}$  filter and then taken for analysis.

### **3.5 Reactor Hydrodynamics**

The main focus of this study is on the interactions in the fluidized bed Fenton process. Although the effect of reactor hydrodynamics was outside the scope of the study as highlighted in Chapter 1, preliminary studies were conducted to establish the minimum superficial velocity and the fluidization patterns of the carriers considered.

The carriers considered were  $\text{SiO}_2$  with particle size of 0.2 – 1 mm and PKSGAC with particle size of 0.5 – 1.7 mm, which falls under Group B and Group D of Gerald particle classification. The theoretical minimum fluidization velocity of the particles was calculated according to Equation 2.9 (Alfredo et al., 2013).

Since there is an overlap in the ranges of particle size, the same minimum superficial fluid velocity was considered to allow proper comparison between the two carriers. During the main experiments, the superficial velocity was kept constant to provide fluidization of 50% in each case.

### **3.6 Experimental Design and Process Optimization**

Design Expert software (Stat-Ease, Inc., USA; Version 8.0.7.1) was used to design the experiments through response surface methodology (RSM). RSM is a multivariate statistical technique that is based on fitting experimental data to a polynomial equation. It is normally used in experimental design where a response or a set of responses are influenced by some variables and an optimum solution is desired. The major advantage

of using RSM is that the interaction of these variables can be studied with a lesser number of experimental runs compared to the conventional one-variable-at-a-time experimental design (Bezerra, Santelli, Oliveira, Villar, & Escaleira, 2008; Mu'azu et al., 2018).

The steps involved in applying RSM for experimental designs and optimization of processes are depicted in Figure 3.3. These include selection of process parameters (independent variables) that have major effects on the FBF process, selection of experimental design domain, conducting the experiments according to the selected experimental domain, fitting the experimental data to the selected model, evaluating the fitness of the model, obtaining the optimum values of the studied parameters and validation experiments.

### **3.6.1 Selection of Design Domains**

RSM procedure requires that the minimum and maximum values of factors are established and the design domain defined (Tarley et al., 2009). Selection of experimental design depends on the type of response that is expected. The first-order models are routinely employed to determine response surface that are linear with respect to all the factors involved. Although this simple model can represent linear response, most of the applications of RSM involves variables with curvature due to interactions of the independent variables. Consequently, higher order models, such as second-order model, are mostly used in RSM applications.

Central composite design (CCD) is among the most widely used design domain. It is based on two-level full/fractional factorial design having additional points and at least one central point in the experimental domain (Tarley et al., 2009). In other words, CCD considers a two-level full factorial design ( $2^f$  experiments), having a star design ( $2^f$  experiments) and a central point, requiring  $N = 2^f + 2f + 1$  experiments to examine the  $f$  factors (Dejaegher & Vander Heyden, 2011). The points of the full factorial design are

situated at the factor levels  $-1$  and  $+1$ , those of the star design at the factor levels  $0$ ,  $-\alpha$  and  $+\alpha$ , and the center point at the factor levels  $0$ . Depending on  $\alpha$  value, different types of CCD can be obtained. The first is face-centered CCD (FCCD) which assumes  $|\alpha| = 1$  and examines the factors at three levels. The other, circumscribed CCD (CCCD) with  $|\alpha| > 1$  examines the factors at five levels. Another type is the so-called rotatable CCCD, where the  $\alpha$  level is  $|\alpha| = (2f)^{1/4}$ , i.e. 1.41 and 1.68 for 2 and 3 factors, respectively.

A CCD with  $k$  factors ( $x_1 \dots \dots x_k$ ) can be characterized by the following (Ferreira et al., 2007):

- i. A factorial (or cubic) design, containing a total of  $n_{\text{fact}}$  points with coordinates  $x_i = -1$  or  $x_i = +1$ , for  $i = 1, \dots \dots, k$ ;
- ii. An axial part formed by  $n_{ax} = 2k$  points with all their coordinates null except for one that is set equal to a certain value  $\alpha$  (or  $-\alpha$ );
- iii. A total of  $n_c$  runs performed at the center point, where, of course,  $x_i = \dots x_k = 0$

Building a CCD requires the specification of the three parts described above. This includes determining the number of cubic points, the value of  $\alpha$  and the number of replications are to be at the center point. The specification of these will determine the nature of the CCD as explained previously

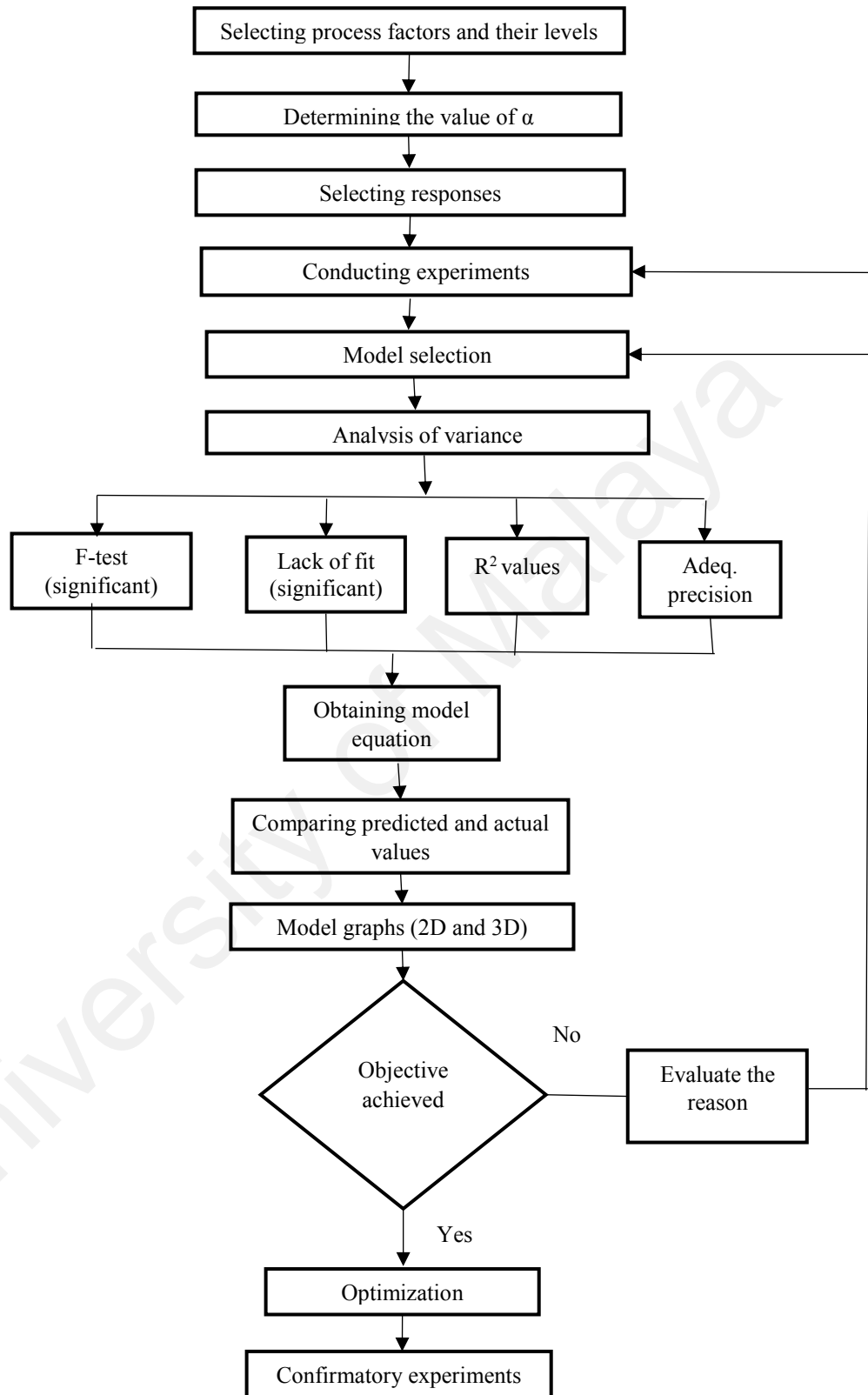


**Figure 3.3 Central composite design flowchart**

Due to the advantages of FCCD, it was used as the design domain in this study. The FC-CCD is based on three levels of variable, minimal ( $X_i$ , min), mid-point ( $X_i$ , mid) and maximal ( $X_i$ , max), corresponding to -1, 0 and +1 of each variable (Mu'azu et al., 2018; Rai, Mohanty, & Bhargava, 2016). Thus, four operating parameters, namely [Dye]/[Fe<sup>2+</sup>] (wt/wt), [Fe<sup>2+</sup>]/[H<sub>2</sub>O<sub>2</sub>] (wt/wt) pH and time were studied at three different levels (4<sup>3</sup>) following the FC-CCD (Raheem et al., 2018). As shown in Table 3.2, these variables are varied at three different levels (-1, 0, +1). The responses were the color removal ( $Y_1$ ) and COD removal ( $Y_2$ ), which are fitted to a second order model according to Equation 3.1 (Mu'azu et al., 2018).

$$Y = \beta_0 + \sum_{i=1}^k \beta_i x_i + \sum_{i=1}^k \beta_{ii} x_i^2 + \sum_{i=1}^{k-1} \sum_{j=2}^k \beta_{ij} x_i x_j + \varepsilon \quad (3.1)$$

Unlike the common practice of studying the effects of Fe<sup>2+</sup> and H<sub>2</sub>O<sub>2</sub> concentrations, their dimensionless ratios of (Dye/Fe<sup>2+</sup> and Fe<sup>2+</sup>/H<sub>2</sub>O<sub>2</sub>) were considered in this study. Previous studies have adopted this approach due to the significance of these ratios (Chen et al., 2015). The range of the variables were selected based on previous studies (Asghar, 2016) and preliminary experiments.

**Table 3.2: Experimental ranges of the process variables**

Independent variables	Coded	Low level (-1)	Medium level (0)	High level (+1)
[Dye]/[Fe <sup>2+</sup> ], (wt/wt)	A	10	30	50
[Fe <sup>2+</sup> ]/[H <sub>2</sub> O <sub>2</sub> ], (wt/wt)	B	5	15	25
pH	C	3	6	9
Time (min)	D	15	37.5	60

The obtained experimental results were input into the DOE and analyzed using the response surface regression procedure in the Design Expert. Second order polynomial equations were used to fit the regression coefficients and ANOVA was used to test the significance of the models. Process optimization was performed to maximize the color and COD removals by the fluidized bed Fenton process.

### 3.7 Analytical Methods

#### 3.7.1 Inductively Couple Plasma

To compare the iron removal by the conventional Fenton and fluidized bed Fenton process, the iron concentration was measured using inductively couple plasma mass spectroscopy (ICP, Optima 7000 DV, Perkin Elmer).

#### 3.7.2 Chemical Oxygen Demand (COD)

The COD of the initial and treated samples were measured according to the Standard Methods for the Examinations of Water and Wastewater (APHA, 1992). 3 ml of samples were added to a prepared COD test cells purchased from Merck and Co. The cells were then heated at 148 °C for 2 hours using a thermo-reactor (Spectroquant® TR 420). The COD was measured using a UV Spectrophotometer (Spectroquant® Pharo 300, Merck, Germany) at 254 nm. The COD removal was calculated as according to Equation 3.2.

$$\% \text{ COD Removal} = \frac{\text{COD}_o - \text{COD}_f}{\text{COD}_o} \times 100 \quad (3.2)$$

#### 3.7.3 Color Removal

The color of the dye solution was measured as an absorbance at 595 nm using a Spectrophotometer (Spectroquant® Pharo 300, Merck, Germany). The percent color removal is reported as the difference between the initial absorbance ( $A_o$ ) and absorbance at a time, t ( $A_t$ ) as shown in Equation 3.3.

$$\% \text{ Color removal} = \frac{A_o - A_t}{A_o} \times 100 \quad (3.3)$$

### 3.7.4 pH Measurement

pH measurements were performed using a digital pH meter (CyberScan pH 300, EUTECH Instruments). All measurements were done at 25 °C. H<sub>2</sub>SO<sub>4</sub> and NaOH were used for the pH adjustment.

### 3.8 Quantum Computational Method

Quantum chemical calculations are used to complement experimental investigations through theoretical prediction of complex processes (Hehre, 2003). With quantum chemical calculations, properties of molecules such as chemical structure and geometry, reactivity, and stability can be accurately predicted. Different models are used to perform quantum simulations. The most common among these, is the density functional models or density functional theory (DFT).

To study the interaction of SiO<sub>2</sub>, Fenton reagents and the organic pollutant, density functional theory (DFT) was applied. First, identification of possible molecular structures (reactants, intermediates and products) was made by considering the study conducted by Zegliński, Piotrowski, & Piekoś, (2006). Table 3.3 shows the molecular structures and other details of the species used in this study. GaussView 05 was utilized to develop ab initio geometries of the studied species while Gaussian 09W software package was employed to perform the quantum chemical calculations.

The geometries of the considered structures were fully optimized at Beck's 3-parameter Lee-Yang-Parr (B3LYP) level of study with 6-311++G (d,p) as a basis set. The generated equilibrium optimized geometries were then used to obtain the total electronic energy (E), HOMO energy, LUMO energy, HOMO-LUMO energy gap and dipole moment. Subsequently, these quantum parameters were utilized to calculate the global hardness ( $\eta$ ), global softness (S), electronegativity ( $\chi$ ), chemical potential ( $\mu$ ) and electrophilicity index ( $\omega$ ). The computation of these parameters is important since it helps to study the reactivities and interactions of molecules (Liu, Chen, Zhang, & Li, 2014). In this regard,

high values of HOMO exhibit the ability of a molecule to accept electrons while low values of LUMO show the propensity of a molecule to accept electrons.

**Table 3.3: Details of the chemical species for quantum analysis**

Molecule	Structure	Chemical Formula	Molecular weight (g/mole)
RB5		$C_{26}H_{21}N_5Na_4O_{19}S_6$	991.789
Disilicic Acid (Silica Gel)		$H_2O_5Si_2$	174.211
Ferrous ion	$Fe^{2+}$	$Fe^{+2}$	55.845
Ferric ion	$Fe^{3+}$	$Fe^{+3}$	55.845
Hydrogen peroxide	$HO-OH$	$H_2O_2$	34.0147
Protonated hydrogen peroxide		$H_3O_2$	35
Hydronium Ion		$H_3O^+$	19.0232
Hydroxyl radical	$OH^\bullet$	$HO^\bullet$	17.007
Water		$H_2O$	18.01528

To determine the thermodynamic feasibility of reacting systems, frequency calculations were also performed at the same level of study. From these, thermodynamic parameters like entropy, enthalpy, Gibb's free energy and heat of formation were obtained. The free energy values provide a way to determine the thermodynamic feasibility of chemical reactions. Negative values for  $\Delta G$  and  $\Delta H$  indicate that the reaction is thermodynamically feasible and spontaneous. The same concept was used to investigate the interaction of

silica with reacting species. The description of the quantum chemical parameters and thermodynamic parameters are provided below.

### 3.8.1 Quantum Chemical Parameters

In quantum simulation, different parameters are used to predict the behavior and chemical reactivity of molecular species. The output of quantum simulation include important information on molecules like highest occupied molecular orbital (HOMO) energy, lowest unoccupied molecular orbitals (LUMO) energy and dipole moment (Asghar, 2016). From these basic information, other quantum chemical parameters including HOMO-LUMO energy gap, ionic potential (IP), electron affinity (EA), global hardness ( $\eta$ ), global softness ( $\sigma$ ), electronegativity ( $\chi$ ), electrophilicity index ( $\omega$ ) and chemical potential ( $\mu$ ) are computed.

#### (a) HOMO-LUMO energy

The HOMO and LUMO energies are directly related to IP and EA and were computed according to Equation 3.4 and Equation 3.5 (Wolinski, Hinton, & Pulay, 1990):

$$IP = -E_{HOMO} \quad (3.4)$$

$$EA = -E_{LUMO} \quad (3.5)$$

#### (b) Global hardness/softness

The hardness ( $\eta$ ) of a molecule is a qualitative indication of the extent of its electron cloud distortion in an electric field (Pilli, Banerjee, & Mohanty, 2015). On the other hand, softness ( $\sigma$ ) is a reciprocal of the hardness and denotes the susceptibility of a molecule to be deformed mechanically. These were computed according to Equation 3.6 and Equation 3.7:

$$\eta = \frac{(E_{LUMO} - E_{HOMO})}{2} = \frac{(IP - EA)}{2} \quad (3.6)$$

$$\sigma = \left(\frac{1}{\eta}\right) = \left(\frac{2}{E_{LUMO}-E_{HOMO}}\right) = \left(\frac{2}{IP-EA}\right) \quad (3.7)$$

**(c) Electronegativity**

Electronegativity is the propensity of a molecule to attract electrons which can be quantified through HOMO and LUMO energies according to Equation 3.8 (Pearson, 1986):

$$\chi = -\left(\frac{E_{HOMO}-E_{LUMO}}{2}\right) = \left(\frac{IP+EA}{2}\right) \quad (3.8)$$

**(d) Chemical potential**

The chemical potential of a molecule represents the tendency of an electron to escape and is and can be computed according to Equation 3.9 (Kavitha, Sundaraganesan, & Sebastian, 2010).

$$\mu = \left(\frac{E_{HOMO}-E_{LUMO}}{2}\right) = -\left(\frac{IP+EA}{2}\right) \quad (3.9)$$

**(e) Electrophilicity index**

Electrophilicity index ( $\omega$ ) is the tendency of a substance to accept electrons from its surrounding and can be calculated by Equation 3.10 (Parr, Szentpály, & Liu, 1999).

$$\omega = \left(\frac{\mu^2}{2\eta}\right) = \left(\frac{\left(\frac{E_{HOMO}-E_{LUMO}}{2}\right)^2}{E_{LUMO}-E_{HOMO}}\right) = \left(\frac{\left(\frac{IP+EA}{2}\right)^2}{IP-EA}\right) \quad (3.10)$$

### 3.8.2 Thermodynamic Parameters

Besides the chemical parameters, quantum chemical calculations can also be used to compute some thermodynamic properties of molecular species. In this case, vibrational frequencies in conjunction with molecular geometry are used to calculate the thermodynamic quantities of molecules. These vibrational frequencies are due to the

interatomic motion within the molecule and depend on the second derivative of energy with respect to atomic structure (Hehre, 2003). The commonly calculated thermodynamic parameters include entropy, enthalpy, heat energy value, dipole moment and Gibbs free energy. The necessary connections among these quantities can be provided by the standard thermodynamic relationship:

$$\Delta G = \Delta H - T\Delta S \quad (3.11)$$

$$\Delta H = \Delta E - P\Delta V \quad (3.12)$$

Alternatively,

$$\Delta_r H^\circ(298K) = \sum_{prod} \Delta_f H_{prod}^\circ - \sum_{react} \Delta_f H_{react}^\circ \quad (3.13)$$

$$\Delta_r G^\circ(298K) = \sum_{prod} \Delta_f G_{prod}^\circ - \sum_{react} \Delta_f G_{react}^\circ \quad (3.14)$$

These thermodynamic quantities provide better understandings on the nature of interaction and feasibility of chemical reactions under certain conditions.

### 3.9 Safety Measures

The material safety data sheet (MSDS) shows that some of the chemicals used in this study can be hazardous. For the safety of the person handling these chemicals, appropriate precautionary measures were taken as highlighted in Table 3.4. Consequently, all chemicals were stored in a storeroom at temperature not above 30 °C and proper ventilation was maintained. In addition, during experiments, appropriate protections such laboratory coat, latex gloves and protective glasses were used to prevent any accident. Proper hand washing, and equipment cleaning were ensured after experiments. The disposal of residual chemicals and treated samples were in accordance with the established procedure.

**Table 3.4: Safety measures**

<b>Chemical</b>	<b>Comment on hazard</b>	<b>Safety measures</b>
H <sub>2</sub> O <sub>2</sub>	<ul style="list-style-type: none"><li>• Hazardous to skin/eye contact and ingestion</li><li>• Over-exposure by inhalation may cause respiratory irritation</li></ul>	<ul style="list-style-type: none"><li>• The container was kept in a dry, cool and well-ventilated area away from sources of ignition and combustible materials</li><li>• Lab-coat, hand gloves and goggles were used to avoid contact with skin and eyes</li></ul>
FeSO <sub>4</sub> .7H <sub>2</sub> O	<ul style="list-style-type: none"><li>• Irritant to skin/eye contact</li><li>• Hazardous in case of swallow or inhalation</li><li>• Toxic to liver, kidney and cardiovascular system</li></ul>	<ul style="list-style-type: none"><li>• Lab-coat and hand globes were used while handling the chemical</li><li>• Contact with skin and eye was avoided</li><li>• The container was kept away from incompatibles materials</li></ul>
NaOH	<ul style="list-style-type: none"><li>• Very hazardous in case of skin and eye contact</li><li>• Very hazardous in case of inhaling and ingestion</li></ul>	<ul style="list-style-type: none"><li>• Contact with skin and eyes was avoided using goggles and hand globes</li><li>• The container was kept away from incompatibles such as oxidizing and reducing agents</li></ul>
H <sub>2</sub> SO <sub>4</sub>	<ul style="list-style-type: none"><li>• Very hazardous in case of skin and eye contact</li><li>• Very hazardous in case of inhaling and ingestion</li><li>• Severe over-exposure can result in death</li></ul>	<ul style="list-style-type: none"><li>• The container was kept locked up in a dry place</li><li>• Contact with body was avoided using lab-coat, splash goggles and hand globes</li><li>• The chemical was kept away from incompatible materials</li></ul>
SiO <sub>2</sub>	<ul style="list-style-type: none"><li>• Slightly hazardous in case of skin and eye contact (irritant)</li><li>• Slightly hazardous in case of ingestion and inhalation.</li></ul>	<ul style="list-style-type: none"><li>• Contact with body was prevented using lab-coat and hand globes</li><li>• The container was kept tightly closed in a cool, well-ventilated area</li></ul>

## CHAPTER 4: PERFORMANCE OF FLUIDIZED BED FENTON PROCESS

This chapter discusses the performance of FBF process in degrading a model recalcitrant pollutant, RB5. The flow of the discussion is based on Figure 4.1 It covers the performance of the FBF process in removing color and COD from the synthetic dye solution, degradation mechanism, kinetic of COD removal, effect of operational parameters, process optimization and performance comparison between FBF process and conventional Fenton oxidation.

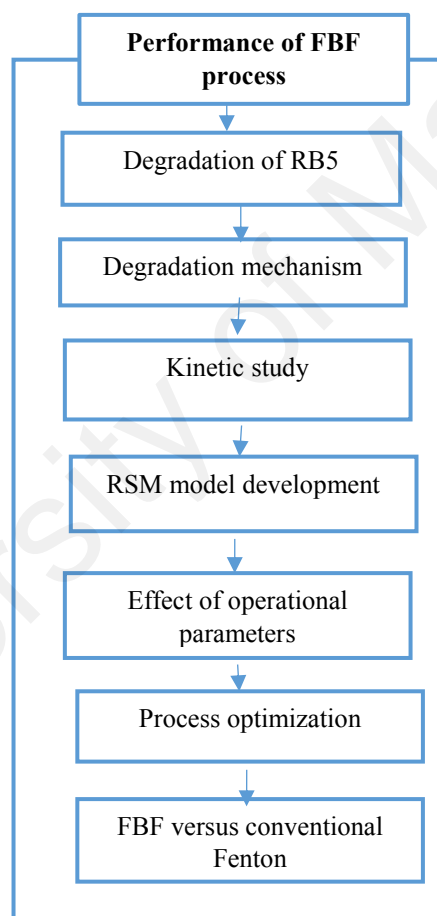


**Figure 4.1: Steps in evaluating fluidized bed Fenton process**

### 4.1. Degradation of Reactive Black 5

The degradation of the RB5 was monitored based on the COD and color removal from the synthetic dye solution. The initial color of the dye based on the absorbance at 595 nm

was found to be 1.38 while the initial COD was 400 mg/L. While the color removal represents the degradation of the dye, the COD removal gives a measure of the extent of mineralization of the dye. Figure 4.2 and Table 4.1 show the rate of color removal and COD removal over 60 min of FBF process.

**Table 4.1:** Percentage COD and color removal

Time	COD removal (%)	Color removal (%)
5	1.75	91.93
10	54.25	94.48
20	65.25	97.49
30	65.75	98.13
40	66.75	98.37
50	68.75	98.55
60	69.75	98.44

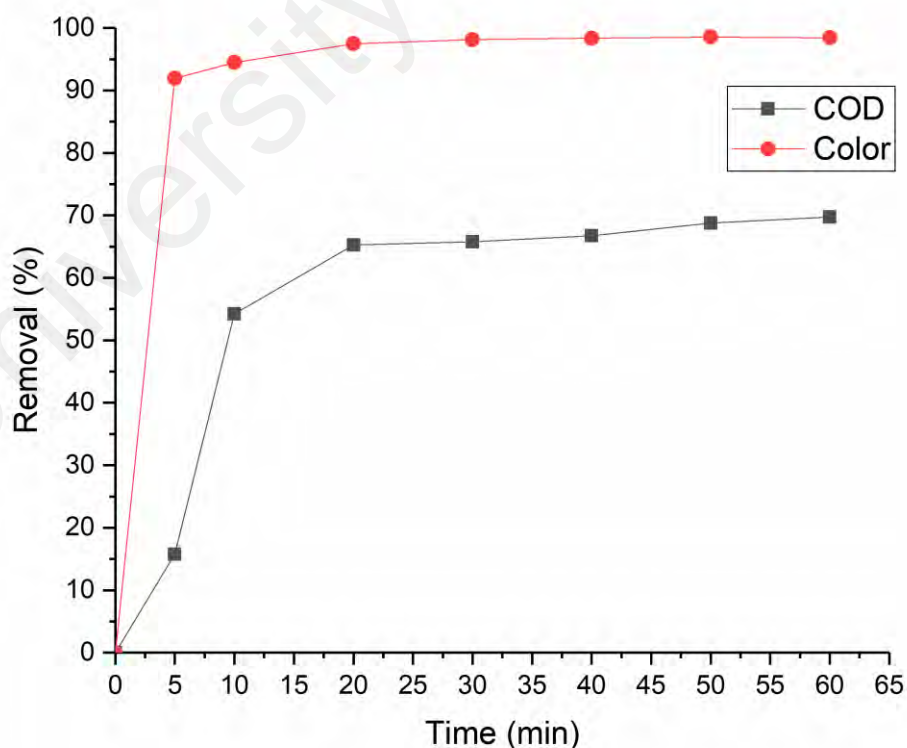


**Figure 4.2:** COD and color removals (Experimental conditions: carrier loading = 30 g, [Dye/Fe<sup>2+</sup>] = 10, [H<sub>2</sub>O<sub>2</sub>/Fe<sup>2+</sup>] = 25, pH = 3)

The color removal occurred very fast and more than 90% color removal was obtained within the first 5 min of the FBF process. There was no significant difference between the color removals at the two extreme periods. For the COD removal, however, only about 15% removal was achieved at the end of 5 min. The COD removal then rose sharply to 54% after 10 min. At the end of 60 min, the COD removal was about 70%.

A molecule of RB5 comprises H-Acid (1- amino-8-hydroxynaphthalene-3,6- disulfonic acid) and two molecules of vinyl sulfone, VS (4-aminophenyl sulfonyl- $\beta$ -hydroxy ethyl sulfato ester sodium salt), which are joined through azo (-N=N) bonds (Patel, Ruparelia, & Patel, 2011). These azo bonds are electron-deficient groups and can be easily reduced into corresponding amines, resulting in the decolorisation of the dye. Thus, two absorption bands at 599 nm and 388 nm commonly characterized RB5. The peak at 595 nm corresponds to the color of the dye and its disappearance represents decolorisation of the dye (Vasconcelos, Ponce-De-León, Nava, & Lanza, 2016). On the other hand, the peak at 388 nm represents the aromatic components and its disappearance indicates degradation of the aromatic compounds (Ersöz, 2014).

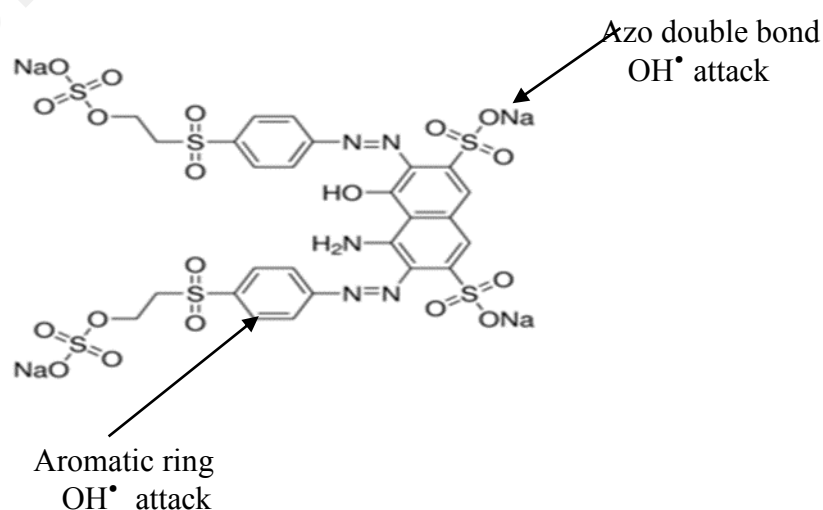


**Figure 4.3: Degradation of Reactive Black 5**

During Fenton oxidation,  $\text{OH}^\bullet$  attacks the  $\text{N}=\text{N}$  bonds, destructing the conjugated  $\pi$  systems, leading to a rapid color removal from the dye (Nordin et al., 2017). Since the azo bonds are easily broken, the color removal occurred very fast in this study and the process could remove more than 90% of the initial color within 5 min. This shows that  $\text{OH}^\bullet$  is very effective in the cleavage of the double azo bonds, leading to the colour removal (Figure 4.3). Similar result was presented by Su et al. (2011) and Weng, Lin, & Yuan, (2013). However, the color removal could also occur due to other processes such as surface complexation between dye molecule and hydro iron moiety, as well as other adsorption processes as described by previous studies (Daneshvar, Oladegaragoze, & Djafarzadeh, 2006; Nam & Tratnyek, 2000; Şengil & Özacar, 2009).

The mineralization of the dye was not as fast as the color removal since longer time is needed to destroy the adjacent ring structure compared to the azo double bonds (Lucas & Peres, 2006; Nordin et al., 2017). Although high color removal from the dye was obtained within short time, the presence of the aromatic groups and some intermediates contributed to the COD of the dye solution. Consequently, only about 70% COD removal was achieved after 1 h of the FBF process. This result is similar to that reported by Pukdee-Asa et al. (2012) using FBF but higher than that reported by Su et al. (2011).

#### **4.2 Kinetic of COD Removal by Fluidized Bed Fenton**

The rate of pollutant degradation is one of the most important considerations in wastewater treatment process. Thus, information on the kinetic order and the corresponding rate constant is significant. The time-evolution of the COD removal by the FBF process has been presented in Figure 4.2. As can be observed, most of the COD removal occurred within the first 20 min of the reaction. For example, about 55% COD removal was obtained in the first 10 min of the process. This increased to about 65% after 20 min. Thereafter, it nearly remained the same and reached about 70% after 60 min. This

observation is due to the rapid production of the hydroxyl radicals at the beginning of the Fenton oxidation. Thus, higher degradation is obtained at the initial stage of the treatment. Similar observations were reported previously (Chen et al., 2016; Fan, Ding, Huang, Chen, & Ren, 2017).

In order to find the reaction order that can describe the COD removal, the COD removal-time data was fitted to first-order, second-order and pseudo-second orders kinetic models according to Equations 4.2 to 4.4.

First-order

$$\frac{d_c}{d_t} = -k_1 t \quad (4.2)$$

Second-order

$$\frac{1}{c_t} = \frac{1}{c_0} + k_2 t \quad (4.3)$$

Pseudo-second order

$$\frac{t}{c_t} = \frac{1}{k_2' c_e^2} + \left(\frac{1}{c_e}\right) t \quad (4.4)$$

Figure 4.4 shows the graph for the pseudo second-order model, first-order and second-order models. Table 4.2 provides the values of the rate constant for each case and the corresponding R<sup>2</sup>.

**Table 4.2: Reaction order for COD removal**

Reaction order	Rate constant	R <sup>2</sup>
First-order	0.0100 s <sup>-1</sup>	0.8271
Second-order	0.0001 L mg <sup>-1</sup> s <sup>-1</sup>	0.8929
Pseudo-second-order	0.00332 L mg <sup>-1</sup>	0.9966

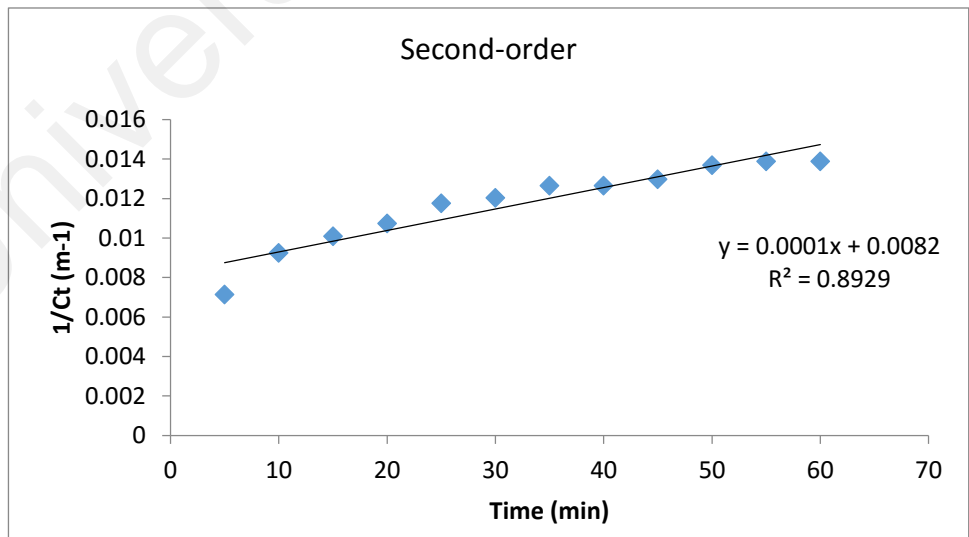
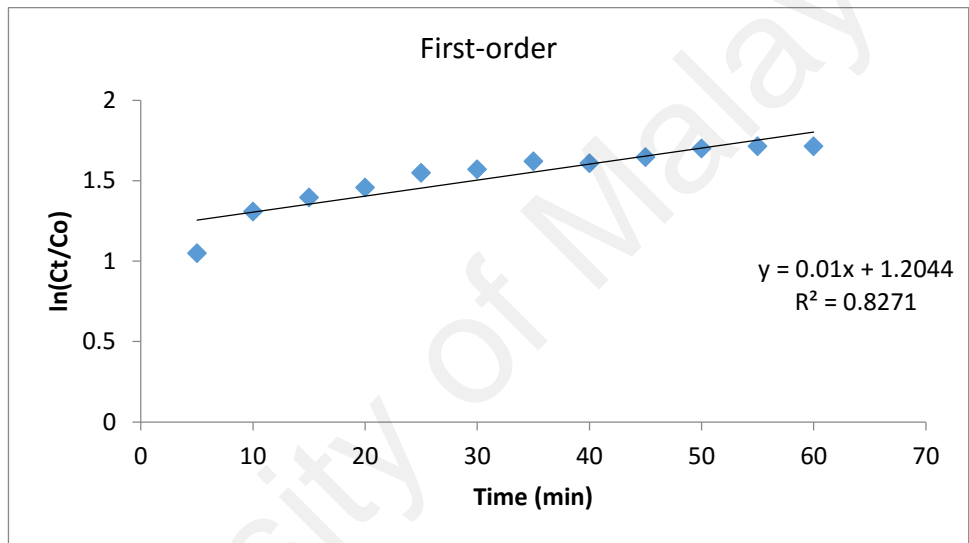
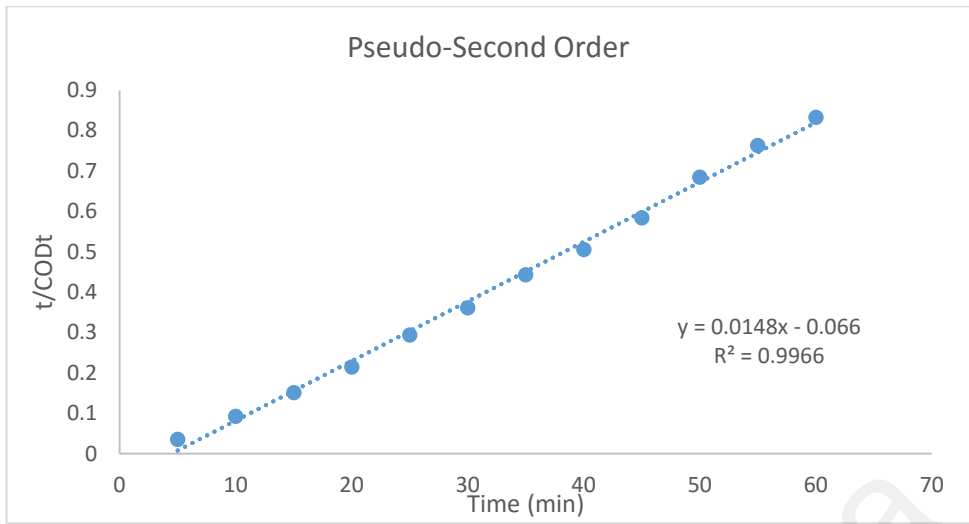


**Figure 4.4: Kinetic orders for COD removal**

It can be observed from Table 4.2 that the regression coefficient of the pseudo-second-order reaction is the highest. Thus, the kinetics of the COD removal follows a second-order reaction, with a rate constant of  $0.00332 \text{ L mg}^{-1}$ . Previous studies have reported similar order of reaction for RB5 degradation using Fenton oxidation (Argun & Karatas, 2011; Kusvuran, Irmak, Yavuz, Samil, & Erbatur, 2005). Similarly, Luna et al., (2013) reported that the degradation of acetaminophen using FBF process could be described by a pseudo-second-order kinetic model.

The reaction rate obtained here showed that the rate of COD removal by the FBF process depends on the initial concentration of COD. This can be represented by Equation 4.5 (Bautista, Mohedano, Gilarranz, Casas, & Rodriguez, 2007).

$$-r_{COD} = k[\text{COD}]^2[\text{OH}\cdot] \cong k'[\text{COD}]^2 \quad (4.5)$$

The implication of Equation 4.5 is that the COD removal will be more rapid at the initial stage of the reaction. This agrees with the experimental observations where the highest COD removal occurred in the first 15 minutes of the process. As the COD was depleted, the rate of removal also decreased. The observations of the kinetics of COD removal obtained in this study is consistent with the established literature as discussed above.

### **4.3 Comparison of Fluidized Bed Fenton and Conventional Fenton**

Since FBF is a modification of conventional Fenton oxidation, it is pertinent that their treatment performances are compared. Thus, experiments were conducted to compare the performance of the two processes in removing the RB5 from synthetic solution under the same conditions.

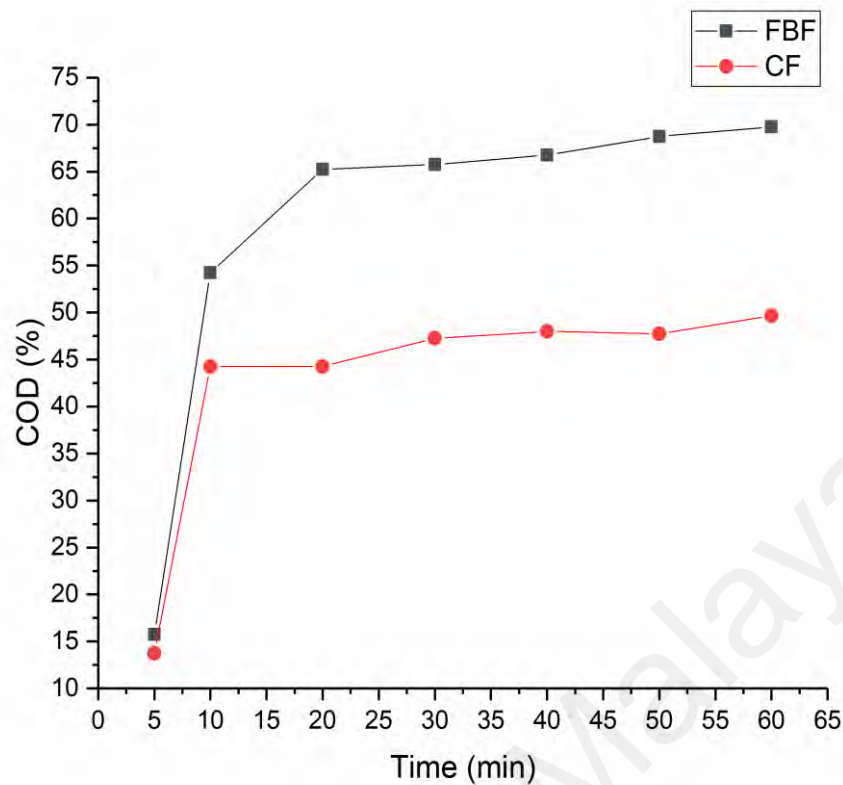


**Figure 4.5: COD removal by fluidized bed Fenton and conventional Fenton (Experimental conditions:  $[\text{Dye}/\text{Fe}^{2+}] = 10$ ,  $[\text{H}_2\text{O}_2/\text{Fe}^{2+}] = 25$ ,  $\text{pH} = 3$ , carrier loading = 30 g).**

Figure 4.5 compares the COD removals of FBF process and conventional Fenton oxidation. In the first 10 min, the rates of COD removal in both processes are nearly the same. In the FBF process, the homogeneous reaction between  $\text{Fe}^{2+}$  and  $\text{H}_2\text{O}_2$  is the dominant process in the first few minutes. Consequently, there was no significant difference between FBF process and conventional Fenton oxidation at the initial stages. However, after the first 10 min, the rate of COD removal in the FBF process became significantly higher than the conventional Fenton oxidation. For example, after 30 minutes, the FBF process removed 65.75% of the initial COD whilst the conventional Fenton oxidation could only remove 44.25% of the initial COD within the same time. At the end of 60 minutes, about 70% COD removal efficiency was achieved in the FBF process whereas the conventional Fenton oxidation removed only about 50%. Thus, the

performance of FBF process is about 20% more than that of conventional Fenton oxidation in terms of COD removal.

The higher performance of the FBF process can be attributed to the additional heterogeneous reaction as well as the excellent mixing achieved in the process. A similar result was obtained by Liu et al. (2014) where FBF process was reported to perform 15 – 20% higher than conventional Fenton oxidation for the removal of COD from recalcitrant organic silicon wastewater. Su et al. (2013) also reported that FBF process achieved 15 – 20% higher removal efficiency compared to conventional Fenton in the removal of monoethanolamine and phosphate from thin-film transistor liquid crystal display (TFT-LCD) wastewater.

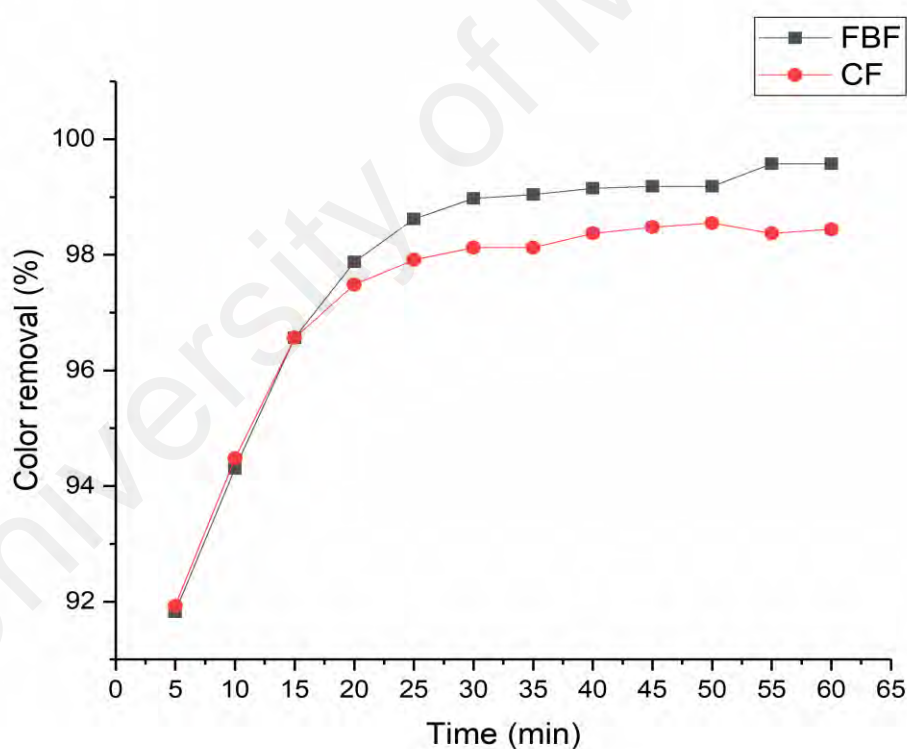


**Figure 4.6: Color removal by fluidized bed Fenton and conventional Fenton (Experimental conditions:  $[Dye/Fe^{2+}] = 10$ ,  $[H_2O_2/Fe^{2+}] = 25$ ,  $pH = 3$ , carrier loading = 30 g).**

Figure 4.6 compares the color removal by the FBF process and conventional Fenton oxidation. For the color removal, there was no difference between FBF process and conventional Fenton oxidation in the first 15 min. Both processes could remove about 96.5% of the initial color at the end of the first 15 min. However, just after 20 min of reaction, the rate of color removal in the FBF process increased slightly above that of conventional Fenton oxidation. For example, after 40 min of reaction, the FBF process removed about 99% of the initial color whereas about 98% was removed by the conventional Fenton. At the end of the 60 min, FBF process achieved approximately 100% color removal whilst the conventional Fenton oxidation achieved approximately 98% color removal.

However, the overall performances of the two processes in color removal is not significantly different. This is because the color removal occurs rapidly due to the homogeneous reaction between  $\text{Fe}^{2+}$  and  $\text{H}_2\text{O}_2$  and thus, the heterogeneous part of FBF process has a little role to play in the color removal. Similar observation was reported by Wang et al., (2015) in their study for the degradation of azo dye Orange G using FBF process. The authors concluded that the color removal was due to the homogeneous Fenton reaction while the role of the heterogeneous Fenton process was more significant in the TOC removal.

The results presented in this section show that FBF process can perform better than conventional Fenton oxidation. However, the superiority of the FBF process is manifested more after the initial stage of Fenton oxidation, which is characterized by rapid formation of hydroxyl radicals. Consequently, for treatment processes that occur very fast, such as color removal from synthetic dyes, the performances of FBF process and conventional Fenton oxidation are not significantly different. For treatment process that requires longer time, such as mineralization of organic pollutants, the performance of FBF process is

higher than that of conventional Fenton oxidation due to the combined homogeneous and heterogeneous processes in the former.

#### 4.4 Development of Response Surface Models

Due to the inherent complexity of FBF process, it is important that some models are developed to predict the performance of the process since experimental investigation alone can be daunting. Therefore, models based on RSM were developed to predict the color and COD removal from the dye-containing solution. Both COD removal and color removal were fitted to modified second order polynomial models as shown in Table 4.3. These models were developed according to the procedure outlined in Figure 3.3. In the models, the coded terms A, B, C and D represent the Dye/Fe<sup>2+</sup>, Fe<sup>2+</sup>/H<sub>2</sub>O<sub>2</sub>, pH and time respectively.

**Table 4.3: Response surface models for COD and color removals**

Parameter	Model
COD Removal	$= +74.45 - 5.25A + 0.87B - 1.00C + 0.13D + 0.11AC - 0.48AD - 2.02BC + 0.58BD + 2.98CD + 1.53A^2 + 0.40B^2 - 2.60D^2 + 1.45ABC - 2.27ABD + 0.27ACD + 1.95BCD - 1.89A^2B - 1.11A^2C + 3.61A^2D + 2.36AB^2 - 0.64ABCD$
Color Removal	$= +99.88 - 0.45A - 0.062C + 0.031D - 0.74AB + 0.16AC + 0.60AD + 0.51BD - 0.078CD - 0.64A^2 - 0.44B^2 - 0.53C^2 - 0.039ABC + 0.58ABD - 0.094ACD - 0.043BCD - 0.64A^2B + 0.16A^2C + 0.65A^2D - 0.43AB^2 - 0.051ABCD + 0.70A^2B^2$

In the models, positive coefficients represent synergistic effect on the process performance whereas negative constants represent antagonistic effect on the performances. Thus, for COD removal, Dye/Fe<sup>2+</sup> and pH have negative effects on the process performance. On the other hand, H<sub>2</sub>O<sub>2</sub>/Fe<sup>2+</sup> and time have positive effects on the COD removal. However, the linear interactions between the process variables have mixed effects on the COD removal. Similarly, the quadratic effects of Dye/Fe<sup>2+</sup> and H<sub>2</sub>O<sub>2</sub>/Fe<sup>2+</sup> are positively correlated to the COD removal while the quadratic effect of time has a

negative correlation with the COD removal. The interaction between the quadratic effect of  $\text{Dye/Fe}^{2+}$  and linear effect of  $\text{H}_2\text{O}_2/\text{Fe}^{2+}$  has a negative effect on the COD removal as does the interaction between the quadratic  $\text{Dye/Fe}^{2+}$  and pH. However, the interaction between the quadratic  $\text{Dye/Fe}^{2+}$  and time has a positive effect on the COD removal. The linear interaction between the four process variables has a negative effect on the COD removal.

For the color removal,  $\text{Dye/Fe}^{2+}$  and pH have negative effects on the color removal whereas  $\text{H}_2\text{O}_2/\text{Fe}^{2+}$  and time have positive effects on the color removal. On the other hand, the linear interactions of the parameters have mixed effects. For example, the linear interaction between  $\text{Dye/Fe}^{2+}$  and  $\text{H}_2\text{O}_2/\text{Fe}^{2+}$  has a negative effect while the interaction between  $\text{Dye/Fe}^{2+}$  and pH has a positive effect on the color removal. On the other hand, the quadratic effects of  $\text{Dye/Fe}^{2+}$ ,  $\text{H}_2\text{O}_2/\text{Fe}^{2+}$  and pH have negative relationships with the color removal. Similarly, the linear interaction between the four process parameters has a negative effect on the color removal. However, the interaction between the quadratic effects of  $\text{Dye/Fe}^{2+}$  and  $\text{H}_2\text{O}_2/\text{Fe}^{2+}$  has a positive effect on the color removal.

For both COD removal and color removal, the observations on the effect of the individual parameters agree with the established literature. The analysis shows that  $\text{Dye/Fe}^{2+}$  and pH have negative effects on the Fenton oxidation. It is well established that Fenton oxidation is more effective at acidic pH and the effectiveness of the process decreases with increasing pH above the optimum (Miklos et al., 2018). An increasing  $\text{Dye/Fe}^{2+}$  represents either an increasing dye concentration or a decreasing  $\text{Fe}^{2+}$ . An increase in the initial pollutant concentration at constant Fenton's reagent would result in a lower treatment efficiency since there is a low concentration of  $\text{OH}^\bullet$  compared to the high concentration of the pollutant (Miklos et al., 2018). Similarly, a decrease in  $\text{Fe}^{2+}$  concentration will result in low rate of  $\text{H}_2\text{O}_2$  decomposition and consequently lower

degradation (Shi et al., 2018). H<sub>2</sub>O<sub>2</sub> has a positive effect on the process performance since the efficiency of Fenton oxidation increases with increasing H<sub>2</sub>O<sub>2</sub> (Sruthi, Gandhimathi, Ramesh, & Nidheesh, 2018).

The analysis of the quadratic models has shown the trend of the effect of parameters. However, the mixed effect of the interactions of the parameters indicated that each interaction must be observed closely to identify whether it can significantly affect the process. Although the COD removal and color removal have been fitted to these models, it is necessary to test whether these models can be used to predict these responses.

#### 4.4.1 Fitness of the response surface models

The fitness of the proposed models was tested by considering the P-value, the lack of fit value, adequate precision and the regression coefficient (R<sup>2</sup>). The P-value shows the level of significance of the model and the model terms. Based on the design domain, the P-values that are less than 0.0500 indicate the significance of the respective model or model terms. On the other hand, values higher than 0.0500 indicate that the model or model terms are insignificant. For a model to be valid, the P-value of the “lack of fit F-value” must be insignificant (above 0.0500). “Adequate precision” measures the signal to noise ratio and a ratio greater than 4 is required for the model to be fit.

**Table 4.4: Fitness of the response surface models**

Response (%)	Model	Lack of fit	Adequate precision	R <sup>2</sup>	Adjusted R <sup>2</sup>
COD removal	<0.0001	0.9167	111.852	0.9979	0.9468
Color removal	<0.0001	0.3632	134.887	0.9997	0.9987

From Table 4.4, the P-value of the COD removal and color removal models are both less than 0.0001, indicating that the model is highly significant as there is less than 0.01% probability that the model values are due to noise. For both models, the P-values for lack

of fit are greater than 0.0500, indicating that the models fit the experimental data. For the adequate precision, both models have values above 4. This shows that the models have adequate signal to noise ratio. The regression coefficients ( $R^2$ ) for both models are above 0.900, indicating good agreement between experimental and predicted responses.

The above analysis shows that the proposed models can be used to predict the performance of FBF process for both COD removal and color removal. The analysis of significance of the model was also extended to the model terms, which represent the operational parameters and their interactions, either linear or quadratic. The analysis indicates whether a parameter or interaction of parameters can significantly affect the process performance. The analysis for the test of significance of the parameters and their interactions for COD removal and color removal are presented in Table B1 and Table B2 respectively in Appendix B. The last column in each of the tables indicates the level of significance of the respective variable.

Although this section has evaluated the fitness of the models and the statistical significance of model terms (parameters and their interactions), it is important to quantify the contribution of these model terms to the response.

#### **4.4.2 Contribution of model terms to COD and color removals**

The contribution of each model term to the model output can be quantified using Pareto analysis. Pareto analysis is a simple technique that is widely used to understand and prioritize the contribution of process variables to a particular response (Abdessalem, Oturan, Bellakhal, Dachraoui, & Oturan, 2008; Khataee, Zarei, & Moradkhannejhad, 2010). Quantifying the contribution of the operational parameters can assist in understanding those parameters that have the highest influence and must therefore be properly optimized.

In this study, Pareto analysis was used to calculate the percentage effect of each model term on the COD removal according to Equation 4.6 (Khataee, Marandizadeh, Vahid, Zarei, & Joo, 2013). This gives further significant information on the effect of the process variables on the response.

$$P_i = \left( \frac{b_i^2}{\sum_{i=1}^n b_i^2} \right) \times 100 \quad (4.6)$$

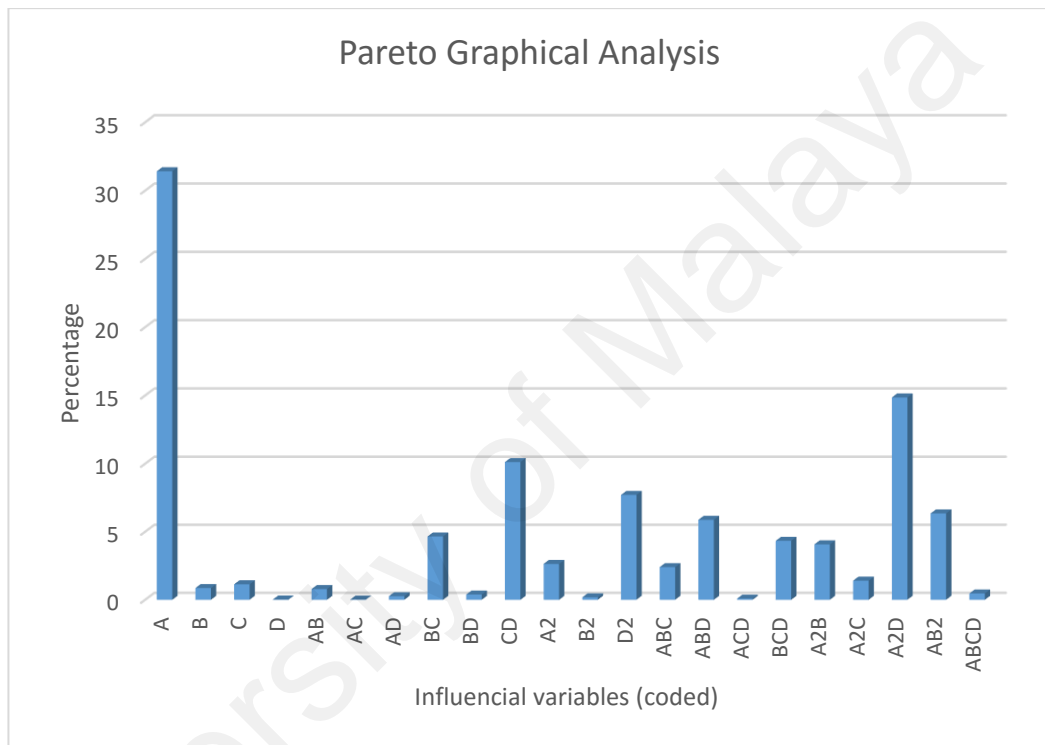


**Figure 4.7: Contributions of model terms to COD removal**

Figure 4.7 shows the Pareto graphical analysis for the COD removal. From the graph, the variables that exerted the highest influence on the COD removal are A (Dye/Fe<sup>2+</sup>) with 31.4%, the interaction between A<sup>2</sup> (Dye/Fe<sup>2+</sup>)<sup>2</sup> and D (Time), with 14.9% and the interaction between C (pH) and D (Time) with 10.1%. Other influential variables include the quadratic effect of D (7.7%), the interaction between A and B<sup>2</sup> (6.3%) and the linear interaction between A, B and D.

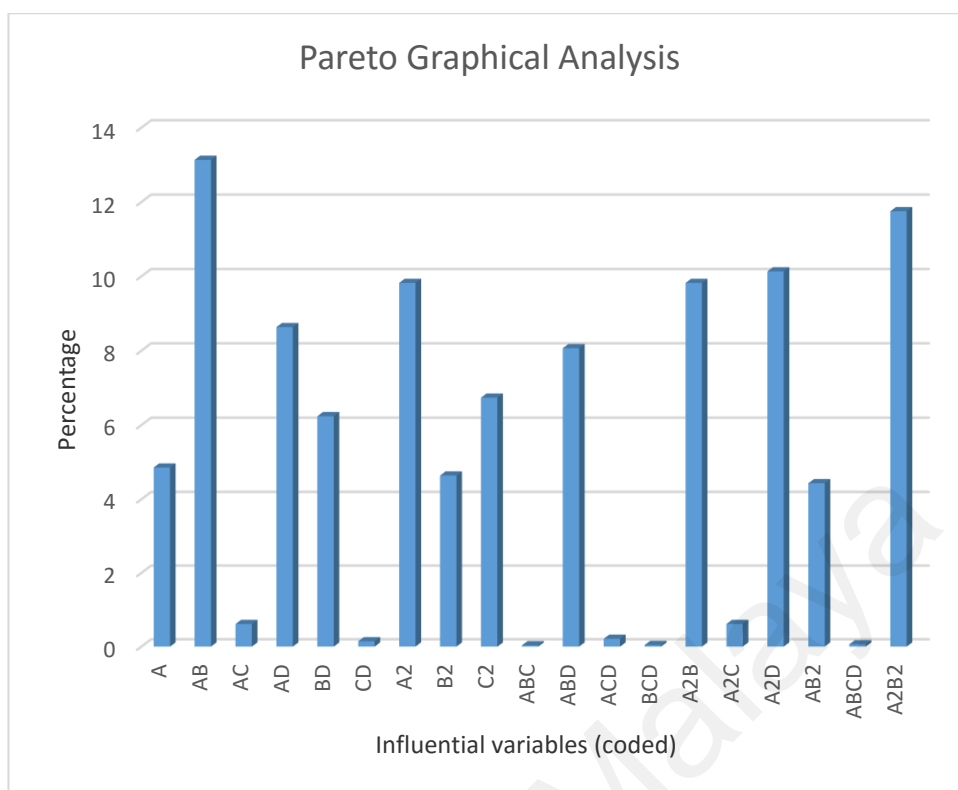


**Figure 4.8: Contributions of model terms to color removal**

The analysis was also performed for color removal. Figure 4.8 shows the graphical presentation of the Pareto analysis for color removal. It can be seen from the graph that the interaction of A (Dye/ $\text{Fe}^{2+}$ ) and B ( $\text{H}_2\text{O}_2/\text{Fe}^{2+}$ ) has the largest contribution (13.1%) to the color removal. This is followed by the interaction effect of the quadratic terms of A and B (11.8%). The contribution of the quadratic effect of A is also significant (9.8%). Other terms with high contributions include the interaction between the quadratic A and linear D (10.1%) and quadratic A and linear D (9.8%). Clearly, all the terms with high contribution involves the contribution of  $\text{Dye}/\text{Fe}^{2+}$ , either linear or quadratic. This further confirms the significance of  $\text{Fe}^{2+}$  in the process.

The analyses presented in this section have shown the quantitative contribution of each significant model term to the model outputs, in this case COD and color removals. For example, the ratio of the initial dye concentration to the catalyst concentration has the highest contribution to the COD removal while the interaction of Dye,  $\text{Fe}^{2+}$  and  $\text{H}_2\text{O}_2$  has

the highest contribution to the color removal. These findings are important since they are useful for process optimization where the influential parameters must be carefully controlled. To further confirm the influence of the independent variables, a perturbation analysis was performed to determine the sensitivity of the response to the independent variables.

#### 4.4.3 Sensitivity of COD and color removal to changes in variables

Perturbation analysis is commonly used to measure the sensitivity of the responses to the independent variables at any point of the design. In this study, perturbation analysis was done to determine the sensitivity of the COD and color removals to the operational parameters. Figure 4.9 shows the perturbation plot for the COD removal.

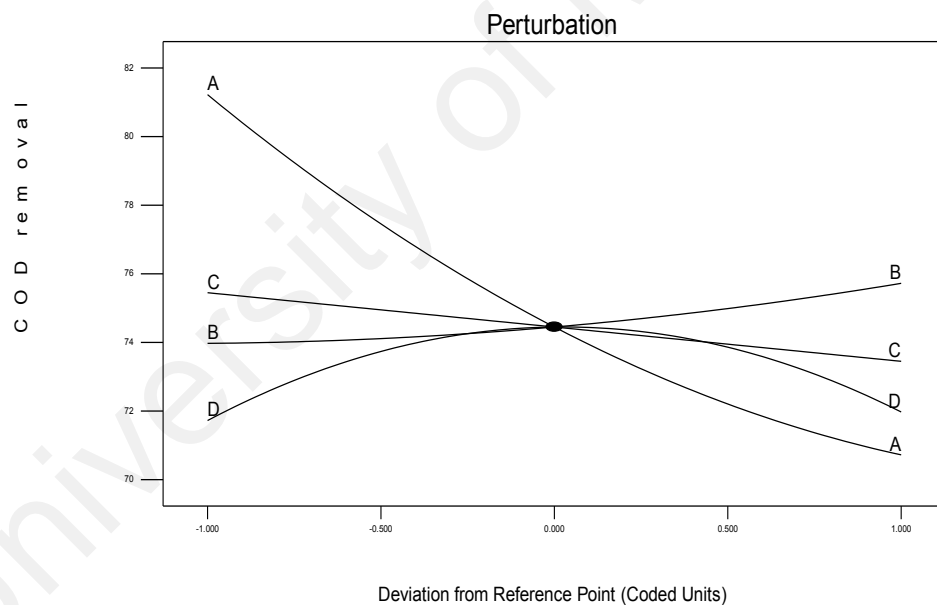


**Figure 4.9: Perturbation plots for COD removal**

Perturbation plots compare the effects of all factors at a point in the design space. A steep slope or curvature in a factor shows that the response is sensitive to that factor. A relatively flat line shows insensitivity to change in that factor. In this case, the perturbation is plotted at the center point of the design space. The process variables at the center are  $\text{Dye}/\text{Fe}^{2+} = 30$ ,  $\text{H}_2\text{O}_2/\text{Fe} = 15$ ,  $\text{pH} = 6$  and  $\text{time} = 37.50$ . From Figure 4.10, the

COD removal is most sensitive to Dye/Fe<sup>2+</sup> (A), followed by the process time (D). Both H<sub>2</sub>O<sub>2</sub>/Fe<sup>2+</sup> (B) and pH (C) appear to have relatively flat lines, indicating their lack of strong influence on the COD removal at the center point.

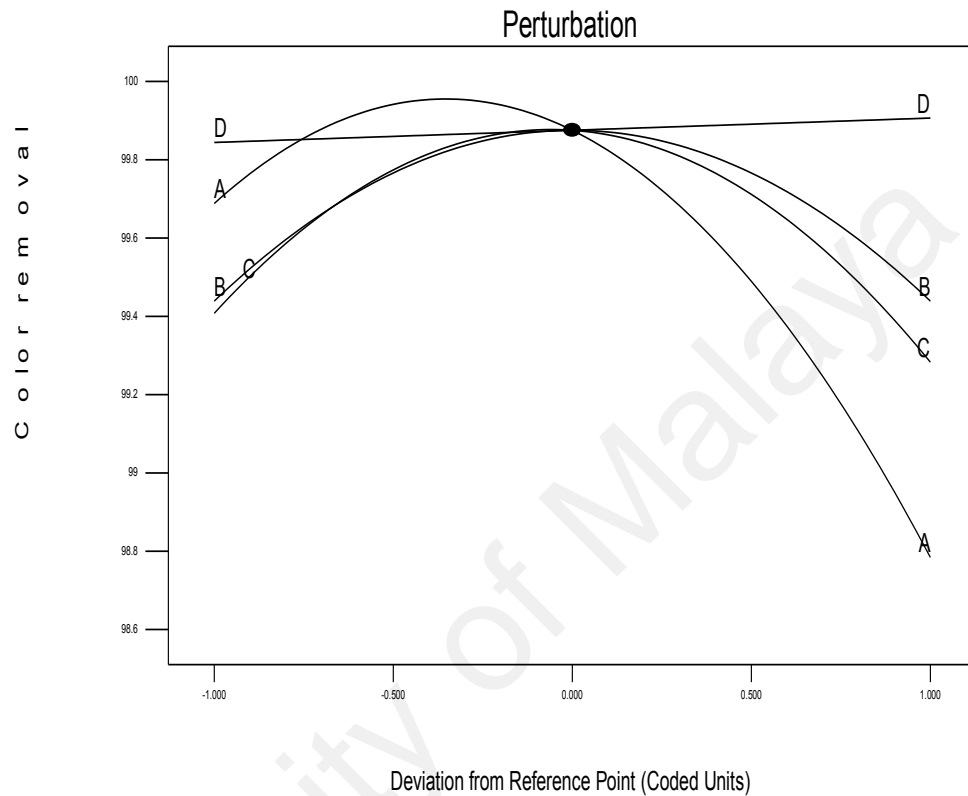


**Figure 4.10: Perturbation plot for color removal**

Figure 4.10 shows the perturbation plots for the color removal at the center point of the design (Dye/Fe<sup>2+</sup> = 30, H<sub>2</sub>O<sub>2</sub>/Fe<sup>2+</sup> = 15, pH = 6 and time = 37.50). The color removal is most sensitive to Dye/Fe<sup>2+</sup> (A). On the other hand, the sensitivities of the color removal to H<sub>2</sub>O<sub>2</sub>/Fe<sup>2+</sup> (B) and pH (C) are nearly the same. However, the graph of time (D) is almost flat, indicating that the color removal is insensitive to the treatment time used. This could be explained by the fact that the color removal is caused by the cleavage of the azo double bond which occurs rapidly within a short period (Wang et al., 2015). In this study, most of the color removal occurred within the first 15 minutes. Consequently, increasing process time beyond this did not substantially increase the color removal.

The results presented in this section have provided further information on the influence of the operational parameters and their interaction on the process performance. The findings of the sensitivity analysis agree with those of Pareto analysis and the established literature. For example, the analysis shows that the color removal is not sensitive to the change in process time. Color removal using Fenton oxidation occurs within a few minutes due to the rapid degradation of the azo double bond, which is responsible for the color.

Although the influence of the operational parameters and their interactions have been evaluated through the analysis of various RSM metrics, it is pertinent to provide a more in-depth discussion on the effect of individual parameters on the process performance.

#### **4.5 Effects of Operational Parameters on COD Removal**

In this section, the effects of the process variables ( $\text{Fe}^{2+}$ ,  $\text{H}_2\text{O}_2$ , pH, Time) on the COD removal and color removal are discussed. In the previous sections, RSM techniques were used to identify those parameters that have significant effects on performance of the FBF process and the extent of the influence were also evaluated. The effects of Fenton's reagent, pH and process time are discussed here.

##### **4.5.1 Effect of Fenton's reagent**

From the model analysis and the Pareto graphical analysis, Dye/ $\text{Fe}^{2+}$  is the most significant parameter affecting COD removal. This is because the dye concentration determines the required amount of the  $\text{OH}^\bullet$  to oxidize the pollutant. On the other hand,  $\text{Fe}^{2+}$  concentration determines the extent of the catalytic production of the  $\text{OH}^\bullet$  from  $\text{H}_2\text{O}_2$ . The significance of  $\text{Fe}^{2+}$  in the fluidized bed Fenton process has been confirmed earlier (Su et al., 2014).

The concentrations of Fenton's reagent ( $\text{Fe}^{2+}$  and  $\text{H}_2\text{O}_2$ ) and their effect on the process performance are key considerations in the application of Fenton oxidation for wastewater treatment.  $\text{Fe}^{2+}$  is present as a homogenous catalyst in the decomposition of  $\text{H}_2\text{O}_2$  to produce  $\text{OH}^\bullet$ . The concentration of Fenton's reagent required for a particular application depends on the type and concentration of the target pollutants. Therefore, the effects of Fenton's reagent were considered in relation to the initial dye concentration.

Generally, increasing  $\text{Fe}^{2+}$  concentration promotes the decomposition of  $\text{H}_2\text{O}_2$ , leading to more  $\text{OH}^\bullet$  generation (Ratanatamskul et al., 2010). However, excess concentration of  $\text{Fe}^{2+}$  may lead to scavenging of  $\text{OH}^\bullet$  as explained by Equation 2.23 where excess  $\text{Fe}^{2+}$  acts as a scavenger and react with  $\text{OH}^\bullet$ , subsequently decreasing their availability to oxidize organic pollutants. Moreover, excess  $\text{Fe}^{2+}$  concentration may lead to the generation of large amount of sludge, leading to additional cost due to sludge treatment and disposal (Ratanatamskul et al., 2010). This highlights the necessity of determining an optimum concentration of the catalyst. The amount of  $\text{OH}^\bullet$  that can be produced in the reaction is determined by the concentration of  $\text{H}_2\text{O}_2$ , which decomposes to form  $\text{OH}^\bullet$  (Wang, Zheng, Zhang, & Wang, 2016). Thus,  $\text{H}_2\text{O}_2$  concentration is directly proportional to the concentration of oxidants and consequently, has a positive effect on the process performance. However, excess  $\text{H}_2\text{O}_2$  may inhibit the process performance due to scavenging reactions as explained earlier. The excess  $\text{H}_2\text{O}_2$  acts as radical scavenger, decreasing the amount of the available  $\text{OH}^\bullet$  through converting it to the less reactive hydroperoxyl radical ( $^\bullet\text{O}_2\text{H}$ ) (Argun & Karatas, 2011).

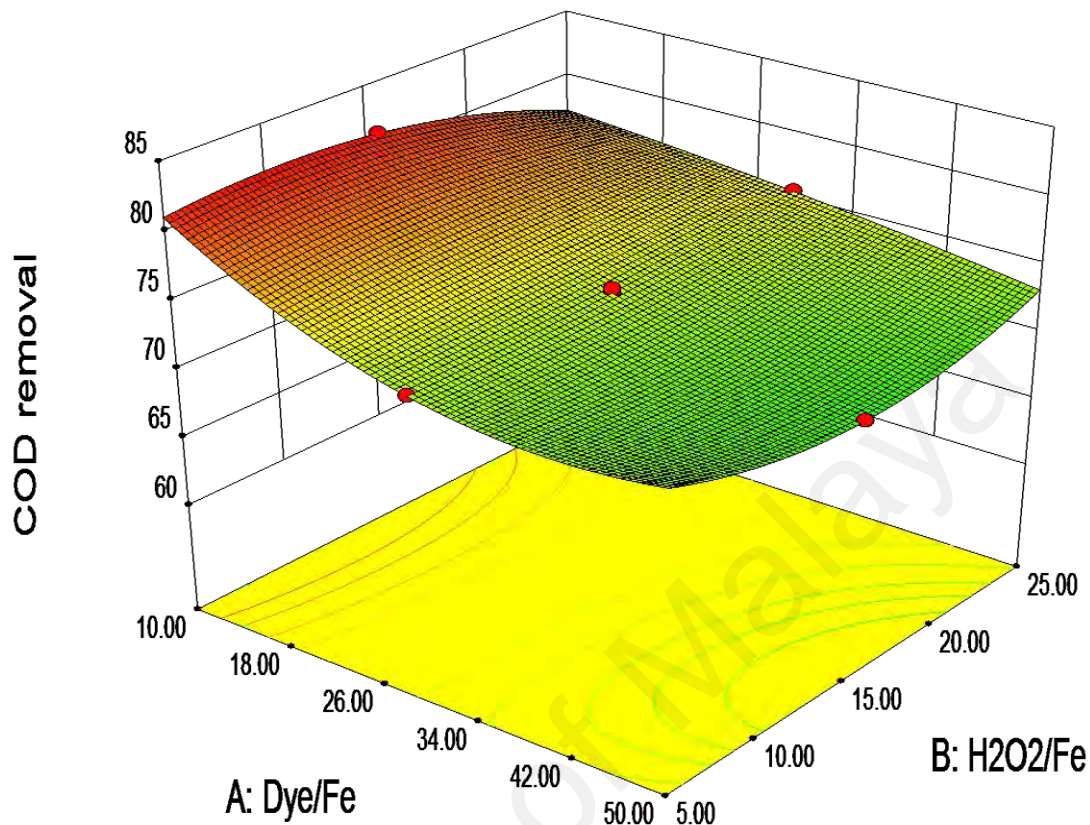


**Figure 4.11: Effect of Dye/Fe<sup>2+</sup> and H<sub>2</sub>O<sub>2</sub>/Fe<sup>2+</sup> on COD removal**

Figure 4.11 shows the effect of Dye/Fe<sup>2+</sup> and H<sub>2</sub>O<sub>2</sub>/Fe<sup>2+</sup> on the COD removal. The COD removal decreases with an increase in the Dye/Fe<sup>2+</sup> concentration. This is because increasing Dye/Fe<sup>2+</sup> indicates that the concentration of Fe<sup>2+</sup> is decreasing since the dye concentration was kept constant. This shows that high concentration of Fe<sup>2+</sup> promotes OH<sup>•</sup> production and hence, higher COD removal. The highest COD removal occurs when the Dye/Fe<sup>2+</sup> is 10. From the experimental data, high COD removals are found when the Dye/Fe<sup>2+</sup> is in the range of 10 to 18 as can be seen in Figure 4.11.

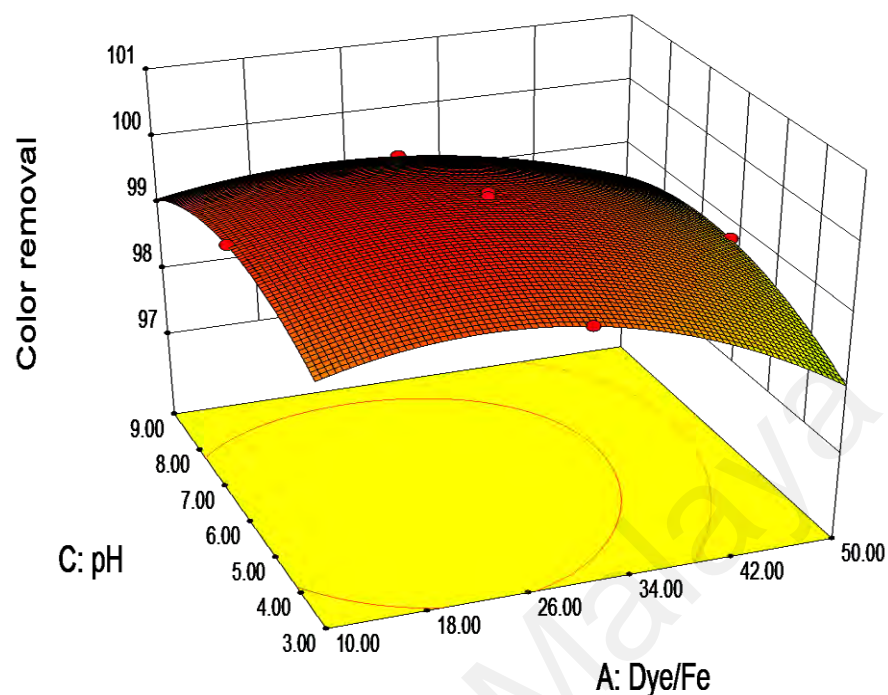


**Figure 4.12: Effect of Dye/Fe<sup>2+</sup> on color removal**

The effect of Dye/Fe<sup>2+</sup> on color removal is shown in Figure 4.12. The color removal increases when the Dye/Fe<sup>2+</sup> was increased from 10 to 30. This was due to the increase in the catalyst concentration, which enhances the production of hydroxyl radicals. However, when the ratio increases above 30, the color removal begins to increase again. For example, the color removal was 99.78% at Dye/Fe<sup>2+</sup> of 18, decreased to 99.44% at Dye/Fe<sup>2+</sup> of 30 and then raised again to 99.73 % at Dye/Fe<sup>2+</sup> of 45. The decrease in the color removal was due to the scavenging effect of Fe<sup>2+</sup> as explained above. Thus, for the color removal, the optimum Dye/Fe<sup>2+</sup> lies around 30.

The effect of H<sub>2</sub>O<sub>2</sub>/Fe<sup>2+</sup> on the COD removal can be observed in Figure 4.11. It can be seen that the COD removal increases with increase in H<sub>2</sub>O<sub>2</sub>/Fe<sup>2+</sup> from 5 to 15. Thereafter, the COD removal decreases with increase in H<sub>2</sub>O<sub>2</sub>/Fe<sup>2+</sup>. The highest COD removal occurred at H<sub>2</sub>O<sub>2</sub>/Fe<sup>2+</sup> of 15. The reduction in the COD removal can be explained by the scavenging effects of H<sub>2</sub>O<sub>2</sub>. Excess H<sub>2</sub>O<sub>2</sub> can scavenge the available OH<sup>•</sup> and decrease

its availability to degrade the target compound as shown in Equations 4.7 and 4.8 (Matira et al., 2015). Another plausible explanation is that there could be a recombination of OH<sup>•</sup> when its concentration is in excess as shown in Equation 4.9 (Muruganandham & Swaminathan, 2004).



The effect of H<sub>2</sub>O<sub>2</sub>/Fe<sup>2+</sup> on color removal follows similar trend as that observed for COD removal. The color removal increases as the H<sub>2</sub>O<sub>2</sub>/Fe<sup>2+</sup> was increased from 5 to about 15, and then decreased again. As the H<sub>2</sub>O<sub>2</sub>/Fe<sup>2+</sup> increases, more hydroxyl radicals are formed leading to the rapid degradation of the dye. However, excess H<sub>2</sub>O<sub>2</sub>/Fe<sup>2+</sup> can lead to complexation that may produce compounds, which can increase the color of the solution (Lucas & Peres, 2006; Xu, Li, Wang, & Gu, 2004).

From the foregoing discussion, it can be concluded that the Fenton's reagent has a positive effect on the performance of the FBF process. Fe<sup>2+</sup> plays a significant role in catalysing the oxidant to generate OH<sup>•</sup> and no scavenging effect was observed within the range of Fe<sup>2+</sup> concentrations used. The concentration of H<sub>2</sub>O<sub>2</sub> also affects the process performance positively. However, a reduction in the process performance was observed when the H<sub>2</sub>O<sub>2</sub> was increased above certain concentration. This indicates a scavenging effect of the excess H<sub>2</sub>O<sub>2</sub> as observed in previous studies (Lucas & Peres, 2006; Xu et al., 2004).

The catalytic performance of Fe<sup>2+</sup> and the reactivity of hydroxyl radical are affected by the pH of the solution. This makes pH an important parameter for FBF process.

#### 4.5.2 Effect of pH

Solution pH is one of the main operational parameters that has a significant impact on the performance of Fenton oxidation. Effective degradation of pollutants in Fenton oxidation is restricted to low pH since  $\text{Fe}^{2+}$  requires acidic condition to maintain its catalytic role (Usman et al., 2016). The optimum pH for Fenton oxidation is between 2.8 to 3.5 (Villegas-Guzman et al., 2017). At higher pH, the catalytic role of iron is impaired as  $\text{Fe}^{3+}$  precipitates as iron oxy-hydroxide (Clarizia et al., 2017).

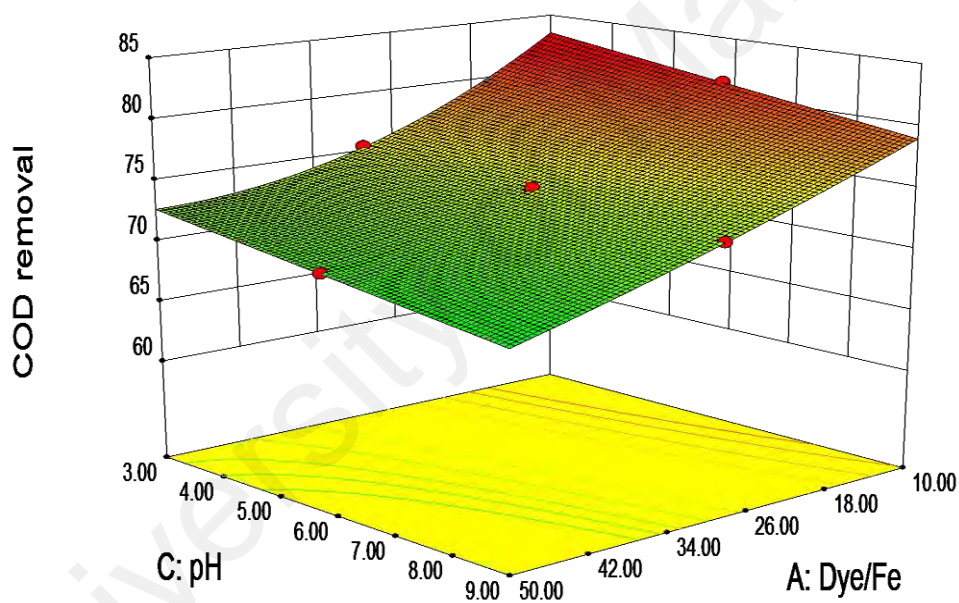


**Figure 4.13: Effects of pH and Dye/ $\text{Fe}^{2+}$  on COD removal**

The effect of pH on the COD removal is depicted in Figure 4.13. The COD removal decreases when the pH increases from 3 to 9. Similar observation was reported previously (Acisli et al., 2017; Babuponnusami & Muthukumar, 2014). High pH leads to coagulation and complex formation because of the conversion of ferric iron to Fe-OH compounds (Matira et al., 2015; Mollah, Schennach, Parga, & Cocke, 2001). However, in this study,

the effect of pH was not very significant. For example, the difference in COD removal between pH 3 and 4 is not more than 3%. Thus, unlike conventional Fenton oxidation, the effect of pH on the FBF process was not very significant. This could be due to the presence of SiO<sub>2</sub> which induced heterogeneous Fenton reaction.

The effect of pH on the color removal is shown in Figure 4.12. There was a slight increase in color removal as the pH was increased from 3 to 6. For example, the color removal was 99.23% at pH 3 and increased to 99.65% at pH 5. However, when the pH was raised above 6, the color removal decreased slightly. Similar observation was made by Buthiyappan et al., (2016) who reported pH 6 as the optimum for decolorisation of dye using Fenton oxidation. They also reported a decreased in the decolorisation when the pH exceeded 6. The lower decolorisation at acidic pH can be attributed to the scavenging effects of H<sup>+</sup> and precipitation of iron hydroxide (Kwon et al., 1999). This observation is consistent with previous studies (Bautista et al., 2007; Deng & Englehardt, 2006).

The results presented showed that both COD and color removals were affected by the initial pH of the solution, which is consistent with established literature on Fenton oxidation as discussed above. The highest COD removal was obtained around pH 3 whilst the highest color removal occurred at pH 6. Although pH and Fenton's reagent are the mostly considered due to their significant effect on the process performance, process time is another parameter of practical importance.

#### **4.5.3 Effect of process time**

The effect of process time on the COD removal can be observed from Figure 4.14. The process time has a positive effect on the COD removal. As the process time increased from 15 min to 60 min, the COD removal increased from 74% to 83%. However, this increase was more noticeable between 15 to 30 min. Above 30 min, the changes in COD removal was not very significant. For example, at 37.5 min, the COD removal was already

81.25% and only increased to 82.8% at 50 min. This shows that most of the degradation occurred below 30 min. The degradation occurred very rapidly in the first few minutes, followed by a slower rate of reaction. This agrees with the theory of two-stage kinetics for COD removal where the pollutants oxidation is characterized by a rapid initial degradation, followed by a slower removal rate (Brink, Sheridan, & Harding, 2017; Chen et al., 2016).

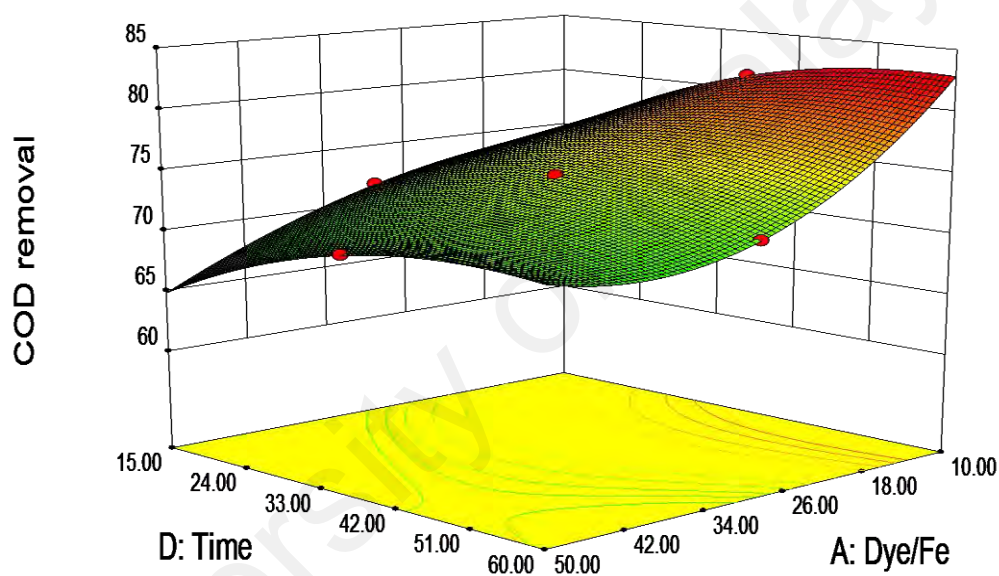


**Figure 4.14: Effects of Dye/Fe<sup>2+</sup> and Time on COD removal**

The effect of process time was not significant on the color removal as high color removals were obtained even at the shortest time investigated. More than 90% of the initial color could be removed even under 15 min. Increasing the reaction time beyond 15 min did not substantially increase the color removal. This is because color removal occurs with the destruction of the color-bearing azo double bonds of the dye. Thus, the OH<sup>\*</sup> can easily conjugate the double bond within few minutes of the process, leading to the color removal (Patel et al., 2011).

This section discussed the effect of individual operational parameters ( $\text{Fe}^{2+}$ ,  $\text{H}_2\text{O}_2$ , pH, time) on the performance of FBF process. Different trend of the effects of parameters were observed for COD removal and color removal. For example, the COD removal decreased with initial pH from 3 to 9, while the color removal increased from pH 3 to 6, and then decreased as discussed above. Nevertheless, the results showed that the effects of these parameters are more pronounced on the COD removal compared to the color removal. Thus, COD removal is a better response to investigate the effects of these parameters.

Although these results have shown the effect of each parameter and where the highest COD removal and color removal can be obtained for each parameter, it is more practical to determine the optimum combinations of these parameters. Thus, numerical optimization was conducted to establish the optimum condition for both COD and color removal.

#### **4.6 Optimization of Fluidized Bed Fenton Process**

One of the most important consideration in FBF process is the optimization of the process parameters. Process optimization is not only important from economic viewpoint, but it is also necessary to avoid scavenging effects of the Fenton's reagent. Thus, the degradation of the model dye pollutant was optimized using the RSM. In the CCD of the Design-Expert, the process parameters (Dye/ $\text{Fe}^{2+}$ ,  $\text{Fe}^{2+}/\text{H}_2\text{O}_2$ , pH, time) were chosen as the variables to be optimized while the responses (COD and color removals) were set to be maximized. Table 4.5 shows the specified conditions for the numerical optimization. The range of Dye/ $\text{Fe}^{2+}$  was 10 to 50,  $\text{Fe}^{2+}/\text{H}_2\text{O}_2$  was 5 to 25, pH was 3 to 9 whilst time was set between 15 to 60 min. The target COD and color removals were set to be maximized. The objective was to obtain the maximum degradation of the pollutant under the optimum conditions.

**Table 4.5: Constrains for the optimization of color and COD removals**

Name	Goal	Lower limit	Upper limit	Lower weight	Upper weight	Importance
A:Dye/Fe <sup>2+</sup>	is in range	10	50	1	1	3
B:H <sub>2</sub> O <sub>2</sub> /Fe <sup>2+</sup>	is in range	5	25	1	1	3
C:pH	is in range	3	9	1	1	3
D:Time	Is in range	15	60	1	1	3
COD removal (%)	Maximize	56.75	100	1	1	3
Color removal (%)	maximize	93.86	100	1	1	3

Based on the selected range of the operational parameters, the software gave 53 possible solutions. The solution with the highest desirability was selected for validation. The experimental conditions, the predicted and actual responses are shown in Table 4.6. The process parameters suggested by the model are Dye/Fe<sup>2+</sup> = 10, H<sub>2</sub>O<sub>2</sub>/Fe<sup>2+</sup> = 25, pH = 3.09 and time = 45.52 min. With these values, the model predicted the COD removal to be 83.28% while the color removal is 99.99%. After running the experiment with the suggested variables, the COD removal was found to be 80% whereas the color removal was 99.94% as shown in Table 4.6. These values are closed to those predicted by the RSM model, indicating that the model can be accurately used to predict the performance of the process.

**Table 4.6: Results of numerical optimization for COD and color removal**

Initial dye (mg/L)	Dye/Fe <sup>2+</sup> (wt/wt)	H <sub>2</sub> O <sub>2</sub> /Fe <sup>2+</sup> (wt/wt)	pH	Time (min)	COD Removal (%)		Color removal (%)	
					Pred.	Exp.	Pred.	Exp.
500	10	25	3.09	45.52	83.28	80.00	99.99	99.94

To understand the sensitivities of the responses to the process variables at the optimum conditions, perturbation graphs are plotted and are shown in Figure B1 of Appendix B. It can be seen from the graphs that the COD removal is most sensitive to Dye/Fe<sup>2+</sup>. This is followed by the sensitivity to pH. However, the sensitivities of the COD removal to

$\text{H}_2\text{O}_2/\text{Fe}^{2+}$  and time are not very high. Thus, at the optimum conditions,  $\text{Dye}/\text{Fe}^{2+}$  and pH are the parameters that exert the greatest influence on the COD removal. In the case of color, the removal is most sensitive to  $\text{Dye}/\text{Fe}^{2+}$ , followed by  $\text{H}_2\text{O}_2/\text{Fe}^{2+}$  and pH. On the other hand, the color removal is insensitive to change in time, which agrees with the findings presented in the previous sections.

The results of the optimization show that the predicted COD removal and color removal are nearly the same with the experimental results. This indicated that the numerical optimization based on the RSM technique can be used to optimize the operational parameters of FBF process. Overall, it shows that the developed RSM models can be used to predict the performance of the FBF process as supported by the results of the model validation and the statistical analysis presented earlier.

#### **4.7 Summary**

In this chapter, the performance of the FBF process has been evaluated and the effects of operational parameters have been elucidated. The performance of the process was optimized and compared with the conventional Fenton oxidation. These results addressed the first objective of the study and set the stage for the second objective since proper investigation of the effect of solid carriers can only be properly done when operational parameters have been optimized.

## CHAPTER 5: EFFECT OF CARRIERS ON FLUIDIZED BED FENTON

This chapter discusses the effect of SiO<sub>2</sub> as the carriers in FBF process and its interactions with the Fenton's reagent and organic pollutant. These results are discussed in two parts. The first part presents the results of quantum chemical simulation, which was conducted to predict the nature of the interactions among the SiO<sub>2</sub>, Fenton's reagent and RB5. This is followed by the results of the experimental investigations conducted to validate the theoretical results. Figure 5.1 depicts the different aspects discussed in this section.

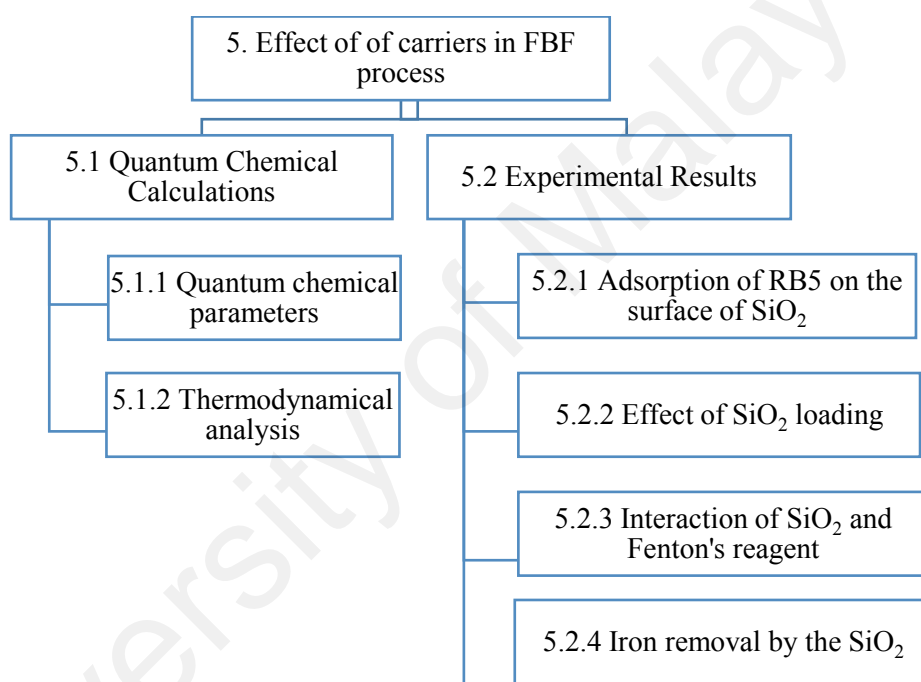


**Figure 5.1: Flow of discussion on the effect of SiO<sub>2</sub>**

### 5.1 Quantum Chemical Calculations

This section presents the results of quantum chemical calculations used to predict the nature of interaction between SiO<sub>2</sub>, Fenton's reagent and the RB5. The quantum chemical calculations were performed using the chemical structures presented in Table 3.2, following their optimization using B3LYP level of study with 6-311++G (d,p) as the basis set. Based on the calculations, the electronic, structural and thermodynamic properties of the molecules were obtained. These results are presented in two parts, based on the findings of quantum chemical parameters and thermodynamic parameters.

### 5.1.1 Quantum Chemical Parameters

Fenton oxidation is carried out using Fenton reagent ( $\text{Fe}^{+2}$ ,  $\text{H}_2\text{O}_2$ ) under strict acidic condition. For efficient performance of Fenton oxidation, pH plays an important role due to possible formation of iron-water complexes ( $\text{FeOH}^{+2}$ ,  $\text{Fe}(\text{OH})^{+2}$ ) and decomposition of  $\text{H}_2\text{O}_2$  (Pignatello, Oliveros, & MacKay, 2006). However, the FBF process could enhance the efficiency of Fenton reaction since different processes occur simultaneously (Fan et al., 2017; Ratanatamskul et al., 2010). Thus, the efficiency of the process would depend on the interaction among  $\text{Fe}^{2+}$ ,  $\text{H}_2\text{O}_2$ , organic pollutant and the fluidized carriers.

Quantum chemical simulations were conducted to study interactions of Fenton's reagent with the fluidized bed carriers. The molecular structures of the chemical species involved in Fenton oxidation were optimized and are shown in Figure 5.2 and Figure 5.3. Based on the optimized geometries, quantum parameters were obtained and compared as shown in Figure 5.4.

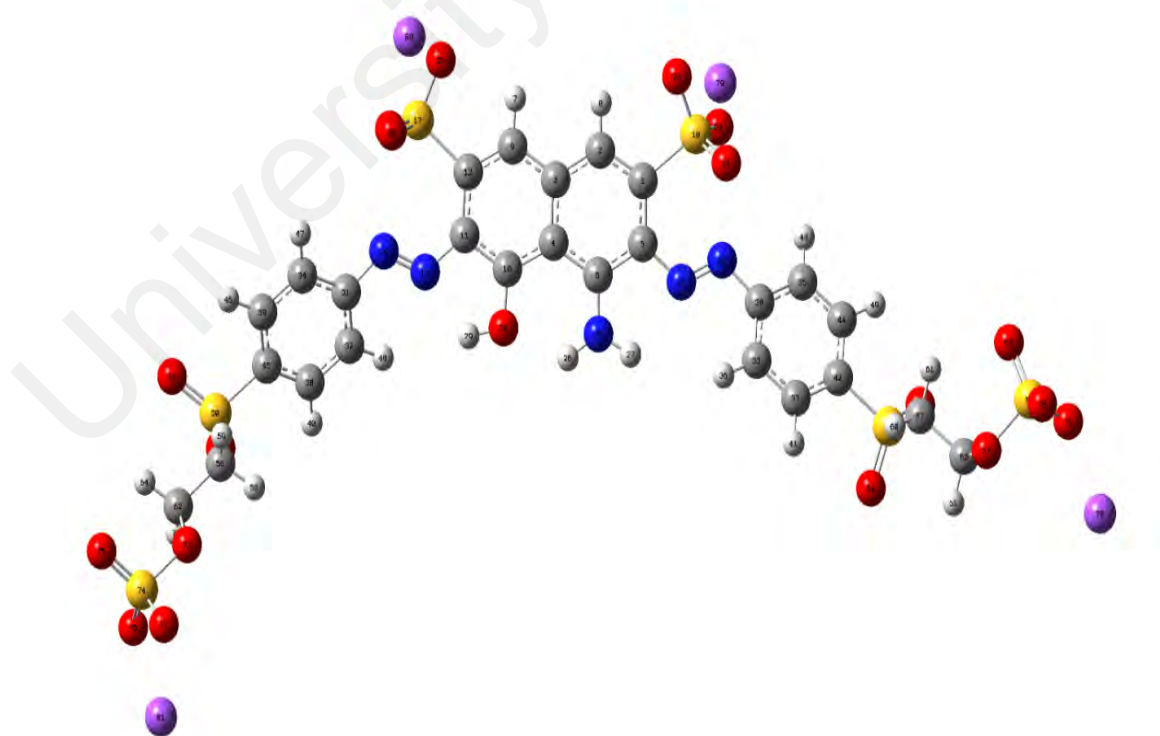


Figure 5.2: Optimized geometry of Reactive Black 5 dye



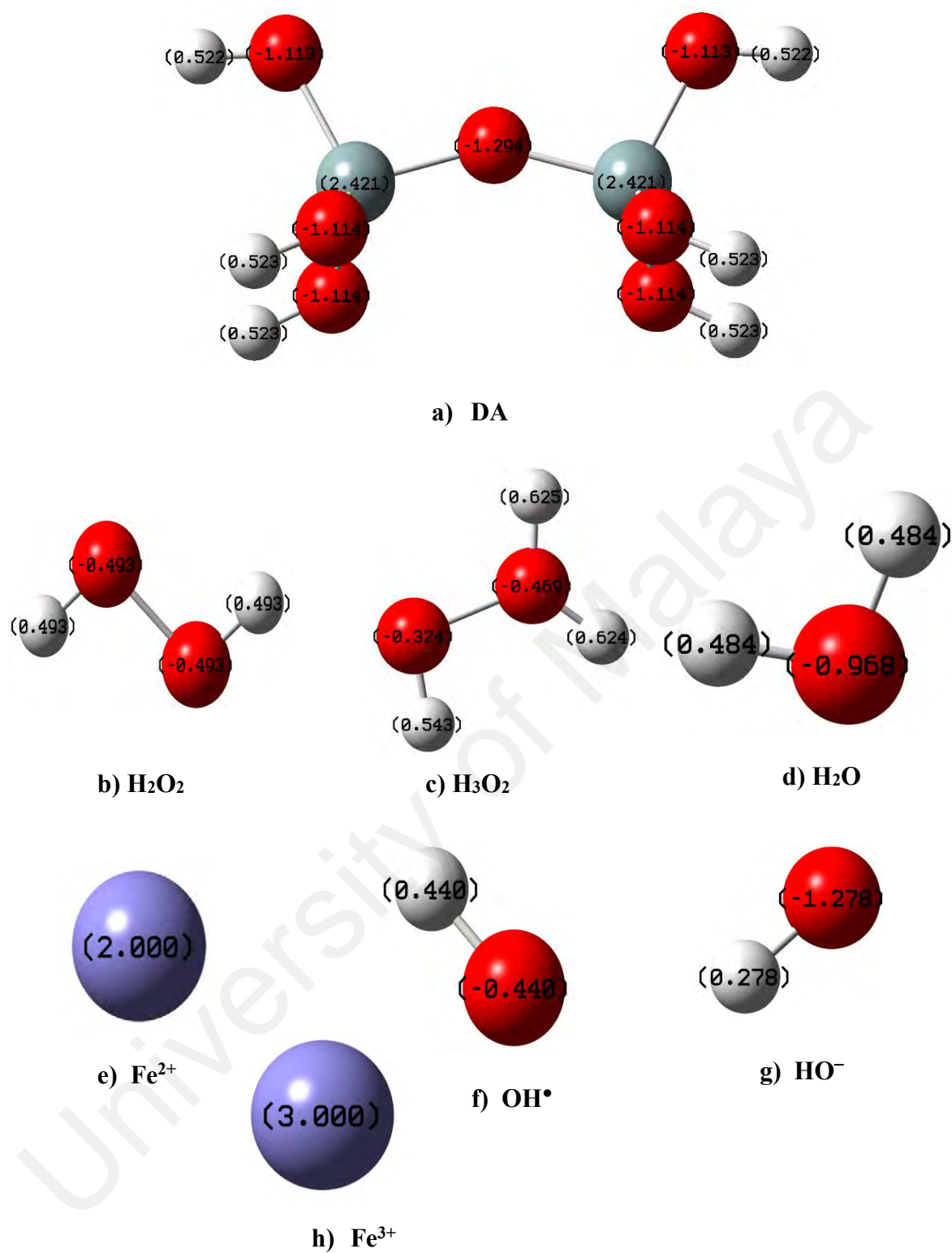
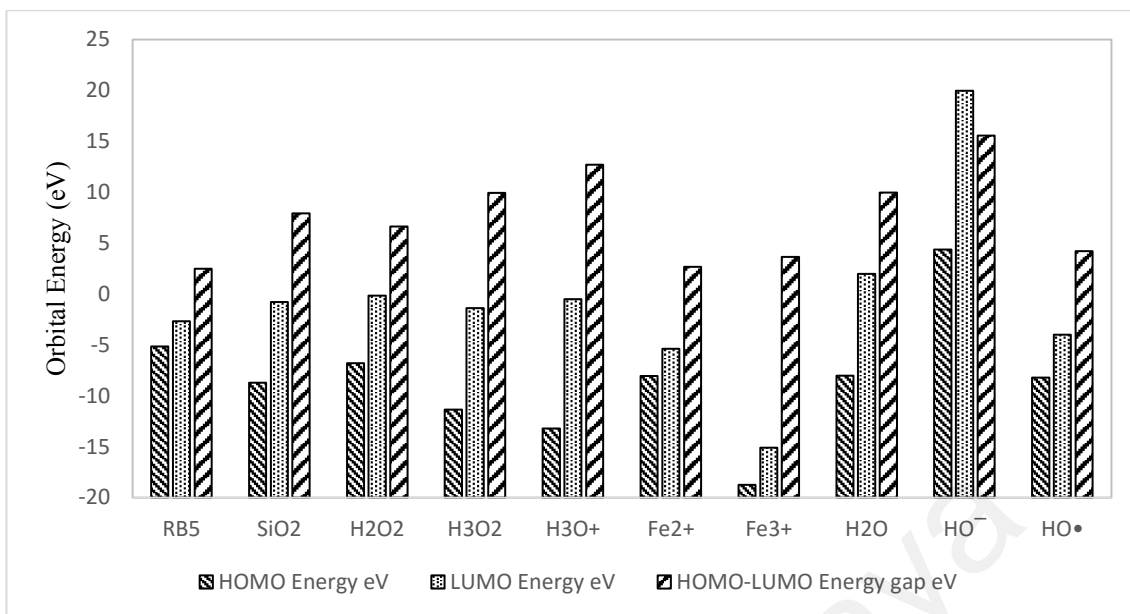


Figure 5.3: Optimized geometries of molecules

H-atom
  O-atom
  C-
  Si-atom



**Figure 5.4: Energy level diagram of the studied molecules**

The comparisons shown in Figure 5.4 are based on the HOMO and LUMO energies of the molecules as well as the HOMO-LUMO energy gap of each molecule. The values of the HOMO/LUMO energy and HOMO-LUMO energy gap of each molecule will give an idea about the possible interaction of the molecule with another available molecule. These comparisons are discussed in subsequent sections.

#### 5.1.1.1 HOMO-LUMO Energies

RB5 with a high HOMO value of -5.15 eV and OH<sup>•</sup> with a low LUMO value of -3.99 eV exhibit electron donating and electron accepting tendencies respectively. This observation is exactly in agreement with Frontier Molecular Orbital theory (FMO) (Liu et al., 2014). In this study, OH<sup>•</sup> radicals are derived from ferrous-catalyzed H<sub>2</sub>O<sub>2</sub> and SiO<sub>2</sub> is used as the fluidization medium. Therefore, it is imperative to study the chemical reactivity and interaction of these species in degrading RB5.

Since the reaction medium for Fenton oxidation is aqueous in nature, it is expected that water molecules with a slightly lower HOMO energy will show affinity for RB5. Therefore, due to a higher LUMO value of 1.97 eV, water molecule will transfer its

electron to RB5 dye. As a result, hydrolysis of dye takes place (Vončina & Majcen-Le-Marechal, 2003). Similarly, water molecule will also show propensity to donate its electron to  $\text{Fe}^{2+}$  molecule due to small LUMO energy value of -5.37 eV. Contrarily,  $\text{H}_2\text{O}_2$  molecule due to high HOMO value of -6.8 eV will show nucleophilic characteristic towards water molecule. Under acidic conditions,  $\text{H}_3\text{O}^+$  ion (as a representative of  $\text{H}^+$  in aqueous solution) with low HOMO and LUMO energy values of -13.2 eV and -0.49 eV respectively will exhibit electrophilic character and as a result protonation of  $\text{H}_2\text{O}_2$  and  $\text{Fe}^{2+}$  may take place. However, according to simulation results,  $\text{H}_3\text{O}^+$  ions will show high affinity for  $\text{H}_2\text{O}_2$  as compared to  $\text{Fe}^{2+}$ . This is because,  $\text{H}_2\text{O}_2$  shows slightly higher HOMO (-6.8 eV) and significantly higher LUMO (-0.15 eV) energies, which causes  $\text{H}_3\text{O}^+$  ions to interact strongly with HOMO of  $\text{H}_2\text{O}_2$ . As a result, protonation of  $\text{H}_2\text{O}_2$  takes place. Protonation results in a significant reduction of both HOMO and LUMO energies of  $\text{H}_2\text{O}_2$ . Therefore, due to lower LUMO value of -1.40 eV, abstraction of electron from the HOMO of  $\text{Fe}^{2+}$  (-8.05 eV) takes place.

The findings of these calculations are in accordance with the available literature (Rodrigues, Borges, Lima, & Madeira, 2018; Saini et al., 2016). Therefore, as per Equation 1.1,  $\text{OH}^\bullet$  radical and  $\text{Fe}^{3+}$  are produced. However, in the presence of  $\text{HO}^-$ , reduction of both  $\text{Fe}^{2+}$  and  $\text{H}_2\text{O}_2$  will take place due to the high HOMO and LUMO values of  $\text{HO}^-$  ( $E_{\text{HOMO}} = 4.38$  eV;  $E_{\text{LUMO}} = 19.96$  eV). This observation is in accordance with previous findings where the decomposition of  $\text{H}_2\text{O}_2$  at higher pH values was reported (Ntampeglitis, Riga, Karayannis, Bontozoglou, & Papapolymerou, 2006).

$\text{SiO}_2$  with relatively lower HOMO value of -8.72 eV does not exhibit electron donating tendency in the presence of Fenton's reagent, RB5,  $\text{HO}^-$  and water. However, due to lower LUMO energies, it may slightly show a tendency to take-up the electrons from  $\text{H}_2\text{O}$ ,  $\text{H}_2\text{O}_2$ , and  $\text{H}_3\text{O}^+$  molecules. Previous studies have also pointed to the possible interaction between  $\text{H}_2\text{O}_2$  and  $\text{SiO}_2$  through hydrogen bonding (Zegliński et al., 2006)

Furthermore, due to its comparatively higher  $E_{\text{HOMO}}$  of -8.72 eV,  $\text{SiO}_2$  shows a tendency to donate electrons to  $\text{Fe}^{3+}$  (having -18.74 eV). This points to a possibility of crystallization of iron oxide on the surface of the carriers, which is one of the characteristics of FBF process (Matira et al., 2015).

While the values of the HOMO and LUMO energies gave an insight about the tendency of a molecule to accept/donate an electron, the difference between these two values (HOMO-LUMO energy gap) for each molecule can also be used to predict their reactiveness.

#### 5.1.1.2 HOMO-LUMO Energy gap

The HOMO-LUMO energy gap can also be used to predict the reactivity of interacting molecules. It is defined as a potential difference for the electron to transfer between two interacting orbitals during chemical reaction. From HOMO-LUMO energy gap, it is found that RB5 with the lowest energy gap is polarizable in nature. Thus, water molecule during its interaction with RB5 dye shares its HOMO with the LUMO of dye molecule due to its energy gap of 2.48 eV. From the data plotted as Figure 5.4, it is observed that  $\text{OH}^\bullet$  with comparatively higher value of 4.22 eV will be reactive towards RB5, which has a lower  $E_{\text{HOMO-LUMO}}$  value of 2.48 eV.

Furthermore,  $\text{SiO}_2$  with higher  $E_{\text{HOMO-LUMO}}$  energy gap value of 7.92 eV will be stable but may show its reactivity towards  $\text{Fe}^{2+}$ ,  $\text{Fe}^{3+}$  and RB5 due to their lower  $E_{\text{HOMO-LUMO}}$  energy gaps (Fan et al., 2017). Indeed previous studies have shown the strong feasibility of adsorption of cationic dyes on the surface of silica (Parida, Dash, Patel, & Mishra, 2006). On the other hand, it has also been found that protonated  $\text{H}_2\text{O}_2$  has higher  $E_{\text{HOMO-LUMO}}$  value as compared to  $\text{H}_2\text{O}_2$ . Interaction of  $\text{Fe}^{2+}$  and  $\text{H}_3\text{O}_2$  results in the transfer of electron from HOMO of  $\text{Fe}^{2+}$  to LUMO of  $\text{H}_3\text{O}_2$  because of the smaller energy gap of -6.65 eV. Thus, HOMO of  $\text{Fe}^{2+}$  will be shared with LUMO of  $\text{H}_3\text{O}_2$  and Fenton oxidation

takes place. The produced  $\text{OH}^\bullet$  is highly unstable because it possesses lower LUMO and lower HOMO values of  $-4.18 \text{ eV}$  and  $-8.21 \text{ eV}$ , it readily shares its LUMO with HOMO of dye molecule. Because of  $\text{OH}^\bullet$  production, other side products such as  $\text{Fe}^{3+}$  and  $\text{HO}^-$  are produced. In Fenton oxidation,  $\text{Fe}^{3+}$  will be slightly reactive and because of the smaller LUMO value of  $-15.09 \text{ eV}$ , electrons transfer from HOMO of  $\text{OH}^\bullet$  and residual  $\text{H}_2\text{O}_2$  may take place. As a result, scavenging of  $\text{OH}^\bullet$  and  $\text{H}_2\text{O}_2$  may take place (Karthikeyan, Titus, Gnanamani, Mandal, & Sekaran, 2011).

### 5.1.1.3 Global Hardness and Global Softness

Other quantum chemical parameters that are imperative to discuss are hardness and softness of species. The hardness of a specie is a qualitative indication of its stability and is a measure of resistance of chemical potential to variation in the number of electrons (Pilli et al., 2015). A large difference between LUMO and HOMO energy values indicates that the chemical is hard, and a small difference indicates that the molecule is polarizable and reactive in nature.

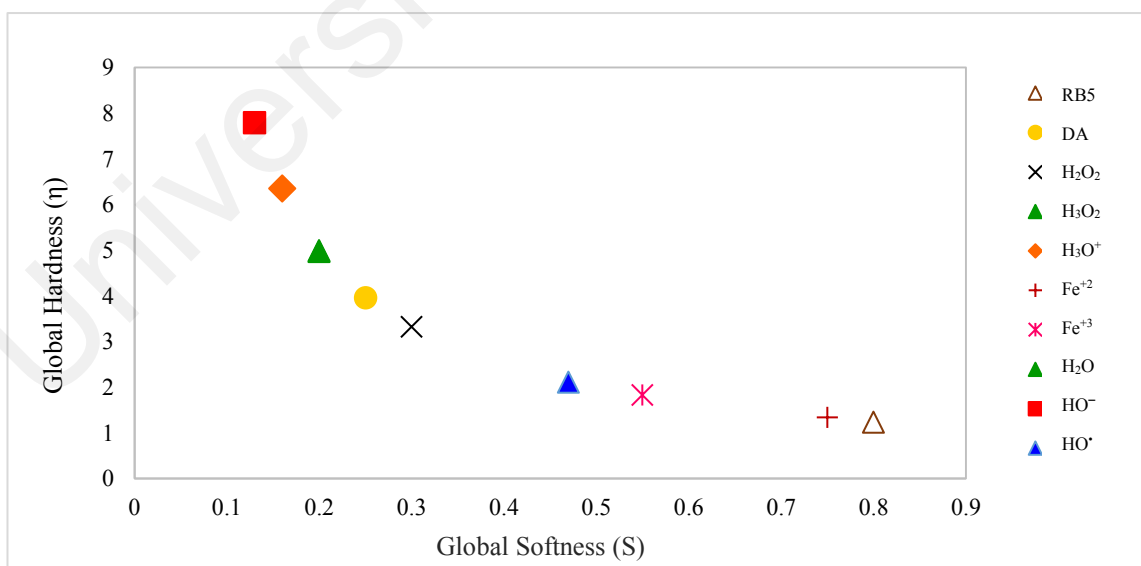
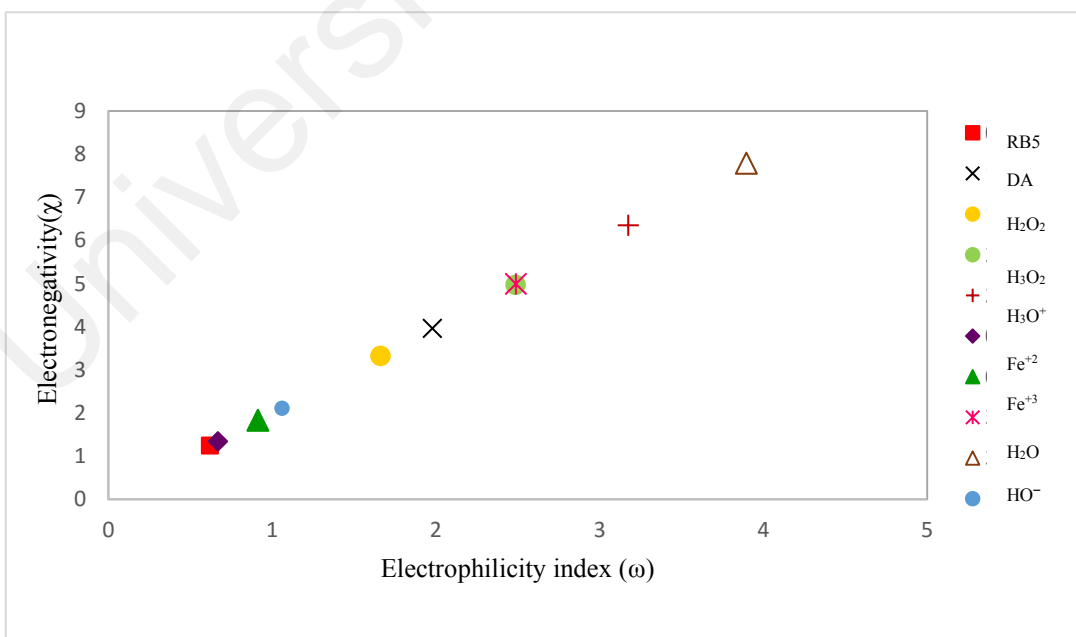


Figure 5.5: Global hardness versus softness of the molecules

The values of global hardness and global softness obtained from simulation are presented as Figure 5.5. A comparative analysis of different values shows that RB5 with the lowest hardness value of 123 eV is soft in nature and HO<sup>-</sup> ion with high hardness value of 7.79 eV is hard in nature. However, Fenton's reagent and fluidized bed carrier lie in the middle of the hardness scale. Therefore, RB5 shows the propensity to be attacked by the oxidant. Furthermore, SiO<sub>2</sub> will also tend to show its affinity to Fenton's reagent and RB5 due to lower hardness values.

#### 5.1.1.4 Electrophilicity Index

Considering the  $E_{\text{HOMO}}$  and  $E_{\text{LUMO}}$  values, electronegativity ( $\chi$ ) and electrophilicity index ( $\omega$ ) are quantum chemical parameters that measure the electron escaping and electron accepting tendency of interacting chemicals. The relationship between  $\chi$  and  $\omega$  is represented as Figure 5.6. Based on Sanderson's electronegativity equalization principle, the movement of electrons will be from the least electronegative molecule to the molecule that shows high electronegativity.



**Figure 5.6: Electronegativity versus electrophilicity index**

From the overall trend depicted in Figure 5.6,  $\text{Fe}^{2+}$  with low electronegative value of 1.34 eV will show electron-donating tendency towards  $\text{H}_3\text{O}_2$ . On the other hand, RB5 with electronegativity value of 1.25 eV will show its tendency towards  $\text{OH}^\bullet$  and Fenton's reagent. On the other hand,  $\text{SiO}_2$  with comparatively higher electronegativity value shows its tendency to accept electrons from Fenton's reagent and RB5.

Parr et al., (1999) explained that lower value of  $\omega$  shows the affinity of a specie towards nucleophile while electrophile is characterized by a high value of  $\omega$ . Thus, from values presented in Figure 5.6, it is found that among Fenton's reagent,  $\text{Fe}^{2+}$  shows the characteristics of nucleophile and will donate electron to  $\text{H}_3\text{O}_2$  because of its high value of  $\omega$ . On the other hand, RB5 will show the nucleophilic character during its interaction with the  $\text{OH}^\bullet$ . However,  $\text{SiO}_2$  with higher  $\omega$  value will show electrophilic character towards Fenton reagents and RB5.

### 5.1.2 Thermodynamic feasibility of interactions

To determine the thermodynamic feasibility of the reacting systems, frequency calculations were performed at the same level of DFT study as described before. From these, thermodynamic parameters (entropy, enthalpy, heat of formation, Gibb's free energy) were obtained. Free energy values provide a way to determine the thermodynamic feasibility of a chemical reaction under certain conditions. Negative values for  $\Delta G$  and  $\Delta H$  indicate that the reaction is thermodynamically feasible and spontaneous. The same concept was used to investigate the interaction of silica with reacting species.

Since different reactants are potentially present in the FBF process, it is necessary to determine the interactions that are most likely to occur under the experimental conditions. The reactants as well as the products that may likely formed in the process are shown in Table 5.1. After identifying the possible reactants and products, frequency calculations of the molecules were conducted to establish feasibility of each interaction. The

simulation results were used to obtain the total electronic energies for each molecule. From these, the change in Gibbs free energy ( $\Delta G$ ) and change in energy of formation ( $\Delta H$ ) for each reaction pathway were determined according. The calculated values of  $\Delta G$  and  $\Delta H$  for each reactant and possible products are shown in Table 5.2.

**Table 5.1: Total and Gibb's free energies of the reactants and products**

<b>Molecule</b>	<b>H (kcal/mol)</b>	<b>G (kcal/mol)</b>
H <sub>2</sub> O	- 240.1273692	- 227.0412756
H <sub>2</sub> O <sub>2</sub>	- 377.60226	- 356.73818
H <sub>3</sub> O <sup>+</sup>	- 177.240827	- 155.8257932
H <sub>3</sub> O <sub>2</sub>	- 237.3123593	- 208.8811362
SiO <sub>2</sub>	- 97920.27047	- 97579.00543
SiO <sub>2</sub> -H <sub>2</sub> O	- 97920.27047	- 97850.65513
SiO <sub>2</sub> - H <sub>2</sub> O <sub>2</sub>	- 98012.91228	- 97936.06991
SiO <sub>2</sub> -H <sub>3</sub> O <sub>2</sub>	- 97644.92284	- 97551.73886
SiO <sub>2</sub> - H <sub>3</sub> O <sup>+</sup>	- 1843.48319	- 1697.705087

From these values, the enthalpy and Gibb's free energy for each reaction are computed and compared. A reaction is thermodynamically feasible with high spontaneity when  $\Delta G$  and  $\Delta H$  are negative. On the other hand, the lower the Gibb's free energy, the more thermodynamically feasible a reaction is. The enthalpies and Gibb's free energies for the possible reactions are shown in Table 5.2. The interaction energies were computed by taking the differences between fragments and complexes from Table 5.1. It can be observed that all the heat of formation of the possible products are negative, except the formation of SiO<sub>2</sub>-H<sub>3</sub>O<sup>+</sup> (95648.13519 kcal/mol). This shows that the interaction of SiO<sub>2</sub>-H<sub>2</sub>O, SiO<sub>2</sub>-H<sub>2</sub>O<sub>2</sub> and SiO<sub>2</sub>-H<sub>3</sub>O<sub>2</sub> are thermodynamically feasible. From the analysis of Gibb's free energies, the most thermodynamically favorable interaction is the formation of SiO<sub>2</sub>-H<sub>2</sub>O ( $\Delta G = -44.60843088$  kcal/mol), followed by SiO<sub>2</sub>-H<sub>2</sub>O<sub>2</sub> ( $\Delta G = -0.3263052$  kcal/mol). The interactions between SiO<sub>2</sub> and H<sub>3</sub>O<sub>2</sub> ( $\Delta G = 236.1477007$  kcal/mol) and SiO<sub>2</sub>- H<sub>3</sub>O<sup>+</sup> ( $\Delta G = 96037.12613$  kcal/mol) are not thermodynamically feasible.

**Table 5.2: Interaction energies of possible complexes**

Product	$\Delta H$ (kcal/mol)	$\Delta G$ (kcal/mol)
SiO <sub>2</sub> -H <sub>2</sub> O	- 365.7655388	- 44.60843088
SiO <sub>2</sub> - H <sub>2</sub> O <sub>2</sub>	- 320.9324594	- 0.3263052
SiO <sub>2</sub> -H <sub>3</sub> O <sub>2</sub>	- 93.23292576	236.1477007
SiO <sub>2</sub> - H <sub>3</sub> O <sup>+</sup>	95648.13519	96037.12613

The high thermodynamic stability of complexes SiO<sub>2</sub>-H<sub>2</sub>O and SiO<sub>2</sub>-H<sub>2</sub>O<sub>2</sub> is due to the fact the SiO<sub>2</sub> exists as a network of Si-O bonds, which are highly polar. Due to the presence of silanol group (Si-OH) on the surface of the silica, it is always embedded with multilayer of water and hence strongly hydrophilic (Parida et al., 2006). This explains why the adsorption of water onto the silica is the most thermodynamically favorable. The adsorbed water molecule will first settle on the part of the silanols as SiOH-O<sub>2</sub>H complex, and the next molecule of water will lead to the formation of SiOH-O<sub>2</sub>H-O<sub>2</sub>H (Yamauchi & Kondo, 1988). The adsorption of H<sub>2</sub>O (and other small molecules) can occur on either site of the silanol as discussed by Yamauchi & Kondo, (1988). In the case of H<sub>2</sub>O<sub>2</sub>, the feasibility of complexation is due to its favorable geometry, which can form strong hydrogen bond to the oxygen of the siloxane bridge (Si-O-Si) of the silica network (Zegliński et al., 2006). It is possible that the O-H group present in both SiO<sub>2</sub>, H<sub>2</sub>O<sub>2</sub> and water played a significant role in the formation of stable complexes.

The results of quantum chemical parameters (HOMO-LUMO energy gaps, hydrophilicity, electronegativity, global hardness and softness) and analysis of interaction energies (Enthalpy and Gibb's free energy) indicate that many interactions are theoretically possible in the FBF process. These results are supported by experimental results that are presented in the subsequent sections. For example, the analysis of FTIR that will be subsequently presented has shown evidence of possible interactions of SiO<sub>2</sub> and H<sub>2</sub>O<sub>2</sub> in the process. Thus, it is evident that beside the more commonly discussed

interaction of SiO<sub>2</sub> and iron, other interactions could occur in FBF process, which may have affect the process performance.

Although the results presented in this section have provided insights into the feasibility and nature of interactions among the fluidized carrier, Fenton's reagent and the organic pollutant, it is necessary that experimental investigation are conducted to validate these predictions.

## **5.2 Experimental Results of the Effect of Carrier**

The effect of SiO<sub>2</sub> as the carriers in FBF process was investigated by studying various aspects of the carriers and their effects on the process performance. The aspects investigated include adsorption of the pollutant by the carrier, the effect of carrier loading in the reactor, iron removal through by the carriers, and the interaction of the carrier with Fenton's reagent and organic pollutant.

### **5.2.1 Adsorption of pollutant on the surface of carrier**

Previous literature on FBF process focused mainly on the crystallization of iron oxide on the carriers. The possible removal of the pollutant through adsorption on the surface of the carriers was scarcely investigated. Therefore, in this work, controlled experiments were conducted to determine the specific contribution of the carrier and Fenton's reagent to the pollutant removal during the FBF process. Experiments were performed with (i) SiO<sub>2</sub> alone, (ii) Fe<sup>2+</sup> + SiO<sub>2</sub> and (iii) SiO<sub>2</sub> + H<sub>2</sub>O<sub>2</sub>.

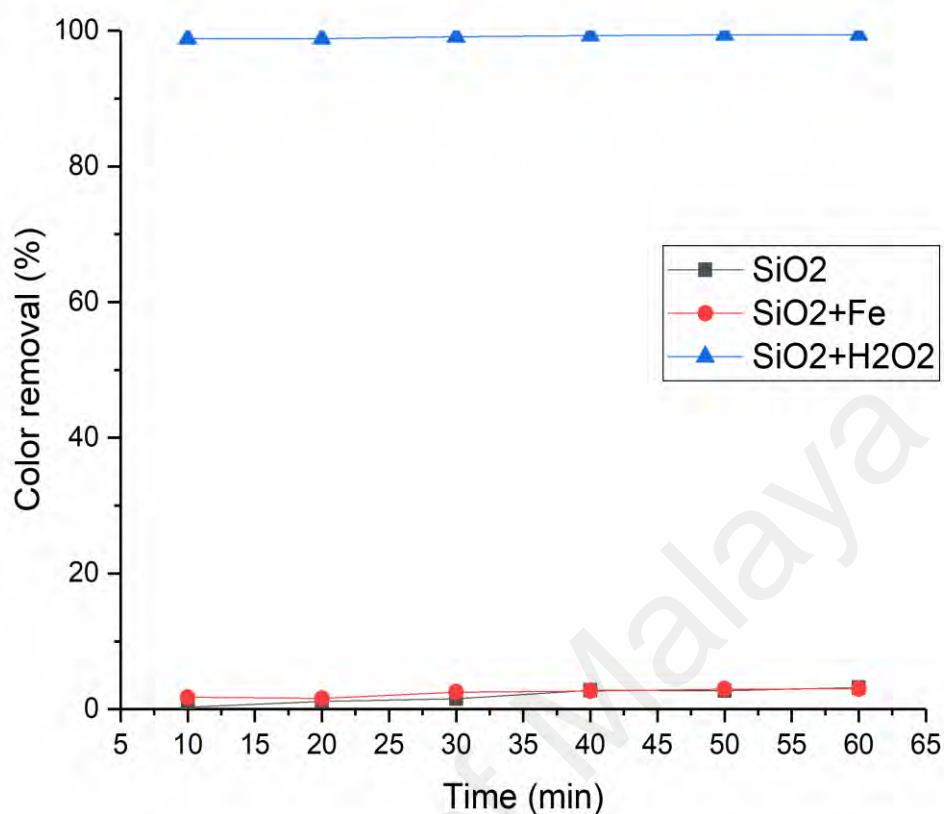


**Figure 5.7: Contribution of different components to color removal (Experimental conditions:  $[\text{Dye}/\text{Fe}^{2+}] = 10$ ,  $[\text{H}_2\text{O}_2/\text{Fe}^{2+}] = 25$ ,  $\text{pH} = 3$ ).**

Figure 5.7 shows the color removal by the controlled experiments. With  $\text{SiO}_2$  alone in the reactor, there was a negligible color removal in the 60 minutes of the process. In the presence of  $\text{SiO}_2$  alone, the dye removal is attributed to the adsorption of the dye on the surface of the fluidized  $\text{SiO}_2$ . The adsorption properties of silica are due to the hydroxyl function,  $\text{Si}-\text{OH}$ , on the surface of the silica (Zegliński et al., 2006). Although  $\text{N}=\text{N}$  bonds could be cleavage through surface complexation (Ziane, Bessaha, Marouf-Khelifa, & Khelifa, 2018), the color removal was rather low. However, the COD removal obtained with  $\text{SiO}_2$  alone was about 24% as shown in Table 5.3. This shows that the adsorption by the  $\text{SiO}_2$  is higher through the aromatic groups of the dye. In general, the low removal efficiency by the  $\text{SiO}_2$  could also be attributed to the short process time, as longer period will be required to reach equilibrium. However, since the objective was to quantify the

adsorption that could occur during the FBF process, the removal was not evaluated beyond 60 min.

**Table 5.3: COD removal by different processes**

Process	SiO <sub>2</sub>	SiO <sub>2</sub> +Fe	SiO <sub>2</sub> +H <sub>2</sub> O <sub>2</sub>	SiO <sub>2</sub> +Fe <sup>2+</sup> + H <sub>2</sub> O <sub>2</sub>
COD removal (%)	23.5	17.25	24*	69.75

\*Scavenging effect

When the catalyst (Fe<sup>2+</sup>) was introduced into the system, the color removal remained very low (Figure 5.7). This is because the SiO<sub>2</sub> and catalyst cannot effectively remove the pollutant through adsorption (Fan et al., 2017). However, in the case of COD removal, the SiO<sub>2</sub>+Fe<sup>2+</sup> process, removed about 17.25% of the initial COD (Table 4.8). The lower COD removal by the SiO<sub>2</sub>+Fe<sup>2+</sup> compared to SiO<sub>2</sub> alone could be due to the possible interaction between SiO<sub>2</sub> and Fe<sup>2+</sup>, which might have reduced the number of active sites for the dye adsorption.

When the process was conducted with SiO<sub>2</sub>+H<sub>2</sub>O<sub>2</sub>, the color removal rose sharply. More than 90% color removal was obtained in the first 10 minutes of the process and nearly complete removal was achieved after 60 minutes. This high removal is due to the oxidation ability of the H<sub>2</sub>O<sub>2</sub>. This indicates that H<sub>2</sub>O<sub>2</sub> can act as an oxidant in the decolorisation of the dye. Additionally, the results of quantum chemical calculations indicated that H<sub>2</sub>O<sub>2</sub> can easily formed complexes with SiO<sub>2</sub>. Therefore, the contribution of color removal through surface complexation may be significant.

In the case of COD removal (Table 5.3), a scavenging effect of H<sub>2</sub>O<sub>2</sub> was observed, leading to the increased in the final COD of the treated solution. Most of the H<sub>2</sub>O<sub>2</sub> remained in the solution, leading to the complexation between SiO<sub>2</sub>, H<sub>2</sub>O<sub>2</sub> and the dye. Once the catalyst was introduced into the system, the decomposition of H<sub>2</sub>O<sub>2</sub> occurs

rapidly and hydroxyl radicals are generated to drive the mineralization of the dye. Consequently, the COD removal increased to about 70% at the end of the process. This removal was due to the synergy between SiO<sub>2</sub> and the Fenton's reagent since only about 49.67% removal was obtained for H<sub>2</sub>O<sub>2</sub>+Fe<sup>2+</sup>.

The results presented in this section show that the SiO<sub>2</sub> also contributed to the pollutant removal through adsorption onto its surfaces. Thus, the pollutant removal by FBF process is likely due to the synergy between Fenton oxidation and adsorption by the carriers. This observation is clearer in the case of COD removal. However, for the color removal, adsorption by the SiO<sub>2</sub> did not play a significant role in the color removal. Although these results have shown that the SiO<sub>2</sub> can contribute to the pollutant removal through adsorption, it is important to examine how the carrier loading affect the performance of the FBF process. The next section discussed the effect of carrier loading on the process performance.

### **5.2.2 Effect of carrier loading**

It has been shown in the previous section that the fluidized carrier can contribute to the removal of pollutants through adsorption. In this section, the effect of carrier loading on the performance of FBF process was investigated by varying the amount of SiO<sub>2</sub> (10g, 20g and 30 g) in the fluidized bed reactor. Figure 5.8 shows the COD removal efficiencies for the three different loadings as the contact time was varied from 10 to 60 min.

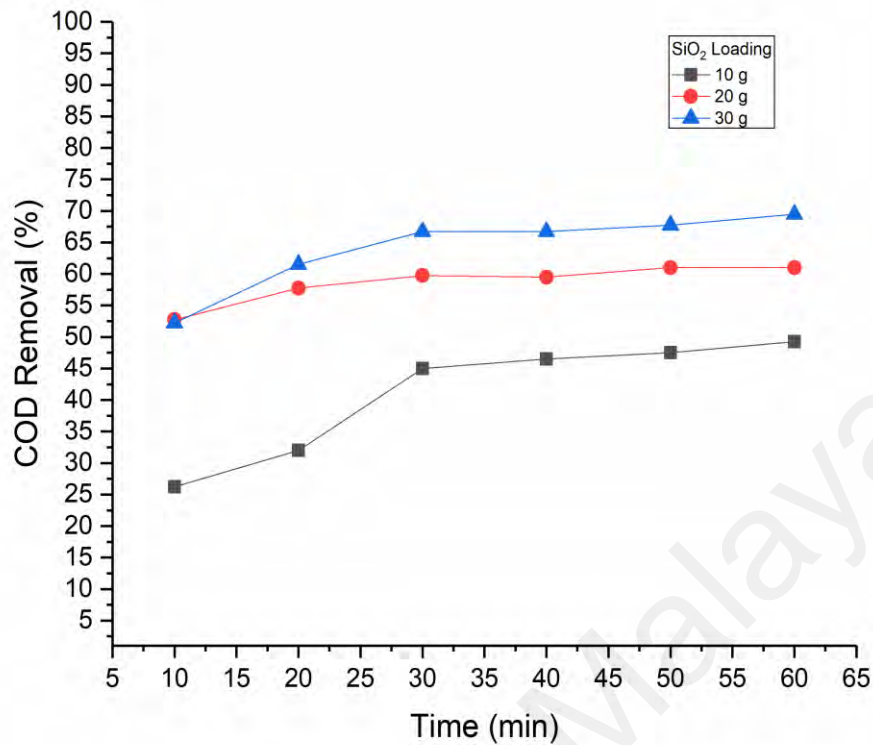


**Figure 5.8: Effect of SiO<sub>2</sub> loading on COD removal (Experimental conditions: [Dye/Fe<sup>2+</sup>] = 10, [H<sub>2</sub>O<sub>2</sub>/Fe<sup>2+</sup>] = 25, pH = 3).**

In all cases, the COD removal efficiency increased with increased in the contact time. It was observed that the COD removal increased as the SiO<sub>2</sub> loading was increased. The highest COD removal obtained with 10 g SiO<sub>2</sub> was about 49% after 60 min. However, the removal efficiency rose to 61% when the SiO<sub>2</sub> loading was increased to 20 g. The highest COD removal was obtained with the SiO<sub>2</sub> loading of 30 g. However, the difference between the performance of 20 g and 30 g SiO<sub>2</sub> was not significant. Anand et al. (2015) reported similar results.

The increase in the COD removal with the increased SiO<sub>2</sub> loading is due to the additional adsorption surfaces provided by the carriers and the increased agitation in the reactor (Anand et al., 2015). However, as discussed earlier, and as reported by Pukdee-Asa et al. (2012), the adsorption of dye by the SiO<sub>2</sub> is relatively low. Therefore, the increased in the COD removal could largely be due to enhanced particles agitation. Since high particle

loading could lead to settling of excess SiO<sub>2</sub> (Chou, Liao, Perng, & Chang, 2004), the loading of 30 g/L was considered as the optimum.

Although there was increase in the performance of FBF process with increased carrier loading as discussed above, some previous studies have observed the effect of carrier loading to be insignificant. For example, Anotai et al. (2012) reported that the loading of carrier was not a significant factor in their study for the degradation of o-toluidine using FBF process. On the other hand, Muangthai et al. (2010) reported that the amount of carrier has a slight effect on the removal of 2,4-Dichlorophenol using FBF process. Thus, the effect of carrier loading observed in this study agrees with the findings of Muangthai et al. (2010).

### **5.2.3 Interaction of carrier with Fenton's reagent**

The possible interactions between the fluidized carriers, Fenton's reagent and organic pollutant can be investigated through the analysis of the surface characteristics and composition of the fluidized carrier before and after the FBF process. Therefore, to investigate these interactions between SiO<sub>2</sub>, Fenton's reagent and RB5, Fourier transform infrared analysis (FTIR), field emission scanning electron microscopy (FESEM) and energy dispersive x-ray (EDX) were performed on the SiO<sub>2</sub> before and after the FBF process. The changes in the surface functional groups, morphology and elemental composition were analyzed and discussed in this section.

#### **5.2.3.1 Fourier Transform Infrared Analysis**

The Fourier transform infrared analysis was conducted in the absorption range of 500 – 4500 cm<sup>-1</sup> using Parking Elmer Spectrophotometer (Frontier). The FTIR spectrum of the SiO<sub>2</sub> before and after the FBF process are shown Figure 5.9.

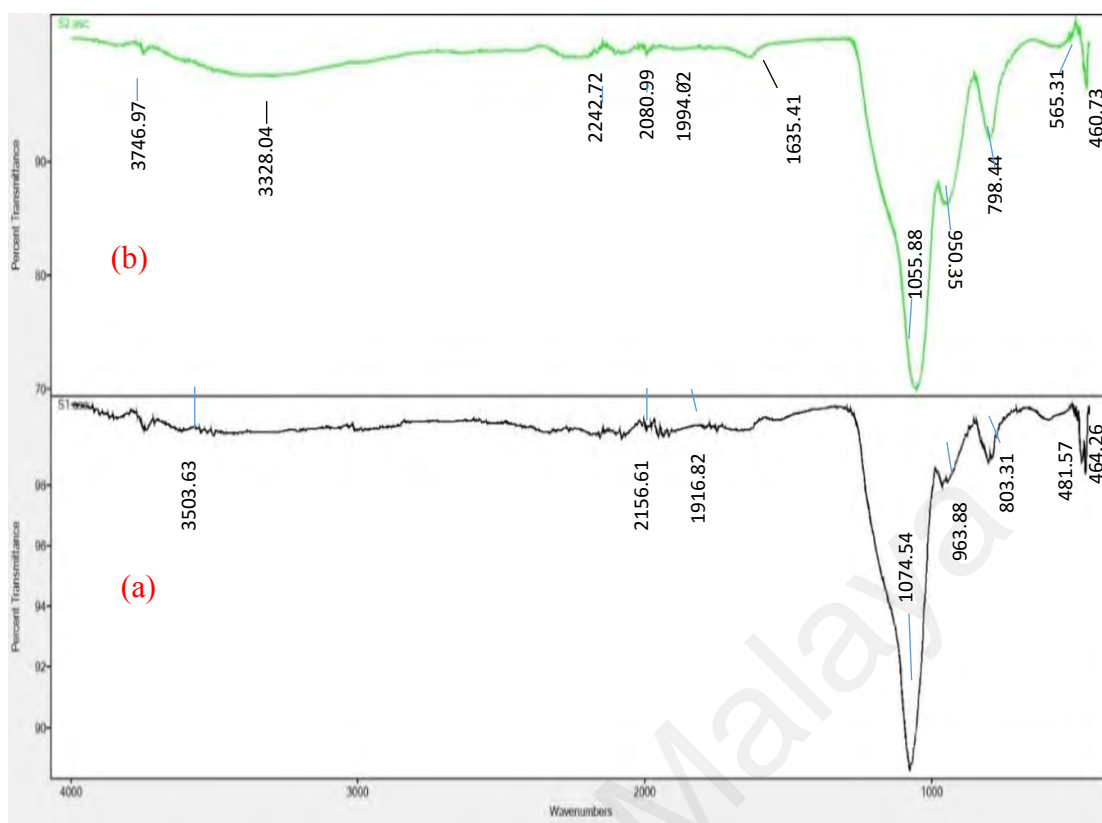


**Figure 5.9: FTIR of SiO<sub>2</sub> (a) before and (b) after fluidized bed Fenton**

It is pertinent to note that SiO<sub>2</sub> exists as a network of Si-O-Si bonds, with silanol groups (Si-OH). From Figure 5.9 (a), the pure SiO<sub>2</sub> exhibited a band in the range of 1040-1150 cm<sup>-1</sup>, which can be assigned to the asymmetric stretching vibration mode of the silanol bridge (Si-O-Si) (Bulkin, Swart, & Lacquet, 1995). The characteristic intense Si-O-Si peak at 1074 cm<sup>-1</sup> is due to the oxygen content of the SiO<sub>2</sub> (Li et al., 2013). Additional less intense peaks can be observed between 500 and 1000 cm<sup>-1</sup> which are due to the bending of OH of the silanol group (Si-OH) (Parida et al., 2006).

After the FBF process, the characteristic peak at 1074 cm<sup>-1</sup> became more intense and shifted to 1055 cm<sup>-1</sup> which is due to the stretching vibration of Fe-O-Si (Quy et al., 2013). The new peak at 565.31 cm<sup>-1</sup> is also attributed to the Fe-O bond (Namduri & Nasrazadani, 2008). A new band also appeared at 1635 cm<sup>-1</sup>, which is due to the bending modes for adsorbed water molecules. Additionally, another broad band appeared around 3400 cm<sup>-1</sup> after the treatment. This band corresponds to the stretching vibration of O-H from the Si-

OH condensation and remaining adsorbed water (Tran, Pham, Le, Nguyen, & Tran, 2013). It can also result from the interaction of  $\text{SiO}_2$  and  $\text{H}_2\text{O}_2$ . Indeed, the new band at  $3746\text{ cm}^{-1}$  has been shown to be contributed by the interaction of  $\text{SiO}_2$  and  $\text{H}_2\text{O}_2$  (Zegliński et al., 2006). It can be observed that most of the characteristic peaks of  $\text{SiO}_2$  became more intense and slightly shifted to lower frequencies after the treatment. These results show that beside Fenton reaction, other interactions between  $\text{SiO}_2$ , Fenton's reagent and dye are possible.

### 5.2.3.2 Morphology and Elemental Composition of $\text{SiO}_2$

One of the processes that occur in fluidized bed Fenton is the possible crystallization or sedimentation of iron oxides on the surface of the fluidized carriers (Garcia-Segura et al., 2016; Pukdee-Asa, et al., 2011). The implication of this is that the sludge production will be reduced and the iron oxide-coated carriers can act as heterogeneous catalyst in the process (Huang, Huang, Cheng, & Huang, 2009). Thus, FESEM/EDX analysis was conducted to investigate the surface morphology of the  $\text{SiO}_2$  before and after the FBF process.

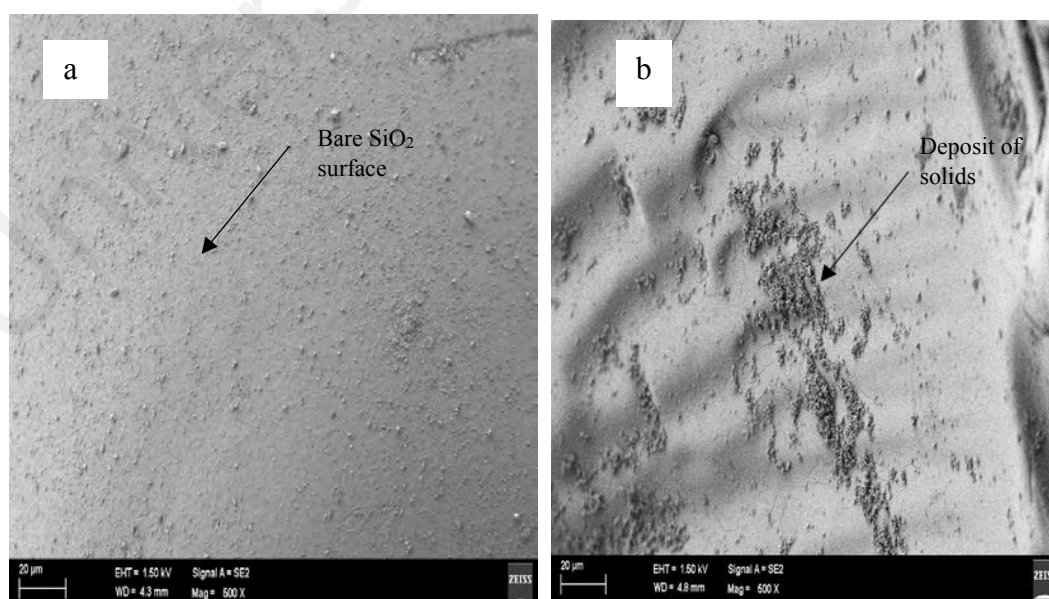


**Figure 5.10: FESEM of  $\text{SiO}_2$  (a) before treatment (b) after treatment**

Figure 5.10 shows the morphologies of the SiO<sub>2</sub> before (a) and after (b). It can be seen clearly that there are changes in the surface of the carrier. While Figure 5.10 (a) shows the rough bare surface of SiO<sub>2</sub>, Figure 5.10 (b) depicts the changes and formation of solids on the surface of the carrier. Sedimentation is one of the possible mechanisms of iron removal in FBF process (Pukdee-Asa, et al., 2011).

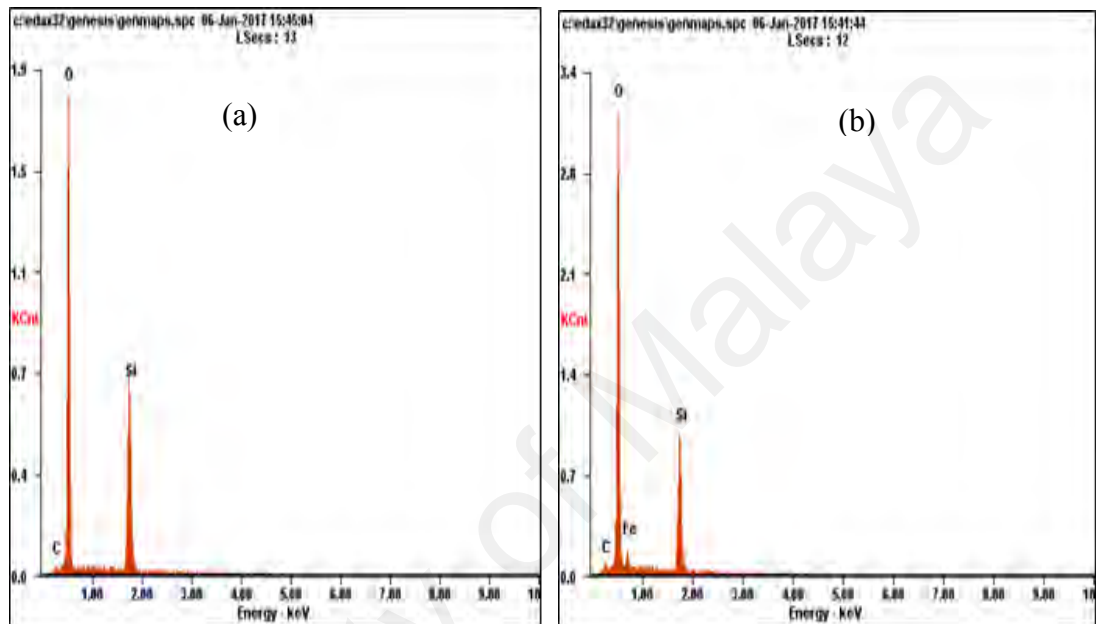


**Figure 5.11: Elemental mapping of SiO<sub>2</sub> (a) before and (b) after treatment**

Figure 5.11 shows the EDX graphs for the SiO<sub>2</sub> before and after the FBF process. Figure 5.11 (a) shows that the major constituents of carrier prior to the FBF process were carbon, oxygen and silicon. However, after the treatment, Fe becomes part of the constituents of the carrier (Figure 5.11(b)), signifying the possible formation of iron oxide on the carriers. Table 5.4 shows the proportions of each element in the carriers. The proportion of oxygen increased from 45.17% to 46.68% and Fe forms about 10.45% of the carriers after the FBF process.

**Table 5.4: Elemental composition of the carrier**

Element	C	O	Si	Fe	Total
<b>Before</b>	01.27	45.17	53.56	-	100%
<b>After</b>	01.53	46.68	41.34	10.45	100%

The results presented here have shown the possible interactions between SiO<sub>2</sub> and Fenton's reagent. The study of the surface functional groups using FTIR have confirmed that SiO<sub>2</sub> interacted with both Fe<sup>2+</sup> and H<sub>2</sub>O<sub>2</sub> as spectrum peaks that suggest their interactions were obtained. The morphological analysis of the SiO<sub>2</sub> before and after the process shows that there was formation of iron oxide on the surface of the carrier, which is further supported by the elemental composition analysis. The findings in these sections support the quantum simulation presented in section 5.1, which pointed to the possibility of interaction of SiO<sub>2</sub> and H<sub>2</sub>O<sub>2</sub> in addition to the commonly discussed iron oxide crystallization.

#### 5.2.4 Iron removal in fluidized bed Fenton

One of the objectives of FBF process is the possibility of reducing the generation of iron sludge. To investigate the fate of iron in the FBF process, the total Fe<sup>2+</sup> concentration was monitored for both FBF process and conventional Fenton processes. Figure 5.12 shows the percentage of the remaining Fe<sup>2+</sup> in the effluent of both FBF process and conventional Fenton oxidation.

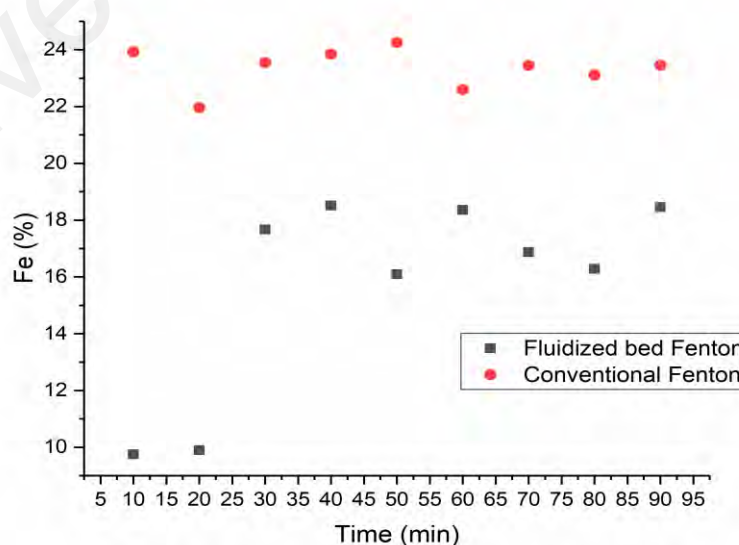


**Figure 5.12: Iron removal by fluidized bed Fenton and conventional Fenton (Experimental conditions: [Dye/Fe<sup>2+</sup>] = 10, [H<sub>2</sub>O<sub>2</sub>/Fe<sup>2+</sup>] = 25, pH = 3).**

The FBF process exhibited lower  $\text{Fe}^{2+}$  concentration in the treated solution throughout the process time. In the first 20 minutes of the FBF process, only about 10% of the initial  $\text{Fe}^{2+}$  concentration was in the treated solution in contrast to about 22% in the conventional Fenton oxidation. In both processes, however, the total  $\text{Fe}^{2+}$  concentration in the effluent fluctuates. At the end of 90 minutes, about 18% of the initial iron concentration remained in the effluent of the FBF process. On the average, the FBF process resulted in about 10% higher  $\text{Fe}^{2+}$  removal compared to the removal obtained with conventional Fenton oxidation.

The higher consumption of  $\text{Fe}^{2+}$  in the FBF process is due to the presence of the fluidized  $\text{SiO}_2$ , which induces iron crystallization. This also points to the possibility that part of the dissolved iron might have crystallized on the surface of the  $\text{SiO}_2$  and hence, its low concentration in the case of the FBF process. Previous studies have pointed out the higher removal of iron by the FBF process in comparison with conventional Fenton oxidation (Anotai et al., 2012; Anotai et al., 2009; Chou & Huang, 1999). For example, Muangthai, et al. (2010) reported 16% and 10% iron removals for FBF process and conventional Fenton oxidation respectively.

### **5.3 Summary**

The theoretical and experimental results presented in this section have shown that different interactions can occur in FBF process. The results of quantum chemical calculations indicated that the fluidized carrier can interact with the Fenton's reagent and the organic pollutant. These predictions were supported by the experimental results presented. The fluidized carrier is therefore an important parameter that can affect the performance of the FBF process. Thus, the type and properties of the carrier can be manipulated towards enhancing the performance of the FBF process. To this end, the

feasibility of using an alternative carrier that can enhance the performance of the FBF process forms the third objective of this study.

University of Malaya

## **CHAPTER 6: PALM KERNEL SHELL ACTIVATED CARBON AS CARRIER**

It has been highlighted previously that the type and characteristics of carriers can be manipulated to enhance the performance of the FBF process. In this section, the possibility of using a palm kernel shell GAC to enhance the performance of the FBF process was investigated. Palm kernel shell is one of the byproducts of palm oil processing which is cheap and readily available. Consequently, PKSGAC was evaluated as an alternative to SiO<sub>2</sub>. This section presents the characteristics of the PKSGAC and its performance as carriers in fluidized bed Fenton process. The performance of the PKSGAC was also compared with that of SiO<sub>2</sub>.

### **6.1 Characteristics of Palm Kernel Shell Granular Activated Carbon**

The properties of the PKSGAC were studied by different physical analysis. The particle size distribution was studied using Malvern Mastersizer. The total surface charge of the PKSGAC was analyzed through zeta potential analysis. The textural properties were investigated using BET analysis. Surface morphology was studied using SEM analysis. The composition and surface functional groups were studied through EDX and FTIR analyses. These results are discussed in this subsection.

#### **6.1.1 Particle size distribution**

The particle size distribution of the PKSGAC was analyzed using a Malvern Mastersizer and the distribution is shown in Figure 6.1. The particle size ranges between 0.020 μm to 2000 μm. The surface weighted mean diameter of the PKSGAC is 125.580 μm. From Figure 6.1, the highest proportion of the particle size falls around 1000 μm.

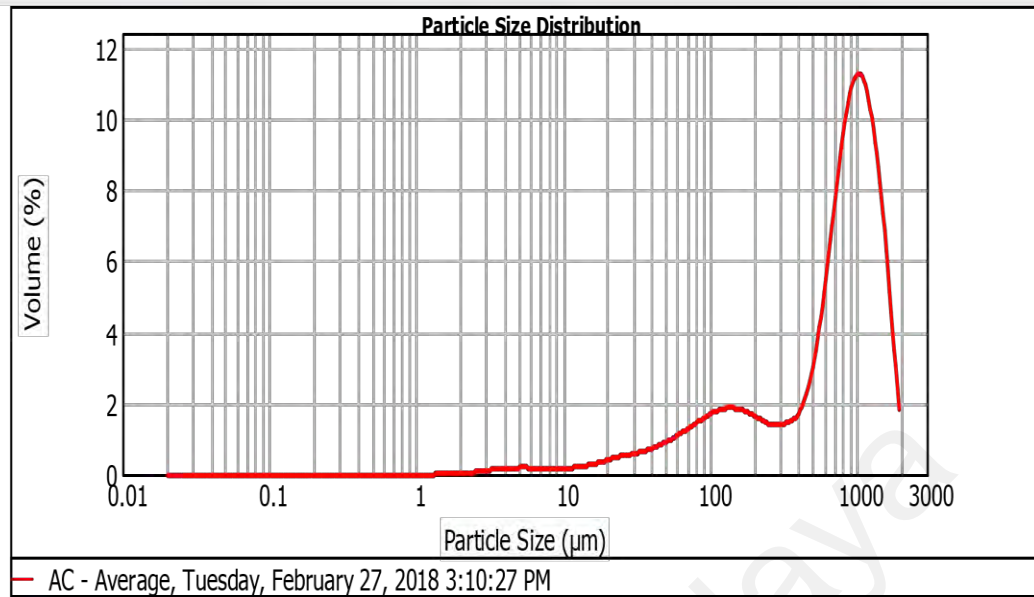


Figure 6.1: Particle size distribution of palm kernel shell

### 6.1.2 Textural analysis

The BET surface area and pore size of the PKSGAC were determined by N<sub>2</sub> adsorption-desorption method. The surface area and pore size are presented in Table 6.1 while Figure 6.2 depicts the adsorption/desorption isotherm.

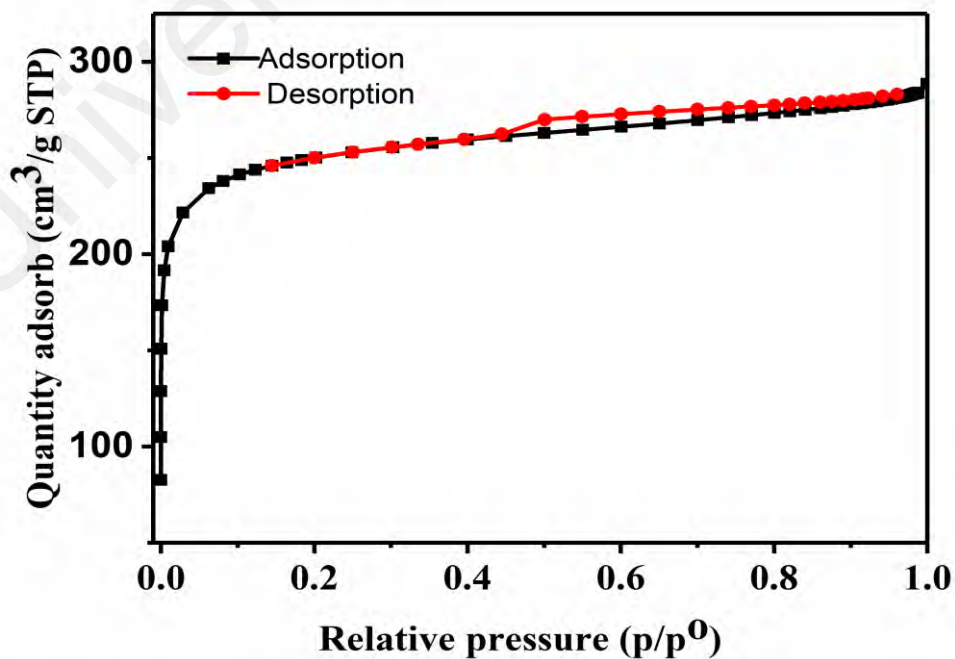


Figure 6.2: N<sub>2</sub> adsorption/desorption isotherm of palm kernel shell

**Table 6.1: Textural properties of palm kernel shell**

Sample	BET Surface area (m <sup>2</sup> /g)	Langmuir Surface area (m <sup>2</sup> /g)	Pore volume (cm <sup>3</sup> /g)	Pore size (nm)
PKSGAC	949.56	1043.94	0.45	1.88

The average pore size of PKSGAC is 1.88 nm, indicating that it contains microporous particles. The calculated BET surface area is 949.56 m<sup>2</sup>/g, which is in the typical range of the surface of areas of AC. The single adsorption/desorption total pore volume measurement shows that micropore volume constitutes more than 67% of the total pore volumes, indicating that the PKSGAC is largely microporous. Similar observations on granular activated carbon have reported previously (Mazarji, Aminzadeh, Baghdadi, & Bhatnagr, 2017; Xu et al., 2019). This is further proved by the N<sub>2</sub> adsorption/desorption isotherm shown in Figure 6.2. The N<sub>2</sub> adsorption/desorption exhibited a type I isotherm, which is typically obtained with microporous solids. The isotherm displayed an H4 hysteresis containing a slit-like pores, which shows that the PKSGAC contains limited amounts of mesopores Chan et al., 2009; Mazarji et al., 2017).

### 6.1.3 Zeta potential

Zeta potential is a measure of the magnitude of charge repulsion/attraction at the interface of solid particle and its liquid medium. It reflects the effective charge at the surface of the particles and is therefore an important parameter to understand the stability of particles, and mechanism of particle interactions. Since zeta potential can affect the possible interactions between PKSGAC and Fenton's reagent, the zeta potential of the PKSGAC was measured at different pH values using a Malvern Zetasizer.

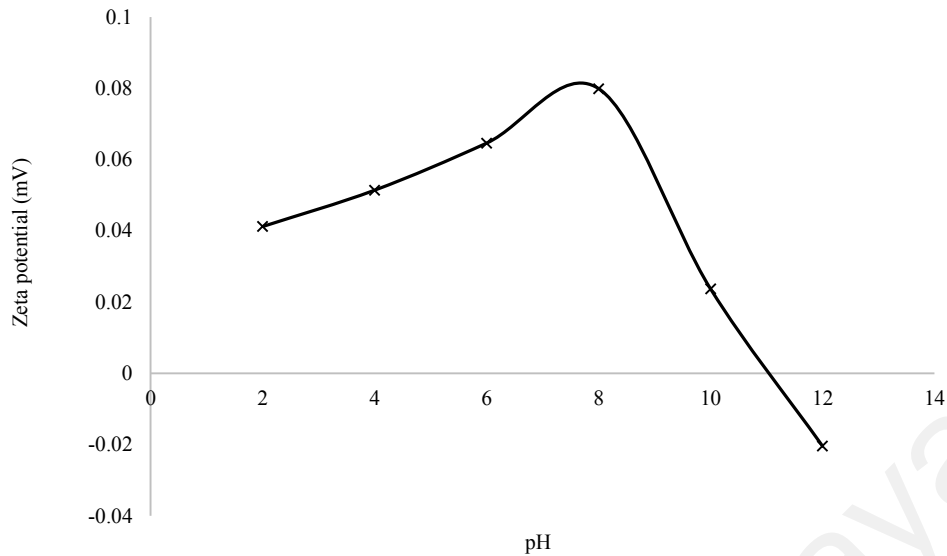


**Figure 6.3: Point of zero charge of palm kernel shell**

To determine the point of zero charge ( $\text{pH}_{\text{pzc}}$ ) of the PKSGAC, the values of zeta potential were plotted against pH (Figure 6.3). The point of zero charge occurs at pH 11. The implication is that the surface of the PKSGAC is acidic at pH values less than 11, and basic at pH values above 11. Consequently, at pH values below 11, the surface of the PKSGAC will be favorable to the homogeneous Fenton reaction, which requires acidic environment.

#### **6.1.4 Morphology and elemental composition of palm kernel shell**

Analysis of morphology and elemental composition are some of the approaches that can be used to gain insight into the possible interaction between fluidized carriers and Fenton's reagent. Thus, the morphology and elemental composition of the PKSGAC were studied using scanning electron microscopy (SEM) and energy dispersive x-ray analysis (EDX).

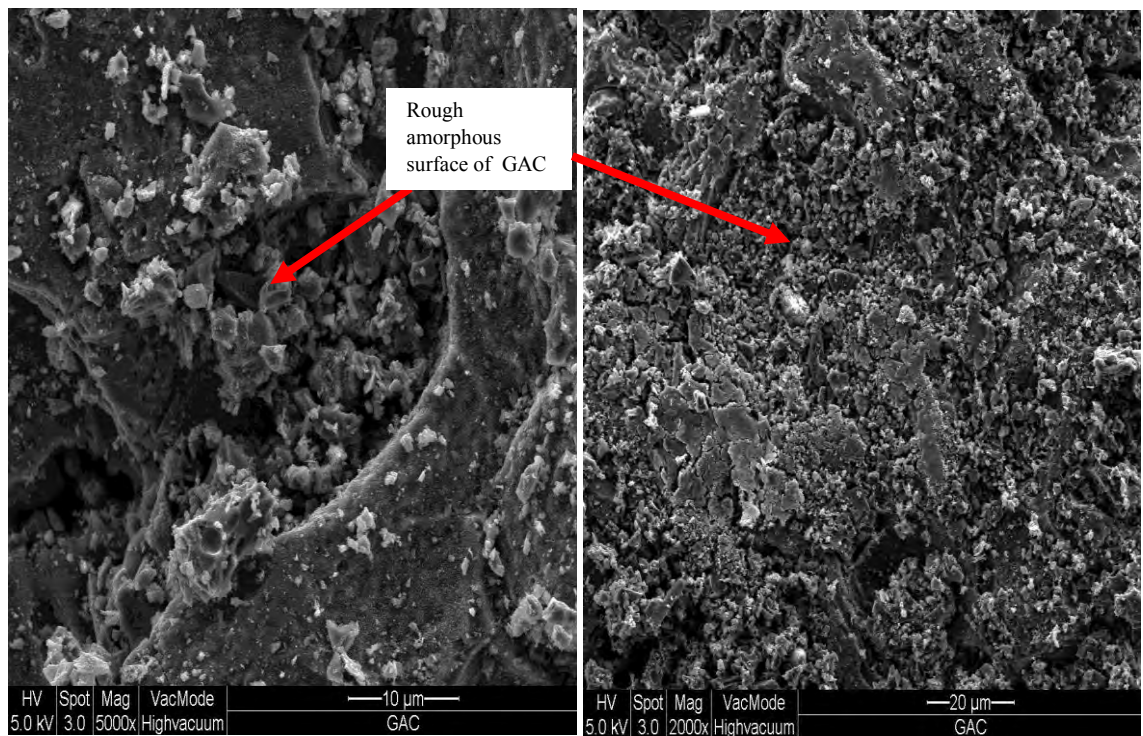


**Figure 6.4: SEM of palm kernel before fluidized bed Fenton**

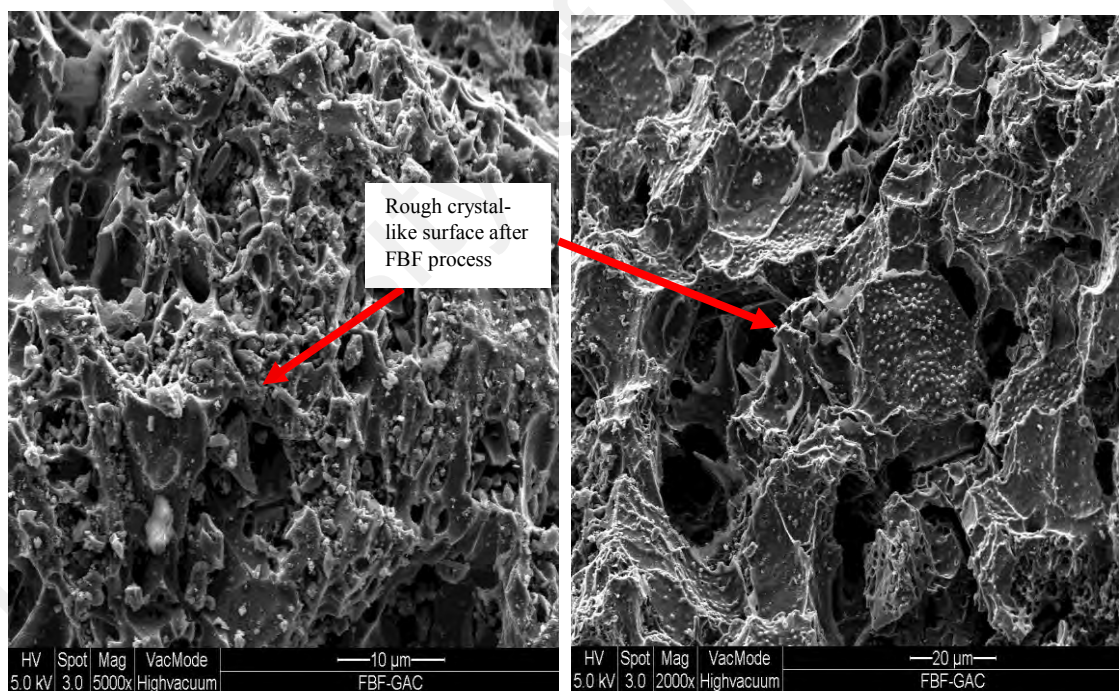


**Figure 6.5: SEM of palm kernel shell after fluidized bed Fenton**

Figure 6.4 shows the morphology of the fresh PKSGAC, displaying a granular structure, with an irregular rough surface that is typical of activated carbon (Gonçalves, Nakamura, Furtado, & Veit, 2017; Kwon et al., 2018; Mines et al., 2018). On the other hand, Figure 6.5 displays the PKSGAC after the FBF process. The changes in the morphology of the

carrier can be seen as the surface displays a rough, crystalline structure compared to the amorphous structure of Figure 6.4.

To further understand the interaction of PKSGAC with Fenton's reagent, energy dispersive x-ray analysis was conducted to investigate the elemental composition of the PKSGAC before and after the FBF process. Table 6.2 shows the elemental composition and the percentage weight of the elements in the PKSGAC before and after the FBF process. Before the FBF process, C (86.59%) and O (10.18%) were the major constituents of the activated carbon, though traces of other elements (including F, Mg, Al and Si) were observed in the elemental mapping. These traces are likely due to impurities from the preparation of the activated carbon. Iron was not detected in the elemental mapping. However, after the FBF process, Fe (about 14%) was detected in the elemental composition. Furthermore, the percentage weight of C decreased from 86.59% to 53.59% while that of O increased from 10.18% to 29.66%. The decreased in the C content is due to the surface coating of the PKSGAC by the iron oxide and other hydrolysis products. The appearance of Fe and the increase of O can be attributed to the formation of iron oxide on the surface of the PKSGAC, which is one the processes that occur in FBF (Garcia-Segura et al., 2016).

**Table 6.2: Elemental composition of palm kernel shell**

<b>Element (%)</b>	<b>C</b>	<b>O</b>	<b>Fe</b>	<b>Others</b>	<b>Total</b>
<b>Before FBF process</b>	86.59	10.18	-	3.26	100%
<b>After FBF process</b>	53.59	29.66	14.82	1.93	100%

Analysis of the morphology and elemental composition of fluidized bed carriers is one of the approaches to understand the possible interactions in FBF process. The results discussed in this section have shown that iron oxide formed on the surface of the PKSGAC due to the presence of Fe and the increased amount of O after the FBF process.

These observations agree with the results of quantum chemical calculations presented earlier. In addition, the analysis of the surface functional group of the PKSGAC, which is presented in the next section, further agrees with these results.

### 6.1.5 Analysis of surface functional groups

The study of the surface functional groups of the fluidized carrier before and after the FBF process can help in understanding the interaction of the carriers and Fenton's reagent. Therefore, FTIR analysis was used to study the surface functional groups of the PKSGAC before and after the FBF process.

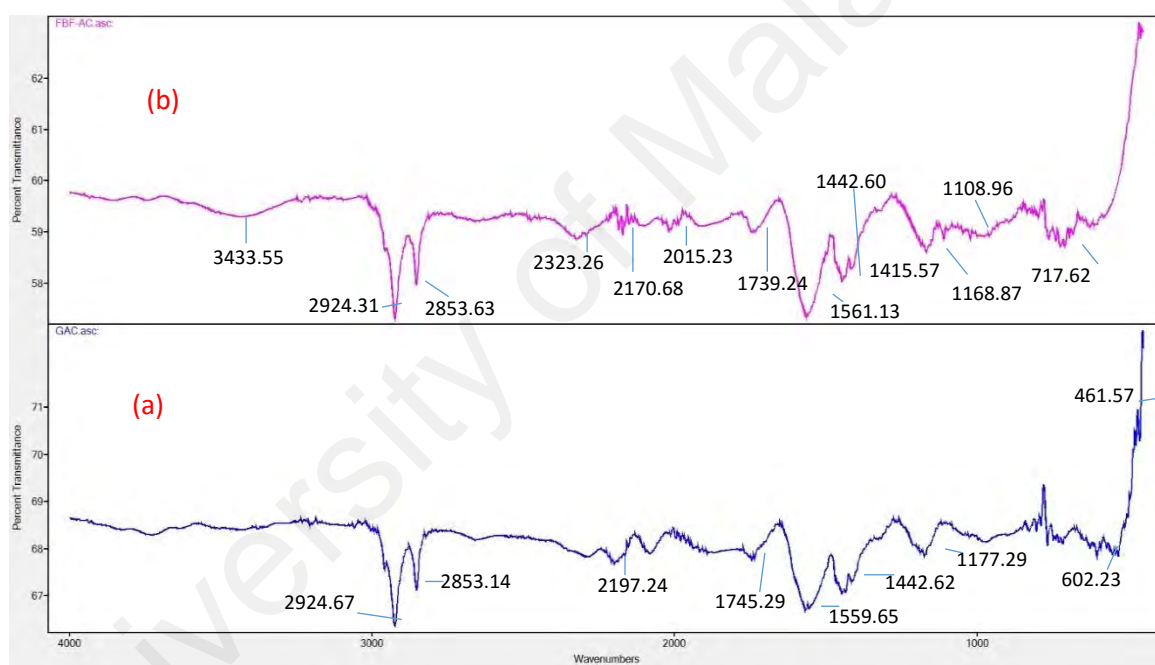


**Figure 6.6: FTIR of palm kernel shell (a) before and (b) after fluidized bed Fenton**

The spectra of the PKSGAC before and after the FBF process are shown in Figure 6.6. The results of the FTIR analysis of the fresh PKSGAC is similar to that reported by Misnon, Zain, Aziz, Vidyadharan, & Jose, (2015) in their study for electrochemical properties of palm kernel shell activated carbon. The wide weak band around  $3700\text{ cm}^{-1}$  is due to the O – H stretching mode resulting from absorption of water molecules and alcohols (Kundu, Sen Gupta, Hashim, & Redzwan, 2015; Mahapatra, Ramteke, &

Paliwal, 2012). The two sharp peaks at 2924 and 2853  $\text{cm}^{-1}$  can be assigned to the asymmetric and symmetric C–H stretching (Grzyb et al., 2010). The relatively weak peak at 1748  $\text{cm}^{-1}$  is due to the stretching of C=O and the peak at 1559  $\text{cm}^{-1}$  is assigned to the stretching mode from carbonyl group C=C (Zheng, Zhao, & Ye, 2014). The weak peak at 1177  $\text{cm}^{-1}$  is due to the stretching mode of C–O–C (Misnon et al., 2015). The region of 700 – 600  $\text{cm}^{-1}$  showing weak bands can be assigned to the vibration of C–H bending (Mahapatra et al., 2012).

After the FBF process, the intensities of the bands decreased. A new broad and strong band appeared at 3433  $\text{cm}^{-1}$ , which can be due to O–H stretching resulting from adsorbed water or hydroxyl groups on the surface of the GAC (Misnon et al., 2015). Additional peaks are also observed at 2323  $\text{cm}^{-1}$ , 2015  $\text{cm}^{-1}$ , 1108  $\text{cm}^{-1}$  and 1020  $\text{cm}^{-1}$ . On the other hand, the band at 461  $\text{cm}^{-1}$  totally disappeared. The appearances of new peaks and the disappearance of the initial ones indicate the possible interactions between the PKSGAC, Fenton's reagent and the pollutant.

Some changes were observed in the analysis of the FTIR spectrum of the PKSGAC after the FBF process. These changes pointed to the possible interactions between the PKSGAC, Fenton's reagent and the organic pollutant. Taking the results presented in previous sections into cognizance, the results of the FTIR analysis have provided support on the possible nature of interaction between PKSGAC and Fenton's reagent.

## **6.2 Performance of Palm Kernel Shell Activated Carbon**

In order to investigate the potential of the PKSGAC as an alternative carrier in FBF process and to compare its performance with  $\text{SiO}_2$ , its efficiency in the removal of RB5 was evaluated. These results are discussed in this section, while comparing with the performance of  $\text{SiO}_2$  as discussed in Chapter 5.

### 6.2.1 Effect of pH on the performance of palm kernel Shell

Fenton oxidation is strongly affected by the solution pH, which is required to be kept within a narrow acidic range for effective performance of the process. The optimum pH to ensure catalytic ability of  $\text{Fe}^{2+}/\text{Fe}^{3+}$  is usually between 2.8 and 3.5 (Vitale et al., 2016). This represents one of the major limitations of homogeneous Fenton oxidation. Higher pH above this range leads to precipitation of oxyhydroxide while lower pH slows down the reactivity of  $\text{Fe}^{2+}$  (Vitale et al., 2016). Therefore, the effect of pH on the FBF process using PKSGAC as the carrier was investigated. The effect of pH on the process performance was studied under pH 3 and 7. The objective was to find out whether the PKSGAC can assist in conducting the FBF process under circumneutral pH.

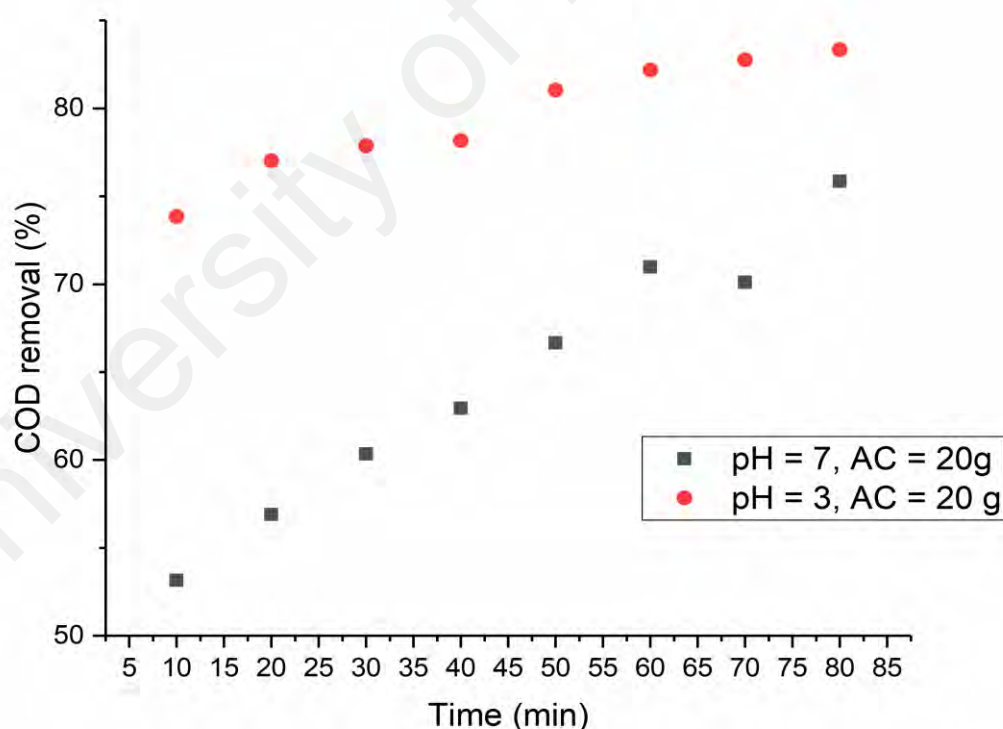


**Figure 6.7: Effect of pH on COD removal (Experimental conditions: carrier loading = 20 g,  $[\text{Dye}/\text{Fe}^{2+}] = 10$ ,  $[\text{H}_2\text{O}_2/\text{Fe}^{2+}] = 25$ )**

Figure 6.7 shows the rate of COD removal under the two different pH conditions. The COD removal under pH 3 is superior to that of pH 7 throughout the process time. The

rate of COD removal is faster under pH 3. For example, the COD removal under pH 3 was about 74% in the first 10 minutes whilst it was only about 53% for pH 7 within the same time. At the end of 60 minutes, the COD removal was more than 80% for pH 3 whereas it was only about 69% for pH 7.

Under pH 3,  $\text{Fe}^{2+}$  remains in solution and exerts its catalytic ability to decompose  $\text{H}_2\text{O}_2$  effectively. Consequently, the removal of the organic pollutant is dominated by oxidation through Fenton reactions. Additionally, the PKSGAC exerts its optimum adsorption capacity towards the pollutant. This indicates the rapid rate of COD removal. On the other hand, pH 7 slows down Fenton reaction due to the precipitation of insoluble iron oxides (Villegas-Guzman et al., 2017). These iron oxides are precipitated on the surface of PKSGAC and can subsequently act as heterogeneous Fenton catalyst (Chen et al., 2016; Garcia-Segura et al., 2016; Lyu, Zhou, & Wang, 2016). However, the crystallization of iron oxide on the surface of PKSGAC may also reduce the adsorption sites for the pollutant. The low COD removal under this condition is therefore due to the lower homogeneous reaction and adsorption sites for the pollutant.

From Figure 6.7, the difference between the COD removal at pH 3 and pH 7 is not very significant. For example, at the end of the 80 min of the process, the difference in the COD removal was only 7%. This shows that the possibility of conducting the process at circumneutral pH should be considered.

Figure 6.8 shows the color removal from the RB 5 for the two pH conditions. Although in each case more than 99% color removal can be achieved in the first 10 minutes, there was little difference in the overall color removal between the two different pH conditions. In the first 10 minutes, for example, about 99.75% color removal was achieved under pH 7 and 99.35% color removal was achieved under pH 3. After that, the color removal fluctuated, and then remained nearly the same throughout the process. Unlike COD

removal, the color removal was slightly higher at the neutral pH. The decreased in color removal at acidic pH has been attributed to the scavenging effects of  $H^+$  and precipitation of iron hydroxide (Kwon et al., 1999). This observation is consistent with many previous studies using Fenton oxidation (Bautista et al., 2007; Deng & Englehardt, 2006).

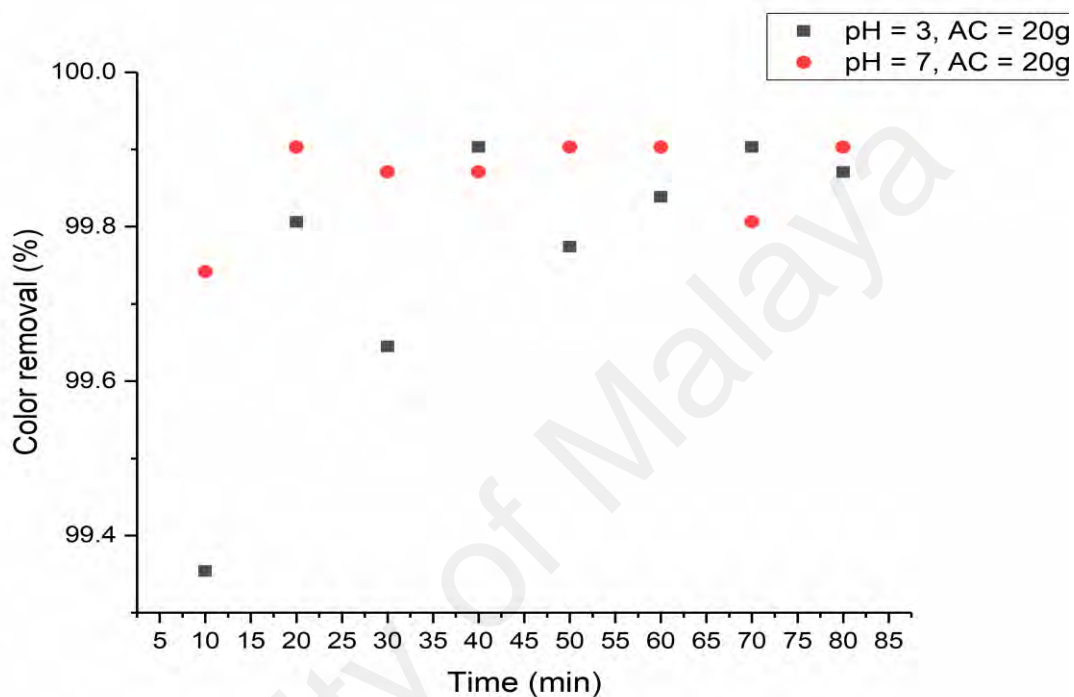


**Figure 6.8: Effect of pH on color removal (Experimental conditions: carrier loading = 20 g,  $[Dye/Fe^{2+}] = 10$ ,  $[H_2O_2/Fe^{2+}] = 25$ )**

Although the performance of the PKSGAC is higher under pH 3 compared to pH 7, there was only about 7% difference in the COD removal after 80 min. Thus, the possibility of cost reduction by conducting the process under the neutral pH must be considered. Large amount of chemicals are used during the acidification and subsequent neutralization processes that are necessary in conventional Fenton oxidation (Li, Zhang, Wang, Zheng, & Zheng, 2016; Usman et al., 2016). Eliminating these two steps, through conducting Fenton oxidation at circumneutral pH, can therefore reduce the overall cost of the treatment. In this regard, the PKSGAC offers an advantages since it has the potential to allow the application of the FBF process at circumneutral pH.

### 6.2.2 Adsorption of pollutant by palm kernel shell

To investigate the contribution of PKSGAC through adsorption of the pollutant, controlled experiments were conducted with PKSGAC alone and compared with the combined process (Fenton + PKSGAC). The results of the controlled experiments for COD and color removals are shown in Figure 6.9 and Figure 6.10 respectively.

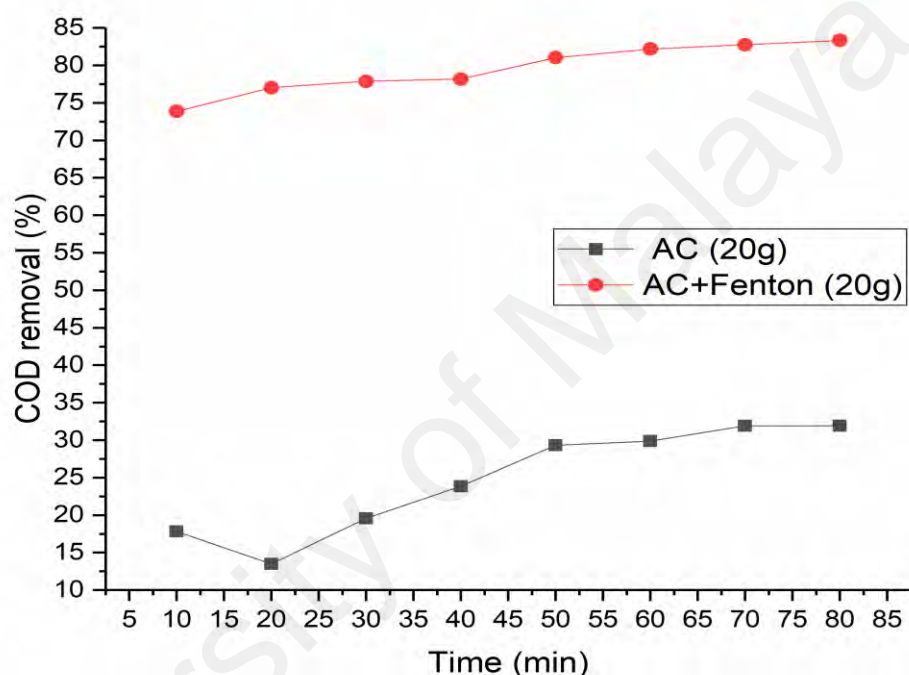


**Figure 6.9: Contribution of adsorption to COD removal (Experimental condition: pH = 3, [Dye/Fe<sup>2+</sup>] = 10, [H<sub>2</sub>O<sub>2</sub>/Fe<sup>2+</sup>] = 25)**

Under adsorption alone, the COD removal was only about 8% in the first 10 minutes and only increased to about 30% after 80 minutes. The COD removal through adsorption alone is due to the high surface area of the PKSGAC (950 m<sup>2</sup>/g) and the presence of surface functional groups. However, for the combined PKSGAC and Fenton oxidation, the removal was more than 70% in the first 10 minutes and reached more than 80% after 80 minutes. Compared to Fenton oxidation, adsorption is a slow process and a very long time may be required to reach equilibrium, hence the lower removal under the designed process time. However, in the presence of Fenton's reagent, the removal of the pollutant

is also driven by the hydroxyl radical oxidation, which has a high oxidation potential (2.8 eV) (Neyens & Baeyens, 2003). Consequently, the COD removal is higher in the combined process due to the synergy of adsorption and Fenton oxidation.

Previous studies have reported similar results when Fenton was integrated with adsorption (Lau, Alberto, Teixeira, Valéria, & Yokoyama, 2016; Li, Bao, Zhang, & Lei, 2015; Li, Zhao, Song, & Guo, 2017). Bel et al. (2018) compared the removal of 2-chlorophenol through adsorption and adsorption-Fenton by Fe-rich clay. The adsorption resulted in 20% removal of 2-chlorophenol, which reached more than 70% under the combined process. Li et al. (2018) have also reported the lower efficiency of adsorption compared to the synergistic performance of the combined adsorption-Fenton oxidation. In the case of adsorption, the removal is through the physico-chemical interaction at the surface of the adsorbent while further degradation is provided when the Fenton oxidation was introduced.

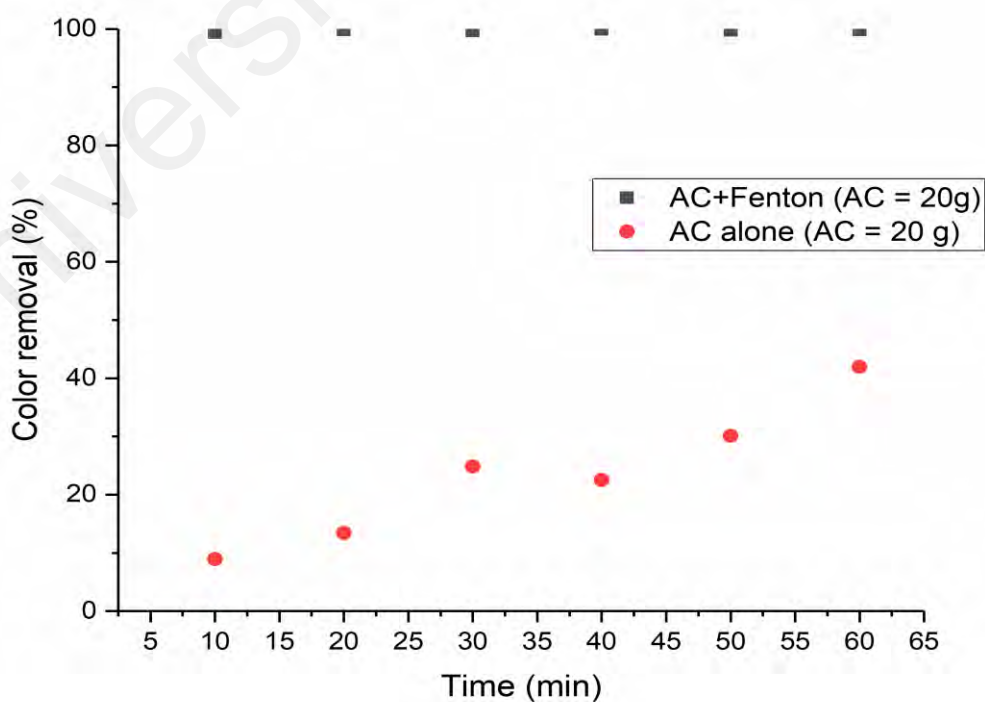


**Figure 6.10: Contribution of adsorption to color removal (Experimental conditions: pH = 20 g, [Dye/Fe<sup>2+</sup>] = 10, [H<sub>2</sub>O<sub>2</sub>/Fe<sup>2+</sup>] = 25)**

In the case of color removal, adsorption alone could remove up to 10% within the first 10 minutes, which increased to about 40% after 60 minutes (Figure 6.10). On the other hand, the combined process achieved nearly complete removal of color after 10 minutes. This also points to the synergy of the combined process. Although the trend shows that higher COD and color removals could be achieved beyond the 80 minutes, the objective was to determine the contribution of the adsorption within the designed time. Consequently, the treatment was stopped at 60 minutes.

The results presented in this section have shown that the carrier (PKSGAC) acted as an adsorbent, besides providing surfaces for the nucleation and precipitation of iron oxide. This means that dual benefits can be achieved when using PKSGAC as an alternative carrier. The contribution of the PKSGAC through adsorption is higher than that of SiO<sub>2</sub> as presented in earlier. This is due to the higher adsorption capacity of the PKSGAC. Thus, PKSGAC presented a better alternative in terms of the simultaneous adsorptive removal of the pollutants by the solid carriers. The next section examines the effect of PKSGAC loading on the performance of the FBF process.

### **6.2.3 Effect of palm kernel shell loading**

Although the main objective of the fluidized carrier is to provide surfaces for the nucleation and crystallization of iron oxide, it can also serve as an adsorbent for the target pollutant. The previous section has quantified the adsorptive removal of the pollutant by the PKSGAC. In this section, the effect of particle loading on the process performance was investigated by varying the amount of the PKSGAC in the fluidized bed reactor (10g, 20 g, 30 g).

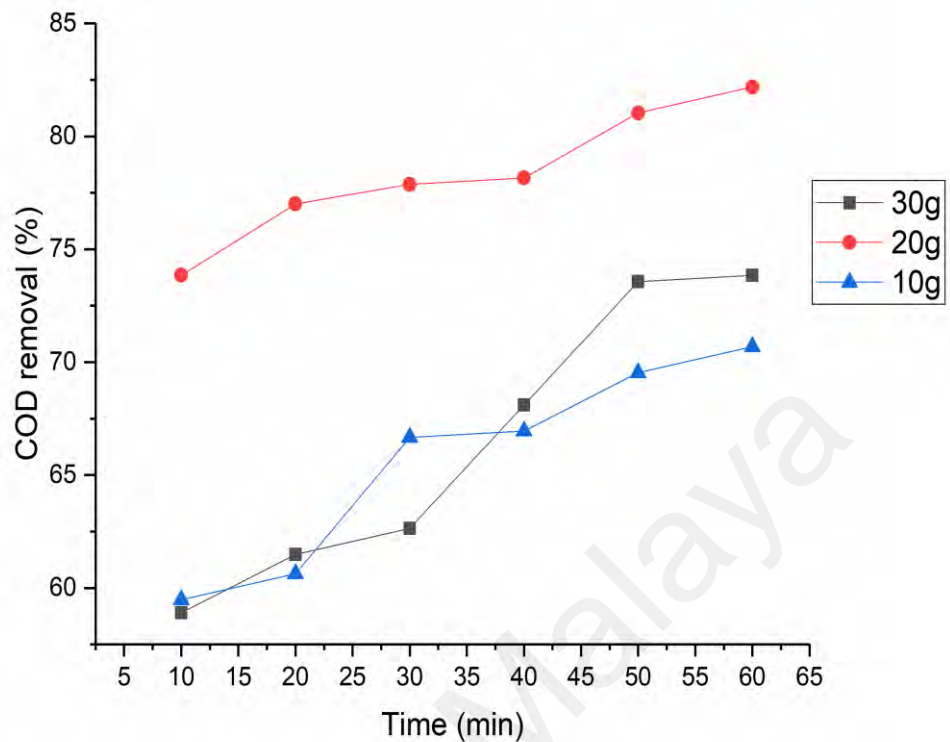


**Figure 6.11: Effect of palm kernel shell loading on COD removal (Experimental conditions: pH = 3, [Dye/Fe<sup>2+</sup>] = 10, [H<sub>2</sub>O<sub>2</sub>/Fe<sup>2+</sup>] = 25)**

Figure 6.11 shows the COD removal for the three different particle loadings. The COD removal increased when the particle loading was increased from 10g to 20g. The increased in the COD removal with the increase in particle loading may be due to two reasons. More adsorption and crystallization sites will become available when the particle loading is increased (Anand et al., 2015). Since the PKSGAC has a large surface area and high adsorption capacity, most of the intermediates can be adsorbed on its surfaces, further reducing the COD of the solution (Lyu et al., 2016). In this case, the PKSGAC serves like a filtration stage, enhancing the process performance (Ramírez-sosa et al., 2013). Consequently, the COD removal increased with an increase in the PKSGAC loading.

Another plausible explanation is that the increase in the loading of the fluidized solid caused an increase in the agitation in the reactor, which may enhance particles mixing

and interaction. However, when the particle loading was increased to 30g, the COD removal decreased. This could be due the excessive settling of particles and poor particle fluidization (Anand et al., 2015). It was observed that as the particle loading was increased from 20g to 30g, particle stacking, and poor fluidization ensued in the reactor.

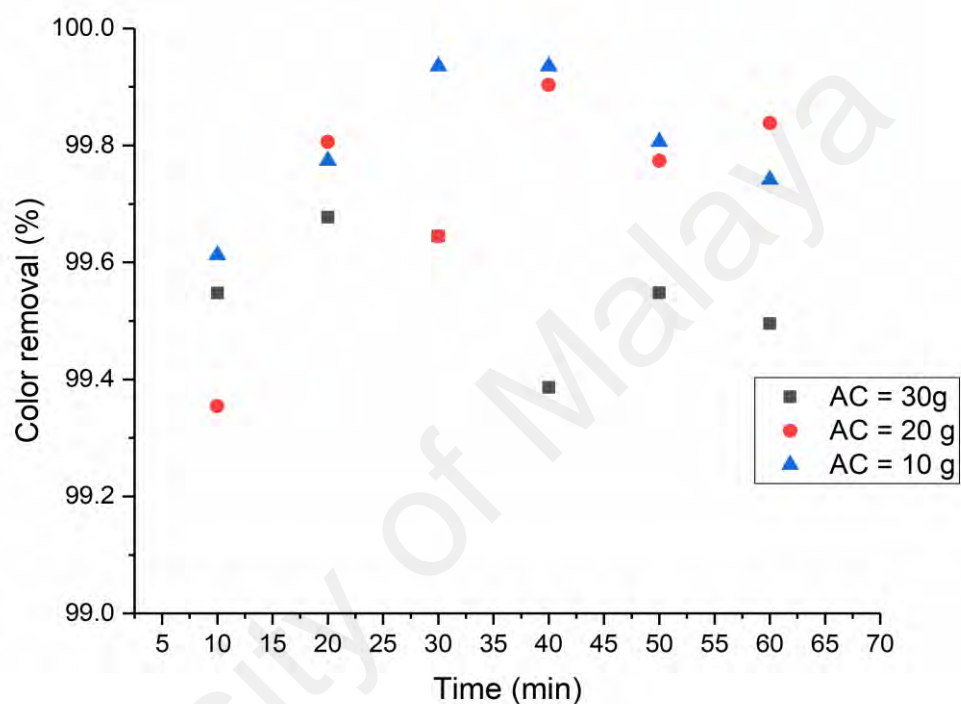


**Figure 6.12: Effect of palm kernel shell loading on color removal**

Figure 6.12 shows the effect of particle loading on color removal using the PKSGAC as a carrier. It is apparent that particle loading does not significantly affect the color removal as more than 99% color removal can be achieved under all the particles loading. However, the color removal was slighter higher in the case of 10g and 20g, compared to 30g. This is likely due to the stacking effect as explain above. The high rate of color removal irrespective of the particle loading is due to the rapid removal of color by the Fenton oxidation. The color of the dye is due to the azo double bond, which can be easily conjugated by the hydroxyl radicals from homogeneous Fenton reaction (Nordin et al., 2017). Thus, the contribution of the PKSGAC to the color removal is insignificant.

Particle loading has a positive effect on the FBF process. The COD removal increased as the PKSGAC loading was increased. This was due to the more adsorption sites and increased agitation, which enhances mass transfer. However, increasing the PKSGAC loading above a particular level resulted in the decrease in the COD removal. This can be attributed to the settling and stacking effect when the loading exceeds the optimum level. In both cases, 20g of PKSGAC was found to be the optimum loading for the FBF process.

#### **6.2.4 Comparison of palm kernel shell and SiO<sub>2</sub>**

One of the objectives of this work is to evaluate the feasibility of utilizing a low-cost palm kernel activated carbon as an alternative carrier in FBF process. Therefore, it is imperative that the alternative carrier is compared with the existing ones. In this section, comparison is made between the PKSGAC and the most commonly used carrier, SiO<sub>2</sub>. These comparisons are in terms of the pollutant removal and hydrodynamics characteristics.

##### **6.2.4.1 Comparison of performance for pollutant removal**

The performance of PKSGAC as an alternative fluidized carrier was compared with the commonly used carrier, SiO<sub>2</sub>. Figure 6.13 shows the COD removal using the two different carriers and the mixture of the two carriers. The PKSGAC exhibited higher COD removal compared to SiO<sub>2</sub>. While more than 70% COD removal was achieved in the first 10 minutes using PKSGAC, only 53% was achieved with the SiO<sub>2</sub> under the same time. At the end of 60 minutes, the COD removal reached 80% in the PKSGAC system while it was about 60% for SiO<sub>2</sub> system.

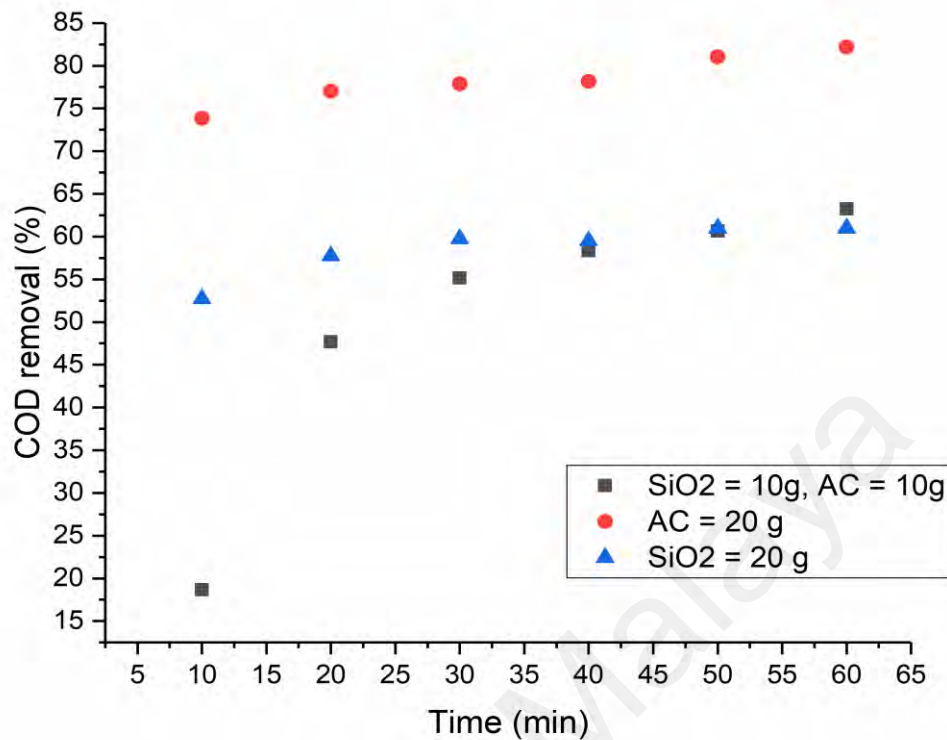


**Figure 6.13: COD removal by palm kernel shell and SiO<sub>2</sub> (Experimental conditions: carrier loading = 20 g, [Dye/Fe<sup>2+</sup>] = 10, [H<sub>2</sub>O<sub>2</sub>/Fe<sup>2+</sup>] = 25, pH = 3)**

The higher COD removal by the PKSGAC system was due to the higher adsorption capacity and surface properties compared to SiO<sub>2</sub>. The removal of pollutant by FBF process occurs through Fenton oxidation and adsorption on the surface of the carriers. As discussed previously, the adsorptive removal of pollutant by PKSGAC is higher than that of SiO<sub>2</sub>. In addition, PKSGAC may offer a higher mass transfer and better hydrodynamics than SiO<sub>2</sub>. Thus, PKSGAC exhibit higher pollutant removal than SiO<sub>2</sub>.

Another advantage of using PKSGAC is that the FBF process performance can still be effective under wider operational pH. The performance of FBF process using PKSGAC was effective between pH 3 and 7. The possibility of using a circumneutral pH condition confers a practical advantage to the use of PKSGAC as an alternative carrier in FBF process.

Although the two carriers were compared in terms of the treatment performance, it is also important to compare their fluidization and hydrodynamic characteristics.

#### **6.2.4.2 Hydrodynamic Characteristics**

The characteristics of solid carriers, such as density and particle size, are important parameters that can affect the fluidization and reactor hydrodynamics (Wirsum et al., 2001). In this regard, the characteristics of PKSGAC are compared with those of SiO<sub>2</sub> in order to evaluate their fluidization and hydrodynamic advantages.

Particle size is an important parameter that affects fluidization as well as heat and mass transfer in the reactor. Kim & Kang, (1997) argued that particle size could be the most important factor that govern mass transfer in FBR. Particle size has a positive effect on the process performance as both heat and mass transfer increase with increase in particle size (Begum & Radha, 2015). In this study, PKSGAC has a particle size of 0.50 – 1.70 mm while the SiO<sub>2</sub> has a particle size of 0.2 – 1 mm. Thus, the two carriers have particles size in Group B and Group D of Geldart classification. However, PKSGAC possesses larger particle size, which means it can offer higher mass transfer than SiO<sub>2</sub>. Thus, the PKSGAC resulted in higher process performance than SiO<sub>2</sub> as presented previously. This results is consistent with previous findings. For example, Fernández et al., (2008) compared the performance of two particles with different range of diameter (0.5 – 0.8 mm) and (0.2 – 0.5 mm) and observed a slightly higher COD removal with the larger particles. Thus, based on the particle size, the PKSGAC offers a better alternative than SiO<sub>2</sub>.

Particle density is an important parameter that can affect the superficial fluidization velocity requirement. Dense particles would require high up-flow velocity to achieve fluidization (Escudero, 2010). This is because as the density increases, the weight of the

initial static bed increases, which will require higher pressure drop to counterbalance the increased weight (Dora et al., 2012). This can be clearly seen from Equation 2.2.7, where the pressure drop across the bed is directly proportional to the particle density. Thus, lighter particles are advantageous. The bulk density of PKSGAC was about  $2.0 \text{ g/cm}^3$  compared to about  $2.65 \text{ g/cm}^3$  for the  $\text{SiO}_2$ . Thus, the use of PKSGAC can result in lower power requirement compared to  $\text{SiO}_2$ .

### **6.3 Summary**

These findings show that PKSGAC offers many advantages as a carrier in FBF process compared to the commonly used,  $\text{SiO}_2$ . These include higher pollutant removal, potential higher mass transfer and better hydrodynamic characteristics. Thus, the use of PKSGAC can enhance the effectiveness of the FBF process.

## CHAPTER 7: CONCLUSION AND RECOMMENDATIONS

### 7.1 Conclusion

This study was conducted with the aim of enhancing the performance of FBF process for recalcitrant wastewater treatment. To achieve this, the effect of operational parameters on the performance of FBF process was investigated and optimized. Under the optimum conditions, a detailed investigation on the effect of fluidized carrier and its interaction with Fenton's reagent was conducted using theoretical and experimental techniques. For the experimental approach, quantum chemical simulation was used to predict the reactivity and thermodynamic feasibilities of different possible interactions among the fluidized carrier, Fenton's reagent and the organic pollutant. Subsequently, the experimental results of the effect of carrier loading, adsorption of organic pollutant on the carrier surface as well as analysis of surface composition and morphology of the carrier were used to validate the theoretical findings. With the clear understanding of the effect of the carrier, a feasibility study was conducted on the use of a low-cost material as an alternative carrier in the FBF process. The major conclusions drawn from the study are presented according to the objectives as follows:

#### Objective 1

1. Under optimum experimental conditions ( $\text{Dye}/\text{Fe}^{2+} = 10$ ,  $\text{H}_2\text{O}_2/\text{Fe}^{2+} = 25$ ,  $\text{pH} = 3.09$  and  $\text{time} = 45.52 \text{ min}$ ), the FBF process achieved 99.94% color removal and 80% COD removal from the synthetic dye-solution. This performance was about 20% higher than that of conventional Fenton oxidation
2. The RSM models developed exhibited more than 90% correlation coefficient, indicating it is suitability to predict the process performance of the fluidized bed

Fenton process. There was only 3% between the predicted and experimental results under optimum condition.

3. Analysis of the effect of operational parameters shows that the initial concentration of iron and the initial concentration of the pollutant have the highest influence on the performance of the FBF process.

### **Objective 2**

1. The analysis of quantum chemical parameters showed that the fluidized bed carrier interacts with Fenton's reagent and the organic pollutant. The thermodynamic analysis further revealed that besides iron crystallization on the  $\text{SiO}_2$ , other interactions, such as the formation of complexes between  $\text{SiO}_2$  and  $\text{H}_2\text{O}_2$ , are possible in the FBF process.
2. The experimental analysis revealed that the carrier can adsorb the organic pollutant on its surface and also induce the crystallization of iron oxide. Analysis of the carrier composition and surface characteristics before and after the FBF process showed that there was interaction between  $\text{SiO}_2$ , Fenton's reagent and the pollutant.
3. The agreement between the quantum chemical simulation and the experimental results indicates that the former can be used to predict the complex interactions occurring in the FBF process.

### **Objective 3**

1. The FBF-PKSGAC process performed 20% higher than FBF- $\text{SiO}_2$  for COD removal under the following conditions: carrier loading = 20 g,  $[\text{Dye}/\text{Fe}^{2+}] = 10$ ,  $[\text{H}_2\text{O}_2/\text{Fe}^{2+}] = 25$ ,  $\text{pH} = 3$ .
2. The effectiveness of the process using PKSGAC can be maintained up to  $\text{pH} 7$ , signifying the potential of the PKSGAC to eliminate the  $\text{pH}$  limitation associated with Fenton oxidation.

3. The analysis of the surface and composition of the PKSGAC before and after FBF process shows evidence of interactions with the Fenton's reagent and organic pollutant.

In general, the results of this study have shown that the complex interactions in FBF process can be investigated and optimized through theoretical and experimental approaches. The quantum chemical simulation predicted the possible interactions in the process, which are supported by the experimental results. The overall results show that beside the commonly discussed interaction of SiO<sub>2</sub> and iron species, there are possibilities of other interactions such as the interaction between SiO<sub>2</sub> and H<sub>2</sub>O<sub>2</sub>. Consequently, such interactions must be considered in the design and optimization of FBF process. The performance of the FBF process can be further enhanced by the use of PKSGAC as a carrier, which offers better treatment performance and hydrodynamic characteristics than the commonly used carrier.

## **7.2 Recommendation for Future Work**

Based on the outcome of this work, the following recommendations are made:

1. This study focused on the fluidized carrier and its effect on the performance of the FBF process. To effectively achieve this objective, the effect of the reactor hydrodynamics was not considered since it represents a different aspect of the process. However, future study may be conducted to investigate the effect of hydrodynamics on the performance of the FBF process. In this regard, the use of appropriate techniques such as CFD modelling is recommended due to the inherent complexity of the process.

2. The quantum chemical calculations was applied to predict the interactions using SiO<sub>2</sub> as the commonly used carrier. Future studies may consider using different carriers so that further comparison can be made.
3. Although laboratory scales studies can provide useful information for process development, pilot scale studies are necessary towards industrial applications. Thus, future studies are needed on scaling-up of FBF process.

### **7.3 Knowledge Contribution**

This study contributed to knowledge in the following ways:

1. This study has developed a theoretical and experimental methodology that can be used to study the complex interactions in FBF process and other similar processes. These techniques have not been used before and will therefore be useful toward understanding and optimization of FBF process.
2. The findings of the detailed investigations of various aspects of FBF process will be useful to future studies on FBF process.
3. The developed correlation for predicting the performance of the FBF process could be used by other researchers and can be extended to the treatment of similar recalcitrant pollutants.
4. The information on the possible interactions in the FBF process will stimulate the interest of researcher and can serve as a starting point for further research.
5. The findings of the possible use of an alternative carrier can stimulate further research in that direction.

This work has so far produced five papers in journals indexed in web of science, three manuscript are under review while two are being prepared. A book chapter and two conference papers have also been produced.

#### **7.4 Potential Real Applications of the Study**

The findings of this study have shown that FBF process can be applied for the treatment of wastewaters containing recalcitrant pollutants, with reduced process time and chemical consumption compares to conventional Fenton oxidation. Fluidized bed reactor is an established technology and thus, FBF process can be easily scaled-up to pilot and industrial applications. The technology will be suitable to cottage and small-scale industries generating recalcitrant wastewater. However, an important challenge in the use of the FBF process is the inherent complexity of the process. The techniques adopted herein to establish the effect of solid carrier and its interaction with Fenton's reagent will be valuable towards the design and optimization of FBF process.

University of Malaya

## REFERENCES

- Abdel-Aziz, M. H., El-Abd, M. Z., & Bassyouni, M. (2016). Heat and mass transfer in three phase fluidized bed containing high density particles at high gas velocities. *International Journal of Thermal Sciences*, 102, 145–153.
- Abdessalem, A. K., Oturan, N., Bellakhal, N., Dachraoui, M., & Oturan, M. A. (2008). Experimental design methodology applied to electro-Fenton treatment for degradation of herbicide chlortoluron. *Applied Catalysis B: Environmental*, 78(3–4), 334–341.
- Acisli, O., Khataee, A., Darvishi Cheshmeh Soltani, R., & Karaca, S. (2017). Ultrasound-assisted Fenton process using siderite nanoparticles prepared via planetary ball milling for removal of reactive yellow 81 in aqueous phase. *Ultrasonics Sonochemistry*, 35, 210–218.
- Adewuyi, Y. G. (2001). Sonochemistry: Environmental science and engineering applications. *Industrial and Engineering Chemistry Research*, 40, 4681–4715.
- Adewuyi, Y. G. (2005). Sonochemistry in environmental remediation. 1. Combinative and hybrid sonophotochemical oxidation processes for the treatment of pollutants in water. *Environmental Science & Technology*, 39(10), 3409–3420.
- Aghdasinia, H., Bagheri, R., Vahid, B., & Khataee, A. (2016). Central composite design optimization of pilot plant fluidized-bed heterogeneous Fenton process for degradation of an azo dye. *Environmental Technology (United Kingdom)*, 37(21), 2703–2712.
- Ahmadi, M., Ramavandi, B., & Sahebi, S. (2015). Efficient Degradation of a Biorecalcitrant Pollutant from Wastewater Using a Fluidized Catalyst-Bed Reactor. *Chemical Engineering Communications*, 202, 1118–1129.
- Akilamudhan, P., Sivakumar, P., Mohanraj, R., & Senthilkumar, K. (2014). Prediction of Solid holdup in an Internal Loop Airlift Fluidized Bed Reactor. *International Journal of ChemTech Research*, 6(9), 4460–4467.
- Alalm, M. G., Tawfik, A., & Ookawara, S. (2015a). Comparison of solar TiO<sub>2</sub> photocatalysis and solar photo-Fenton for treatment of pesticides industry wastewater: Operational conditions, kinetics, and costs. *Journal of Water Process Engineering*, 8, 55–63.
- Alalm, M. G., Tawfik, A., & Ookawara, S. (2015b). Degradation of four pharmaceuticals by solar photo-Fenton process: Kinetics and costs estimation. *Journal of Environmental Chemical Engineering*, 3(1), 46–51.
- Amorim, C. C., Leão, M. M. D., Moreira, R. F. P. M., Fabris, J. D., & Henriques, A. B. (2013). Performance of blast furnace waste for azo dye degradation through photo-fenton-like processes. *Chemical Engineering Journal*, 224(1), 59–66.
- Anand, A. A. ., Adish Kumar, S., Rajesh Banu, J., & Ginni, G. (2015). The performance of fluidized bed solar photo Fenton oxidation in the removal of COD from hospital wastewaters. *Desalination and Water Treatment*, 3994, 1–7.

- Andalib, M., Elbeshbishy, E., Mustafa, N., Hafez, H., Nakhla, G., & Zhu, J. (2014). Performance of an anaerobic fluidized bed bioreactor (AnFBR) for digestion of primary municipal wastewater treatment biosolids and bioethanol thin stillage. *Renewable Energy*, *71*, 276–285.
- Anotai, J., Chen, C., Bellotindos, L. M., & Lu, M. (2012). Treatment of TFT-LCD wastewater containing ethanolamine by fluidized-bed Fenton technology. *Bioresource Technology*, *113*, 272–275.
- Anotai, J., Sakulkittimasak, P., Boonrattanakij, N., & Lu, M. (2009). Kinetics of nitrobenzene oxidation and iron crystallization in fluidized-bed Fenton process. *Journal of Hazardous Materials*, *165*, 874–880.
- Anotai, J., Su, C., Tsai, Y., & Lu, M. (2010). Effect of hydrogen peroxide on aniline oxidation by electro-Fenton and fluidized-bed Fenton processes. *Journal of Hazardous Materials*, *183*(1–3), 888–893.
- Anotai, J., Thuptimdang, P., Su, C., & Lu, M. (2012). Degradation of o -toluidine by fluidized-bed Fenton process : statistical and kinetic study. *Environ Sci Pollut Res*, *19*, 169–176.
- Aparicio, M. A., Eiroa, M., Kennes, C., & Veiga, M. C. (2007). Combined post-ozonation and biological treatment of recalcitrant wastewater from a resin-producing factory. *Journal of Hazardous Materials*, *143*(1–2), 285–90.
- APHA. (1992). Standard Methods for the Examination of Water and Wastewater. *Water Environment Federation*, *18th*, 9–45.
- Argun, M. A., & Karatas, M. (2011). Application of fenton process for Decolorization of Reactive Black 5 from Synthetic Wastewater: Kinetics and Thermodynamics. *Environmental Progress and Sustainable Energy*, *30*(4), 540–548.
- Asghar, A. (2016). *In situ Production of Hydrogen Peroxide and Electricity Generation for Textile Wastewater Treatment in Microbial Fuel Cell*. University of Malaya.
- Asghar, A., Raman, A. A. A., & Daud, W. M. A. W. (2015). Advanced oxidation processes for in-situ production of hydrogen peroxide/hydroxyl radical for textile wastewater treatment: A review. *Journal of Cleaner Production*, *87*(1), 826–838.
- Askaripour, H., & Dehkordi, A. M. (2015). Effects of Initial Static Bed Height on Fractional Conversion and Bed Pressure Drop in Tapered-in and Tapered-out Fluidized Bed Reactors. *International Journal of Multiphase Flow*, *08*(006).
- Askaripour, H., & Dehkordi, A. M. (2016). Effects of initial static bed height on fractional conversion and bed pressure drop in tapered-in and tapered-out fluidized bed reactors. *International Journal of Multiphase Flow*, *79*, 50–61.
- Babuponnusami, A., & Muthukumar, K. (2014). A review on Fenton and improvements to the Fenton process for wastewater treatment. *Journal of Environmental Chemical Engineering*, *2*(1), 557–572.
- Barros, W. R. P., Steter, J. R., Lanza, M. R. V., & Tavares, A. C. (2016). Catalytic activity

of  $\text{Fe}_{3-x}\text{Cu}_x\text{O}_4$  ( $0 \leq x \leq 0.25$ ) nanoparticles for the degradation of Amaranth food dye by heterogeneous electro-Fenton process. *Applied Catalysis B: Environmental*, 180, 434–441.

- Bautista, P., Mohedano, A. F., Gilarranz, M. A., Casas, J. A., & Rodriguez, J. J. (2007). Application of Fenton oxidation to cosmetic wastewaters treatment. *Journal of Hazardous Materials*, 143(1–2), 128–134.
- Begum, S. S., & Radha, K. V. (2015). Gas – Liquid Mass Transfer Studies in Inverse Fluidized Bed Biofilm Reactor for the Biodegradation of Industrial Effluent Rich in Phenolic Compounds. *Environmental Progress & Sustainable Energy*, 35, 433–438..
- Bel H. H., Sdiri, A., Ltaief, W., Da Costa, P., Gálvez, M. E., & Ben Zina, M. (2018). Efficient removal of cadmium and 2-chlorophenol in aqueous systems by natural clay: Adsorption and photo-Fenton degradation processes. *Comptes Rendus Chimie*, 21, 253–262.
- Bellotindos, L. M., Lu, M., Methatham, T., & Lu, M. (2014). Factors affecting degradation of dimethyl sulfoxide (DMSO) by fluidized-bed Fenton process. *Environ Sci Pollut Res*, 21, 14158–14165.
- Bezerra, M. A., Santelli, R. E., Oliveira, E. P., Villar, L. S., & Escaleira, L. A. (2008). Response surface methodology (RSM) as a tool for optimization in analytical chemistry. *Talanta*, 76(5), 965–977.
- Bilinska, L., Gmurek, M., & Ledakowicz, S. (2016). Comparison between industrial and simulated textile wastewater treatment by AOPs - Biodegradability, toxicity and cost assessment. *Chemical Engineering Journal*, 306, 550–559.
- Bora, L. V., & Mewada, R. K. (2017). Visible/solar light active photocatalysts for organic effluent treatment: Fundamentals, mechanisms and parametric review. *Renewable and Sustainable Energy Reviews*, 76, 1393–1421.
- Brink, A., Sheridan, C. ., & Harding, K. G. (2017). The Fenton oxidation of biologically treated paper and pulp mill effluents: A performance and kinetic study. *Process Safety and Environmental Protection*, 107, 206–215.
- Briones, R. M., de Luna, M. D. G., & Lu, M.-C. (2012). Optimization of acetaminophen degradation by fluidized-bed Fenton process. *Desalination and Water Treatment*, 45, 100–111.
- Broséus, R., Vincent, S., Aboulfadl, K., Daneshvar, A., Sauvé, S., Barbeau, B., & Prévost, M. (2009). Ozone oxidation of pharmaceuticals, endocrine disruptors and pesticides during drinking water treatment. *Water Research*, 43(18), 4707–4717.
- Buffiere, P., Moletta, R., & Elmaleh, S. (1998). Anaerobic digestion of wine distillery wastewater in down-flow fluidized bed. *Water Research*, 32(12), 3593–3600.
- Bulkin, P. V, Swart, P. L., & Lacquet, B. M. (1995). Effect of process parameters on the properties of electron cyclotron resonance plasma deposited silicon-oxynitride. *Journal of Non-Crystalline Solids*, 187, 403–408.

- Burghate, S. P., & Ingole, N. W. (2013). Fluidized Bed Biofilm Reactor – A Novel Wastewater Treatment Reactor. *International Journal of Research in Environmental Science and Technology*, 3(4), 145–155.
- Casas, E. M., & Bester, K. (2015). Can those organic micro-pollutants that are recalcitrant in activated sludge treatment be removed from wastewater by biofilm reactors (slow sand filters)? *The Science of the Total Environment*, 506–507, 315–22.
- Chang, S. S., Clair, B., Ruelle, J., Beauchêne, J., Di Renzo, F., Quignard, F., ... Gril, J. (2009). Mesoporosity as a new parameter for understanding tension stress generation in trees. *Journal of Experimental Botany*, 60, 3023–3030.
- Chen, C.-Y., Wu, P.-S., & Chung, Y.-C. (2009). Coupled biological and photo-Fenton pretreatment system for the removal of di-(2-ethylhexyl) phthalate (DEHP) from water. *Bioresource Technology*, 100 (19), 4531-4534.
- Chen, C., & Qiu, M. (2014). Combined treatment of the municipal landfill leachate by fluidized bed Fenton process. *Desalination and Water Treatment*, 52(28–30), 5327–5332.
- Chen, M., Ren, H., Ding, L., & Gao, B. (2015). Effect of different carriers and operating parameters on degradation of flax wastewater by fluidized-bed Fenton process. *Water Science and Technology*, 71(12), 1760–1767.
- Chen, T.-C., Matira, E. M., Lu, M.-C., & Dalida, M. L. P. (2016). Degradation of dimethyl sulfoxide through fluidized-bed Fenton process. *Int. J. Environ. Sci. Technol.*, 300, 1–12.
- Cheng, H., Chou, S., Chen, S., & Yu, C. (2014). Photoassisted Fenton degradation of phthalocyanine dyes from wastewater of printing industry using Fe (II)/ $\gamma$ -Al<sub>2</sub>O<sub>3</sub> catalyst in up-flow fluidized-bed. *Journal of Environmental Sciences*, 26(6), 1307–1312.
- Choi, H. S., & Shin, M. (1999). Hydrodynamics Study of Two Different Inverse Fluidized Reactors for the Application of Wastewater Treatment. *Korean J. Chem. Eng.*, 16(5), 670–676.
- Choi, J., Min, J., Lee, W., & Lee, S. B. (2000). Approximated Solution of Model for Three-Phase Fluidized Bed Bio- film Reactor in Wastewater Treatment. *Biotechnology Bioprocess*, 5(1), 65–70.
- Choi, W., Termin, A., & Hoffmann, M. R. (1994). The role of metal ion dopants in quantum-sized TiO<sub>2</sub>: Correlation between photoreactivity and charge carrier recombination dynamics. *The Journal of Physical Chemistry*, 98(51), 13669–13679.
- Chou, S., & Huang, C. (1999). Application of a supported iron oxyhydroxide catalyst in oxidation of benzoic acid by hydrogen peroxide. *Chemosphere*, 38(12), 2719–2731.
- Chou, S., Huang, C., & Huang, Y. H. (1999). Effect of Fe(II) on catalytic oxidation in a fluidized bed reactor. *Chemosphere*, 39(12), 1997–2006.
- Chou, S., Liao, C. C., Perng, S. H., & Chang, S. H. (2004). Factors influencing the

- preparation of supported iron oxide in fluidized-bed crystallization. *Chemosphere*, 54(7), 859–866.
- Chowdhury, P., & Viraraghavan, T. (2009). Sonochemical degradation of chlorinated organic compounds, phenolic compounds and organic dyes – A review. *Science of the Total Environment*, 407(8), 2474–2492.
- Chun, J., Lee, H., Lee, S. H., Hong, S. W., Lee, J., Lee, C., & Lee, J. (2012). Magnetite/mesocellular carbon foam as a magnetically recoverable fenton catalyst for removal of phenol and arsenic. *Chemosphere*, 89(10), 1230–1237.
- Clarizia, L., Russo, D., Di Somma, I., Marotta, R., & Andreozzi, R. (2017). Homogeneous photo-Fenton processes at near neutral pH: a review. *Applied Catalysis B: Environmental*, 209, 358–371.
- Daneshvar, N., Oladegaragoze, A., & Djafarzadeh, N. (2006). Decolorization of basic dye solutions by electrocoagulation: An investigation of the effect of operational parameters. *Journal of Hazardous Materials*, 129(1–3), 116–122.
- Davarnejad, R., & Azizi, J. (2016). Alcoholic wastewater treatment using electro-Fenton technique modified by Fe<sub>2</sub>O<sub>3</sub> nanoparticles. *Journal of Environmental Chemical Engineering*, 4(2), 2342–2349.
- Dejaegher, B., & Vander Heyden, Y. (2011). Experimental designs and their recent advances in set-up, data interpretation, and analytical applications. *Journal of Pharmaceutical and Biomedical Analysis*, 56(2), 141–158.
- Delebarre, A., Morales, J., & Ramos, L. (2004). Influence of the bed mass on its fluidization characteristics. *Chemical Engineering Journal*, 98, 81–88.
- Deng, Y., & Englehardt, J. D. (2006). Treatment of landfill leachate by the Fenton process. *Water Research*, 40, 3683–3694.
- Dewil, R., Mantzavinos, D., Poulios, I., & Rodrigo, M. A. (2017). New perspectives for advanced oxidation processes. *Journal of Environmental Management*, 195, 93–99.
- Dias, F. F., Oliveira, A. A. S., Arcanjo, A. P., Moura, F. C. C., & Pacheco, J. G. A. (2016). Residue-Based Iron Catalyst for the Degradation of Textile Dye via Heterogeneous photo-Fenton. *Applied Catalysis B: Environmental*, 186, 136–142.
- Diz, H., & Novak, J. (1998). Fluidized Bed for Removing Iron and Acidity from Acid Mine Drainage. *Journal of Environmental Engineering*, 124(8) 701–708.
- Dong, S., Zhang, X., He, F., Dong, S., & Wang, B. (2014). Visible-light photocatalytic degradation of methyl orange over spherical activated carbon-supported and Er<sup>3+</sup>: YAlO<sub>3</sub>-doped TiO<sub>2</sub> in a fluidized bed. *J Chem Technol Biotechnol*, 90, 880–887.
- Dora, D. T. K., Mohanty, Y. K., & Roy, G. K. (2012). Hydrodynamics of three-phase fluidization of a homogeneous ternary mixture of irregular particles. *Chemical Engineering Science*, 79, 210–218.

- Dora, T. K., Mohanty, Y. K., Roy, G. K., & Sarangi, B. (2013). Adsorption studies of As (III) from wastewater with a novel adsorbent in a three-phase fluidized bed by using response surface method. *Journal of Environmental Chemical Engineering*, 1(3), 150–158.
- Dutta, S., & Suci, G. D. (1992). An Experimental Study of the Effectiveness of Baffles and Internals in Breaking Bubbles in Fluid Beds. *Journal of Chemical Engineering of Japan*, 25(3), 345–348.
- Efstathios, E., & Michaelides, S. (2013). Fluidized Bed Reactors. In *Heat and Mass Transfer in Particulate Suspensions* (pp. 89–119). New York: Springer.
- Ersöz, G. (2014). Fenton-like oxidation of Reactive Black 5 using rice husk ash based catalyst. *Applied Catalysis B: Environmental*, 147, 353–358.
- Escudero, D. R. (2010). *Bed height and material density effects on fluidized bed hydrodynamics*. Iowa State University. Retrieved from <http://lib.dr.iastate.edu/cgi/viewcontent.cgi?article=2653&context=etd>
- Fan, D., Ding, L., Huang, H., Chen, M., & Ren, H. (2017). Fluidized-bed Fenton coupled with ceramic membrane separation for advanced treatment of flax wastewater. *Journal of Hazardous Materials*, 340, 390–398.
- Fernández, N., Montalvo, S., Borja, R., Guerrero, L., Sánchez, E., Cortés, I., ... Raposo, F. (2008). Performance evaluation of an anaerobic fluidized bed reactor with natural zeolite as support material when treating high-strength distillery wastewater. *Renewable Energy*, 33(11), 2458–2466.
- Ferreira, S. L. C., Bruns, R. E., da Silva, E. G. P., dos Santos, W. N. L., Quintella, C. M., David, J. M., ... Neto, B. B. (2007). Statistical designs and response surface techniques for the optimization of chromatographic systems. *Journal of Chromatography A*, 1158(1–2), 2–14.
- Forster, C. F. (1980). Aeration of fluidised bed reactors. *Environmental Technology Letters*, 1(5), 253–258.
- Garcia-Segura, S., Bellotindos, L. M., Huang, Y.-H., Brillas, E., & Lu, M.-C. (2016). Fluidized-bed Fenton process as alternative wastewater treatment technology—A review. *Journal of the Taiwan Institute of Chemical Engineers*, 67, 211–225.
- Garcia, E. H., Rodriguez, A., Prados, A., & Klein, J. (1999). A fluid dynamic model for three-phase airlift reactors. *Chemical Engineering Science*, 54, 2359–2370.
- Geldart, D. (1973). Types of Fluidization. *Powder Technology*, 7, 285–292.
- Glaze, W. H., Kang, J. W., & Chapin, D. H. (1987). The chemistry of water treatment processes involving ozone, hydrogen peroxide and ultraviolet radiation. *Ozone: Science & Engineering: The Journal of the International Ozone Association*, 9(9), 335–352.
- Gogate, P. R. (2008). Treatment of wastewater streams containing phenolic compounds using hybrid techniques based on cavitation: A review of the current status and the

way forward. *Ultrasonics Sonochemistry*, 15, 1–15.

Gomes, J., Costa, R., Quinta-ferreira, R. M., & Martins, R. C. (2017). Application of ozonation for pharmaceuticals and personal care products removal from water. *Science of the Total Environment*, 586, 265–283.

Gonçalves, G. da C., Nakamura, P. K., Furtado, D. F., & Veit, M. T. (2017). Utilization of brewery residues to produce granular activated carbon and bio-oil. *Journal of Cleaner Production*, 168, 908–916.

Gonzalez, G., Herrera, M. G., Garcia, M. T., & Pena, M. M. (2001). Biodegradation of phenol in a continuous process: comparative study of stirred tank and fluidized-bed bioreactors. *Bioresource Technology*, 76, 245–251.

Gorji-kandi, S., Alavi-amleshi, S. M., & Mostoufi, N. (2015). Experimental investigating the effect of bed geometry on solids mixing in fluidized beds. *Particulate Science and Technology*, 6351, 1–7.

Grzyb, B., Hildenbrand, C., Berthon-Fabry, S., Bégin, D., Job, N., Rigacci, A., & Achard, P. (2010). Functionalisation and chemical characterisation of cellulose-derived carbon aerogels. *Carbon*, 48(8), 2297–2307.

Guo, S., Yuan, N., Zhang, G., & Yu, J. C. (2017). Graphene modified iron sludge derived from homogeneous Fenton process as an efficient heterogeneous Fenton catalyst for degradation of organic pollutants. *Microporous and Mesoporous Materials*, 238, 62–68.

Han, H., Lee, W., Kim, Y., Kwon, J., Choi, H., Kang, Y., & Kim, S. (2003). Phase Hold-up and Critical Fluidization Velocity in a Three-Phase Inverse Fluidized Bed. *Korean J. Chem. Eng.*, 20(1), 163–168.

Hehre, W. J. (2003). *A Guide to Molecular Mechanics and Quantum Chemical Calculations*. California: Wavefunction, Inc.

Heijnen, J. J., Mulder, A., Enger, W., & Hoeks, F. (1989). Review on the application of anaerobic fluidized bed reactors in waste-water treatment. *The Chemical Engineering Journal*, 41(3).

Herrmann, J. M. (2010). Fundamentals and misconceptions in photocatalysis. *Journal of Photochemistry and Photobiology A: Chemistry*, 216(2–3), 85–93.

Hou, X., Huang, X., Jia, F., Ai, Z., Zhao, J., & Zhang, L. (2017). Hydroxylamine Promoted Goethite Surface Fenton Degradation of Organic Pollutants. *Environmental Science & Technology*, acs.est.6b05906.

Huang, C. P., Dong, C., & Tang, Z. (1993). Advanced chemical oxidation: Its present role and potential future in hazardous waste treatment. *Waste Management*, 13(5–7), 361–377.

Huang, C. P., Huang, Y. F., Cheng, H. P., & Huang, Y. H. (2009). Kinetic study of an

- immobilized iron oxide for catalytic degradation of azo dye reactive black B with catalytic decomposition of hydrogen peroxide. *Catalysis Communications*, 10(5), 561–566.
- Huang, C. P., & Huang, Y. H. (2009). Application of an active immobilized iron oxide with catalytic H<sub>2</sub>O<sub>2</sub> for the mineralization of phenol in a batch photo-fluidized bed reactor. *Applied Catalysis A: General*, 357(2), 135–141.
- Huang, J., Yan, J., & Wu, C. (2000). Comparative bioparticle and hydrodynamic characteristics of conventional and tapered anaerobic fluidized-bed bioreactors. *Journal of Chemical Technology & Biotechnology*, 75, 269–278.
- Huang, Y. F., & Huang, Y. H. (2009). Behavioral evidence of the dominant radicals and intermediates involved in Bisphenol A degradation using an efficient Co<sup>2+</sup>/PMS oxidation process. *Journal of Hazardous Materials*, 167(1–3), 418–426.
- Irmak, S., Erbatur, O., & Akgerman, A. (2005). Degradation of 17 $\beta$ -estradiol and bisphenol A in aqueous medium by using ozone and ozone/UV techniques. *Journal of Hazardous Materials*, 126(1–3), 54–62.
- Jaafari, J., Mesdaghinia, A., Nabizadeh, R., & Hoseini, M. (2014). Influence of upflow velocity on performance and biofilm characteristics of Anaerobic Fluidized Bed Reactor ( AFBR ) in treating high-strength wastewater. *Journal of Environmental Health Science & Engineering*, 12(139), 1–10.
- Jena, H. M., Roy, G. K., & Meikap, B. C. (2009). Hydrodynamics of a gas – liquid – solid fluidized bed with hollow cylindrical particles. *Chemical Engineering and Processing: Process Intensification*, 48, 279–287.
- Jin, Y., Wei, F., & Wang, Y. (2003). Effect of Internal Tubes and Baffles. In W.-C. Yang (Ed.), *Handbook of Fluidization and Fluid-Particle Systems* (pp. 171–200). New York: Marcel Dekker, Inc.
- Jordening, H.-J., & Buchholz, K. (1999). Fixed Film Stationary Bed and Fluidized Bed Reactors. In H.-J. Rehm & G. Reed (Eds.), *Biotechnology: Environmental Processes I* (2nd ed., Vol. 11a, pp. 493–512). Weinheim, Germany: Wiley-VCH Verlag, GmbH.
- Jovanovic, M., Grbavcic, Z., Rajic, N., & Obradovic, B. (2014). Removal of Cu (II) from aqueous solutions by using fluidized zeolite A beads : Hydrodynamic and sorption studies. *Chemical Engineering Science*, 117, 85–92.
- Karthikeyan, S., Titus, A., Gnanamani, A., Mandal, A. B., & Sekaran, G. (2011). Treatment of textile wastewater by homogeneous and heterogeneous Fenton oxidation processes. *Desalination*, 281(1), 438–445.
- Kavitha, E., Sundaraganesan, N., & Sebastian, S. (2010). Molecular structure, vibrational spectroscopic and HOMO, LUMO studies of 4-nitroaniline by density functional method. *Indian Journal of Pure and Applied Physics*, 48(1), 20–30.
- Khan, M. J. H., Hussain, M. A., Mansourpour, Z., Mostoufi, N., Ghasem, N. M., & Abdullah, E. C. (2014). CFD simulation of fluidized bed reactors for polyolefin

production – A review. *Journal of Industrial and Engineering Chemistry*, 20(6), 3919–3946.

- Khataee, A., Marandizadeh, H., Vahid, B., Zarei, M., & Joo, S. W. (2013). Combination of photocatalytic and photoelectro-Fenton/citrate processes for dye degradation using immobilized N-doped TiO<sub>2</sub> nanoparticles and a cathode with carbon nanotubes: Central composite design optimization. *Chemical Engineering and Processing*, 73, 103–110.
- Khataee, A. R., Zarei, M., & Moradkhannejhad, L. (2010). Application of response surface methodology for optimization of azo dye removal by oxalate catalyzed photoelectro-Fenton process using carbon nanotube-PTFE cathode. *Desalination*, 258(1–3), 112–119.
- Kim, S.-M., & Vogelpohl, A. (1998). Degradation of Organic Pollutants by the Photo-Fenton-Process. *Chemical Engineering & Technology*, 21(2), 187–191.
- Kim, S. D., & Kang, Y. (1997). Heat and mass transfer in three-phase fluidized-bed reactors--an overview. *Chemical Engineering Science*, 52(21), 3639–3660.
- Kulkarni, S. J., Tapre, R. W., Patil, S. V., & Sawarkar, M. B. (2013). Adsorption of Phenol from Wastewater in Fluidized Bed Using Coconut Shell Activated Carbon. *Procedia Engineering*, 51, 300–307.
- Kundu, A., Sen Gupta, B., Hashim, M. A., & Redzwan, G. (2015). Taguchi optimization approach for production of activated carbon from phosphoric acid impregnated palm kernel shell by microwave heating. *Journal of Cleaner Production*, 105, 420–427.
- Kunii, D., & Levenspiel, O. (1991). *Fluidization Engineering*. (H. Brenner, Ed.) (Second ed.). Boston: Butterworth-Heinemann.
- Kusvuran, E., Irmak, S., Yavuz, H. I., Samil, A., & Erbatur, O. (2005). Comparison of the treatment methods efficiency for decolorization and mineralization of Reactive Black 5 azo dye. *Journal of Hazardous Materials*, 119(1–3), 109–116.
- Kwon, B., Lee, D. S. O. O., Kang, N., & Yoon, J. (1999). Characteristics of P-chlorophenol oxidation by Fenton's reagent. *Water Research*, 33(9), 2110–2118.
- Kwon, K. M., Kim, I. G., Nam, Y. S., Choi, J., Cho, W. Il, Oh, I. H., ... Nah, I. W. (2018). Catalytic decomposition of hydrogen peroxide aerosols using granular activated carbon coated with manganese oxides. *Journal of Industrial and Engineering Chemistry*, 62, 225 – 230.
- Lakshmi, A. C. V., Balamurugan, M., Sivakumar, M., Samuel, T. N., & Velan, M. (2000). Minimum fluidization velocity and friction factor in a liquid-solid inverse fluidized bed reactor. *Bioprocess Engineering*, 22, 461–466.
- Lau, A., Alberto, L., Teixeira, C., Valéria, F., & Yokoyama, L. (2016). Evaluation of the mercaptobenzothiazole degradation by combined adsorption process and Fenton reaction using iron mining residue. *Environmental Technology*, 38(16), 2032–2039.

- Li, F., Bao, J., Zhang, T. C., & Lei, Y. (2015). A combined process of adsorption and Fenton-like oxidation for furfural removal using zero-valent iron residue. *Environmental Technology*, 36(24), 3103–3111.
- Li, G., Xu, Q., Jin, X., Li, R., Dharmarajan, R., & Chen, Z. (2018). Enhanced adsorption and Fenton oxidation of 2,4-dichlorophenol in aqueous solution using organobentonite supported nZVI. *Separation and Purification Technology*, 197, 401–406.
- Li, H., Priambodo, R., Wang, Y., Zhang, H., & Huang, Y. (2015). Mineralization of bisphenol A by photo-Fenton-like process using a waste iron oxide catalyst in a three-phase fluidized bed reactor. *Journal of the Taiwan Institute of Chemical Engineers*, 53, 68–73.
- Li, K., Zhao, Y., Song, C., & Guo, X. (2017). Magnetic ordered mesoporous Fe<sub>3</sub>O<sub>4</sub>/CeO<sub>2</sub> composites with synergy of adsorption and Fenton catalysis. *Applied Surface Science*, 425, 526–534.
- Li, M., Zeng, L., Chen, Y., Zhuang, L., Wang, X., & Shen, H. (2013). Realization of Colored Multicrystalline Silicon Solar Cells with SiO<sub>2</sub>/SiN<sub>x</sub>: H Double Layer Antireflection Coatings. *International Journal of Photoenergy*, 352473, 1–8.
- Li, N., An, J., Zhou, L., Li, T., Li, J., Feng, C., & Wang, X. (2016). A novel carbon black graphite hybrid air-cathode for efficient hydrogen peroxide production in bioelectrochemical systems. *Journal of Power Sources*, 306, 495–502.
- Li, S., Zhang, G., Wang, P., Zheng, H., & Zheng, Y. (2016). Microwave-enhanced Mn-Fenton process for the removal of BPA in water. *Chemical Engineering Journal*, 294, 371–379.
- Lima, M. J., Silva, C. G., Silva, A. M. T., Lopes, J. C. B., Dias, M. M., & Faria, J. L. (2017). Homogeneous and heterogeneous photo-Fenton degradation of antibiotics using an innovative static mixer photoreactor. *Chemical Engineering Journal*, 310, 342–351.
- Lin, C., Zhang, W., & Yuan, M. (2014). Degradation of polycyclic aromatic hydrocarbons in a coking wastewater treatment plant residual by an O<sub>3</sub>/ultraviolet fluidized bed reactor. *Environ Sci Pollut Res*, 21, 10329–10338.
- Liu, H., Chen, Q., Zhang, S., & Li, X. (2014). Relationship of mineralization of amino naphthalene sulfonic acids by Fenton oxidation and frontier molecular orbital energies. *Chemical Engineering Journal*, 247, 275–282.
- Liu, J., Li, J., Mei, R., Wang, F., & Sellamuthu, B. (2014). Treatment of recalcitrant organic silicone wastewater by fluidized-bed Fenton process. *Separation and Purification Technology*, 132, 16–22.
- Lucas, M. S., & Peres, J. A. (2006). Decolorization of the azo dye Reactive Black 5 by Fenton and photo-Fenton oxidation. *Dyes and Pigments*, 71(3), 236–244.
- Luna, M. D. G. de, Briones, R. M., Su, C., & Lu, M. (2013). Kinetics of acetaminophen degradation by Fenton oxidation in a fluidized-bed reactor. *Chemosphere*, 90(4),

1444–1448.

- Luo, Y., Guo, W., Hao, H., Duc, L., Ibney, F., Zhang, J., ... Wang, X. C. (2014). A review on the occurrence of micropollutants in the aquatic environment and their fate and removal during wastewater treatment. *Science of the Total Environment*, 473–474, 619–641.
- Lyu, C., Zhou, D., & Wang, J. (2016). Removal of multi-dye wastewater by the novel integrated adsorption and Fenton oxidation process in a fluidized bed reactor. *Environmental Science and Pollution Research*, 23(20), 20893–20903.
- Ma, J., Yang, Q., Wen, Y., & Liu, W. (2017). Fe-g-C<sub>3</sub>N<sub>4</sub>/graphitized mesoporous carbon composite as an effective Fenton-like catalyst in a wide pH range. *Applied Catalysis B: Environmental*, 201, 232–240.
- Mackul'ak, T., Mosný, M., Grabic, R., Golovko, O., Koba, O., & Birošová, L. (2015). Fenton-like reaction: A possible way to efficiently remove illicit drugs and pharmaceuticals from wastewater. *Environmental Toxicology and Pharmacology*, 39(2), 483–488.
- Mahapatra, K., Ramteke, D. S., & Paliwal, L. J. (2012). Production of activated carbon from sludge of food processing industry under controlled pyrolysis and its application for methylene blue removal. *Journal of Analytical and Applied Pyrolysis*, 95, 79–86.
- Mailler, R., Gasperi, J., Coquet, Y., Bulete, A., Vulliet, E., Deshayes, S., ... Rocher, V. (2016). Removal of a wide range of emerging pollutants from wastewater treatment plant discharges by micro-grain activated carbon in fluidized bed as tertiary treatment at large pilot scale. *Science of the Total Environment*, 542, 983–996.
- Martínez-Huitle, C. A., & Brillas, E. (2009). Decontamination of wastewaters containing synthetic organic dyes by electrochemical methods: A general review. *Applied Catalysis B: Environmental*, 87(3–4), 105–145.
- Mason, T. J., & Lorimer, J. P. (1988). *Sonochemistry: Theory, applications and uses of ultrasound in chemistry*. New York: New York: Ellis Horwood Ltd.
- Matira, E. M., Chen, T.-C., Lu, M.-C., & Dalida, M. L. P. (2015). Degradation of dimethyl sulfoxide through fluidized-bed Fenton process. *Journal of Hazardous Materials*, 300, 218–226.
- Mazarji, M., Aminzadeh, B., Baghdadi, M., & Bhatnagar, A. (2017). Removal of nitrate from aqueous solution using modified granular activated carbon. *Journal of Molecular Liquids*, 233, 139–148.
- Meng, C. N., Jin, B., Chow, C. W. K., & Saint, C. (2010). Recent developments in photocatalytic water treatment technology: A review. *Water Research*, 44(10), 2997–3027.
- Midha, V., Jha, M. K., & Dey, A. (2012). Sulfide oxidation in fluidized bed bioreactor using nylon support material. *Journal of Environmental Sciences*, 24(3), 512–519.

- Miklos, D. B., Remy, C., Jekel, M., Linden, K. G., Drewes, J. E., & Hübner, U. (2018). Evaluation of advanced oxidation processes for water and wastewater treatment – A critical review. *Water Research*, *139*, 118–131.
- Mines, P. D., Uthuppu, B., Thirion, D., Jakobsen, M. H., Yavuz, C. T., Andersen, H. R., & Hwang, Y. (2018). Granular activated carbon with grafted nanoporous polymer enhances nanoscale zero-valent iron impregnation and water contaminant removal. *Chemical Engineering Journal*, *339*, 22–31.
- Miralles-Cuevas, S., Audino, F., Oller, I., Sánchez-Moreno, R., Pérez, J. A.S., & Malato, S. (2014). Pharmaceuticals removal from natural water by nanofiltration combined with advanced tertiary treatments (solar photo-Fenton, photo-Fenton-like Fe(III)-EDDS complex and ozonation). *Separation and Purification Technology*, *122*, 515–522.
- Mison, I. I., Zain, N. K. M., Aziz, R. A., Vidyadharan, B., & Jose, R. (2015). Electrochemical properties of carbon from oil palm kernel shell for high performance supercapacitors. *Electrochimica Acta*, *174*(1), 78–86.
- Mohamed, H. H., & Bahnemann, D. W. (2012). The role of electron transfer in photocatalysis: Fact and fictions. *Applied Catalysis B: Environmental*, *128*, 91–104.
- Mollah, M. Y., Schennach, R., Parga, J. R., & Cocke, D. L. (2001). Electrocoagulation (EC)--Science and Applications. *Journal of Hazardous Materials*, *84*(1), 29–41.
- Mostoufi, N., & Chaouki, J. (2001). Local solid mixing in gas–solid fluidized beds. *Powder Technology*, *114*(1–3), 23–31.
- Mu'azu, N. D., Haladu, S. A., Jarrah, N., Zubair, M., Essa, M. H., & Ali, S. A. (2018). Polyaspartate extraction of cadmium ions from contaminated soil: Evaluation and optimization using central composite design. *Journal of Hazardous Materials*, *342*, 58–68.
- Muangthai, I., Ratanatamsakul, C., & Lu, M. (2010). Removal of 2, 4-Dichlorophenol By Fluidized-Bed Fenton Process. *Sustainable Environmental Research*, *20*(5), 325–331.
- Munoz, M., de Pedro, Z. M., Casas, J. A., & Rodriguez, J. J. (2015). Preparation of magnetite-based catalysts and their application in heterogeneous Fenton oxidation - A review. *Applied Catalysis B: Environmental*, *176–177*, 249–265.
- Muruganandham, M., & Swaminathan, M. (2004). Decolourisation of Reactive Orange 4 by Fenton and photo-Fenton oxidation technology. *Dyes and Pigments*, *63*(3), 315–321.
- Nakada, N., Shinohara, H., Murata, A., Kiri, K., Managaki, S., Sato, N., & Takada, H. (2007). Removal of selected pharmaceuticals and personal care products (PPCPs) and endocrine-disrupting chemicals (EDCs) during sand filtration and ozonation at a municipal sewage treatment plant. *Water Research*, *41*, 4373–4382.
- Nam, S., & Tratnyek, P. G. (2000). Reduction of azo dyes with zero-valent iron. *Water Research*, *34*(6), 1837–1845.

- Nam, W., Kim, J., & Han, G. (2002). Photocatalytic oxidation of methyl orange in a three-phase fluidized bed reactor. *Chemosphere*, *47*, 1019–1024.
- Nam, W., Woo, K., & Han, G. (2009). Photooxidation of anionic surfactant (sodium lauryl sulfate) in a three-phase fluidized bed reactor using TiO<sub>2</sub>/SiO<sub>2</sub> photocatalyst. *Journal of Industrial and Engineering Chemistry*, *15*(3), 348–353.
- Namduri, H., & Nasrazadani, S. (2008). Quantitative analysis of iron oxides using Fourier transform infrared spectrophotometry. *Corrosion Science*, *50*(9), 2493–2497.
- Navarro, S., Fenoll, J., Vela, N., Ruiz, E., & Navarro, G. (2011). Removal of ten pesticides from leaching water at pilot plant scale by photo-Fenton treatment. *Chemical Engineering Journal*, *167*(1), 42–49.
- Neyens, E., & Baeyens, J. (2003). A review of classic Fenton's peroxidation as an advanced oxidation technique. *Journal of Hazardous Materials*, *98*, 33–50.
- Nguyen-tien, K., Patwari, A. N., Schume, A., & Deckwer, W.-D. (1984). Liquid Dispersion in Three-phase Fluidized Beds. *Journal of Chemical Engineering of Japan*, *1249*(1973), 3–4.
- Nikolov, V., Farag, I., & Nikov, I. (2000). Gas-liquid mass transfer in bioreactor with three-phase inverse fluidized bed. *Bioprocess Engineering*, *23*, 427–429.
- Nordin, N., Ho, L. N., Ong, S. A., Ibrahim, A. H., Wong, Y. S., Lee, S. L., ... Oon, Y. L. (2017). Hybrid system of photocatalytic fuel cell and Fenton process for electricity generation and degradation of Reactive Black 5. *Separation and Purification Technology*, *177*, 135–141.
- Ntampeglitis, K., Riga, A., Karayannis, V., Bontozoglou, V., & Papapolymerou, G. (2006). Decolorization kinetics of Procion H-ex1 dyes from textile dyeing using Fenton-like reactions. *Journal of Hazardous Materials*, *136*(1 SPEC. ISS.), 75–84.
- Ochieng, A., Odiyo, J. O., & Mutsago, M. (2003). Biological treatment of mixed industrial wastewaters in a fluidised bed reactor. *Journal of Hazardous Materials*, *96*, 79–90.
- Ochieng, A., Ogada, T., Sisenda, W., & Wambua, P. (2002). Brewery wastewater treatment in a fluidised bed bioreactor. *Journal of Hazardous Materials*, *90*, 311–321.
- Olowson, P. A. (1994). Influence of pressure and fluidization velocity on the hydrodynamics of a fluidized bed containing horizontal tubes. *Chemical Engineering Science*, *49*(15), 2437–2446.
- Onysko, K. A., Robinson, C. W., & Budman, H. M. (2002). Improved Modelling of the Unsteady-State Behaviour of an Immobilized-Cell, Fluidized-Bed Bioreactor for Phenol Degradation. *The Canadian Journal of Chemical Engineering*, *80*, 239–252.
- Parida, S. K., Dash, S., Patel, S., & Mishra, B. K. (2006). Adsorption of organic molecules on silica surface. *Advances in Colloid and Interface Science*, *121*(1–3), 77–110.

- Parr, R. G., Szentpály, L. V., & Liu, S. (1999). Electrophilicity index. *Journal of the American Chemical Society*, *121*(9), 1922–1924.
- Parthiban, R., Iyer, P. V. R., & Sekaran, G. (2007). Anaerobic tapered fluidized bed reactor for starch wastewater treatment and modeling using multilayer perceptron neural network. *Journal of Environmental Sciences*, *19*, 1416–1423.
- Patel, U. D., Ruparelia, J. P., & Patel, M. U. (2011). Electrocoagulation treatment of simulated floor-wash containing Reactive Black 5 using iron sacrificial anode. *Journal of Hazardous Materials*, *197*, 128–136.
- Pearson, R. G. (1986). Absolute electronegativity and hardness correlated with molecular orbital theory. *Proceedings of the National Academy of Sciences of the United States of America*, *83*, 8440–8441.
- Pen, R. I. Æ. F. J., & Jose, X. S. Æ. (2008). Feasibility study of degradation of phenol in a fluidized bed bioreactor with a cyclodextrin polymer as biofilm carrier. *Biodegradation*, *19*, 589–597.
- Perdigo, A., Petre, A., Rosal, R., Rodri, A., Agu, A., & Ferna, A. R. (2010). Occurrence of emerging pollutants in urban wastewater and their removal through biological treatment followed by ozonation. *Water Research*, *44*, 578–588.
- Pignatello, J. J. (1992). Dark and photoassisted iron(3+)-catalyzed degradation of chlorophenoxy herbicides by hydrogen peroxide. *Environmental Science & Technology*, *26*(5), 944–951.
- Pignatello, J. J., Oliveros, E., & MacKay, A. (2006). Advanced oxidation processes for organic contaminant destruction based on the fenton reaction and related chemistry. *Critical Reviews in Environmental Science and Technology*, *36*(1), 1–84.
- Pilli, S. R., Banerjee, T., & Mohanty, K. (2015). HOMO-LUMO energy interactions between endocrine disrupting chemicals and ionic liquids using the density functional theory: Evaluation and comparison. *Journal of Molecular Liquids*, *207*, 112–124.
- Pouran, S. R., Abdul Raman, A. A., & Wan Daud, W. M. A. (2014). Review on the application of modified iron oxides as heterogeneous catalysts in Fenton reactions. *Journal of Cleaner Production*, *64*, 24–35.
- Pouran, S.R., Abdul Aziz, A. R., & Wan Daud, W. M. A. (2015). Review on the main advances in photo-Fenton oxidation system for recalcitrant wastewaters. *Journal of Industrial and Engineering Chemistry*, *21*, 53–69.
- Poyatos, J. M., Muñio, M. M., Almecija, M. C., Torres, J. C., Hontoria, E., & Osorio, F. (2010). Advanced oxidation processes for wastewater treatment: State of the art. *Water, Air, and Soil Pollution*, *205*, 187–204.
- Pozzo, R. L., Giombi, J. L., Baltanás, M. a, & Cassano, A. E. (2000). The performance in a fluidized bed reactor of photocatalysts immobilized onto inert supports. *Catalysis Today*, *62*(2–3), 175–187.

- Pukdee-Asa, M., Su, C. C., Ratanatamskul, C., & Lu, M. C. (2012). Degradation of azo dye by the fluidised-bed Fenton process. *Coloration Technology*, 128(1), 28–35.
- Qin, T. F., Shen, B. X., Zhou, Q. X., & Liu, J. C. (2014). Biodegradation Performance of an Inner-Loop Three-Phase Fluidized-Bed Bioreactor to Treat Petrochemical Wastewater. *Petroleum Science and Technology*, 32(October), 848–855.
- Quy, D. Van, Hieu, N. M., Tra, P. T., Nam, N. H., Hai, N. H., Son, N. Thai, ... Luong, N. H. (2013). Synthesis of Silica-Coated Magnetic Nanoparticles and Application in the Detection of Pathogenic Viruses. *Journal of Nanomaterials*, 2013(3), 1–6.
- Raheem, A., Ji, G., Memon, A., Sivasangar, S., Wang, W., Zhao, M., & Taufiq-Yap, Y. H. (2018). Catalytic gasification of algal biomass for hydrogen-rich gas production: Parametric optimization via central composite design. *Energy Conversion and Management*, 158, 235–245.
- Rai, A., Mohanty, B., & Bhargava, R. (2016). Supercritical extraction of sunflower oil: A central composite design for extraction variables. *Food Chemistry*, 192, 647–659.
- Ramamoorthy, S., & Subramanian, N. (1981). Axial solid mixing and bubble characteristics in gas-fluidized beds with vertical internals. *Chemical Engineering Journal*, 22(3), 237–242.
- Ramírez-sosa, D. R., Castillo-borges, E. R., Méndez-novelo, R. I., Sauri-rianchó, M. R., Barceló-quintal, M., & Marrufo-gómez, J. M. (2013). Determination of organic compounds in landfill leachates treated by Fenton – Adsorption. *Waste Management*, 33, 390–395.
- Ratanatamskul, C., Chintitanun, S., Masomboon, N., & Lu, M. (2010a). Inhibitory effect of inorganic ions on nitrobenzene oxidation by fluidized-bed Fenton process. *Journal of Molecular Catalysis A: Chemical*, 331, 101–105.
- Ratanatamskul, C., Narkwittaya, S., Masomboon, N., & Lu, M.-C. (2010b). Oxidation of 2,6-dimethylaniline by the fluidized-bed Fenton Process. *Reac Kinet Mech Cat*, 101, 301–311.
- Ratanatamskul, C., Narkwittaya, S., Masomboon, N., & Lu, M. (2011). Effect of carrier composition on 2,6- dimethylaniline degradation in aqueous solution by fluidized-bed Fenton process. *Environmental Technology*, 32(11), 1233–1237.
- Reinhold, G., Merrath, S., Lennemann, F., & Markl, H. (1996). Modelling the Hydrodynamics and the Liquid-Mixing Behaviour of a Biogas Tower Reactor. *Chemical Engineering Science*, 51(17), 4065–4073.
- Ribeiro, M. C. M., Starling, M. C. V. M., Leão, M. M. D., & de Amorim, C. C. (2017). Textile wastewater reuse after additional treatment by Fenton's reagent. *Environmental Science and Pollution Research*, 24, 6165.
- Rodrigues, C. S. D., Borges, R. A. C., Lima, V. N., & Madeira, L. M. (2018). p-Nitrophenol degradation by Fenton's oxidation in a bubble column reactor. *Journal of Environmental Management*, 206, 774–785.

- Rusevova, K., Kopinke, F. D., & Georgi, A. (2012). Nano-sized magnetic iron oxides as catalysts for heterogeneous Fenton-like reactions-Influence of Fe(II)/Fe(III) ratio on catalytic performance. *Journal of Hazardous Materials*, 241–242, 433–440.
- Sabarunisha, S. B., & Radha, K. V. (2014). Hydrodynamic behavior of inverse fluidized bed biofilm reactor for phenol biodegradation using *Pseudomonas fluorescens*. *Korean J. Chem. Eng.*, 31(3), 436–445.
- Saini, R., Raghunath, C. V., Pandey, P., & Kumar, P. (2016). Optimization of Fenton oxidation for the removal of methyl parathion in aqueous solution. *Perspectives in Science*, 1980, 670–672.
- Şengil, I. A., & Özacar, M. (2009). The decolorization of C.I. Reactive Black 5 in aqueous solution by electrocoagulation using sacrificial iron electrodes. *Journal of Hazardous Materials*, 161(2–3), 1369–1376.
- Shemer, H., Kunukcu, Y. K., & Linden, K. G. (2006). Degradation of the pharmaceutical Metronidazole via UV, Fenton and photo-Fenton processes. *Chemosphere*, 63(2), 269–276.
- Shi, X., Tian, A., You, J., Yang, H., Wang, Y., & Xue, X. (2018). Degradation of organic dyes by a new heterogeneous Fenton reagent - Fe<sub>2</sub>GeS<sub>4</sub>nanoparticle. *Journal of Hazardous Materials*, 353, 182–189.
- Shih, Y., Tsai, M., & Huang, Y. (2013). Mineralization and defluoridation of 2,2,3,3-tetrafluoro-1-propanol (TFP) by UV oxidation in a novel three-phase fluidized bed reactor (3P-FBR). *Water Research*, 47(7), 2325–2330.
- Si, C., Zhou, J., & Guo, Q. (2011). Characterization of pressure fluctuation signals in an acoustic bubbling fluidized bed. *Journal of the Taiwan Institute of Chemical Engineers*, 42(6), 929–936.
- Sruthi, T., Gandhimathi, R., Ramesh, S. T., & Nidheesh, P. V. (2018). Stabilized landfill leachate treatment using heterogeneous Fenton and electro-Fenton processes. *Chemosphere*, 210, 38–43.
- Stahelin, J., & Hoigne, J. (1985). Decomposition of ozone in water in the presence of organic solutes acting as promoters and inhibitors of radical chain reactions. *Environmental Science and Technology*, 19(12), 1206–1213.
- Su, C.-C., Fan, C.-C., Anotai, J., & Lu, M.-C. (2014). Effect of the iron oxide catalyst on o-toluidine oxidation by the fluidized-bed fenton process. *Environmental Technology*, 35(1–4), 89–94.
- Su, C., Chen, C., Anotai, J., & Lu, M. (2013). Removal of monoethanolamine and phosphate from thin-film transistor liquid crystal display (TFT-LCD) wastewater by the fluidized-bed Fenton process. *Chemical Engineering Journal*, 222, 128–135.
- Su, C., Pukdee-Asa, M., Ratanatamskul, C., & Lu, M.-C. (2011). Effect of operating parameters on the decolorization and oxidation of textile wastewater by the fluidized-bed Fenton process. *Separation and Purification Technology*, 83, 100–105.

- Su, C., Pukdee-asa, M., Ratanatamskul, C., & Lu, M. (2011). Effect of operating parameters on decolorization and COD removal of three reactive dyes by Fenton's reagent using fluidized-bed reactor. *Desalination*, 278(1–3), 211–218.
- Suslick, K. S. (1989). The Chemical Effects of Ultrasound. *Scientific American*, 260, 80–86.
- Suslick, K. S. (1990). Sonochemistry. *Science*, 247(4949), 1439–1445.
- Tang, W. Z., & Huang, C. P. (1996). 2,4-Dichlorophenol Oxidation Kinetics by Fenton's Reagent. *Environmental Technology*, 17(12), 1371–1378.
- Tarley, C. R. T., Silveira, G., dos Santos, W. N. L., Matos, G. D., da Silva, E. G. P., Bezerra, M. A., ... Ferreira, S. L. C. (2009). Chemometric tools in electroanalytical chemistry: Methods for optimization based on factorial design and response surface methodology. *Microchemical Journal*, 92(1), 58–67.
- Tisa, F., Aziz, A. R. A., & Mohd, W. W. A. (2014). Applicability of fluidized bed reactor in recalcitrant compound degradation through advanced oxidation processes: A review. *Journal of Environmental Management*, 146, 260–275.
- Tran, T. N., Pham, T. V. A., Le, M. L. P., Nguyen, T. P. T., & Tran, V. M. (2013). Synthesis of amorphous silica and sulfonic acid functionalized silica used as reinforced phase for polymer electrolyte membrane. *Advances in Natural Sciences: Nanoscience and Nanotechnology*, 4, 1–6.
- Umar, M., Roddick, F., Fan, L., & Abdul, H. (2013). Application of ozone for the removal of bisphenol A from water and wastewater – A review. *Chemosphere*, 90(8), 2197–2207.
- Usman, M., Hanna, K., & Haderlein, S. (2016). Fenton oxidation to remediate PAHs in contaminated soils: A critical review of major limitations and counter-strategies. *Science of the Total Environment*, 569–570, 179–190.
- Vasconcelos, V. M., Ponce-De-León, C., Nava, J. L., & Lanza, M. R. V. (2016). Electrochemical degradation of RB-5 dye by anodic oxidation, electro-Fenton and by combining anodic oxidation-electro-Fenton in a filter-press flow cell. *Journal of Electroanalytical Chemistry*, 765, 179–187.
- Villegas-Guzman, P., Giannakis, S., Torres-Palma, R. A., & Pulgarin, C. (2017). Remarkable enhancement of bacterial inactivation in wastewater through promotion of solar photo-Fenton at near-neutral pH by natural organic acids. *Applied Catalysis B: Environmental*, 205, 219–227.
- Vimonses, V., Jin, B., Chow, C. W. K., & Saint, C. (2010). Development of a pilot fluidised bed reactor system with a formulated clay – lime mixture for continuous removal of chemical pollutants from wastewater. *Chemical Engineering Journal*, 158(3), 535–541.
- Vinod, A. V., & Reddy, G. V. (2005). Simulation of biodegradation process of phenolic wastewater at higher concentrations in a fluidized-bed bioreactor. *Biochemical Engineering Journal*, 24, 1–10.

- Vitale, A. A., Bernatene, E. A., & Pomilio, A. B. (2016). New Insights of the Fenton Reaction Using Glycerol as the Experimental Model. Effect of  $O_2$ , Inhibition by  $Mg^{2+}$ , and Oxidation State of Fe. *The Journal of Physical Chemistry A*, *120*, 5435–5445.
- Vončina, D. B., & Majcen-Le-Marechal, A. (2003). Reactive dye decolorization using combined ultrasound/ $H_2O_2$ . *Dyes and Pigments*, *59*(2), 173–179.
- Wang, J. L., & Xu, L. J. (2012). Advanced oxidation processes for wastewater treatment: Formation of hydroxyl radical and application. *Critical Reviews in Environmental Science and Technology*, *42*(3), 251–325.
- Wang, N., Zheng, T., Zhang, G., & Wang, P. (2016). A review on Fenton-like processes for organic wastewater treatment. *Journal of Environmental Chemical Engineering*, *4*(1), 762–787.
- Wang, Y., Feng, C., Li, Y., Gao, J., & Yu, C.-P. (2016). Enhancement of Emerging Contaminants Removal Using Fenton Reaction Driven by  $H_2O_2$ -producing Microbial Fuel Cells. *Chemical Engineering Journal*, *307*, 679–686.
- Wang, Y., Priambodo, R., Zhang, H., & Huang, Y. (2015). Degradation of the azo dye Orange G in a fluidized bed reactor using iron oxide as a heterogenous photo-Fenton catalyst. *RSC Advances*, *5*, 45276–45283.
- Wei, B. C., Xie, B., & Xiao, H. (2000). Hydrodynamics in an Internal Loop Airlift Reactor with a Convergence-Divergence Draft Tube. *Chemical Engineering Technology*, *23*, 38–45.
- Weipeng, Z., Yumei, Y., Guangji, Z., & Chao, Y. (2014). Mixing Characteristics and Bubble Behavior in an Airlift Internal Loop Reactor with Low Aspect Ratio. *Chinese Journal of Chemical Engineering*, *22*(6), 611–621.
- Weng, C. H., Lin, Y. T., & Yuan, H. M. (2013). Rapid decoloration of Reactive Black 5 by an advanced Fenton process in conjunction with ultrasound. *Separation and Purification Technology*, *117*, 75–82.
- Wirsum, M., Fett, F., Iwanowa, N., & Lukjanow, G. (2001). Particle mixing in bubbling fluidized beds of binary particle systems. *Powder Technol.*, *120*, 63–69.
- Wolinski, K., Hinton, J. F., & Pulay, P. (1990). Efficient Implementation of the Gauge-Independent Atomic Orbital Method for NMR Chemical Shift Calculations. *Journal of the American Chemical Society*, *112*(23), 8251–8260.
- Wu, C., & Huang, J. (1996). Bioparticle characteristics of tapered anaerobic fluidized-bed bioreactors. *Water International*, *30*(1), 233–241.
- Xu, J., Gao, N., Zhao, D., An, N., Li, L., & Xiao, J. (2019). Bromate reduction and reaction-enhanced perchlorate adsorption by  $FeCl_3$ -impregnated granular activated carbon. *Water Research*, *149*, 149–158.
- Xu, X. R., Li, H. Bin, Wang, W. H., & Gu, J. D. (2004). Degradation of dyes in aqueous solutions by the Fenton process. *Chemosphere*, *57*(7), 595–600.

- Yamauchi, H., & Kondo, S. (1988). The structure of water and methanol adsorbed on silica gel by FT-NIR spectroscopy. *Colloid and Polymer Science*, 266(9), 855–861.
- Yan, C., Fan, Y., Lu, C., Zhang, Y., Liu, Y., Cao, R., ... Xu, C. (2009). Solids mixing in a fluidized bed riser. *Powder Technology*, 193(1), 110–119.
- Yang, W.-C. (2003). *Handbook of Fluidization and Fluid-Particle System. Chemical Engineering*. New York: Marcel Dekker, Inc.
- Yu, J., Ji, M., & Yue, P. L. (1999). A three-phase fluidized bed reactor in the combined anaerobic / aerobic treatment of wastewater. *Journal of Chemical Technology & Biotechnology*, 626, 619–626.
- Zegliński, J., Piotrowski, G. P., & Piekos, R. (2006). A study of interaction between hydrogen peroxide and silica gel by FTIR spectroscopy and quantum chemistry. *Journal of Molecular Structure*, 794(1–3), 83–91.
- Zhang, T., Wei, C., Feng, C., & Zhu, J. (2012). A novel airlift reactor enhanced by funnel internals and hydrodynamics prediction by the CFD method. *Bioresource Technology*, 104, 600–607.
- Zhao, J., Zhong, X., & Xu, H. (1992). A model of solid backmixing between stages in a gas-fluidized bed with perforated baffles. *Powder Technology*, 73(1), 37–41.
- Zheng, J., Zhao, Q., & Ye, Z. (2014). Preparation and characterization of activated carbon fiber (ACF) from cotton woven waste. *Applied Surface Science*, 299, 86–91.
- Zhong, W., Jin, B., Zhang, Y., Wang, X., & Xiao, R. (2008). Fluidization of Biomass Particles in a Gas - Solid Fluidized Bed. *Energy and Fuels*, 22(12), 4170–4176.
- Zhu, J., Salah, M., & Zhou, Y. (1997). Radial and axial voidage distribution in circulating fluidized bed with ring-type internals. *Journal of Chemical Engineering of Japan*, 30(5), 928–937.
- Ziane, S., Bessaha, F., Marouf-Khelifa, K., & Khelifa, A. (2018). Single and binary adsorption of reactive black 5 and Congo red on modified dolomite: Performance and mechanism. *Journal of Molecular Liquids*, 249, 1245–1253.

## LIST OF PUBLICATIONS AND PAPERS PRESENTED

### ISI-indexed Publications

1. **Bello, M. M.**, Raman, A. A. A., & Purushothaman, M. (2017). Applications of fluidized bed reactors in wastewater treatment: A review of the major design and operational parameters. *Journal of Cleaner Production*, 141, 1492 -1514 <https://doi.org/10.1016/j.jclepro.2016.09.148>
2. **Bello, M. M.**, & Raman, A. A. A. (2017). Trend and current practices of palm oil mill effluent polishing: Application of advanced oxidation processes and their future perspectives. *Journal of Environmental Management*, 198, 170 – 182. <https://doi.org/10.1016/j.jenvman.2017.04.050>
3. **Bello, M. M.**, Raman, A. A. A. (2018) Synergy of adsorption and advanced oxidation processes in recalcitrant wastewater treatment. *Environmental Chemistry Letters* <https://doi.org/10.1007/s10311-018-00842-0>
4. **Bello, M. M.**, Raman, A. A. A., & Asghar, A. (2019). A review on approaches for addressing the limitations of Fenton oxidation for recalcitrant wastewater treatment. *Process Safety and Environmental Protection* <https://doi.org/10.1016/j.psep.2019.03.028>
5. **Bello, M. M.**, Raman, A. A. A., & Asghar, A. (2019). Fenton oxidation treatment of recalcitrant dye in fluidized bed reactor: role of SiO<sub>2</sub> as carrier and its interaction with Fenton's reagent. *Environmental Progress and Sustainable Energy* <https://doi.org/10.1002/ep.13188>
6. **Bello, M. M.**, & Raman, A. A. A. Interaction patterns in fluidized bed Fenton process for degradation of recalcitrant pollutants: theoretical and experimental insights. *Chemical Papers* (Under Review: Revision requested)
7. **Bello, M. M.**, Y'ng, T.S., Raman, A. A. A. Integrated fluidized bed adsorption-Fenton oxidation to remove recalcitrant pollutants. *Chemical Engineering Communications* (Under Review: Revision requested)
8. **Bello, M. M.**, Raman, A. A. A., & Asghar, A. Enhancing fluidized bed Fenton process for recalcitrant wastewater treatment using palm kernel shell activated carbon *Journal of Cleaner Production* (Under review)
9. **Bello, M. M.**, & Raman, A. A. A. Comparing the performance of SiO<sub>2</sub> and palm kernel shell GAC as carriers in fluidized bed Fenton process for wastewater treatment. (In preparation).
10. **Bello, M. M.**, Raman, A. A.A. Fe-loaded palm kernel shell GAC as heterogeneous catalyst in fluidized bed Fenton process for removal of recalcitrant pollutants. (in preparation)

### **Book Chapter**

1. **Bello M.M.** and Raman, A.A.A. (2018). Adsorption and oxidation techniques to remove organic pollutants from water. In G. Grini & E. Litchfouse (Eds.), *Green Adsorbent for Pollutants Removal Fundamentals and Design* (1<sup>st</sup> ed., pp. 51- 63). Springer International Publishing

### **Conference papers**

1. **Bello, M. M., & Raman, A. A. A.** (2017). Performance of Fluidized bed Fenton process in Degrading Acid Blue 113. IOP Conference Series: Materials Science and Engineering, 210(1), 1–8. <https://doi.org/10.1088/1757-899X/210/1/012006>
2. **Bello, M. M., & Raman, A. A. A.** Treatment of recalcitrant wastewater using Fenton oxidation in a fluidized bed reactor. 4th International Symposium on Current Progress in Mathematics and Sciences 2018 (Accepted).

University of Malak